In presenting this thesis or dissertation as a partial fulfillment of the requirements for an advanced degree from Emory University, I hereby grant to Emory University and its agents the non-exclusive license to archive, make accessible, and display my thesis or dissertation in whole or in part in all forms of media, now or hereafter known, including display on the world wide web. I understand that I may select some access restrictions as part of the online submission of this thesis or dissertation. I retain all ownership rights to the copyright of the thesis or dissertation. I also retain the right to use in future works (such as articles or books) all or part of this thesis or dissertation.

Signature:

_____	_____
Jameson T. L. Berry	Date

Enhancing Oncolytic Reovirus with Doxorubicin for Triple-Negative Breast Cancer Therapy

By

Jameson T. L. Berry
Doctor of Philosophy

Graduate Division of Biological and Biomedical Science
Cancer Biology

_____
Bernardo A. Mainou, Ph.D.
Advisor

_____
Curtis J. Henry, Ph.D.
Committee Member

_____
Gregory B. Lesinski, Ph.D., MPH
Committee Member

_____
Mehul S. Suthar, Ph.D.
Committee Member

_____
Periasamy Selvaraj, Ph.D.
Committee Member

Accepted:

_____
Lisa A. Tedesco, Ph.D.
Dean of the James T. Laney School of Graduate Studies

_____
Date

Enhancing Oncolytic Reovirus with Doxorubicin for Triple-Negative Breast Cancer Therapy

By

Jameson T. L. Berry
B.S., Arizona State University, 2016

Advisor: Bernardo A. Mainou, Ph.D.

An abstract of
A dissertation submitted to the Faculty of the
James T. Laney School of Graduate Studies of Emory University
in partial fulfillment of the requirements for the degree of
Doctor of Philosophy
in the Graduate Division of Biology and Biomedical Science,
Cancer Biology
2020

Abstract

Enhancing Oncolytic Reovirus with Doxorubicin for Triple-Negative Breast Cancer Therapy
By Jameson T. L. Berry

Breast cancer is the leading cause of cancer-related deaths in women in the United States. The triple-negative (TNBC) subtype associates with higher rates of relapse, decreased survival, aggressive metastatic disease, and limited therapeutic options. Mammalian orthoreovirus (reovirus) selectively infects and kills transformed cells, and a serotype 3 reovirus (T3C$) is in clinical trials to assess oncolytic efficacy against several cancers. To engineer a reovirus with increased oncolysis against TNBC, we coinfected MDA-MB-231 TNBC cells with Type 1 Lang (T1L), Type 2 Jones (T2J), and Type 3 Dearing (T3D) reoviruses. After serial passage of cells, we isolated the reassortant r2Reovirus that is composed of T1L and T3D genes. r2Reovirus infects TNBC cells more efficiently and reduces cell viability with faster kinetics than parental T1L or T3D and T3C$. Pretreating cells with topoisomerase inhibitors, including doxorubicin, enhances r2Reovirus infectivity and cytotoxicity in TNBC cells and leads to stimulation of DNA damage response pathway activation and Type III interferon production. To develop a mechanism of codelivery of drug and virus, we conjugated doxorubicin to r2Reovirus (reo-dox). Reo-dox induces cytotoxicity in TNBC cells more efficiently than r2Reovirus alone. Conjugation has minimal effects on virus biology, and host response to reo-dox is altered compared virus alone or with exogeneous doxorubicin. Crosslinked doxorubicin retains the ability to damage DNA and promote damage response pathway activation. Importantly, r2Reovirus and reo-dox significantly reduce primary TNBC tumor burden *in vivo*, with greater reduction in metastatic burden after reo-dox inoculation. Crosslinking chemotherapeutic agents to oncolytic viruses facilitates functional drug delivery to cells targeted by the virus, making it a viable approach for combination therapy against TNBC. Together, these studies identify a new reassortant reovirus with improved oncolysis against TNBC that can be enhanced by classical combination with topoisomerase inhibitors or by novel chemical conjugation. Adapting viruses to target tumor cells is an important step in generating improved individualized therapies to address tumor heterogeneity, and novel drug delivery mechanisms that enhance combination therapy and anti-tumor immune responses will benefit the long-term systemic response to treatment, improving quality of life and care of patients.

Enhancing Oncolytic Reovirus with Doxorubicin for Triple-Negative Breast Cancer Therapy

By

Jameson T. L. Berry
B.S., Arizona State University, 2016

Advisor: Bernardo A. Mainou, Ph.D.

A dissertation submitted to the Faculty of the
James T. Laney School of Graduate Studies of Emory University
in partial fulfillment of the requirements for the degree of
Doctor of Philosophy
in the Graduate Division of Biology and Biomedical Science,
Cancer Biology
2020

Acknowledgements

In the Spring Semester of 2016, I was like any college senior, trying to finalize my plans for the next step in my career, in life. Before me stood two distinct trajectories: accept a placement as Japan Exchange and Teaching English teacher in that country for a year or two, or pursue my PhD studies immediately at Emory University. If I had elected for the overseas job, I would likely have come back to graduate studies, but I'm certain I would not have had the opportunity to join Bernardo's lab. And what an opportunity I would have missed out on! By God's grace and a providential push in the right direction, I've been blessed to enjoy three years of dissertation research with a small team of amazing scientists beyond what I could have hoped for!

Bernardo, thank you for gladly taking me in to the BAM-fam. Not only did I get to conduct research in my primary field of interest, I got to do so in the lab of someone who cares about his team like family. You've always expressed interest in my personal life and made sure that I had a balance between efforts in lab and being a human being outside ECC 510. Additionally, your willingness to let me propose a new project idea, seek out how to make it a reality, and pursue it as my dissertation project has meant so much to me as I've grown up as an independent scientist. It's a special opportunity, and it takes an outstanding PI to support that. And thanks for keeping me around and believing in me even after my seahorse obsession….yep, I'm letting that live on in writing!

Lab life would not have been nearly as enjoyable if not for a terrific friend in the trenches day-in and day-out. Roxana, I couldn't have asked for a better labmate to go through the struggles and victories of grad school with. You've always been happy to help answer questions and check my math. I hope I've been as good of a sounding board for experiment ideas and data analysis for you as you've been for me. It has meant a lot to me too to have such a thoughtful and caring friend who is genuinely interested in life events, big and small. Growing up in lab the last couple years, I've enjoyed having you as an incredible role model and big sister figure, so to speak. I've been inspired by your scientific curiosity, inventiveness, and overall drive to get where you want to be. The CDC is lucky to have you, and I hope to see great advances in health sciences with your name tied to them! It's been a fun run, and it's exciting that we're getting to cross the finish line as labmates and as a whole lab at the same time.

To my cohort, it's been a fun four years, and it's hard to believe we're starting to wrap things up already. Cara, Rae, and Brandon, all of you are incredible scientists and I'm excited to see where your careers take you in the future. Thank you for being a support group, whether studying for quals, bouncing ideas, or just checking in periodically. Best of luck to you all!

Mom and Dad, thank you for being supportive of me moving 2000 miles away to advance my interest in the sciences. I know it hasn't always been easy, but your support and encouragement to pursue my studies at Emory has been invaluable. Thanks for wanting to see my papers even though they're written for a technical audience with different science background. When I talk about my project with you, I appreciate that you always listen and even ask questions! Learning to explain my work to you has helped me to improve my communication skills; I can't guarantee you'll understand everything in my public defense, but I know you'll recognize a few things, like

reo-dox. It means a lot that you support and show interest in my interests. I can't wait to celebrate with y'all in person! Love you guys so much!

To my brother, Tanyon, and sister-in-law, Lindsey, thank you that despite the distance from Decatur to Tempe, we stay in touch and try to keep up with each other's lives. Tanyon, you really are the best little brother a guy could ask for. We have so many silly stories from growing up, and when one of those memories comes to mind, it brings a smile and happy thoughts that can turn any day around. Glad we still wish each other a happy Fumbleknob day, and it's something special to be able to quote (and misquote) movies and games out of context and still be able to know what and why the other is referencing! *Kawana-botah* indeed. And Lindsey, it's a blessing to have a siter-in-law who fits right in to the nerdiness and weirdness that is my family, while bringing your own geeky fandoms along. If it wasn't for you, I don't know if Elizabeth and I would have gotten hooked on Doctor Who! Love you two, and looking forward to the years ahead.

To my Lifegroup and church family, all of you have been there through this journey with me. You've listened to every uncertainty I've had about my pursuit of the PhD, encouraged me as I've gone back and forth on what career trajectory I think I should be pursuing. Thank you for your prayers and helping me keep this stage in my life and career in the perspective of Christ.

I want to specifically acknowledge Emily and Roger. I'm extremely grateful that you took the crazy step to move across the country and start a new life in Atlanta. God has blessed Elizabeth and me so much not only by leading y'all to join Resonate, but also by the fact that you live just down the road. In the last couple years, you've become two of our closest friends. Your hospitality and aid last summer getting us moved into our new apartment and housing us while we got the break-in sorted out is just a small testament to your servant hearts. Also, it's been too long since the last time we had y'all over for dinner (or invited ourselves, with the gift of dessert in tow of course!). Love you both.

Tim and Margaret, thank you for accepting me with open arms into your family. Not everyone can say they have terrific parents-in-law, but I'm one of the lucky few. You're two of the most thoughtful folks I know, and you're always interested in my life and making sure I feel comfortable, cared for, and included. I'm so happy that y'all are now part of my family and I get to share future milestones with you!

Thank you to my fantastic dissertation committee, current and previous members. Greg, Curtis, Mehul, Selva, and Dolores, I looked forward to sharing my project with you over the last two years at every meeting, whether it was as a group, meeting in your office, or sitting down to talk over coffee. Thank you for the guidance, enthusiasm, and interest in my science and my development as a scientist.

Elizabeth, you've been with me every step of the way. Thank you for choosing to pursue your graduate studies in Atlanta when you could have chosen to go to Pennsylvania or California, or stayed back home in Texas. After a long day or week in lab, driving across town or knowing you were coming over for dinner was always a highlight! Thanks for being my adventure buddy, exploring new places and trying new foods around the city and state. Thanks for saying "yes" even when I took you up to Tallulah Gorge super early in the morning and we couldn't even get a pass

to go to the gorge floor, and for bearing with me as I drove you through rural North Georgia to stage two of my proposal. You're the best road trip companion, and while I don't particularly want to drive through a hurricane again anytime soon, there's no one else I'd rather do that with (plus it makes a fun story from the first week of being married!). You are an incredibly smart woman whose curiosity truly knows no bounds. I'm proud of you for realizing that you didn't want a PhD, for moving on from a rough research experience, to landing an awesome job where you are getting to research and develop some very neat new technologies! You value friendships and care for others so deeply, and anyone who knows you can see you have Christ's heart for your neighbors. You help me steer back in the right direction, and I know I can always count on your advice. I'm incredibly blessed to call you me best friend, and God has provided in you an *ezer* beyond what I could ask. You bring out the best in me, and challenge me to grow into a better reflection of Christ in love, thoughtfulness, selflessness, and humility. You're the bestest wifey ever, the jelly to my peanut butter, and one of these days, the trophy wife you always dreamed of becoming! I love you lots and am so grateful that you've been by my side through this chapter, and that we get to share in every chapter here on out.

In memory of

Boyd P. Lane, Jr.

Miss and love you, Grandad.

Table of Contents

List of Figures and Tables

List of Abbreviations

ABCB1 – ATP-binding cassette sub-family B member 1
ADC – antibody-drug conjugate
AKT – protein kinase B
AMP – adenosine monophosphate
AP-1 – activator protein 1
AP-2 – activator protein 2
ATM – ataxia telangiectasia-mutated
ATP – adenosine triphosphate
BRCA1 – breast cancer type 1 susceptibility protein (gene, italicized)
CARD – caspase activation and recruitment domains
Cdc25 – cell division cycle 25
Cdk – cyclin dependent kinase
cGAMP – cyclic GMP-AMP
cGAS – cyclic GMP-AMP synthase
Chk – checkpoint kinase
Cip – Cdk-interacting protein
Cxcl – C-X-C motif chemokine
Cxcr – C-X-C motif chemokine receptor
(i/m)DC – ([im]mature) dendritic cell
DNA – deoxyribonucleic acid
dsRNA – double-stranded RNA
EGFR – epidermal growth factor receptor
eIF2α/B – eukaryotic initiation factor-2α/B
ELISA – enzyme-linked immunosorbent assay
ER – estrogen receptor
ERK – extracellular signal-regulated kinase
GDP – guanine diphosphate
GEF – guanine nucleotide exchange factor
GM-CSF – granulocyte-macrophage colony-stimulating factor
GMP – guanine monophosphate
GRB2 – growth factor receptor-bound protein 2
GTP – guanine triphosphate
(γ)H2AX – (phosphorylated) H2A histone family member X
HER2 – human epidermal growth factor receptor 2
HR – hormone receptor
HSV1 – herpes simplex virus type-1
ICP – infected cell protein
IFI16 – interferon gamma inducible protein 16
IFN – interferon (genes italicized)
IHC – immunohistochemistry
IL-28R – interleukin 28 receptor
IRES – internal ribosomal entry site
IRF – interferon regulatory factor
ISVP – infectious subvirion particle

JAM-A – junctional adhesion molecule A
KSR1 – kinase suppressor of Ras 1
MAPK – mitogen-activated protein kinase
MAVS – mitochondrial activator of viral signaling
MDA5 – melanoma differentiation-associated protein 5
MDM2 – mouse double minute 2 homolog
MDR1 – multidrug resistance protein 1
MEK – mitogen-activated protein kinase kinase
MFI – mean fluorescence intensity
MOI – multiplicity of infection
MRE11 – meiotic recombination 11
MRN – MRE11-RAD50-NBS1
mRNA – message RNA
MSL – mesenchymal stem-like
MTD – maximum tolerated dose
NBS1 – Nijmegen breakage syndrome 1; nibrin
NCC – NIH Clinical Collection
NF-κB – nuclear factor kappa-light-chain-enhancer of B cells
NgR1 – nogo receptor 1
NGS – next generation sequencing
NK cell – natural killer cell
OV – oncolytic virus
OXPHOS – oxidative phosphorylation
PARP – poly ADP-ribose polymerase
PCR – polymerase chain reaction
PDX – patient-derived xenograft
PFU – plaque forming unit
P-gp – P-glycoprotein
PI3K – phosphoinositide 3-kinase
PIP2/3 – phosphatidylinositol (4,5)-bisphosphate/(3,4,5)-triphosphate
PKR – protein kinase R
PR – progesterone receptor
PRR – pattern recognition receptor
PTEN – phosphatase and tensin homolog deleted on chromosome 10
qPCR – quantitative PCR
Rb – retinoblastoma protein
RIG-I – retinoic acid inducible gene I
RNA – ribonucleic acid
ROS – reactive oxygen species
RTK – receptor tyrosine kinase
SCID – sever combined immunodeficient
SMCC – succinimidyl 4-(n-maleimidomethyl)cyclohexane-1-carboxylate
SOS – son of sevenless
ssRNA – single-stranded RNA
STAT – signal transducer and activator of transcription
STING – stimulator of interferon genes

T1L – type 1 Lang
T2J – type 2 Jones
T3A – type 3 Abney
T3C$ -- type 3 “Cashdollar”; used in oncolytic reovirus clinical trials
T3D – type 3 Dearing
TAA – tumor associated antigen
TANK – TRAF family member-associated NF-κB activator
TBK1 – TANK binding kinase 1
TCID – tissue culture infectious dose
TIL – tumor infiltrating lymphocyte
TNBC – triple-negative breast cancer
TRAF6 – tumor necrosis factor receptor associated factor 6
T-Vec – talimogene laherparepvec, an oncolytic HSV
VSV – vesicular stomatitis virus

Chapter 1: Introduction

CANCER

Cancer is broadly defined as a collection of vastly different diseases stratified not only by organ site but also by affected tissue. Cancers typically are diseases related to aging and are second to heart disease as the leading cause of death in the United States (1). Between patients and within the tumor tissue of a single patient, there can exist numerous differences in genetic composition, tumor progression, immune response to the cancer, and therapeutic resistance (2-5). Along with differences in and among cancer cells themselves, tumor tissues thrive by virtue of using other cell types in their microenvironments (6, 7): cancer cells can promote angiogenesis to generate a blood supply through newly formed vascular endothelial cells (8); cancer associated fibroblasts support some tumor tissue growth and can aid a cancer in shielding itself from immune detection (9); cancer cells often evolve to evade immune detection, but inflammation in the tumor microenvironment can lead to signaling that promotes cancer cell survival (10).

When a cancer is diagnosed, it is assigned a classification based on the type of cancer, extent of disease, and spread of cancerous cells throughout the body. Stage IV, aggressive cancers are typically associated with metastasis, or spread of cancer cells from the primary tumor to secondary, distant sites throughout the body. Metastatic disease can be more difficult to detect and treat, and survival is severely negatively impacted by metastases. Whereas the 5-year survival rates for local disease (cancer only in the primary tissue) is ~80%, the average for metastatic cancer is ~20% (averages from 19 different organs and tissue sites) (11, 12).

Breast cancer

According to the American Cancer Society, breast cancer continually accounts for the largest number of new diagnoses in women in the United States with a projected 276,000 (30%) new cases for 2020. Breast cancer has been second to lung cancers as the leading cause of cancer-related mortality in women in the United States since the late 1980s, and is projected to account

for 42,000 individuals (15%) in 2020 (11). Global estimations reflect a similar pattern; breast cancers are projected as the most prevalent new diagnosis in women, accounting for ~20-30% of cases across all levels of the Human Development Index (a measure of standard of living, education, and life expectancy by location) (13). The World Health Organization indicates that breast cancer and lung cancer were the more prominent cancers globally in 2018 (14). While increased self-examination and mammographic screening correlate with a higher incidence of breast cancer in the United States, mortality rates have not been affected. Increased screening and adjuvant therapy have aided in minimizing metastatic disease, but it remains the leading cause of death from breast cancer (15) with a 5-year survival rate of 27% for distant disease compared to 86-99% survival among patients with local or regional disease (11, 12).

Triple-negative breast cancer

Breast cancers can be classified into four distinct molecular subtypes based upon cellular expression of surface receptor proteins: estrogen receptors (ER) and progesterone receptors (PR) (together referred to as hormone receptor [HR]) and human epidermal growth factor receptor 2 (HER2). Breast cancers are most commonly Luminal A (HR+/HER2-). The characteristically less aggressive subtype can respond well to hormone therapy and prognosis trends favorably (16, 17). Luminal B (HR+/HER2+) are typically higher grade than luminal A; higher grade cancers are further progressed and tend to associate with poorer outcomes. HER2-enriched (HR-/HER2+) tumors are targetable with HER2-directed therapies, which has improved outcomes for patients with this classification of breast cancer (18, 19).

The fourth subtype, triple-negative (TNBC, also basal-like), is characterized by the lack of ER, PR, and HER2 on cell surfaces. The lack of hormone and growth factor receptors on TNBC cells poses a limitation to development of targeted therapies, and prognosis is poorer than other

subtypes. TNBC accounts for 10-20% of breast cancers. The disease tends to affect younger women, is more prevalent in women of African descent, and women with germline *BRCA1* mutations are at greater risk for TNBC (20). Treatment for TNBC is limited to surgical resection of tumors, radiation therapy, and broadly acting chemotherapeutics.

DOXORUBICIN

Doxorubicin (adriamycin, abbreviated henceforward as dox) is an anthracycline class antineoplastic drug that has been in frontline use for cancer, including breast cancer, therapy over the past four decades (21-23). Dox inhibits topoisomerase II enzyme by intercalation with DNA, leading to DNA double strand breaks and activation of resultant programmed cell death (24, 25). Dox can also activate cell death by the production of reactive oxygen species (ROS) in tumor and healthy cells (26, 27). Systemic administration of dox as a cancer therapy has faced the significant drawback of non-specific cytotoxicity, largely attributed to ROS generation, in various organs, namely heart, liver, and kidneys (25). Dox does not directly impact neural tissue as the drug cannot cross the blood brain barrier (28). However, ROS-related damage has been documented in the brain after prolonged systemic dox treatment (25, 29). Various efforts are being made to improve targeted delivery of dox to cancer cells and circumvent drug resistance mechanisms (30).

Evolution of drug resistance diminishes the long-term efficacy of chemotherapeutic drugs. Normal cells and cancer cells (though to a greater degree) express P-gp (P-glycoprotein, also MDR1: multidrug resistance protein 1), a drug efflux pump encoded by *ABCB1* (ATP-binding cassette sub-family B member 1) (31). P-gp is a transmembrane protein that resides in the plasma membrane of the cell. It binds a variety of hydrophobic drugs, including dox, and releases drugs into the extracellular space through an ATP hydrolysis-mediated conformational change of P-gp (32). In some cancer cells, dox treatment correlates with increased expression of drug efflux pumps

(33). More recently, sorcin (SOluble Resistance-related Calcium-binding proteIN) was identified to bind with high affinity to dox. Further, dox treatment leads to sorcin redistribution from the plasma membrane to a cytosol-diffused pattern, indicating that cancer cells can adapt to and sequester chemotherapeutic agents throughout the cell, not only at the membrane efflux pumps (34).

Nanoparticle delivery systems encompass many efforts to enhance dox delivery to tumor cells. FDA-approved methods include pegylated and unpegylated liposomes with dox concealed in an aqueous core (27, 35). Studies using liposome-encapsulated dox indicate that dox accumulates to greater concentrations in tumor tissues compared to free systemic dox and yields a better safety profile for patients (36). Other studies have encapsulated dox in micelles (37) and exosomes (37, 38) enhancing the cytotoxic effect of dox directed at tumor cells.

Preclinical studies indicate potential efficacy of combining nanoparticle-delivered dox with efflux pump inhibitors (30). Nanoparticle delivery undermines the presentation of dox to efflux pumps by avoiding dox diffusion across the cell membrane and releasing dox intracellularly (30). Further inhibition of factors contributing to drug resistance enhance the potency of dox in treated cancer cells.

To direct dox to cancer cells, antibody-drug conjugates (ADCs) have also been developed (39). ADCs utilize monoclonal antibodies raised against tumor-specific antigens with crosslinked cytotoxic cargo (40) and have been an area of study since at least the early 1990’s. One of the first-generation ADCs described involved dox conjugated to the chimeric monoclonal antibody BR96, which binds an antigen abundantly presented in human cancers and related to Lewis Y carbohydrate (41-44). Contemporary efforts utilize nanoparticle-encapsulated dox conjugated to

antibodies as a strategy in a variety of cancers including HER2+ breast cancers (45-47), although development of targeted therapies toward TNBC remains an issue.

Topoisomerase

Chemotherapeutic agents can kill cells through the inhibition of proteins and enzymes involved in DNA replication and cell cycle progression. While a myriad of targets exist, the work detailed herein focuses on inhibition of topoisomerase enzymes. Topoisomerases are classified as type I and type II, where type I cleaves DNA one strand at a time and type II cleaves both strands of DNA simultaneously during the catalytic process. The first topoisomerase was discovered in 1971 by Dr. James C. Wang who detailed a novel protein ω from *E. coli* that could decrease the linking number of helical DNA without altering the physical properties of the molecule (48). Protein ω would later be termed *E. coli* type IA topoisomerase, reflecting the function of the enzyme to alter the linking number of circular DNA and form different topoisomers (topological isomers) of the macromolecule through relaxation of negative supercoils. The mammalian counterpart, eukaryotic Top1 (type IB topoisomerase), emerged from the work of Champoux and Dulbecco. This topoisomerase is distinct from *E. coli* type IA because it relaxes positive and negative DNA supercoils and forms a 3’ tyrosyl-DNA covalent catalytic intermediate rather than a 5’ intermediate (49). Top3 and Top1mt (eukaryotic type IA and human mitochondrial type IB topoisomerases, respectively) were discovered in the late 1990s and early 2000s (50, 51). Shortly after the initial bacterial discovery by Wang, the second class of topoisomerase enzymes, initially termed DNA gyrase (*E. coli* topoisomerase II [type IIA]), was documented (52). Humans express two isotypes of the topoisomerase protein, topoisomerase IIα and IIβ, both of which are type IIA. Topoisomerase II relaxes DNA supercoils during DNA replication, simplifying DNA topology

(53). Inhibition of topoisomerase II leads to suspension of relegation of DNA double strand breaks, promoting apoptotic cell death (54, 55).

DNA double strand break response

Upon DNA double strand break formation, a series of protein recruitment and activation at the site of damage gives rise to either repair of damage or fating to apoptotic cell death. Upon double strand break damage, H2A histone family member X (H2AX) is phosphorylated on Ser139 (γH2AX) by the kinase ataxia telangiectasia-mutated (ATM) (56, 57). Inactive, dimerized ATM autophosphorylates at Ser1981, leading to dimer dissociation and increased kinase activity (58). The tri-protein MRN complex (MRE11-RAD50-NBS1) recognizes sites of DNA double strand breaks, associates with the damage site, and recruits ATM, facilitating the targeted phosphorylation of ATM substrates (59). ATM phosphorylates Chk1 at serine 345 (60)and Chk2 at threonine 68 (61). Activation of both Chk1 and Chk2 leads to inhibition of Cdc25 phosphatase, impairing cell cycle progression from G2 to M phase (62). Active ATM can also directly phosphorylate p53 at Ser15 (63). Active p53 in turn acts as a transcription factor for a variety of genes involved in cell cycle arrest and apoptosis. Cdk (cyclin-dependent kinase)-interacting protein (Cip) p21 binds cyclin-Cdk complexes, attenuating phosphorylation of Rb (retinoblastoma protein) and restricting G1/S progression (64). p53 can decrease cyclin B1 transcription (65), and p53-mediated upregulation of 14-3-3σ leads to inactivation of Cdc25C and Cdc2 (66), leading to a deficit in signals to allow progress through G2/M phase. G2/M arrest is favored by DNA damage due to the inhibition of Cdc25C phosphatase by Chk1, Chk2, and p53 (62, 66-68). Pro-apoptotic Bcl-2 family member Bax as well as BH3-only members Puma, Noxa, and Bid can be transcriptionally upregulated by active p53, leading to an increase in the abundance of pro-apoptotic proteins in the cell and favoring mitochondrial release of cytochrome c, caspase

activation, and apoptosis (69-72). The accumulation of pro-apoptotic signals and extensive DNA damage burden ultimately fates cells for transition from cell cycle arrest to apoptotic death (67).

ONCOLYTIC VIRUSES

In 1904, Dr. George Dock documented a case of reduction in leukemic cells in patient blood after the patient contracted influenza (73). The work of Dr. Dock highlights an important link between viral infection and cancer therapy. While the concept of oncolytic virotherapy has roots as far as the early 20th Century, serious consideration of viruses for cancer therapy was emphasized decades later from 1950-1970 (74). However, only wild-type viruses were assessed at the time, as these trials predate advanced molecular biology technology used to engineer chimeric species, introduce immunostimulatory genes, and delete genes promoting virulence. Intensive study and development of viruses for enhanced therapy has been rejuvenated only recently with the advent of genetic engineering technologies and contemporary knowledge of virus-host interactions, making oncolytic virotherapy a competitive approach in a world of effective chemotherapeutics and targeted immunotherapies.

Oncolytic virotherapy embraces aspects of virus and cancer cell biology. First, many viruses selectively replicate within and kill host cells, particularly cancer cells, which tend to have dysregulated antiviral responses as part of their malignant phenotype (75). Cell lysis and other means of virus egress from cells releases progeny viral particles to amplify infection in neighboring cells. While cellular antiviral responses may be subverted, infection can still activate the innate immune response, releasing cytokines like Type-I and -III interferons (IFN) that attract lymphocytes to the infected tumor microenvironment. Dying tumor cells can releases tumor-associated antigens (TAAs) that further augment a tumor-directed immune response, supporting adaptive systemic antitumor immunity to target cancer cells at distant, uninfected sites (76).

Oncolytic viruses remain largely absent from clinical use. To date, only one has received FDA approval in the United States. Talimogene laherparepvec (T-Vec, Oncovex^{GM-CSF}, Imlygic®) is an engineered herpes simplex virus type-1 (HSV1) that has been developed for treating inoperable melanoma (ClinicalTrials.gov identifier NCT00769704) (77-80). Liu *et al.* described the generation of T-Vec in 2003. Using a JS1 clinical isolate of HSV1, neurovirulence factor genes Infected Cell Protein (ICP) 34.5 and ICP47 were removed, and the virus was engineered to overexpresses granulocyte-macrophage colony-stimulating factor (GM-CSF) (81). ICP34.5 blocks the action of protein kinase R (PKR)-mediated host cell translation shutoff, a cellular defense mechanism to inhibit viral replication (81, 82). As many cancer cells already exhibit disabled PKR signaling, removal of ICP34.5 helps target HSV replication to tumor cells only, and ICP34.5 deletion in laboratory isolated HSVs (1716 [based on Glasgow strain 17+] and G207) was documented as nonneruovirulent and favorable for malignant gliomas (83, 84). Mutation to increase the expression of US11 was included to enhance ICP34.5 mutant HSV replication (85-87), and ICP47 was deleted in the process, which normally blocks $CD8^+$ T cell response to HSV (88) and blocks antigen presentation by infected cells (89). Overexpression of GM-CSF further amplifies the immune response to infected tumor cells (81).

Genetic modification of viruses is not limited to making otherwise harmful viruses into relatively safe, therapeutic agents. Several wild-type viruses that do not cause serious disease in humans can be genetically engineered to enhance their oncolytic potential, including the topic of the work describe herein: mammalian orthoreovirus.

REOVIRUS

Mammalian orthoreovirus (reovirus) is a non-enveloped, segmented double-stranded RNA virus. The name “reovirus” derives from the designation as Respiratory Enteric Orphan virus.

Reovirus is an orphan virus because it is rarely associated with disease. Most humans have been infected with reovirus during early childhood (90, 91). While reovirus may be implicated in the development of celiac disease (92), the full extent of the role of the virus in human health and disease remains uncertain. The genome of reovirus consists of 10 gene segments classified as L (3 genes), M (3 genes), and S (4 genes). Each gene encodes one or two structural or nonstructural proteins. L1, L2, and L3 code for structural proteins λ3, λ2, and λ1 respectively. M1 and M2 code for structural proteins μ2 and μ1 respectively, and M3 codes for two nonstructural proteins, μNS and μNSC. S1, S2, and S4 encode structural proteins σ1, σ2, and σ3 respectively. S1 also encodes nonstructural σ1s, and S3 encodes nonstructural σNS (93). The μNS and σNS support the formation of inclusion bodies wherein genome is replicated, viral proteins are translated, and progeny virions assemble (93). Reovirus is composed of two concentric capsid layers of 8 different structural proteins. The outer capsid is comprised of λ2, μ1, σ1, and σ3. The inner capsid, or core, also contains λ2 in addition to λ1, λ3, μ2, and σ2. Pentameric λ2 turrets protrude from the core into the outer capsid. Up to 12 σ1 attachment fiber proteins can protrude from the viral particle, one per λ2 pentamer (94). σ1 consists of a globular C-terminal head, a central body, and elongated N-terminal tail which inserts in the turret pentamers (93, 95-97).

Reovirus discovery and isolation

Reovirus was first isolated and identified in the laboratory of Dr. Albert Sabin in 1954 from stool samples of children (98, 99). Three distinct serotypes of reovirus were defined by the end of the 1950s: Type 1 Lang (100), the prototype reovirus; Type 2 Jones (101); and Type 3 Dearing (101). A second serologically identical Type 3 reovirus (Abney) was also defined by Dr. Leon Rosen (102). The serotypes of reovirus are defined by attachment fiber-specific neutralizing antibodies (93) and hemagglutination inhibition (103).

Reovirus cell entry

Reovirus cell attachment is facilitated through an adhesion-strengthening mechanism. Outer capsid attachment fiber protein σ1 engages in low-affinity binding with cell-surface carbohydrates (104, 105). Type 1 reoviruses bind with terminal sugar moieties *N*-acetylneuraminic acid and *N*-acetylgalactosamine of the oligosaccharide portion of ganglioside GM2 (GM2 glycan) in the globular head domain of σ1 (106). Type 3 reovirus attachment fibers engage sialylated oligosaccharides (107). Subsequently, reovirus binds with a proteinaceous surface receptor, junctional adhesion molecule A (JAM-A), a protein which typically localizes to cellular tight junctions, through high-affinity binding of the σ1 head domain (104, 108, 109). After binding with JAM-A, reovirus particles begin endocytosis in a β1 integrin-dependent and clathrin-mediated manner(110, 111) (112). As the endosome traffics through the cytoplasm, the pH of the endosomal compartment decreases. Acidification yields an environment amenable to cathepsin protease activity (113-117). Cathepsins B, L (acid-dependent), and S (active at neutral pH) proteolytically remove σ3 from the reovirus outer capsid and cleave μ1 into ϕ and particle-associated δ fragments (114, 118). Conformational change of σ1 also occurs; combined the events in the late endosome form the infectious subvirion particle (ISVP) (93, 113-115, 118, 119). The ϕ fragment creates pores in the endosomal membrane, allowing for viral core translocation into the cellular cytoplasm (120, 121). In the cytoplasm, transcriptionally active cores undergo primary transcription of message-sense single-stranded RNA (ssRNA) mediated by core-associated viral λ3 RNA-dependent RNA polymerase (122), with posited helicase activities attributed to μ2 and λ1 (93, 123). Nonstructural viral proteins σNS and μNS associate with endoplasmic reticulum and endoplasmic reticulum-Golgi intermediate compartment, thinning membrane tubules and cleaving the intracellular membranes to remodel the membranes. μNS, σNS, and the remodeled membranes

together form globular structures called inclusion bodies, or viral factories (124, 125). Further transcription, translation, and viral assembly occur within these viral factories (126, 127). mRNA is synthesized with the negative-sense RNA as a template. Translation of structural proteins proceeds using positive-sense genomic RNA and newly synthesized mRNAs. As translation

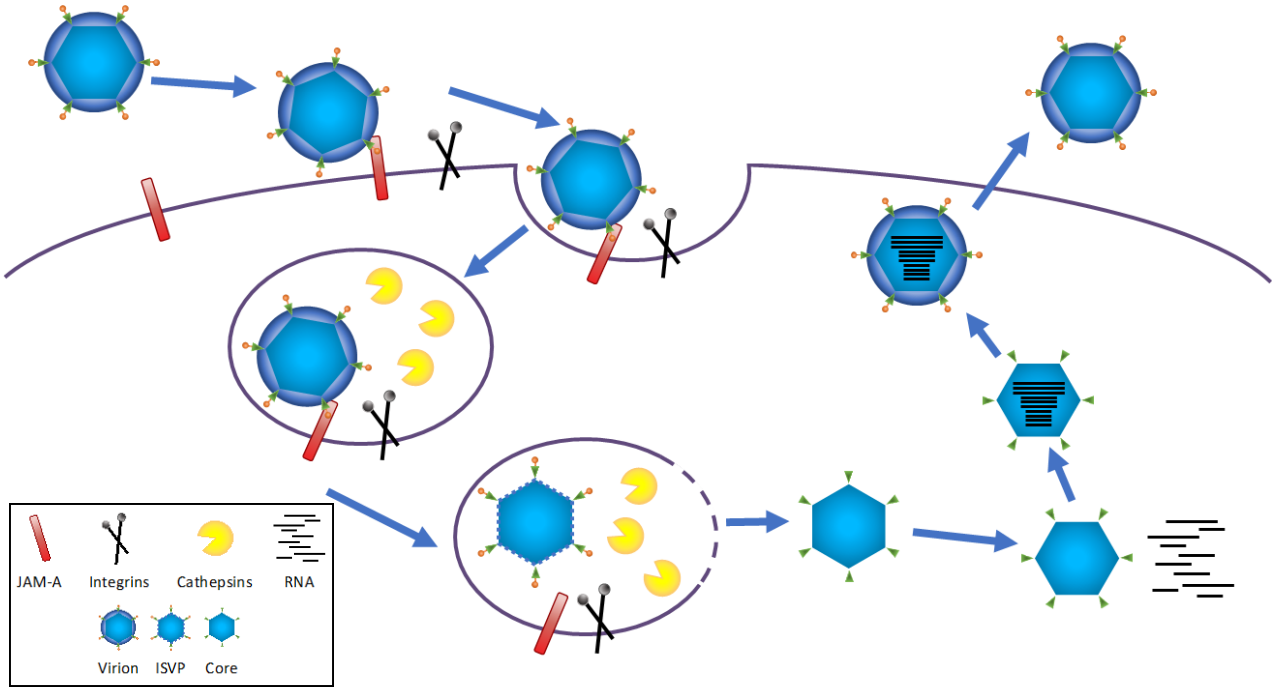

Figure 1.1. Reovirus entry pathway in epithelial cells.
Reovirus attachment fiber σ1 engages cell surface carbohydrate and JAM-A. Clathrin-mediated endocytosis internalizes the virus. In the late endosome, cathepsins B, L and S proteolytically uncoat reovirus forming ISVPs. Nonstructural proteins σNS and μNS remodel endoplasmic reticulum membranes to form viral factories in the cytoplasm. Within the viral factories, genomic RNA and proteins are amplified and self-assemble into new viral particles. Virions egress through an undefined mechanism.

proceeds, newly synthesized inner capsid proteins assemble with viral RNA as progeny cores, which in turn contribute to further transcription and translation. During the process, newly translated outer capsid proteins accumulate in the viral factories; assembly of these proteins on progeny cores inhibits further full-length RNA transcription (128). Progeny virions are complete after σ1 trimers insert into λ2 channels. The mechanism of reovirus egress remains poorly understood, though lytic and nonlytic methods have been proposed.

Virus-host response

Mammalian cells are equipped to mount an innate immune response to viral infection. Various pattern recognition receptors (PRRs) contribute to the response to foreign antigens. Retinoic acid inducible gene I (RIG-I) and melanoma differentiation-associated protein 5 (MDA5) recognize viral RNA in the cytosol (129). Binding of viral RNA to either PRR invokes a conformational change of the protein to an active state in which the terminal caspase activation and recruitment domains (CARDs) are exposed. While in their active conformation, RIG-I and MDA5 CARDs interact with the CARD of mitochondrial activator of viral signaling (MAVS), a mitochondria-associated adaptor protein that mediates PRR signaling (130-132). The CARD-CARD interaction between RIG-I or MDA5 and MAVS induces active interferon regulatory factor 3 (IRF3) and nuclear factor kappa-light-chain-enhancer of B cells (NF-κB) which serve as transcription factors for Type-I interferons (IFNs) and other inflammatory cytokines (130-132). Viral dsRNA (double-stranded RNA) can also be detected by cellular PKR. When PKR binds dsRNA, PKR forms homodimers. Autophosphorylation leads to direct phosphorylation of eukaryotic initiation factor-2α (eIF2α), thus enhancing its affinity for the guanine nucleotide exchange factor (GEF) eIF2B. Stable eIF2B-eIF2α-GDP prevents future initiation of protein synthesis (133, 134). Reovirus is adapted to circumvent PKR recognition, as outer capsid protein σ3 conceals the dsRNA reovirus genome (135, 136).

Reovirus as an oncolytic

Reovirus has inherent tropism to cancer cells. Many cancer cells harbor constitutively activated Ras. Ligand binding with surface receptor tyrosine kinases (RTKs) (like EGFR, epidermal growth factor receptor) leads to dimerization and phosphorylation of the kinase. GRB2 (growth factor receptor-bound protein 2) binds to the cytosolic tail of the kinase dimer and is bound by SOS (son of sevenless). The GRB2/SOS complex binds with Ras, and SOS acts as a GEF to

displace GDP from Ras and allow for GTP to bind to Ras (137). Active GTP-Ras recruits Raf to the cell surface, releasing Raf from inhibitory binding with 14-3-3 proteins. The Ras-Raf dimer activates KSR1 (kinase suppressor of Ras 1), an enzyme which facilitates Raf phosphorylation of MEK, which in turn activates ERK, regulating proliferation and survival pathway transcriptional programs in the cell (138-140). Ras/MAPK pathway activating mutations are prevalent in many cancers, but highly infrequent in breast cancers (140), with Ras and Raf family member mutations occurring in less than 2% of primary breast tumors (141, 142). Nonetheless, overexpression of RTKs and elevated ERK activity (140, 143, 144), or truncating mutations in *NF1* (neurofibromin), a negative regulator of GDP-Ras exchange to GTP-Ras, can serve as indirect mechanisms to lead breast cancers to rely more on Ras/MAPK activity (140, 142, 145, 146).

Ras-transformed cells express elevated levels of cathepsin B, enhancing the efficiency of reovirus uncoating during endocytic processing (147). Ras proliferative signaling also inhibits PKR from catalyzing the phosphorylation of eIF2α, alleviating the potential for PKR-mediated impairment of translation initiation and minimizing part of the antiviral detection machinery in cells (147, 148).However, PKR activity does not necessarily antagonize reovirus replication (149), and Ras constitutive activation is not the only benefactor to reovirus preference for cancer cells. Overexpression of JAM-A can facilitate greater levels of reovirus attachment to cancer cells compared to untransformed cells (108, 150). Some cancer cells express elevated levels of cathepsins B and L (151-155) which are required for reovirus disassembly and overall oncolysis (114). Untransformed cells in contrast exhibit lower levels of cathepsins, contributing to restriction of reovirus uncoating and less productive infection (156).

Because reovirus infects and replicates more readily in transformed cells, is safe without attenuation and can be administered intravenously and intratumorally (93), it has gained wide

interest for development as an oncolytic virus. A laboratory-isolated type 3 reovirus (Reolysin®, pelareorep) is used in numerous phase I-III clinical trials in a variety of cancers. Table 1.1 outlines many of the trials conducted since the early 2000's using oncolytic reovirus alone or in combination with chemotherapeutic and immunotherapy agents. Natural infection with reovirus is rarely associated with disease and is relatively safe to inject into humans, with asymptomatic or subclinical illness (Table 1.1) (157-159). As most humans have prior exposure to reoviruses, consideration must be given to antibody-mediated neutralization of the virus when reintroduced as an oncolytic agent. In 1998, Coffey *et al.* tested oncolytic reovirus efficacy in immunocompetent CH3 mice with previous exposure to reovirus. Intratumoral reovirus inoculation of ras-transformed CH3 fibroblast tumors resulted in regression of tumors but required a series of repeated virus administration rather than single dose therapy that regressed tumors in an immunocompromised SCID (severe combined immunodeficient) mouse model (160). Several studies have investigated the efficacy of loading adaptive immune cells with oncolytic reovirus to circumvent systemic neutralization and deliver virus to tumor sites. In 2009, Ilett *et al*. described a study in which reovirus was loaded in T cells, immature dendritic cells (iDCs), and mature DCs (mDCs) (161). In reovirus-immune C57Bl/6 mice bearing B16tk melanoma and lymph node metastases, mDCs and T cells loaded with reovirus delivered virus to cancer cells whereas infections with reovirus alone or loaded on iDCs were ineffective. Further, the reovirus-loaded T cell- and mDC-mediated purging of B16tk cells from tumor draining lymph nodes discreetly correlated with TAA-specific adaptive immune response (161). In 2018, a study published by Berkeley *et al*. expanded on the findings of Ilett and others, showing that *in vitro*, antibody-neutralized reovirus could be taken up by monocytes (that circulate in the bloodstream). While antibody-neutralized virus was ineffective at killing melanoma cells, monocytes loaded with neutralized virus delivered replicating virus to

tumor cells and resulted in efficient infection and cell killing (162), indicating a potential role for monocytes to overcome pre-existing immunity against reovirus. Others have assessed the adaptive immune response generated by loading lymphocytes with other oncolytic viruses, including VSV (vesicular stomatitis virus) (163) and PVSRIPO, a chimeric live attenuated poliovirus with the internal ribosomal entry site (IRES) of human rhinovirus (164, 165). Using oncolytic viruses to prime a tumor-specific adaptive immune response highlights the multifaceted nature of oncolytic virotherapy that must be embraced to fully appreciate clinical gains.

Tissue		Trial Location	Phase	Highest doses ($TCID_{50}$*, except where noted)	Combination agent	Participants	Safety/Efficacy	ClinicalTrials.gov identifier	Status	Published Results
Brain cancer	Childhood & early adult brain tumors	US	I	Determining MTD**	sargramostim (GM-CSF)	6		NCT02444546	Active, not recruiting	
	malignant glioma	US	I	1×10^{10}		18	Well tolerated	NCT00528684	Completed 2010	(166)
	malignant glioma	Canada	I	1×10^{9}		12	Well tolerated		Completed 2006	(167)
Gynecologic cancer		US	II	1×10^{10}	paclitaxel	108	No results posted	NCT01199263	Active, not recruiting	
		US	I	1×10^{10}		70	No results posted	NCT00602277	Completed 2016	
			IIB	3×10^{10}	paclitaxel	108				(168)
Colorectal cancer		Canada	II	1×10^{10}	FOLFOX6 and bevacizumab	109	Tolerated, inferior PFS	NCT01622543	Completed 2018	(169)
		US	I	1×10^{10}	FOLFIRI and bevacizumab	36	No results posted	NCT01274624	Completed 2018	
Breast cancer		Canada	II	1×10^{10}	paclitaxel	81	Longer OS, no difference in PFS	NCT01656538	Completed 2018	(170)
Prostate cancer		Canada	II	1×10^{10}	docetaxel and prednisone	85	Tolerated, inferior PFS	NCT01619813	Completed 2016	(171)
Pancreatic cancer		US	II	1×10^{10}	paclitaxel, carboplatin	73	Tolerated, no improvement in PFS	NCT01280058	Completed 2016	(172)
		US	II	1×10^{10}	gemcitabine	34	No results posted	NCT00998322	Completed 2015	
Lung cancer		Canada	II	1×10^{10}	pemetrexed, docetaxel	166	Tolerated, no improvement in PFS	NCT01708993	Completed 2018	(173)
		US	II	1×10^{10}	paclitaxel, carboplatin	37	No results posted	NCT00861627	Completed 2015	
		US	II	1×10^{10}	paclitaxel, carboplatin	32	No results posted	NCT00998192	Completed 2015	
Head and neck cancer		US, UK, Canada, Belgium, etc	III	1×10^{10}	paclitaxel, carboplatin	167	Well tolerated/limited efficacy	NCT01166542	Completed 2014	
		US	II	1×10^{10}				NCT00753038	Completed 2013	
		UK	I, II	3×10^{10}	paclitaxel, carboplatin	31	Well tolerated/limited efficacy		Completed 2012	(174)

Bone and soft tissue Sarcomas		US	II	1×10^{10}		23	Well tolerated/limited efficacy	NCT00651157	Completed 2012	(175)
		US	II	1×10^{10}		53		NCT00503295	Completed 2011	
Skin cancer		US	II	1×10^{10}	paclitaxel, carboplatin	14	No results posted	NCT00984464	Completed 2014	
Hematological cancer		US	I	MTD, capped 4.5×10^{10}	bortezomib and dexamehtasone	14		NCT02514382	Active, not recruiting	
		US	I	1×10^{10}	carfilzomib, dexamethasone	28***		NCT02101944	Recruiting	
		US	I	1×10^{10}		12	No results posted	NCT01533194	Completed 2015	
Childhood solid tumors		US, Canada	I	1×10^{10}	cyclophosphamide	26	No results posted	NCT01240538	Completed 2014	
Advanced solid tumors		UK	I	3×10^{10}	docetaxel	25	Well tolerated		Completed 2008	(176)
		UK	I	1×10^{10}	radiotherapy	23	Well tolerated		Completed 2007	(177)
		UK	I	3×10^{10}		33	Well tolerated, repeated administration		Completed 2007	(158)
		UK	I	3×10^{10}	gemcitabine	16	Well tolerated at 1×10^{10} $TCID_{50}$		Completed 2007	(159)
		Canada	I	1×10^{10} (PFU)		19	Well tolerated/limited efficacy		Completed 2002	(178)

* Tissue culture infectious dose

** Maximum tolerated dose

*** Estimated enrollment

Table 1.1 Overview of clinical trials using Reolysin over the past two decades.
Adapted from Kim 2015, *Naturally occurring reoviruses for human cancer therapy* (179).

SUMMARY AND SCOPE

TNBC is an aggressive form of breast cancer with limited treatment options. Oncolytic reovirus has been studied as a potential therapeutic in a variety of cancers, including breast cancer, but success with the laboratory-isolated serotype 3 reovirus in clinical trials is minimal. Efforts to enhance efficacy include combining reovirus with immunotherapeutic and chemotherapeutic agents (Table 1.1). Chemotherapeutic agents, while extremely effective at killing many cell types, are largely not cancer-specific, and systemic administration associates with off-tumor toxicities. In Chapter II, a reassortant reovirus (r2Reovirus) is engineered with increased infective and cytotoxic efficacy against TNBC cells. Screening of a library of FDA-approved small molecule inhibitors reveals topoisomerase inhibitors as enhancers of reovirus infectivity in TNBC cells. *In vitro* experiments suggest that r2Reovirus infects and kills more potently when combined with topoisomerase inhibitors. The combination promotes DNA damage and innate immune stimulation, highlighting a multifaceted cellular response to the combined agents and promise for future study in TNBC. In Chapter III, doxorubicin, one of the identified topoisomerase inhibitors, is conjugated to r2Reovirus (reo-dox) to enhance cytotoxicity directed at infected cells. Cells infected with reo-dox display similar innate immune activity as those infected with r2Reovirus alone and after doxorubicin pretreatment. Cells infected with reo-dox also display fragmented DNA and activation of double strand break response proteins. Further, 4T1-bearing mice inoculated with r2Reovirus or reo-dox present decreased primary tumor burden, and reo-dox inoculation promotes a greater reduction in metastatic spread to the lungs than r2Reovirus. Crosslinking small molecule inhibitors to reassortant reoviruses may serve as an effective model for enhancing oncolytic activity against a selected tumor and more precisely deliver cargo to cells targeted by the virus.

Chapter 2: Enhanced Killing of Triple-Negative Breast Cancer Cells by Reassortant Reovirus and Topoisomerase Inhibitors

This research was published in *Journal of Virology*.

Authors: Roxana M. Rodríguez Stewart, Jameson T.L. Berry, Angela K. Berger, Sung Bo Yoon, Aspen L. Hirsch, Jaime A. Guberman, Nirav B. Patel, Gregory K. Tharp, Steven E. Bosinger, and Bernardo A. Mainou

Journal of Virology. 2019, Volume 93 Issue 23 e01411-19

Enhanced Killing of Triple-Negative Breast Cancer Cells by Reassortant Reovirus and Topoisomerase Inhibitors

Roxana M. Rodríguez Stewart1,2#, Jameson T.L. Berry1,2^#, Angela K. Berger2,3, Sung Bo Yoon1, Aspen L. Hirsch2,3, Jaime A. Guberman1, Nirav B. Patel4, Gregory K. Tharp4, Steven E. Bosinger4, and Bernardo A. Mainou2,3*

Emory University,[1] Department of Pediatrics,[2] Emory University School of Medicine, Atlanta, GA 30322, Children's Healthcare of Atlanta[3], Atlanta, GA, 30322, Emory Vaccine Center[4], Yerkes National Primate Research Center, Atlanta, GA 30322

# R.M.R.S. and J.T.L.B. contributed equally to this work.

* To whom correspondence should be addressed: Emory University School of Medicine, Department of Pediatrics, ECC 564, 2015 Uppergate Drive, Atlanta, GA 30322. Tel.: (404) 727-1605. Fax: (404) 727-9223. E-mail: bernardo.mainou@emory.edu.

Running Title: Topoisomerase Inhibitors Enhance Reovirus Cell Killing

ABSTRACT

Breast cancer is the second-leading cause of cancer-related deaths in women in the United States. Triple-negative breast cancer constitutes a subset of breast cancer that is associated with higher rates of relapse, decreased survival, and limited therapeutic options for patients afflicted with this type of breast cancer. Mammalian orthoreovirus (reovirus) selectively infects and kills transformed cells and a serotype 3 reovirus is in clinical trials to assess its efficacy as an oncolytic agent against several cancers. It is unclear if reovirus serotypes differentially infect and kill triple-negative breast cancer cells and if reovirus-induced cytotoxicity of breast cancer cells can be enhanced by modulating the activity of host molecules and pathways. Here, we generated reassortant reoviruses by forward genetics with enhanced infective and cytotoxic properties in triple-negative breast cancer cells. From a high-throughput screen of small molecule inhibitors, we identified topoisomerase inhibitors as a class of drugs that enhance reovirus infectivity and cytotoxicity of triple-negative breast cancer cells. Treatment of triple-negative breast cancer cells with topoisomerase inhibitors activates DNA damage response pathways and reovirus infection induces robust production of Type III, but not Type I, interferon. Although Type I and Type III IFN can activate STAT1 and STAT2, triple-negative breast cancer cellular proliferation is only negatively affected by Type I IFN. Together, these data show that reassortant viruses with a novel genetic composition generated by forward genetics in combination with topoisomerase inhibitors more efficiently infect and kill triple-negative breast cancer cells.

IMPORTANCE

Patients afflicted by triple-negative breast cancer have decreased survival and limited therapeutic options. Reovirus infection results in cell death of a variety of cancers, but it is unknown if different reovirus types lead to triple-negative breast cancer cell death. In this study, we generated two novel reoviruses that more efficiently infect and kill triple-negative breast cancer cells. We show that infection in the presence of DNA-damaging agents enhances infection and triple-negative breast cancer cell killing by reovirus. These data suggest that a combination of a genetically engineered oncolytic reovirus and topoisomerase inhibitors may provide a potent therapeutic option for patients afflicted with triple-negative breast cancer.

INTRODUCTION

Breast cancer is the leading cause of cancer and second leading cause of deaths by cancer in women in the United States (180). Triple-negative breast cancer (TNBC) constitutes approximately 15% of breast cancers and has a higher rate of relapse and shorter overall survival after metastasis than other subtypes of breast cancer (181). In addition, compared to other forms of breast cancer, TNBC more frequently affects the young, is more prevalent in African American women, and tumors are larger in size and biologically more aggressive (182). TNBC is characterized by the lack of expression of estrogen receptor (ER), progesterone receptor (PR), and human epidermal growth factor receptor 2 (HER2/neu) and can be classified into seven subtypes based on their genetic signature (182). Although targeted therapies against hormone receptor-positive and HER2-positive breast cancer have been efficacious, the absence of these molecules on TNBC cells has limited treatment to cytotoxic chemotherapy, radiotherapy, and surgery (21, 183). This raises a need for targeted therapeutics against this type of cancer.

The concept that viruses can promote tumor regression is nearly as old as the discovery of viruses (73). The deregulated expression of viral receptors, endocytic uptake molecules, proteases, altered metabolic states, and impaired innate immunity make cancer cells ideally suitable for virus infection and replication (75, 134, 184). In addition to directly impacting cancer cell biology, oncolytic viruses can elicit anti-tumor immune responses and serve as adjuvants for other cancer therapies (185-187). Several viruses are under study to assess their oncolytic properties against several cancers (75, 184). Nonfusogenic mammalian orthoreovirus (reovirus) is a non-enveloped double-stranded RNA (dsRNA) virus in the *Reoviridae* family. A serotype 3 reovirus (Reolysin) is in Phase I and II clinical trials (clinicaltrials.gov: NCT01622543, NCT01656538) to assess its efficacy against a variety of cancers (80). Reovirus can be delivered to patients via intratumoral and intravenous administration and can be effective in combination therapy (188). Reovirus has

an inherent preference to replicate in tumor cells, making it ideally suited for use in oncolytic virotherapies (189, 190). However, the cellular and viral factors that promote preferential reovirus infection of cancer cells are not fully elucidated.

Reovirus has a segmented genome with three large (L), three medium (M), and four small (S) dsRNA gene segments (191). There are three different reovirus serotypes (Type 1, 2, and 3) based on the neutralization ability of antibodies raised against the σ1 attachment protein that is encoded by the S1 gene segment (93, 102). Reoviruses infect most mammals and although humans are infected during childhood, infection seldom results in disease (90, 92, 93, 192). Reovirus induces programmed cell death *in vitro* and *in vivo* (193-200). Although both Type 1 and Type 3 reovirus can induce apoptosis, Type 3 reoviruses induce apoptosis and necroptosis more efficiently in most cells (93, 193, 194). Serotype-dependent differences in apoptosis induction segregate with the S1 and M2 gene segments (201-203). However, there is a limited understanding of the viral factors that determine preferential replication and killing of cancer cells.

In this study, we show that co-infection and serial passaging of parental reoviruses in TNBC cells yields reassortant viruses with enhanced oncolytic capacities compared to parental reoviruses. Reassortant reoviruses have a predominant Type 1 genetic composition with some Type 3 gene segments as well as synonymous and non-synonymous point mutations. We show that reassortant reoviruses have enhanced infective and cytotoxic capacities in TNBC cells compared to parental viruses. To further enhance the oncolytic properties of these reassortant viruses, we used a high-throughput screen of small molecule inhibitors and identified DNA-damaging topoisomerase inhibitors as a class of drugs that reduces TNBC cell viability while enhancing reovirus infectivity. Infection of TNBC cells in the presence of topoisomerase inhibitors results in induction of DNA damage, increased levels of Type III but not Type I interferon, and enhanced cell killing. Although

Type I and Type III IFN can activate STAT1 and STAT2, triple-negative breast cancer cellular proliferation is only negatively affected by Type I IFN. Together, we show that reassortant reoviruses with a novel genetic composition have enhanced oncolytic properties and pairing of topoisomerase inhibitors with reovirus potentiates TNBC cell killing.

RESULTS

Generation of reassortant viruses in triple-negative breast cancer cells by forward genetics.

Reovirus serotypes have distinct infective, replicative, and cell killing properties and the segmented nature of the reovirus genome allows the generation of viruses with novel properties through gene reassortment following co-infection (204, 205). To generate reoviruses with enhanced replicative properties in TNBC cells, MDA-MB-231 cells were co-infected with prototype laboratory strains T1L, T2J, and T3D and serially passaged in these cells ten or twenty times (FIG 2.1A). Following serial passage, individual viral clones were isolated by plaque assay and the gene segment identity for each clone (44 clones following 10 passages, 45 clones following 20 passages) was determined by SDS-gel electrophoresis (FIG 2.1B). Of the 44 isolates analyzed following 10 serial passages, 8 distinct electropherotypes were identified, with 23 isolates (52%) having the same electropherotype (r2Reovirus) (FIG 2.1C). Following 20 serial passages, 6 distinct isolates were identified, including two (r9 and r10) that were not observed after passage 10 (FIG 2.1D). The most predominant electropherotypes following 20 serial passages were r1Reovirus and r2Reovirus, constituting 33% and 27% respectively of all isolates. Illumina Next-Generation Sequencing (NGS) revealed that r1Reovirus is composed of seven gene segments from T1L and three from T3D (L2, M2, S2), while r2Reovirus is composed of nine gene segments from T1L and one from T3D (M2) (FIG 2.2). In addition, both viruses have previously unidentified nonsynonymous point mutations that result in an Ala to Thr substitution at amino acid 160 in L3, an Ile to Val substitution at amino acid 250 in S3, and Val to Ile substitution at amino acid 49 in S4. A Pro to Thr substitution at amino acid 161 is also found in r1Reovirus. In addition, r1Reovirus and r2Reovirus have several synonymous point mutations (Table 2.S1). Interestingly, the r1Reovirus S2 gene segment, but no other gene segment, has single residue variations that range from 35% to 65%. Sanger sequencing of the S2 gene segment from ten r1Reovirus plaque isolates

showed a wide array of mutations distinct from the initial virus isolate (data not shown). These data suggest that the S2 gene segment of r1Reovirus is genetically unstable. We did not detect single residue variations in gene segments from either parental T1L, T2J, or T3D or r2Reovirus, suggesting this is not an intrinsic property of the S2 gene segment carried from parental viruses. Together, these data indicate that co-infection and serial passaging of reoviruses in MDA-MB-231 cells leads to the generation of reassortant reoviruses with novel genetic compositions.

Reassortant reoviruses infect MDA-MB-231cells more efficiently than parental reoviruses.

Reovirus attaches to cells via a strength-adhesion mechanism whereby the viral attachment fiber σ1 binds to cell-surface carbohydrate and proteinaceous receptors JAM-A or NgR1 (106-108, 150, 206). To determine the attachment efficiency of r1Reovirus and r2Reovirus in comparison to parental reoviruses, MDA-MB-231 cells were adsorbed with vehicle (mock) or Alexa 633 (A633)-labeled T1L, T3D, T3C$ (the reovirus strain currently in clinical trials), or reassortant reoviruses at an MOI of 5×10^4 particles/cell and assessed for cell surface reovirus by flow cytometry (FIG 2.3A). Reassortant reoviruses attach to cells with similar efficiency as T1L, but less efficiently than Type 3 reoviruses T3D and T3C$. As reassortant reoviruses contain a T1L S1 gene segment, it is not surprising that they attach to cells to similar levels as parental T1L. These data also indicate that other genetic changes found in r1Reovirus and r2Reovirus do not impact the ability of these viruses to attach to cells.

To determine how genetic changes in r1Reovirus and r2Reovirus affect reovirus infection of TNBC cells, MDA-MB-231 cells were pretreated with DMSO or the cysteine protease inhibitor E64-d, which blocks reovirus cell entry by preventing proteolysis during endocytic uptake (207), adsorbed with mock, T1L, T3D, T3C$, or reassortant reoviruses at an MOI of 100 PFU/cell and

assessed for infectivity after 18 h by indirect immunofluorescence using reovirus-specific antiserum (FIG 2.3B). In contrast to attachment, r1Reovirus and r2Reovirus infect MDA-MB-231 cells more efficiently than parental reoviruses or T3C$, with both reassortant viruses infecting cells over 2-fold more efficiently. Infection with all viruses tested was impaired by E64-d, indicating a similar requirement for proteolytic processing during entry. These data indicate that reassortant reoviruses establish infection more efficiently in MDA-MB-231 cells than parental reoviruses and that infection of these cells requires proteasomal processing of the virion during cell entry.

To determine if the increased infectivity of the reassortant viruses is limited to MDA-MB-231 cells, the infectivity of parental and reassortant reoviruses was assessed on murine L929 fibroblasts, which are highly susceptible to reovirus infection and are used to propagate the virus (FIG 2.3C). L929 cells were adsorbed with mock, T1L, T3D, T3C$, or reassortant reoviruses at an MOI of 5 PFU/cell and assessed for infectivity after 18 h by indirect immunofluorescence using reovirus-specific antiserum. In contrast to that observed in MDA-MB-231 cells, reassortant reoviruses infect L929 cells to similar levels as parental T1L, but less efficiently than both T3D and T3C$. These data indicate that r1Reovirus and r2Reovirus more efficiently infect TNBC cells, but not L929 cells. This suggests that the genetic changes found in the reassortant viruses confer enhanced infection in the TNBC cells used for serial passage at a step after attachment.

Replication kinetics of reassortant reoviruses are similar to T1L but faster than T3D.

To determine the replication efficiency of parental and reassortant reoviruses, MDA-MB-231 cells were adsorbed with mock, T1L, T3D, T3C$ or reassortant reoviruses at an MOI of 10 PFU/cell and assessed for viral replication over a 3 day course of infection (FIG 2.4). Despite the

differences observed in infectivity, all viruses except T3D replicated with similar kinetics, with T3C$ having faster replication kinetics by day 1 post infection (FIG 2.4B) and reaching higher peak titers than all other viruses tested. T1L, T3C$, r1Reovirus, and r2Reovirus had similar replication kinetics at days 2 and 3 post infection. T3D replication kinetics were slower, with lower viral yields, than all other viruses tested. Interestingly, although T3C$ only differs from T3D by 22 amino acids, its replication kinetics are more similar to T1L and the reassortant reoviruses than T3D. These data indicate that although reassortant reoviruses establish infection in MDA-MB-231 cells more efficiently than parental reoviruses, replication kinetics are similar to T1L but significantly enhanced compared to T3D.

r1Reovirus and r2Reovirus impact TNBC cell viability with faster kinetics than parental reoviruses.

Type 3 reoviruses induce cell death more efficiently than Type 1 reoviruses *in vitro* and *in vivo* and T3C$ is currently in clinical trials to test its efficacy as an oncolytic against a variety of cancers (203, 208). To determine the efficacy of viral-induced cytotoxicity in TNBC cells, MDA-MB-231 cells were adsorbed with mock, T1L, T3D, T3C$, r1Reovirus, or r2Reovirus at an MOI of 500 PFU/cell, or treated with staurosporine as a positive control, and assessed for cell viability for 7 days (FIG 2.5A). Compared to mock-infected cells, all reoviruses tested impaired cell viability, with reassortant reoviruses impairing cell viability with the fastest kinetics. In reassortant reovirus-infected cells, cell viability peaked at day 2 post infection, reaching levels similar to staurosporine by day 5 post infection. Cell viability peaked at day 3 post infection in T1L-, T3D-, and T3C$-infected cells reaching staurosporine levels by day 5 with T1L and day 6 with T3C$. At day 3 post infection, cell viability is significantly impaired in reassortant reovirus-infected cells,

but not other reoviruses tested (FIG 2.5A). Overall, the impact on cell viability by reassortant viruses was 1 day ahead of T1L and T3C$ and 2-3 days ahead of T3D. To determine if similar effects on cell viability could be observed in another TNBC cell line, MDA-MB-436 cells were infected with mock, T1L, T3D, T3C$, or r2Reovirus and assessed for cell viability over 6 days (FIG 2.5B). Similar to that observed in MDA-MB-231 cells, r2Reovirus induced cell death with significantly faster kinetics than either parental T1L or T3D, or T3C$. At day 4 post infection, r2Reovirus was the only virus tested to significantly impair MDA-MB-436 cell viability (FIG 2.5B). These data show that reassortant viruses negatively affect cell viability of TNBC cells more efficiently than parental reoviruses and the oncolytic T3C$ strain. These data also suggest that T3D is not efficient at inducing cell death in at least a subset of TNBC cells.

To determine if r1Reovirus and r2Reovirus differ from parental reoviruses in their ability to impair cell viability of non-TNBC cells, L929 cells were adsorbed with mock, T1L, T3D, T3C$, r1Reovirus, or r2Reovirus at an MOI of 500 PFU/cell and assessed for cell viability over a 3 day time course (FIG 2.5C). In contrast to that observed in MDA-MB-231 cells, all reoviruses tested impaired cell viability with relatively similar kinetics except for T3C$, which impaired L929 cell viability with significantly faster kinetics. These data indicate that reassortant viruses induce cell death with faster kinetics than parental reoviruses in TNBC cells and to a lesser extent in L929 cells. Given r2Reovirus had enhanced infectivity and cytotoxicity in MDA-MB-231 compared to parental viruses and r1Reovirus has a genomically unstable S2.2 gene segment, experiments in the rest of this study were performed with r2Reovirus.

Identification of small molecules that impact reovirus infectivity of MDA-MB-231 cells.

The efficacy of reovirus as a mono-oncolytic therapeutic has been limited. Combinatorial therapeutics can enhance efficacy by targeting different pathways that lead to enhanced cancer cell death (209). To identify small molecule inhibitors that enhance the oncolytic potential of reovirus, a high-throughput screen to assess the effect of small molecules from the NIH Clinical Collection I and II (NCC) on reovirus infectivity was performed. The NCC is composed of compounds that have been through Phase I-III clinical trials. To test the effects on reovirus infectivity of compounds in the NCC, MDA-MB-231 cells were pre-treated with vehicle (DMSO), 4 μM E64-d, or 10 μM NCC compounds for 1 h. r2Reovirus was added to cells at an MOI of 20 PFU/cell, incubated for 20 h post infection in the presence of DMSO, 2 μM E64-d, or 5 μM NCC compounds, and scored for infectivity by indirect immunofluorescence using reovirus-specific antiserum (FIG 2.6A, Table 2.S2). Of the 700 compounds in the NCC, 20 increased reovirus infectivity whereas 17 decreased infectivity (FIG 2.6B). Six microtubule-inhibiting compounds impaired reovirus infectivity, corroborating a need for microtubule function in reovirus cell entry (210). The sodium ATPase pump inhibitor digoxin and two serotonin antagonists also impaired reovirus infection, corroborating a role for the sodium ATPase pump and serotonin receptors in reovirus infection (211, 212). Four topoisomerase inhibitors, doxorubicin, epirubicin, etoposide (topoisomerase II inhibitors) and topotecan (topoisomerase I inhibitor), significantly enhanced reovirus infectivity. Topoisomerase inhibitors can sensitize TNBC cells to cell death but it is unknown how they impact reovirus-mediated cell death (213).

Topoisomerase inhibitors enhance reovirus infection of MDA-MB-231 cells without altering viral replication.

To determine if topoisomerase inhibitors affect reovirus infection of TNBC cells, MDA-MB-231 cells were treated with increasing concentrations of doxorubicin, epirubicin, and topotecan for 1 h at 37°C, infected with mock or r2Reovirus at an MOI of 100 PFU/cell, and scored for infectivity by indirect immunofluorescence using reovirus-specific antiserum (FIG 2.7). Reovirus infectivity increased slightly when cells were treated with 0.1 μM and more significantly when treated with 1.0 μM with all three drugs. Treatment of cells with 10 μM doxorubicin or epirubicin decreased infectivity compared to 1.0 μM treatment, likely due to cellular cytotoxicity. In contrast, treatment of cells with 10 μM topotecan enhanced reovirus infectivity more than any other concentration tested. To determine if topoisomerase inhibitors affect reovirus replication in TNBC cells, MDA-MB-231 cells were treated with vehicle (DMSO), 1 μM doxorubicin, epirubicin, or topotecan, adsorbed with mock or r2Reovirus at an MOI of 10 PFU/cell, and assessed for replication over a 3 day time course (FIG 2.8). Treatment of cells with doxorubicin or epirubicin slightly decreased viral titers by day 3 post infection compared to DMSO. Treatment of cells with topotecan slightly affected viral titers at day 0, but replication kinetics were similar to all other conditions at days 1-3, with slightly higher viral yields at day 3.These data indicate that topoisomerase inhibitors augment reovirus infectivity in a concentration-dependent manner while not significantly altering the ability of reovirus to replicate in these cells.

Topoisomerase inhibitors enhance reovirus-mediated cell killing of MDA-MB-231 cells.

To determine if topoisomerase inhibitors confer additive or synergistic effects on reovirus-mediated cytotoxicity, MDA-MB-231 cells were treated with vehicle (DMSO) or increasing concentrations of doxorubicin, epirubicin, or topotecan for 1 h at 37°C, infected with r2Reovirus at an MOI of 200 PFU/cell, and assessed for cell viability over 3 days (FIG 2.9). Treatment with

0.1 μM of all three drugs did not significantly impact cell viability in the presence or absence of r2Reovirus. In the absence of virus, 1.0 μM doxorubicin and epirubicin impaired cell viability to similar levels as virus alone. Addition of reovirus moderately enhanced cytotoxicity compared to either agent alone. These effects can be especially observed at day 3 post infection (FIG 2.9B). Treatment with 10 μM doxorubicin or epirubicin had significant cytotoxic properties in the absence of reovirus. In contrast, 1.0 μM topotecan had significantly diminished cell viability in the absence of reovirus, and addition of reovirus conferred an additive effect on the cytotoxic effects of both topotecan and reovirus. A synergistic cytotoxic effect was observed when reovirus was combined with 10 μM topotecan compared to either agent alone. Together, these data indicate that the combination of topoisomerase inhibitors with reovirus, especially topotecan, enhances the cytopathic properties of drugs and virus in a TNBC cell line.

Activation of DNA damage repair and innate immune signaling pathways following reovirus infection with topoisomerase inhibitors.

Reovirus infection activates innate immune signaling that results in the production of interferon (IFN) (214, 215). Topoisomerase inhibitors, but not reovirus, induce DNA damage repair pathways and can induce innate immune signaling (216). To determine if reovirus infection of TNBC cells impacts DNA damage repair and innate immune pathways, MDA-MB-231 cells were treated with DMSO, doxorubicin, epirubicin, or topotecan for 1 h at 37°C, infected with mock or r2Reovirus, whole cell lysates were collected at 0, 1, and 2 days post infection, and immunoblotted for phosphorylated and total STAT1, STAT2, STAT3, ATM, and p53 (FIG 2.10A). Reovirus infection in the presence of topotecan resulted in increased levels of phosphorylated STAT1 and STAT2 at day 1 post infection (FIG 2.10B). Total levels of STAT1

and STAT2 were slightly elevated in cells treated with doxorubicin, epirubicin, and topotecan compared to DMSO. STAT3 is constitutively activated in 40% of breast cancers and is associated with epithelial to mesenchymal transition (217, 218). Phosphorylated STAT3 was detected in the absence of reovirus regardless of the presence of topoisomerase inhibitors. Infection resulted in decreased levels of phosphorylated STAT3 at 1 and 2 dpi also independent of doxorubicin, epirubicin, or topotecan. These data indicate that reovirus infection of MDA-MB-231 cells promotes activation of innate immune pathways and that infection in the presence of topotecan, but not doxorubicin or epirubicin, enhances the activation of both STAT1 and STAT2. Reovirus infection also dampens the activation of STAT3 independent of topoisomerase inhibitors.

Reovirus infection in the absence of topoisomerase inhibitors slightly affected phosphorylated and total levels of ATM and p53, with phosphorylated ATM levels trending upwards over the times tested (FIG 2.10C). Treatment of cells with topoisomerase inhibitors in the absence of reovirus increased levels of phosphorylated ATM and p53 compared to DMSO-treated cells at all time points tested. The activation of ATM and p53 by topoisomerase inhibitors was not affected by the presence of reovirus. These data suggest that reovirus does not affect the activation of DNA damage signaling activated by topoisomerase inhibitors.

Reovirus infection of TNBC cells results in increased levels of Type III interferon.

To assess if the increased levels of phosphorylated STAT1 and STAT2 correlate with IFN production during reovirus infection, MDA-MB-231 cells were treated with DMSO, doxorubicin, epirubicin, or topotecan for 1 h at 37°C, infected with r2Reovirus at an MOI of 100 PFU/cell, and RNA and supernatants were collected at 0, 8, 12, 24, and 48 h post infection (FIG 2.11). Reovirus mRNA levels were largely unaffected by the presence or absence of topoisomerase inhibitors up

to 12 h post infection and slightly increased in doxorubicin and epirubicin at 24 and 48 h post infection compared to DMSO and topotecan (FIG 2.11A), confirming that topoisomerase inhibitors do not significantly affect reovirus replication. Despite robust infection, negligible levels of *IFNB1* mRNA were observed in the presence or absence topoisomerase inhibitors (FIG 2.11B). In contrast, significant levels of *IFNL1* mRNA were observed starting at 8 h post infection and up to 48 h post infection in infected cells (FIG 2.11C). Also, in infected cells *IFNL1* mRNA levels were higher in DMSO- and topotecan-treated cells at 8 and 12 h post infection than in doxorubicin- and epirubicin-treated cells, with the latter peaking at 24 h post infection. Interestingly, robust levels of *IFNL1* mRNA were observed at 24 h and 48 h in uninfected cells treated with doxorubicin and epirubicin. To determine if increasing levels of *IFNL1* mRNA result in increasing levels of protein, IFNλ levels were assessed by ELISA (FIG 2.11D). Secreted IFNλ was detected only in infected cells, except for low levels at 48 h in uninfected cells. IFNλ was first observed at 12 h post infection only in epirubicin-treated cells. By 24 h post infection, IFNλ was observed at similar levels in cells treated with DMSO, doxorubicin, and topotecan, but not epirubicin. At 48 h post infection, high levels of IFNλ were observed in all infected conditions, with the highest levels observed in topotecan-treated cells. These data further support that topoisomerase inhibitors do not affect overall reovirus replication kinetics and that reovirus infection of MDA-MB-231 cells results in increased levels of Type III, but not Type I, IFN mRNA and protein. Although topoisomerase inhibitors had a modest effect in the induction of *IFNL1* mRNA following reovirus infection, the presence of topotecan had the largest effect on the levels of secreted IFNλ.

Type III IFNs do not affect cell viability of TNBC cells.

Infection of MDA-MB-231 cells results in the production of Type III IFN. To determine if Type I or Type III IFNs impact cell viability of TNBC cells, MDA-MB-231 cells were treated with DMSO, increasing amounts of recombinant human IFNλ or IFNβ, or 1 μM doxorubicin, or infected with r2Reovirus at an MOI of 100 PFU/cell, and assessed for cell viability over 3 days (FIG 2.12A). Treatment of cells with IFNλ did not affect cell viability. In contrast, treatment of cells with IFNβ decreased cell viability in a dose-dependent manner, with cell viability levels reaching those see during reovirus infection with the highest dose tested. To determine if MDA-MB-231 cells can sense Type I and Type III IFNs, cells were untreated or treated with increasing amounts of IFNλ or IFNβ, and assessed for the activation status of STAT1 and STAT2 after 1 h (FIG 2.12B). Compared to untreated cells, phosphorylated STAT1 and STAT2 were observed following treatment with both IFNλ or IFNβ, suggesting that MDA-MB-231 cells can respond to Type I and Type III IFNs. These data suggest that while infection of MDA-MB-231 cells results in robust production of Type III IFN, the cytotoxic effects of reovirus infection are not directly due to antiproliferative effects of the IFNλ produced by these TNBC cells.

DISCUSSION

Reovirus has an inherent preference to replicate in tumor cells, making it ideally suited for use in oncolytic therapy (189, 190). Reovirus can be delivered to patients via intratumoral and intravenous administration and can be effective in combination therapy (188). A Type 3 reovirus (T3C$) is currently in Phase I-II clinical trials against a variety of cancers in combination with several drugs (clinicaltrials.gov: NCT01622543, NCT01656538). In this study, we generated novel reassortant reoviruses with enhanced replicative properties in TNBC cells by coinfection of a TNBC cell line with prototype strains T1L, T2J, and T3D and serial passage. Reassortant reoviruses attach to cells with similar efficiency as T1L, whereas Type 3 reoviruses attach with enhanced efficacy. T1L uses GM2 glycans to attach to cells whereas T3D interacts with α2,3-linked sialic acid (104, 106). High expression of α2,3-sialic acid in breast cancer is associated with greater metastatic potential (219), suggesting the slight enhancement in attachment observed with Type 3 reoviruses could be due to high levels of α2,3-sialic acid present on the surface of MDA-MB-231 cells.

Reassortant viruses did not have mutations in σ1 and the most predominant viruses following serial passaging all had a Type 1 σ1. These data suggest that carbohydrate binding did not drive selection of the reassortant viruses. JAM-A is expressed in normal mammary epithelial cells and high JAM-A expression in breast cancer patients correlates with worse survival and increased recurrence (220, 221). MDA-MB-231 cells express JAM-A (221), although relatively low JAM-A levels may be responsible for the lower infectivity observed by all reoviruses tested in comparison to infection in L929 cells. These data suggest that receptor engagement is not responsible for the enhanced infectivity observed with the reassortant viruses.

During cell entry, reovirus traverses to endosomes where cathepsin proteases cleave outer capsid protein σ3, forming an infectious subvirion particle (ISVP) (114, 207). Both reassortants

have a nonsynonymous mutation in the σ3-encoding S4 gene segment that results in a V49I substitution. This mutation has not been identified to impact reovirus disassembly kinetics, but it is possible it could expedite viral cell entry kinetics. However, reassortant viruses were equally sensitive to E64-d treatment as parental viruses. Although reassortant viruses infected MDA-MB-231 cells more efficiently than T1L, T3D, and T3C$, replication kinetics of the reassortant viruses were similar except for T3D, which had slower replication kinetics. These data indicate that Type 1 reoviruses replicate with enhanced kinetics compared to T3D, but that genetic differences between T3D and T3C$ are sufficient to allow T3C$ to replicate as efficiently as Type 1 viruses. These data also suggest that the enhanced cytotoxic properties of the reassortant viruses over parental viruses are not due to enhanced replication kinetics in MDA-MB-231 cells.

The reovirus L3, S2, and S3 gene segments have distinct roles in reovirus replication. The L3-encoded λ1 protein is a major inner-capsid protein that has phosphohydrolase activity and participates in viral transcription (122, 222). The S2-encoded σ2 protein is essential for the assembly of viral cores (223). The S3-encoded nonstructural protein σNS is required for viral factory formation (224). The similarity in replication efficiency observed between T1L and the reassortant viruses suggests the A160T mutation in L3 and I250V mutation in S3 (found in both reassortants) and the P161T in S3 (in r1Reovirus only) do not impact overall replication efficiency. However, it is possible that point mutations in these gene segments in the reassortant viruses impact the activity of the viral proteins that result in enhanced infectivity or cytotoxicity in the context of TNBC cells. Further characterization of the point mutations found in the reassortant viruses will help elucidate their impact on viral fitness.

Of all the viruses tested in MDA-MB-231 cells, r1Reovirus and r2Reovirus impaired cell viability with the fastest kinetics, and only T3D was severely deficient in killing these cells. The

poor induction of cell death by T3D may be related to its dampened replication in these cells. Differences in the induction of apoptosis by reovirus strains segregate with the M2 and S1 gene segments (203). Apoptosis is activated by fragments of the M2-encoded μ1 protein generated during reovirus cell entry (198, 202, 203, 225, 226). The μ1 protein impacts reovirus infectivity by enhancing reovirus attachment to cells (227). S1 is genetically linked to reovirus induction of apoptosis through the activities of both σ1 and σ1s, although it is unclear if the effects of σ1s on the induction of cell death are independent of its ability to regulate viral protein synthesis and induce cell cycle arrest (228, 229). We did not observe significant levels of cell cycle arrest in MDA-MB-231 cells infected with reassortant reoviruses (data not shown). It is unclear if the enhanced cytopathic properties of reassortant viruses in the context of TNBC cells maps to the T3D M2 gene segment, the various nonsynonymous changes, or a combination of both.

Screening small molecules from the NIH Clinical Collection identified 20 molecules that increase infectivity and 17 molecules that decreased infectivity in MDA-MB-231 cells. Six microtubule-inhibiting drugs, digoxin, and two serotonin antagonists affected reovirus infectivity, corroborating the role of microtubules, the sodium-potassium ATPase pump, and serotonin receptors in reovirus infection (210-212). Of the 17 molecules that enhanced infectivity, 4 are topoisomerase I (topotecan) or II (doxorubicin, epirubicin, and etoposide) inhibitors. Treatment of cells with topoisomerase inhibitors resulted in increased infectivity, with no effect on virus attachment (data not shown) or viral replication, except for slight increases in viral RNA at 24 and 48 h post infection. Topoisomerase inhibitors promote DNA double-strand breaks leading to cell death (230-233). Reovirus infection does not induce DNA double-strand breaks and promotes cell death through the induction of extrinsic and intrinsic apoptosis or necroptosis (193, 194, 198, 203, 234, 235). It is possible that topoisomerase inhibitors positively affect uptake of viral particles

during cell entry that results in enhanced infectivity and that doxorubicin and epirubicin further impact a step late in the viral life cycle that results in enhanced transcription of viral RNA. It is also possible that the additive cytotoxicity observed in MDA-MB-231 cells when both reovirus and topoisomerase inhibitors are present is through the activation of complementary cell death pathways.

Reovirus infection does not impair the DNA double strand break response activated by treatment with topoisomerase inhibitors. Late during infection in the presence of topoisomerase inhibitors, levels of phosphorylated and total p53 were lower than in uninfected cells. It remains to be determined if the effects of reovirus infection on p53 are at the transcriptional, translational, or post-translational level. Reovirus infection can induce higher levels of activated MDM2, which leads to p53 degradation (236). In the context of reovirus infection, it is possible that topoisomerase inhibitors promote p53 stabilization through impairing the activation of MDM2 by the virus. It is also possible the effects on total p53 at late times post infection are due to viral-dependent host translational shutoff. In support of this, total levels of STAT1, STAT2, STAT3, and ATM were also lower at late times of infection.

Reovirus infection of MDA-MB-231 cells resulted in robust expression of Type III, but not Type I, IFN mRNA and protein. Infection in the presence of topoisomerase inhibitors did not significantly affect levels of *IFNL1* mRNA. Interestingly, doxorubicin and epirubicin treatment in the absence of infection results in the induction of *IFNL1* mRNA starting at 24 h reaching similar levels to those detected in virus-infected cells by 48 h. Induction of DNA double strand breaks by topoisomerase inhibitors can result in p53-dependent regulation of Type I IFN through a STING-dependent but cGAS-independent pathway (216). MDA-MB-231 cells express STING (data not shown), suggesting that topoisomerase inhibitors could be inducing transcription of Type III IFN

downstream of the induction of the DNA damage response through a similar mechanism. However, topoisomerase inhibitors did not induce Type I IFN transcription in the presence or absence of reovirus.

Levels of IFNλ were first observed at 12-24 h post infection in the presence or absence of topoisomerase inhibitors, with the highest levels of IFNλ detected at 48 h post infection in the presence of topotecan. IFNλ1, IFNλ2, and IFNλ3 are expressed in breast cancer cells, although their role in mediating innate immunity in these cells is not well characterized (237). Type I and Type III IFN are transcriptionally regulated by the transcription factor IRF3 (238, 239). Reovirus can antagonize IFN production by sequestering IRF3 to viral inclusions (240) and infection of gut epithelial cells *in vitro* and *in vivo* results in upregulated levels of IFNλ mRNA (240-242). It is possible that in MDA-MB-231 cells reovirus is unable to sequester IRF3 to viral inclusions, resulting in robust production of Type III IFN. Reovirus infection of TNBC cells resulted in high levels of secreted IFNλ, with over 200 pg/ml detected at 48 h post infection in the presence or absence of topoisomerase inhibitors. Levels of IFNλ in the presence of topotecan at 48 h post infection reached over 800 pg/ml, levels that are higher than that observed in dendritic cells that have been exposed to a RIG-I agonist (243). It is unclear why topotecan, but not doxorubicin or epirubicin result in significantly higher IFNλ levels, especially considering that *IFNL1* mRNA levels were not different in infected cells in the presence of the different topoisomerase inhibitors. Interestingly, in the absence of reovirus, IFNλ had no effect on MDA-MB-231 cell viability, while IFNβ decreased cell viability in a concentration dependent manner. However, MDA-MB-231 cells responded to Type I and Type III IFN treatment, indicating these cells have functional receptors to detect and activate signaling pathways downstream of ligand engagement. MDA-MB-231 cells can express low basal levels and are responsive to Type I IFNs (244-246). The large levels of Type

III IFN detected in MDA-MB-231 cells, and lack of Type I IFN, indicates that STAT activation observed in these cells is likely in response to the interaction of IFNλ with its receptors.

Despite the robust induction of Type III IFN in response to infection, robust levels of activated STAT1 and STAT2 were only detected in the presence of topotecan. Low levels of activated STAT1 were observed in infected cells in the absence of topoisomerase inhibitors, but no STAT activation was observed in the presence of doxorubicin or epirubicin. It is possible that the low levels of activated STAT1 and STAT2 in infected MDA-MB-231 cells are a result of impaired sensing of IFNλ due to low level expression of the IFNλ receptor. It is also possible that treatment of cells with topotecan may sensitize cells to IFNλ through the upregulation of the IFNλ receptor. Surprisingly, despite high levels of activated STAT1 and STAT2 following reovirus infection of topotecan-treated cells, reovirus infectivity and replication remained unimpaired.

In this study, we generated reoviruses with unique infective and cytotoxic properties by forward genetics following coinfection with three different serotype reoviruses. The novel genetic composition of the reassortant viruses could inform future studies on viral factors that promote infection and killing of cells by reovirus. Through high-throughput screening we identified topoisomerase inhibitors as a class of drug that enhances infection and the cytotoxic properties of reovirus in the context of TNBC. We also show that infection of a breast cancer cell line leads to the robust production of Type III, but not Type I, IFN. This study presents evidence for the pairing of reassortant reoviruses generated by forward genetics with topoisomerase inhibitors identified by high-throughput screening as a promising therapeutic against TNBC.

MATERIALS AND METHODS

Cells, viruses, and antibodies

MDA-MB-231 cells (gift from Jennifer Pietenpol, Vanderbilt University) and MDA-MB-436 cells (ATCC HTB-130) were grown in Dulbecco's Modified Eagle's Medium (DMEM) supplemented with 10% fetal bovine serum (FBS) (Life Technologies), 100 U per ml penicillin and streptomycin (Life Technologies). Spinner-adapted L929 cells (Terry Dermody, University of Pittsburgh) were grown in Joklik's modified MEM with 5% FBS, 2 mM L- glutamine (Life Technologies), penicillin and streptomycin, and 0.25 mg per ml amphotericin B (Life Technologies).

Reovirus strains Type 1 Lang (T1L) and Type 3 Dearing (T3D) working stocks were prepared following rescue with reovirus cDNAs in BHK-T7 cells (gift from Terry Dermody, University of Pittsburgh), followed by plaque purification, and passage in L929 cells (247). Reovirus type 2 Jones (T2J) is a laboratory strain and Type 3 Cashdollar (T3C$) is a distinct Type 3 reovirus (248). Purified virions were prepared using second-passage L929 cell lysate stocks. Virus was purified from infected cell lysates by Vertrel XF (TMC Industries Inc.) extraction and CsCl gradient centrifugation as described (249). The band corresponding to the density of reovirus particles (1.36 g/cm^3) was collected and dialyzed exhaustively against virion storage buffer (150 mM NaCl, 15 mM MgCl2, 10 mM Tris-HCl [pH 7.4]). Reovirus particle concentration was determined from the equivalence of 1 unit of optical density at 260 nm to 2.1×10^{12} particles (250). Viral titers were determined by plaque assay using L929 cells (251). Reovirus virions were labeled with succinimidyl ester Alexa Fluor 488 (A488) (Life Technologies) as described (117, 210).

Reovirus polyclonal rabbit antiserum raised against reovirus strains T1L and T3D was purified as described (252) and cross-adsorbed for MDA-MB-231 cells. Secondary IRDye 680 and

800 antibodies (LI-COR Biosciences) and goat anti-rabbit Alexa Fluor 488 (A488) (Life Technologies).

Serial passage of T1L, T2J, and T3D in MDA-MB-231 cells

MDA-MB-231 cells were adsorbed with T1L, T2J, and T3D at a multiplicity of infection (MOI) of 1 PFU/cell for 1 h at room temperature and incubated for 48 h at 37°C in MDA-MB-231 cell media. Cells were freeze-thawed three times, fresh MDA-MB-231 cells were infected with 500 μl of freeze-thawed cell supernatant, and incubated for 48 h at 37°C. Serial passage was repeated 20 times and individual viral titers were obtained by plaque isolation following plaque assay in L929 cells.

Electrophoretic mobility of reovirus

5×10^{10} particles of purified reovirus or freeze-thawed supernatants containing reovirus mixed with 2X SDS-Sample Buffer (20% Glycerol, 100 mM Tris-HCl [pH 6.8], 0.4% SDS, and 3 mg Bromophenol Blue) were separated by SDS-PAGE using 4-20% gradient polyacrylamide gels (Bio-Rad Laboratories) at 10 mAmps for 16 h. The gel was stained with 5 μg/ml ethidium bromide for 20 min and imaged using a Chemidoc XRS+ (Bio-Rad).

Next Generation Sequencing of Reovirus

RNA from viral preparations of T1L, T2J, T3D, r1Reovirus, and r2Reovirus were obtained using an RNeasy RNA purification kit (Qiagen). Ten nanograms of viral RNA was used as input for cDNA synthesis using the Clontech SMARTer Stranded Total RNA-Seq Kit v2 (Pico Input, Mammalian) according to the manufacturer's instructions. Libraries were validated by capillary

electrophoresis on an Agilent 4200 TapeStation, pooled, and sequenced on an Illumina HiSeq3000 with 100bp paired end reads averaging 13 million reads/sample, yielding an average depth of coverage > 1000 reads. Reads were trimmed of adapter sequence using Trimmomatic (version 0.36, http://www.usadellab.org/cms/?page=trimmomatic) using the TruSeq3-PE-2 paired end adapter reference. Trimmed reads from each sample were aligned to all of the parental strain reference sequences using the Burrows-Wheeler Aligner (BWA version 0.7.10-r789, http://bio-bwa.sourceforge.net/). Deduplication was performed with Picard tools (version 1.74(1243), https://broadinstitute.github.io/picard/), and variation was called, again for each sample against all the parental strain references, using the GATK pipeline's (version 3.4, https://software.broadinstitute.org/gatk/) HaplotypeCaller with ploidy set to 1 and other default parameters. The resultant Variant Call Files (.vcf) were examined for sample similarity/variation from the parental reference strains.

Flow cytometric analysis of cell-surface reovirus

MDA-MB-231 cells were adsorbed with 5×10^3-5×10^4 particles per cell of A633-labeled virus for 1 h at room temperature. Cells were washed with PBS, detached with Cellstripper (Cellgro) for 10 min at 37°C, quenched and washed with PBS containing 2% FBS. Cells were fixed in 1% EM-grade paraformaldehyde (Electron Microscopy Sciences). Mean fluorescence intensity (MFI) was assessed using a CytoFLEX flow cytometer (Beckman Coulter) and quantified using FlowJo software.

Reovirus infectivity assay

Reovirus infectivity was assessed by indirect immunofluorescence (253). MDA-MB-231 and L929 cells were adsorbed with reovirus at a range of MOIs for 1 h at room temperature, washed with PBS, and incubated in media for 16-24 h at 37°C. To assess the effects of topoisomerase inhibitors on reovirus infectivity, cells were pretreated with topoisomerase inhibitors or E64-d for 1 h at 37°C, reovirus was added to cells, and incubated for 18-24 h at 37°C. Cells were fixed with ice-cold methanol and stored at -20°C for at least 30 min. Methanol was removed, cells were washed twice with PBS, and blocked with PBS containing 1% BSA for 15 min at room temperature. Cells were stained with reovirus-specific polyclonal antiserum (1:2000) for 1 h at room temperature, washed twice with PBS, stained with goat anti-rabbit Alexa 488 (1:1000) for 1 h at room temperature, counterstained with 0.5 ng/ml DAPI for 5 min at room temperature, and washed twice with PBS. Immunofluorescence was detected using a Lionheart FX Automated Microscope (Biotek) with a 4x-PLFL phase objective (NA 0.13), and percent infectivity was determined (reovirus positive cells/DAPI positive cells) using Gen5 software (Biotek).

Reovirus replication assay

MDA-MB-231 cells were adsorbed with reovirus at a MOI of 10 PFU/cell for 1 h at room temperature, washed with PBS, and incubated for 0-3 days in MDA-MB-231 media at 37°C. To determine the effects of topoisomerase inhibitors on reovirus replication, MDA-MB-231 cells were treated with vehicle or topoisomerase inhibitors for 1 h at 37°C, media was removed, cells were adsorbed with reovirus at an MOI of 10 PFU/cell for 1 h at room temperature, washed with PBS, and incubated for 0-3 days with complete media containing vehicle or topoisomerase inhibitors at 37°C. Cells were freeze-thawed three times and viral titers were determined by plaque

assay using L929 cells. Viral yields were calculated by dividing viral titers by the viral titer from day 0.

Cell viability assay

Cell viability was assessed by measuring metabolic activity using Presto Blue reagent (Invitrogen). L929, MDA-MB-231, and MDA-MB-436 cells were adsorbed with reovirus at a range of MOIs for 1 h at room temperature or treated with 1 μM staurosporine, washed with PBS, and incubated for 0-7 days at 37°C. To determine the effects of topoisomerase inhibitors on cell viability, cells were pretreated with increasing concentrations of topoisomerase inhibitors for 1 h at 37°C, reovirus was added to cells, and incubated in the presence of the inhibitors for 0-3 days. To determine the effect of recombinant IFNs on cell viability, MDA-MB-231 cells were treated with 10-5000 IU/ml human IFNβ (Peprotech) or 10-1000 ng/ml IFNλ (Peprotech), 1 μM doxorubicin, or infected with reovirus at an MOI of 100 PFU/cell and assessed for cell viability for 0-3 days. Presto Blue was added at each time point for 30 min at 37°C and fluorescence (540 nm excitation/590 nm emission) was measured with a Synergy HT plate reader (Biotek).

Screening of NIH Clinical Collection Small Molecule Inhibitors

The NIH Clinical Collection was obtained from the NIH Roadmap Molecular Libraries Screening Centers Network. MDA-MB-231 cells were treated with DMSO, 4 μM E64-d, or 10 μM of compounds from the NIH Clinical Collection for 1 h at 37°C. Media (mock) or reovirus was added to cells at an MOI of 20 PFU/cell, and incubated for 20 h at 37°C. Cells were fixed and scored for infectivity by indirect immunofluorescence as described previously. Z scores for each well were calculated using the following formula: Z score = (a-b)/c, where a is the percent

infectivity (infected cells/number of cells), b is the median percent infectivity for each plate, and c is the standard deviation of percent infectivity for each plate. Z scores of $-2 > x < 2.0$ were considered significant. Data for all compounds in screen are provided in Table 2.S2.

Immunoblotting for DNA damage response and innate immune molecules

MDA-MB-231 cells were treated with DMSO or 2 μM topoisomerase inhibitors for 1 h at 37°C, infected with mock or reovirus at an MOI of 100 PFU/cell, and incubated for 0-2 days at 37°C. To assess the ability of IFNs to stimulate immune signaling, MDA-MB-231 cells were treated with 10 and 100 ng/ml of IFNλ or 100 and 1000 IU/ml IFNβ for 1 h at 37°C. Whole cell lysates were prepared using RIPA buffer (20 mM Tris-HCl [pH 7.5], 150 mM NaCl, 1 mM EDTA, 1% NP-40, 0.1% sodium dodecyl sulfate, 0.1% sodium deoxycholate) and fresh Protease Inhibitor Cocktail (P8340, Sigma-Aldrich), Phosphatase Inhibitor Cocktail 2 (P5726, Sigma-Aldrich), 1 mM sodium vanadate, and 1 mM phenylmethylsulfonyl fluoride (PMSF) and protein concentration was determined using the DC protein assay (Bio-Rad). Whole cell lysates were resolved by SDS-PAGE in 4-20% gradient Mini-PROTEAN TGX gels (Bio-Rad) and transferred to 0.2 μm pore size nitrocellulose membranes (Bio-Rad). Membranes were incubated for 1 h in blocking buffer (Tris-buffered saline [TBS] with 5% powdered milk), incubated with primary antibodies specific for phospho-STAT1 (Y701, clone D4A7 #7649), -STAT2 (Y690, clone D3P2P, #88410), -STAT3 (Y705, clone D3A7, #9145), -ATM(S1981, clone 10H11.E12, #4526), -p53(S15, #9284), total STAT1 (clone D3A7, #9145), STAT2 (clone D9J7L, #72604), STAT3 (clone 124H6, #9139), ATM (clone D2E2, #2873), p53 (clone 1C12, #2524), and GAPDH (clone GA1R, MA5-15738), and reovirus polyclonal antiserum overnight at 4°C. Antibodies are from Cell Signaling Technology except for GAPDH, ThermoFisher. Membranes were washed with TBS-T (TBS with

0.1% Tween 20) and incubated with secondary antibodies conjugated to IRDye 680 or IRDye 800. Membranes were imaged using a LiCor Odyssey CLx and processed in ImageStudio (LI-COR Biosciences).

qPCR assessment of Type 1 and 3 interferon transcript levels

MDA-MB-231 cells were treated with DMSO or 2 μM topoisomerase inhibitors for 1 h at 37°C, infected with mock or r2Reovirus at an MOI of 100 PFU/cell, and incubated for 0, 8, 12, 24, and 48 h. RNA was isolated using a QIAGEN RNeasy kit with on-column DNase digestion. cDNAs were generated using 500 ng of RNA and random primers with the High-Capacity cDNA Reverse Transcription Kit (ThermoFisher) in a SimpliAmp Thermal Cycler (ThermoFisher). cDNA was diluted 1:5 in nuclease-free water and qPCR reactions were performed in MicroAmp Fast Optical 96-Well Reaction Plates (Applied Biosystems) using PrimeTime qPCR assays (IDT) for *IFNB1*, *IFNL1*, *HPRT1*, and a custom assay for the reovirus S1 gene segment (Probe: 5'-/56-FAM/TCAATGCTG/ZEN/TCGAACCACGAGTTGA/3IABkFQ/-3'; Primer 1: 5'-CGAGTCAGGTCACGCAATTA-3'; Primer 2: 5'-GGATGTTCGTCCAGTGAGATTAG-3') using a 7500 Fast Real-Time PCR System (Applied Biosystems) and accompanying software to analyze qPCR data.

IFNλ ELISA

MDA-MB-231 cells were treated with DMSO or 2 μM topoisomerase inhibitors for 1 h at 37°C, infected with mock or r2Reovirus at an MOI of 100 PFU/cell, and incubated for 0, 8, 12, 24, and 48 h. Cell supernatants were collected and levels of IFNλ were determined with the IFN-

lambda 1/3 DuoSet ELISA kit (R&D Systems). Plates were read on a Synergy HT plate reader (Biotek) using 450 nm for sample detection and 540 nm for wavelength correction.

Statistical analysis

Mean values for quadruplicate experiments were compared using one or two-way analysis of variance (ANOVA) with Dunnett's or Tukey's multiple-comparisons test (Graph Pad Prism). *P* values of < 0.05 were considered statistically significant.

Data Availability

Individual mutations identified in reassortant viruses are listed in Table 2.S1. The read files for this study have been deposited with the NCBI Sequence Read Archive (SRA) and are available via accession PRJNA561538.

ACKNOWLEDGEMENTS

This work was supported by funding from the Children's Healthcare of Atlanta and the Pediatric Research Institute and Winship Comprehensive Cancer Institute #IRG-14-188-01 from the American Cancer Society (B.A.M.). Flow cytometry experiments were performed in the Emory Pediatrics Flow Cytometry Core (UL1TR002378). Imaging was performed at the Emory Integrated Cellular Imaging Core (2P30CA138292-04 and the Emory Pediatrics Institute). The Yerkes NHP Genomics Core is supported in part by NIH P51 OD011132. The funders had no role in the study design, data collection and analysis, decision to publish, or preparation of manuscript.

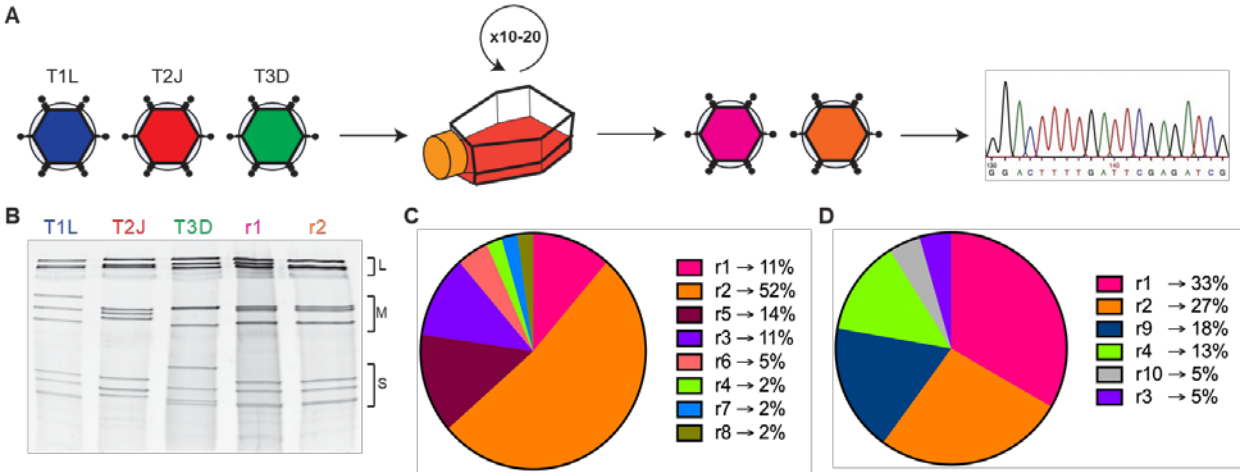

Figure 2.1. Generation of reoviruses by forward genetics in MDA-MB-231 cells.

(A) Triple-negative breast cancer MDA-MB-231 cells were co-infected with T1L, T2J, and T3D and serially passaged ten or twenty times. Virus isolates were obtained following plaque assay on L929 cells and sequenced by Illumina Next-Generation Sequencing. (B) Polyacrylamide gel electrophoresis of reovirus parental strains T1L, T2J, and T3D and r1Reovirus (r1) and r2Reovirus (r2). Strains are differentiated by migration patterns of three large (L), three medium (M), and four small (S) gene segments. (C) Percentage of viral isolates with a specific electropherotype following 10 serial passages in MDA-MB-231 cells (n = 44). r1Reovirus (pink) accounts for 11% of isolates while r2Reovirus (orange) accounts for 52%. (D) Percentage of viral isolates with a specific electropherotype following 20 serial passages in MDA-MB-231 cells (n = 45). r1Reovirus (pink) accounts for 33% of isolates while r2Reovirus (orange) accounts for 27%.

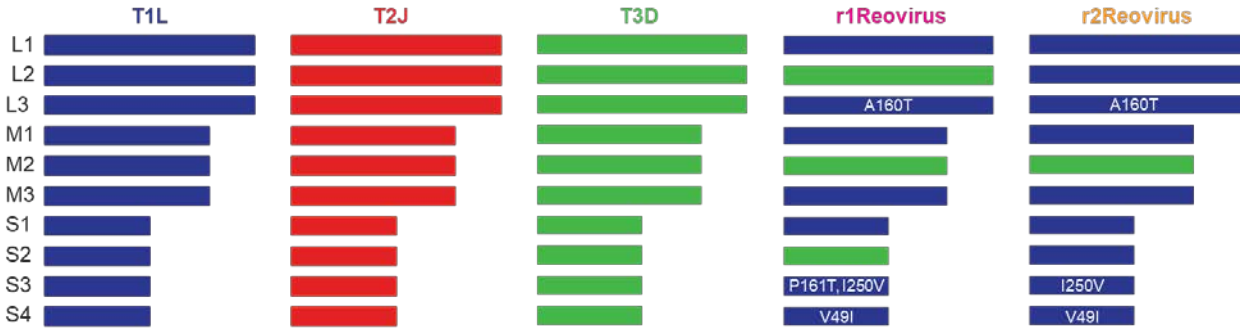

Figure 2.2. Genetic composition of r1Reovirus and r2Reovirus.

The genetic composition of parental and reassortant r1Reovirus and r2Reovirus was determined by Illumina Next-Generation sequencing. r1Reovirus has seven gene segments from T1L and three from T3D (S2, M2, L2) and four nonsynonymous point mutations (L3 A160T, S3 P161T, I250V, and S4 V49I). r2Reovirus has nine gene segments from T1L and one from T3D (M2) and three nonsynonymous point mutations (L3 A160T, S3 I250V, and S4 V49I). Both r1Reovirus and r2Reovirus have several synonymous point mutations.

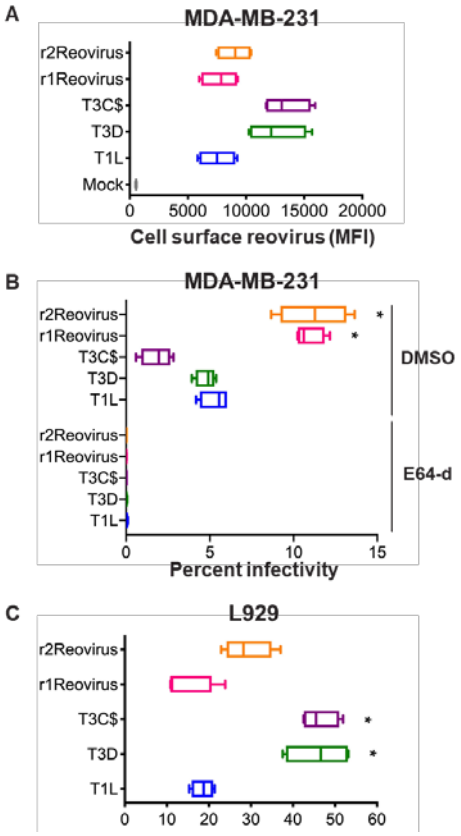

Figure 2.3. Attachment and infectivity of MDA-MB-231 cells by reassortant reoviruses.

(A) MDA-MB-231 cells were adsorbed with A633-labeled T1L, T3D, T3C$, or reassortant reoviruses at an MOI of $5x10^4$ particles/cell and assessed for cell-surface reovirus by flow cytometry. Results are expressed as box and whisker plots of cell surface reovirus mean fluorescence intensity (MFI) for quadruplicate independent experiments. (B) MDA-MB-231 cells were treated with DMSO or 4 μM E64-d and adsorbed with T1L, T3D, T3C$, or reassortant reoviruses at an MOI of 100 PFU/cell and assessed for infectivity after 18 h by indirect immunofluorescence using reovirus-specific antiserum. (C) L929 cells were adsorbed with T1L, T3D, T3C$, or reassortant reoviruses at an MOI of 5 PFU/cell and assessed for infectivity after 18 h by indirect immunofluorescence using reovirus-specific antiserum. Results are expressed as box and whisker plots of percent infectivity for quadruplicate independent experiments. *, $P < 0.0005$ in comparison to T1L by two-way ANOVA with Tukey's multiple comparisons test.

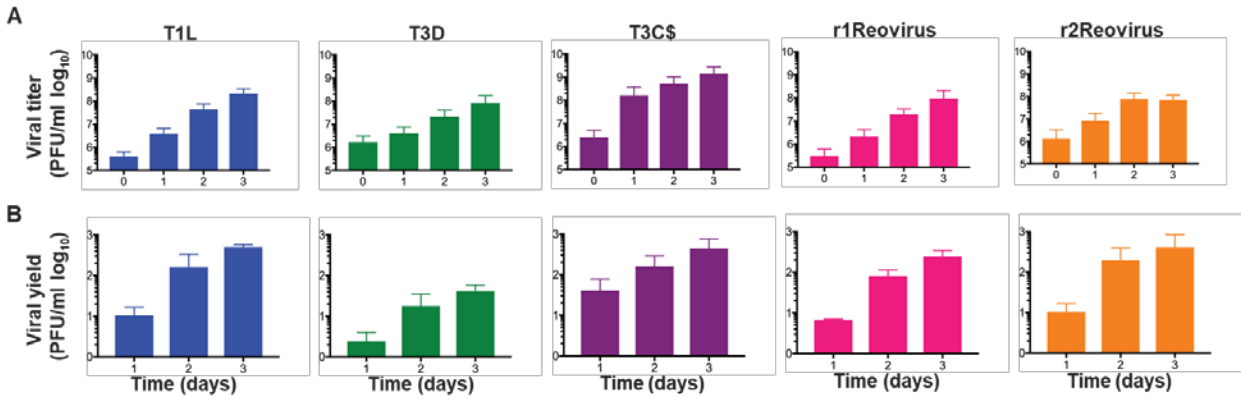

Figure 2.4. Reassortant viruses replicate with similar kinetics than T1L and T3C$, but faster than T3D, in MDA-MB-231 cells.

T1L, T3D, T3C$, r1Reovirus, and r2Reovirus were adsorbed at an MOI of 10 PFU/cell and (A) viral titers and (B) viral yields were determined by plaque assay on L929 cells at 0-3 days post infection. The results are presented as (A) mean viral titers (± SEM) or (B) mean viral yields (± SEM) compared to day 0 post infection.

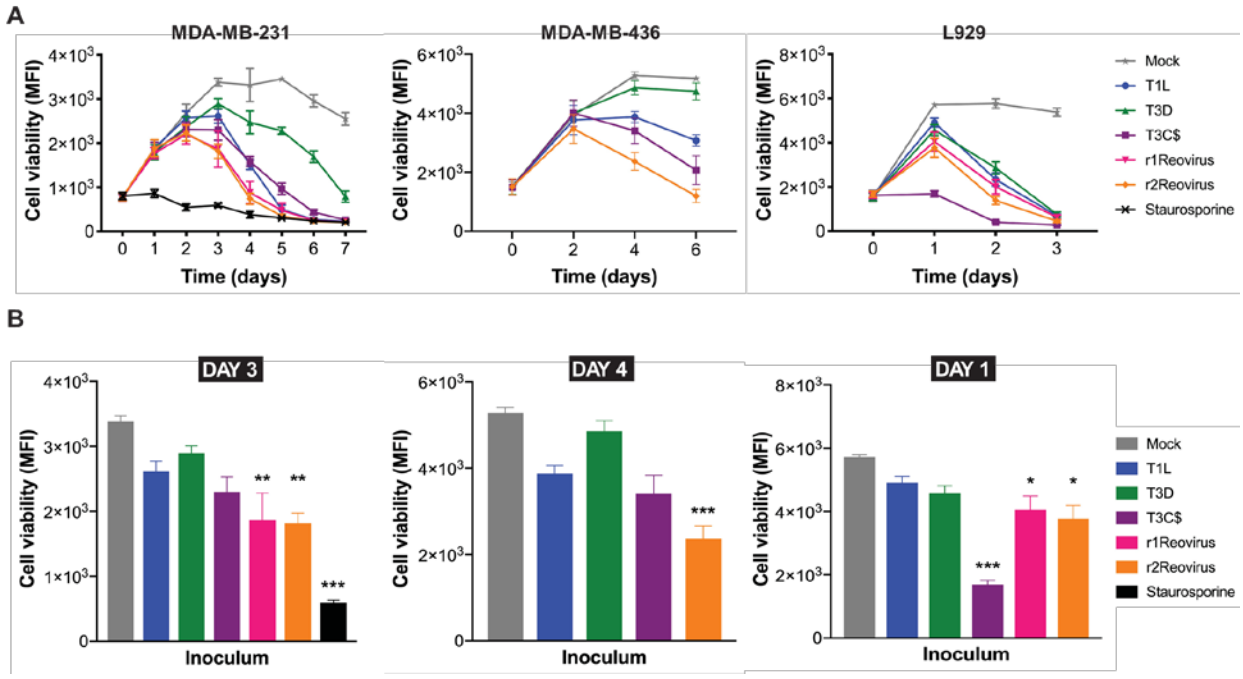

Figure 2.5. Impact on cell viability of TNBC cells and L929 cells following reovirus infection.

(A) MDA-MB-231, (B) MDA-MB-436, and (C) L929 cells were adsorbed with T1L, T3D, T3C$, r1Reovirus, or r2Reovirus at an MOI of 500 PFU/ml or treated with 1 μM staurosporine and cell viability was assessed at times shown. Results are presented as mean fluorescence intensity (MFI) and SEM for four independent experiments. Bottom panel, cell viability for all cell lines in (A-C) for days 3, 4, and 1 post-infection. Error bars represent SEM. *, $P < 0.01$, **, $P \leq 0.001$, ***, $P \leq 0.0001$ in comparison to T1L by two-way ANOVA with Tukey's multiple comparisons test.

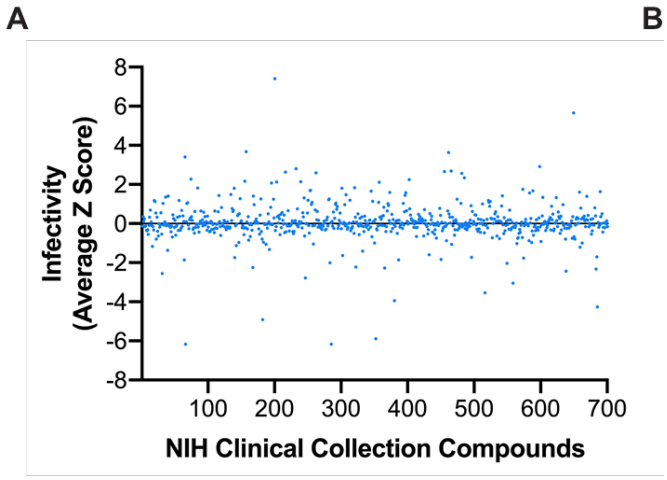

B

I"#$%"&'`)*@+	*-.+/"-.0""+ "!`23/4"&	5%&.6	5%&.7	28+-*.+
!"#`$'%&`(`)+,-.$`(+.`"$`-/	0`1`"`2`3/$4 2/ $6=8$'$	7$9:	:8:.<	7$==
0`1`"8/(4) +,-.$`(+.`"$`-/	0`1`"`2`3/$4 2/ $6=8$'$	>87:	>8><	>8.:;	
!4(6`)`3.(`)	@A	?8><	<8>;	?8;7
B.`C`3.(`) A	A0D42/ >8'$	E8E>	>8F>	?8;?
AG/.428)/ +.-.$`(+.`"$`-/	H`2643`)/ H= I/(/16`"$ A)64C")'26	E89:	?8:>	?8<=
J`3K42646`)	HLMNO"A I/-%(642/	E8>?	?8?=	E88E
P$"1`"2`-/	0`1`"`2`3/$4 2/ $6=8$'$	?8?>	E8E.	E8:=
B)-4)2/6$`)	J/$`"6`)`) ? I/(/16`"$ QHNH0?RA)64C")'26	E877	E8.F	E8;9
@'&./6`)	LLD .%=8$'$	E8>E	?8>9	E8.;
P!'$%&`(`)+,-.$`(+.`"$`-/	0`1`"`2`3/$4 2/ $6=8$'$	?8E<	E8FE	E8.?
S:%)42546)	HLMNO"A I/-%(642/	E8><	E87>	E8.;F
D4 .")`2/6$`) +.-.$`(+.`"$`-/	J/$`"6`)`) ? I/(/16`"$ QHNH0?RA)64C")'26	E879	E877	E8>;
D45"#6`)` 34 ./46/	J/$`"$`)`) 09421`36/$	E8E9	E879	E8?<
T/)1$`1/$`)/ 1+21+46/	O"%C+ J%11$/22`$	E8EE	E8??	E8E7
L/K42646`)	HLMNO"A I/-%(642/	E8>>	E87>	E8E>
O.64546`)	@%(./`2-/ A)4.`C%/	E8FF	E8?<	E8>7
S)"U`&$46/	D.DA I A.1+4	=8:7	E8>=	E8><
!$"1/$`-"`	!"143`)/ NE I/(/16`"$ A)64C")'26	E87;	=8<9	E8>?
VK42546)	HLMNO"A I/-%(642/	=87;	E8<;	E8>=
!")/1/G`.+.-.$`(+.`"$`-/	A(/6.,(+`.`)/26/$42/ `)+'&/6`$	E8>>	E8FF	E8F7

I"#$%"&'`)*@+	*-.+/"-.0""+ "!`23/4"&	5%&.6	5%&.7	28+-*.+
AG/&$'3.(`)	>FJ W7FJ I`&`2"3/2	N:8=9	N8>=	N8=7
H`3"+4$$`)C6`")`/	:F J I`&`2"3/ J%&%)6	N>8:<	N8=F	N=8=7
V"`1/$43`-/ +.-.$`(+.`"$`-/	B1"-N$(/16`$ AC")'26	N>8<9	N87F	N=8>9
!"C"#`)	@4 X A0D42/ DN31	N>8<9	N=$7;	N=$E
Y`)"$/. &`)/ 8$$$49	L'($'6%&%./2	N78:;	N<$:;	N<$E
L/$(416"1%$)/	D%$')/L/64&`.'23 9=8$'$	N7899	N78:9	N7$9<
D`-`U`.'#	L'($'6%&%./2	N78<>	N78;E	N78><
I4 .'#`U`)/ +.-.$`(+.`"$`-/	P26$'C/)1/(/16`$ AC")'26	NE87F	N78=#	N79F>
S.%&)-4G`./	L'($'6%&%./2	N78>?	NE$F7	NE$7
A.&/)-4G`./	L'($'6%&%./2	NE8<;	NE8;<	NE$>
0+`"6+`#`)/	!"143`)/ A)64C")'26	NE8=;	NE$7	NE$<
Y`)($'26`)/ 2%.U45/	L'($'6%&%./2	NE87;	NE$=	NE$7
L/&/)-4G`./	L'($'6%&%./2	NE877	N=$7.	NE$E7
!/2.`"$464-`)/	H`2643`)/H= I/(/16`"$	N=8:7	NE$;F	NE$E<
5654(`)4G`./	S%)C4. D<>F	NE8:>	N=$=9	NE$EE
D.$`3/6+43`)/	$`.`(A(`- A)64C")'26	NE8==	N=$9>	NE$F7
H:#4(+.`"$`+-/)/	M%64546`) `/+,-.$`C/)42/	NE8E=	N=$E	NE$F<

Figure 2.6. Screening of NIH Clinical Collection small molecules for reovirus infectivity. MDA-MB-231 cells were treated with vehicle (DMSO), 4 μM E64-d, or 10 μM compounds from the NIH Clinical collection for 1 h, infected with r2Reovirus at an MOI of 20 PFU/cell in the presence of DMSO, 2 μM E64-d, or 5 μM compounds from the NIH Clinical collection for 20 h. Cells were scored for infectivity by indirect immunofluorescence using reovirus-specific antisera. (A) Data are shown as infectivity from average Z-scores for compounds in the NIH Clinical Collection for duplicate experiments. (B) Compounds from the NIH Clinical Collection that increase (green, top table) or decrease (red, bottom table) infectivity by 2 Z-scores or more. Data are shown for each experimental replicate (Run).

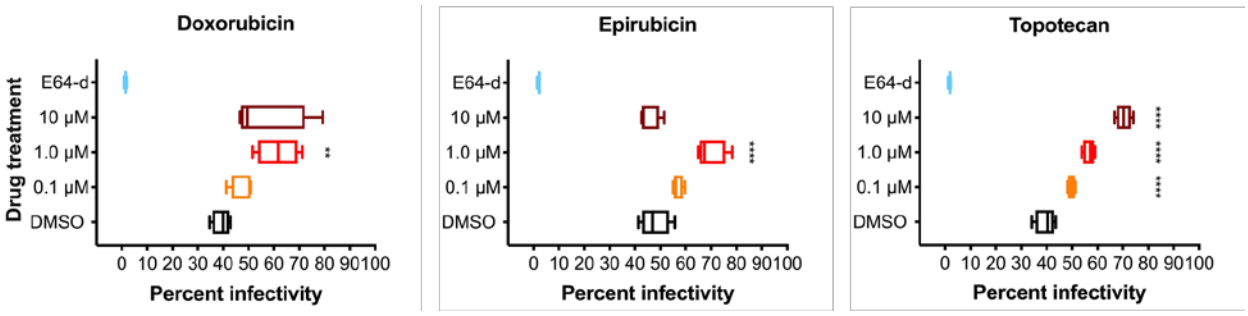

Figure 2.7. Topoisomerase inhibitors enhance reovirus infection of TNBC cells.

MDA-MB-231 cells were treated for 1 h with vehicle (DMSO), 8 μM E64-d, or increasing concentrations doxorubicin, epirubicin, or topotecan and infected with r2Reovirus at an MOI of 100 PFU/cell for 20 h. Cells were assessed for infectivity by indirect immunofluorescence using reovirus-specific antisera. Data are shown as percent infectivity for quadruplicate independent experiments. **, $P \leq 0.01$, ***, $P < 0.001$, ****, $P < 0.0001$ in comparison to DMSO by one-way ANOVA with Dunnett's multiple comparisons test.

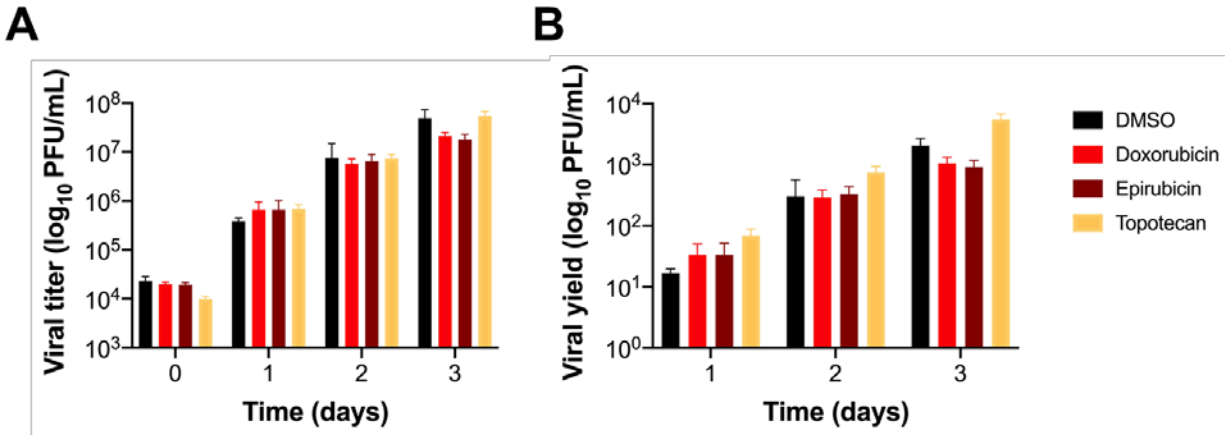

Figure 2.8. Topoisomerase inhibitor drugs do not impair r2Reovirus replication in MDA-MB-231 cells.

MDA-MB-231 cells were treated with vehicle (DMSO), 1 μM topoisomerase inhibitors, adsorbed with r2Reovirus at an MOI of 10 PFU/cell, and assessed for viral replication by plaque assay on L929 cells at days 0-3 post infection. Results are presented as (A) mean viral titers (±SEM) and (B) mean viral yields (±SEM) from day 0.

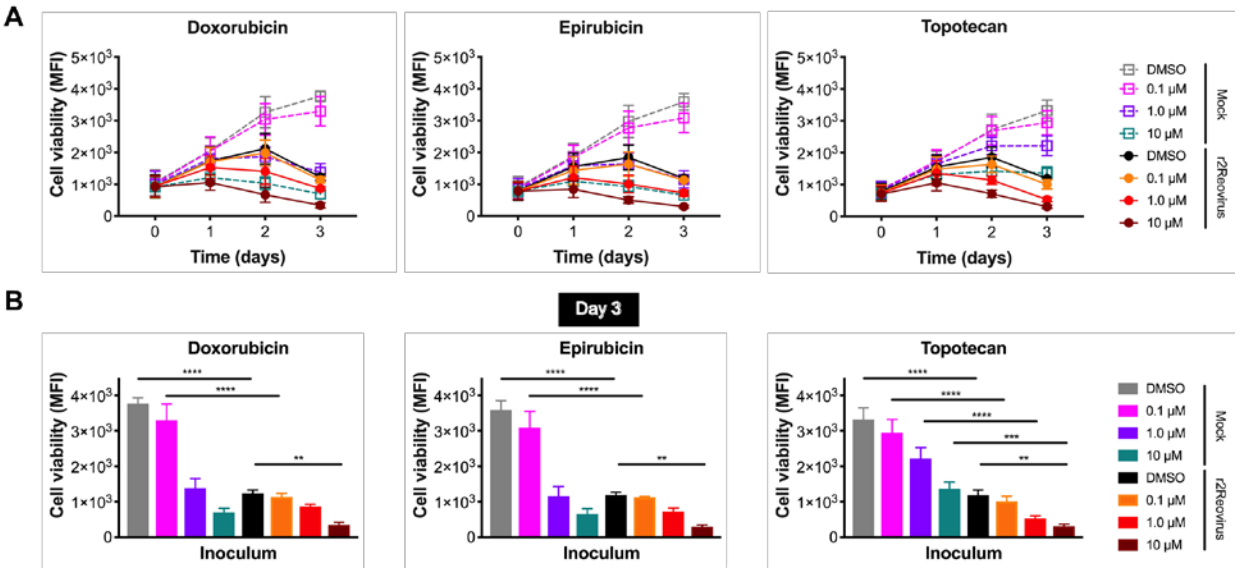

Figure 2.9. Cell viability of MDA-MB-231 cells is impaired by reovirus and topoisomerase inhibitors.

(A) MDA-MB-231 cells were treated with vehicle (DMSO) or increasing concentrations of doxorubicin, epirubicin, or topotecan for 1 h, infected with r2Reovirus at an MOI of 200 PFU/cell, and assessed for cell viability at days 0-3 post infection. Data are shown as mean fluorescence intensity (MFI) for quadruplicate independent experiments. (B) Cell viability for all conditions in (A) for day 3 post infection. Error bars represent SEM. **, $P < 0.01$, ***, $P < 0.001$ by one-way ANOVA with Tukey's multiple comparisons test.

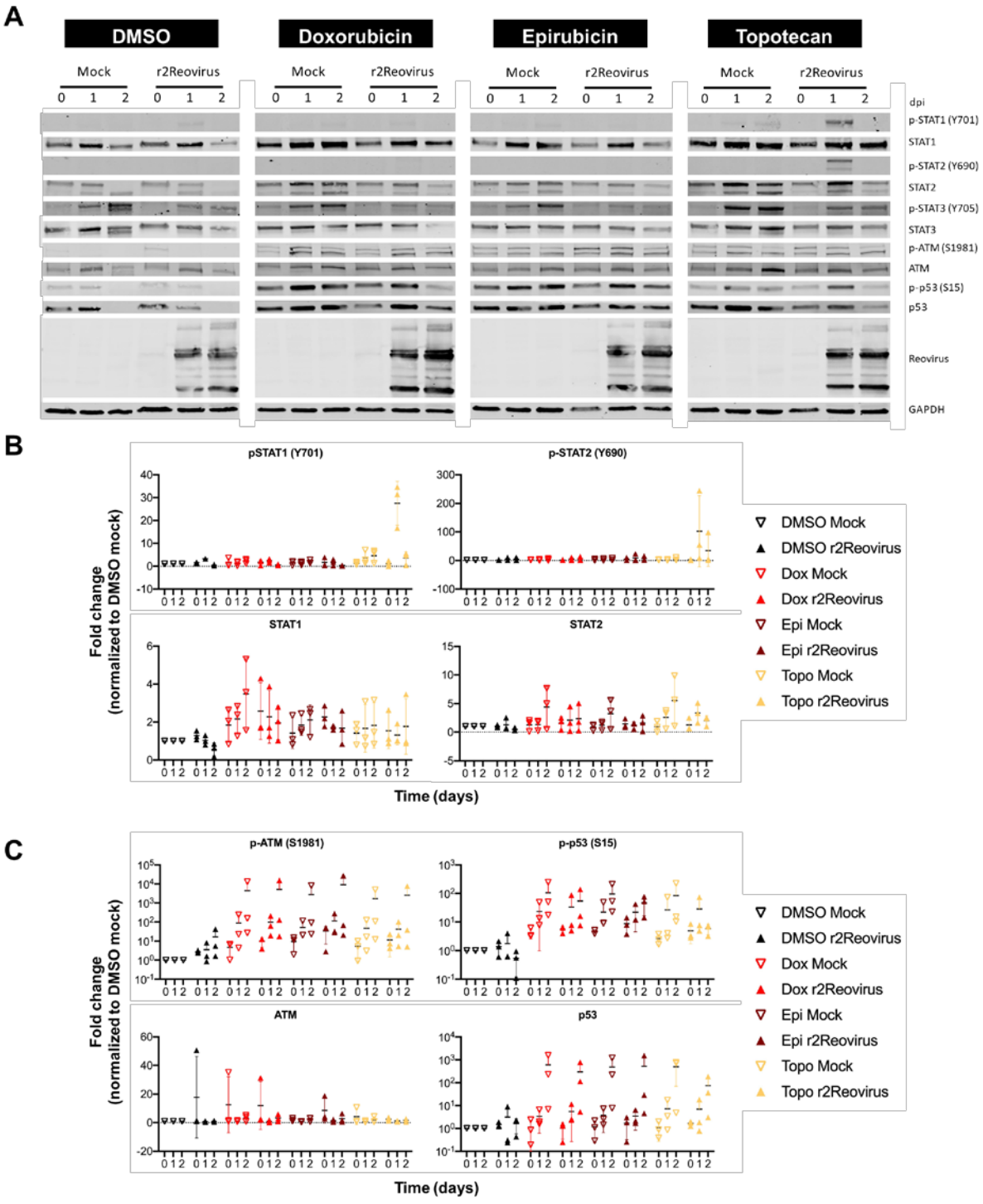

Figure 2.10. Reovirus activates STAT1 signaling and topoisomerase inhibitors activate DNA damage response pathways.

(A) MDA-MB-231 cells were treated with vehicle (DMSO) or 2 μM doxorubicin, epirubicin, or topotecan for 1 h, infected with reovirus at an MOI of 100 PFU/cell, and incubated with DMSO

or 1 μM topoisomerase inhibitors for 0-2 days post infection. Whole cell lysates were resolved by SDS-PAGE and immunoblotted with antibodies specific for phosphorylated and total STAT1, STAT2, STAT3, ATM, p53 and GAPDH and reovirus. Residues recognized by phosphorylation-specific antibodies are shown in parenthesis. (B) Quantitative densitometry of immunoblots from three independent experiments. All data are normalized to GAPDH and DMSO Mock for each corresponding day. Error bars = SEM.

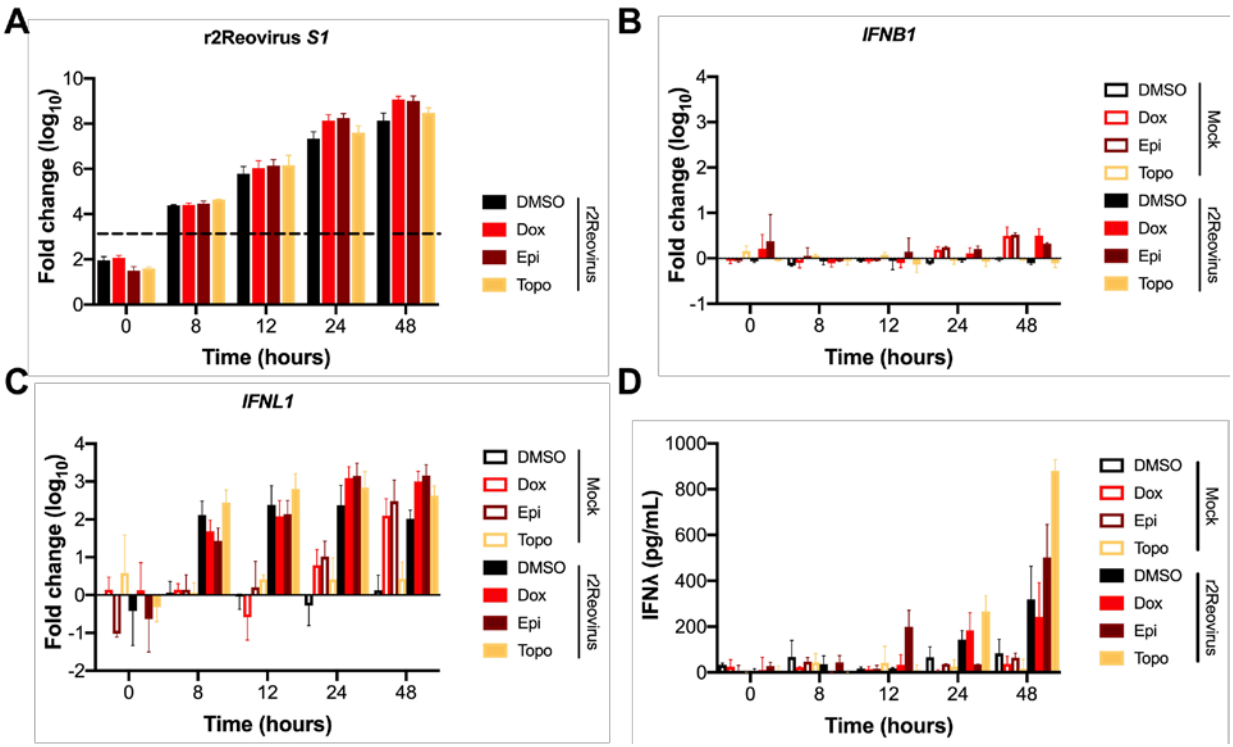

Figure 2.11. Topoisomerase inhibitors and r2Reovirus induce higher levels of *IFNL1* over time than either agent alone.

MDA-MB-231 cells were treated with vehicle (DMSO) or 2 μM doxorubicin, epirubicin, or topotecan, infected with mock or r2Reovirus at an MOI of 100 PFU/cell. RNA was isolated from cells at times shown and qPCR was performed to assess mRNA levels of (A) *IFNB1*, (B) *IFNL1*, and (C) reovirus *S1*. Dashed line in (C) represents background baseline levels observed in mock. Data are shown as fold change normalized to a housekeeping gene for duplicate independent experiments. Error bars = SEM. (D) Levels of IFNλ in cell supernatants were detected by ELISA. Data are shown as pg/ml of IFNλ for duplicate independent experiments.

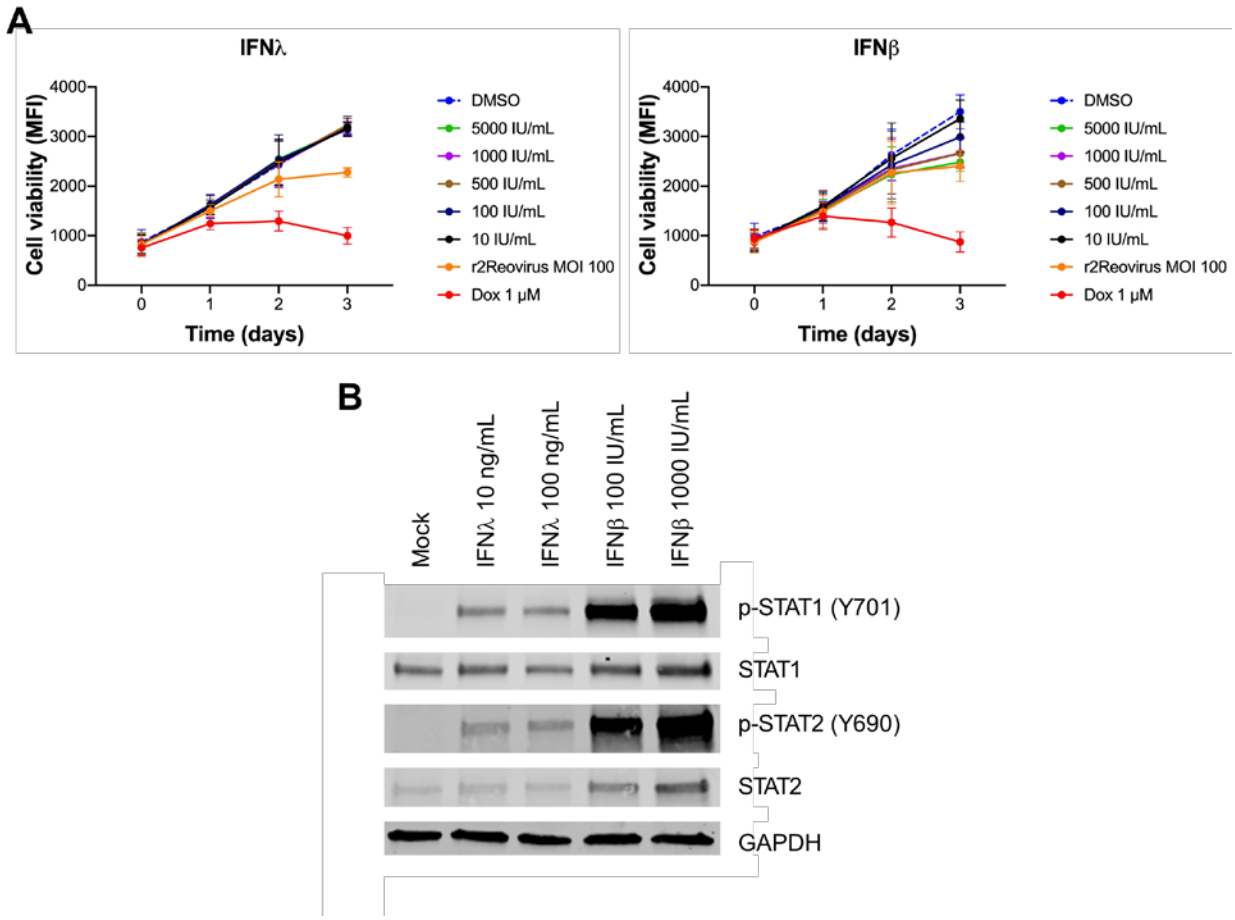

Figure 2.12. IFNλ does not impact MDA-MB-231 cellular proliferation but activates STATs.

(A) MDA-MB-231 cells were treated with DMSO, increasing amounts of recombinant human IFNλ, recombinant human IFNβ, or 1 μM doxorubicin, or infected with r2Reovirus at an MOI of 100 PFU/cell for 1 h and assessed for cell viability at times shown. Data are shown as average MFIs for quadruplicate independent experiments. Error bars = SEM. (B) MDA-MB-31 were untreated or treated with increasing amounts of recombinant human IFNλ or IFNβ for 1h. Whole cell lysates were resolved by SDS-PAGE and immunoblotted with antibodies specific for phosphorylated and total STAT1, STAT2, and GAPDH. Residues recognized by phosphorylation-specific antibodies are shown in parenthesis.

Table 2.S1. List of Synonymous and Nonsynonymous Mutations in r1Reovirus and r2Reovirus.

I. Synonymous mutations

Gene segment	r1Reovirus	r2Reovirus
L1	N/A	N/A
L2	N/A	A318G
L3	C2059T G2062C	C2059T G2062C T3550C
M1	T229C C919T	T229C C919T
M2	N/A	N/A
M3	N/A	N/A
S1	N/A	N/A
S2	See table III	N/A
S3	N/A	N/A
S4	N/A	N/A

II. Non-synonymous mutations

Gene segments	R1Reovirus	R2Reovirus
L1	N/A	N/A
L2	N/A	N/A
L3	G491A (A160T)	G491A (A160T)
M1	N/A	N/A
M2	N/A	N/A
M3	N/A	N/A
S1	N/A	N/A
S2	G1294A (after coding region) See table IV	N/A
S3	C508A (P161T) A775G (I250V) T1170G (after coding region)	A775G (I250V)
S4	G177A (V49I)	G177A (V49I)

III. Synonymous mutations in r1Reovirus S2 gene segment

Mutation	Percentage
G54A	45% A, 55% G
C84T	64% C, 36% T
C87T	64% C, 36% T
A90G	64% A, 36% G

C91T	65% C, 35% G
T96G	65% T, 35%G
C108T	64% C, 35% T
T114C	33% C, 66% T
A123G	67% A, 33% G
A537G	57% A, 42% G
T564C	56% T, 44% C
C573T	59% C, 41% T
T834C	69% T, 31% C
C858T	65% C, 35% T
T939C	67% T, 33% C
A945G	55% A, 45% G
A951G	55% A, 45% G
G954T	55% G, 45% T
C972T	49% C, 51% T
T981C	51% C, 48% T
T990C	50% C, 50% T
A996G	52% A, 48% G
T997C	49% C, 51% T
G1005T	48% G, 52% T
G1011A	51% A, 49% G
A1015C	47% A, 52% C
T1035C	50% C, 49% T
G1044A	45% A, 55% G
G1047A	46% A, 54% G
T1059A	49% A, 51% T
C1062T	52% C, 48% T
C1068T	51% C, 49% T
G1080A	51% A, 49% G
G1107A	51% A, 49% G
G1257A	65% A, 35% G
T1274A	65% A, 35% G

IV. Non-synonymous mutations in r1Reovirus S2 gene segment

Mutation	**Percentage**
G1087A (V357I)	51% A, 49% G
C1174A (H386N)	54% A, 46% C

Table 2.S2 Data from screening of reovirus infectivity using the NIH Clinical Collection.

Data are shown for two independent experiments (Runs). For each run, reovirus focus forming units (FFU), number of cells (DAPI), percent infectivity ([FFU/DAPI]*100), and Z-score based on percent infectivity (Z percent infectivity) were calculated. Z scores for each well were calculated using the following formula: Z score = (a-b)/c, where a is the percent infectivity (infected cells/number of cells), b is the median percent infectivity for each plate, and c is the standard deviation of percent infectivity for each plate. The average Z-score for both runs is also provided (Avg Z % Infectivity). Name for individual compounds and their PubChem ID numbers are provided.

				Run 1					Run 2			Average
NIH Clinical Collection Compound	**PUBCHEM_S**	**FFU**	**DAPI**	**%**	**Z %**		**FFU**	**DAPI**	**%**	**Z %**		**Avg Z %**
(-)-Cotinine	46386857	2092	14619	14.310	0.005		3200	15961	20.049	-0.271		-0.133
(+)-cis-Diltiazem hydrochloride	104170056	3107	16205	19.173	0.309		4354	15018	28.992	0.386		0.347
(+/-)-Norepinephrine hydrochloride	104170127	1659	16363	10.139	-0.005		3611	17031	21.203	0.241		0.118
(+/-)-Vesamicol hydrochloride	46386799	3339	16652	20.052	0.310		4220	15806	26.699	0.191		0.251
1,1-Dimethyl-4-phenylpiperazinium iodide	46387026	2219	16640	13.335	-0.168		3558	17209	20.675	-0.131		-0.149
11-Deoxycortisol	46386963	1498	14406	10.398	0.015		3502	16740	20.920	-0.248		-0.116
19-Norethindrone	104170074	1177	12279	9.585	-0.299		2753	14090	19.539	-0.381		-0.340
19-Norethindrone acetate	104170073	1274	14142	9.009	-0.559		3688	17176	21.472	-0.155		-0.357
19-Nortestosterone	46386764	3024	16219	18.645	-0.313		4047	16035	25.239	-0.309		-0.311
2-Chloroadenosine	46386960	2267	13089	17.320	-0.900		3185	12461	25.560	-0.199		-0.550
2-Pyridylethylamine	46386941	2179	14932	14.593	-0.209		2770	13688	20.237	0.030		-0.089
3-Pyridinemethanol	46386968	1528	14392	10.617	0.370		3663	16448	22.270	0.262		0.316
3,5,3'-Triiodothyronine	104169993	1862	16047	11.603	0.774		3580	16147	22.171	0.604		0.689
3'-Deoxydenosine	46386791	1256	12505	10.044	0.105		3503	16264	21.538	0.071		0.088
4-Phenylbutyric acid	104169967	1360	14260	9.537	-0.129		3506	16692	21.004	-0.069		-0.099
5-Azacytidine	104170170	1068	12621	8.462	-1.197		2646	14413	18.358	-1.152		-1.174
5-Fluoro-2-pyrimidone	46386867	2219	16295	13.618	-0.118		3498	17222	20.311	-0.212		-0.165
5-Fluorouracil	104169952	1393	15561	8.952	-0.590		3902	17874	21.831	-0.052		-0.321
5-Methoxytryptamine	46387021	2778	14304	19.421	1.353		2980	12900	23.101	1.007		1.180
5-Nonyloxytryptamine hydrochloride	46387012	1645	13694	12.013	1.026		4006	15989	25.055	1.210		1.118
6-Aminoindazole	46386887	1161	10946	10.607	0.146		3347	13783	24.284	0.938		0.542
6-Azauridine	46386950	1040	11173	9.308	-0.667		2716	14323	18.963	-0.939		-0.803
7-Nitroindazole	46387020	1763	15869	11.110	0.461		3659	16482	22.200	0.203		0.332
Acarbose	46386746	1447	14712	9.836	-0.337		3456	16945	20.395	-0.433		-0.385
Acebutolol hydrochloride	104170167	1445	16437	8.791	-0.721		3278	17207	19.050	-0.564		-0.643
Acetazolamide	104169989	1752	16398	10.684	0.285		3366	17053	19.738	-0.307		-0.011
Acetylcholine chloride	104170141	1571	16027	9.802	-0.184		3568	17766	20.083	-0.178		-0.181
Acitretin	104170221	954	10320	9.244	-0.429		3301	14286	23.107	0.316		-0.057
Actarit	46386663	2643	14689	17.993	0.891		2509	12093	20.748	0.204		0.548
Acyclovir	104170215	905	10133	8.931	-0.601		2921	14335	20.377	-0.470		-0.536
Albendazole	104170113	484	8774	5.516	-2.463		1068	7911	13.500	-2.642		-2.552
Alfuzosin	46386655	3397	16737	20.296	1.636		3240	15149	21.388	0.423		1.030
Allopurinol	104169990	1633	16071	10.161	0.007		3382	16760	20.179	-0.142		-0.067
Alosetron monohydrochloride	46386816	2464	16744	14.716	0.077		3661	17270	21.199	-0.015		0.031
Alprazolam	46386679	2743	17640	15.550	0.101		3182	15667	20.310	0.055		0.078
Altanserin hydrochloride	46386989	2605	14086	18.494	1.053		3286	13124	25.038	1.667		1.360
Altretamine	104170093	1306	13484	9.686	-0.188		3732	17032	21.912	-0.028		-0.108
AM 404	46386792	2469	16885	14.622	0.060		3562	17168	20.748	-0.115		-0.027
AM-251	46386990	1984	16774	11.828	-1.104		2334	15171	15.385	-1.624		-1.364
Amcinonide	104170128	3267	14451	22.607	1.414		4510	13593	33.179	1.388		1.401
Amiloride hydrochloride hydrate	46386846	3060	15899	19.246	-0.047		4085	15815	25.830	-0.106		-0.077
Aminoglutethimide	104170212	1002	10174	9.849	-0.098		3105	14534	21.364	-0.186		-0.142
Aminolevulinic acid	104170099	1390	14612	9.513	-0.140		3655	17987	20.320	-0.248		-0.194
Amiodarone hydrochloride	46386662	2513	16544	15.190	-1.204		4683	16432	28.499	0.374		-0.415
Amisulpride	46386656	2531	17520	14.446	-0.256		3143	15592	20.158	0.003		-0.126
Amitriptyline hydrochloride	104169995	1440	16507	8.724	-0.757		3353	17749	18.891	-0.624		-0.690
Amlexanox	46386726	3055	17095	17.871	0.852		3362	16587	20.269	0.041		0.446
Amlodipine	46386686	2279	14338	15.895	0.212		2772	13174	21.041	0.305		0.258
Amoxapine	104170044	2879	16193	17.779	-0.140		3826	14489	26.406	-0.233		-0.187
Amoxicillin	104170168	1771	16419	10.786	0.340		3624	17607	20.583	0.009		0.175
Ampicillin sodium	104170166	1056	11444	9.228	-0.718		2966	14616	20.293	-0.469		-0.593
Ampiroxicam	46386688	2512	17079	14.708	-0.172		3211	16208	19.811	-0.115		-0.143
Anagrelide hydrochloride	46386622	3502	17613	19.883	0.235		4408	17653	24.970	-0.401		-0.083
Anastrozole	46386543	1281	12092	10.594	0.359		3381	15069	22.437	0.306		0.333
Argatroban	46386718	3127	17578	17.789	-0.368		4230	16168	26.163	-0.327		-0.348
Aripiprazole	46386763	3374	16153	20.888	1.828		2953	13592	21.726	0.538		1.183
Artemether	46386824	3342	16282	20.526	0.513		4541	16200	28.031	0.233		0.373
Artesunate	46386645	1865	14061	13.264	-0.639		2496	12456	20.039	-0.037		-0.338
Atenolol	104170046	2987	16684	17.903	-0.100		4145	16129	25.699	-0.403		-0.251
Atomoxetine hydrochloride	46386643	1283	11505	11.152	0.487		3432	14268	24.054	0.857		0.672
Atracurium besylate	46386822	1026	10767	9.529	-0.132		3051	14760	20.671	-0.156		-0.144
Atropine	104169991	1559	13940	11.184	0.507		3696	16519	22.374	0.265		0.386
Azasetron hydrochloride	46386991	3040	17554	17.318	0.673		2926	15495	18.884	-0.431		0.121
Azathioprine	104170112	870	14394	6.044	-2.183		2895	17371	16.666	-1.539		-1.861
Azelastine hydrochloride	46386661	3778	13401	28.192	2.981		4751	11858	40.066	3.846		3.413
Azithromycin	104170210	55	11373	0.484	-6.193		518	12392	4.180	-6.153		-6.173
Balsalazide	46386828	1535	15218	10.087	0.125		3716	17221	21.578	0.081		0.103
Beclomethasone	46386972	3160	13887	22.755	1.231		4515	15021	30.058	0.842		1.036
Beclomethasone dipropionate	104170108	3182	14839	21.443	1.040		4222	13242	31.883	1.078		1.059
Benactyzine hydrochloride	46386942	3309	17489	18.920	-0.003		4448	16582	26.824	-0.129		-0.066
Benazepril hydrochloride	46386692	2940	16178	18.173	-0.244		4057	15388	26.365	-0.267		-0.255
Bendrofluazide	104170162	3170	16732	18.946	0.235		4297	15310	28.067	0.164		0.200
Benidipine hydrochloride	46386729	2208	14915	14.804	0.092		3638	15555	23.388	0.473		0.283
Benproperine phosphate	46386752	2243	16122	13.913	2.216		4376	15509	28.216	2.325		2.271
Benzbromarone	46386951	3152	16921	18.628	1.097		2618	13747	19.044	-0.376		0.360
Benztropine mesylate	104170144	1703	15721	10.833	0.287		3770	17371	21.703	0.028		0.158
Benzylimidazole	46386891	1442	14198	10.156	-0.136		3305	16286	20.294	-0.469		-0.303
Bestatin	46386830	2914	15718	18.539	-0.126		4054	15459	26.224	-0.309		-0.218
Beta-estradiol	46386902	3056	16697	18.303	-0.465		3985	16184	24.623	-0.520		-0.492
Betamethasone	104170205	1133	10531	10.759	0.400		3346	13406	24.959	0.849		0.625
Betaxolol hydrochloride	46386993	2129	16847	12.637	-0.291		3535	17047	20.737	-0.117		-0.204
Bethanechol chloride	104170158	1559	14692	10.611	0.149		3558	16932	21.013	-0.215		-0.033
Bicalutamide	46386630	970	9739	9.960	0.066		3255	15632	20.823	-0.117		-0.025
Bifemelane hydrochloride	46386922	4125	17521	23.543	1.856		5491	17516	31.348	1.784		1.820

Bifonazole	46386787	3431	17251	19.889	0.238		4032	16535	24.385	-0.601		-0.182
Bisoprolol fumarate	46386635	2729	17483	15.609	0.120		2583	14978	17.245	-0.990		-0.435
Brimonidine	104170136	3024	17114	17.670	-0.175		4313	15407	27.994	0.147		-0.014
Brucine	46386939	3349	17186	19.487	0.179		4329	15792	27.413	0.048		0.113
Budesonide	104170124	1515	13731	11.033	0.413		3659	15160	24.136	0.886		0.650
Buflomedil hydrochloride	46386737	2377	16676	14.254	-0.005		3641	16946	21.486	0.049		0.022
Bumetanide	104170048	1770	15917	11.120	0.467		3393	15858	21.396	-0.080		0.194
Bupropion hydrochloride	46386703	2495	13648	18.281	-0.209		3130	11501	27.215	-0.012		-0.110
Buspirone hydrochloride	104170171	1776	15931	11.148	0.485		4130	17529	23.561	0.683		0.584
Busulfan	104169996	1776	16484	10.774	0.333		3239	16257	19.924	-0.237		0.048
Calcipotriol	46386727	3168	15943	19.871	0.302		4427	15457	28.641	0.416		0.359
Calcitriol	46386784	2140	16933	12.638	-0.291		3475	15830	21.952	0.153		-0.069
Captopril	104170052	1649	16012	10.299	-0.047		3859	17280	22.332	0.250		0.101
Carbamazepine	104170177	1420	14442	9.832	-0.339		3450	16689	20.672	-0.335		-0.337
Carbidopa	104170225	1579	14418	10.952	0.506		4092	17858	22.914	0.260		0.383
Carbinoxamine maleate	104170100	3120	17319	18.015	-0.064		3891	14868	26.170	-0.290		-0.177
Carisoprodol	104170000	2536	13797	18.381	0.054		3564	12989	27.439	0.014		0.034
Carmofur	46386675	3031	17357	17.463	-0.473		4247	16313	26.034	-0.366		-0.419
Carvedilol	46386749	1683	16972	9.916	-0.123		3381	17973	18.812	-0.654		-0.388
CCPA	46386935	1369	13492	10.147	0.153		3484	16159	21.561	0.077		0.115
Cefaclor	46386958	3056	16843	18.144	-0.253		4090	15671	26.099	-0.347		-0.300
Cefatrizine propylene glycol	46386659	2516	17111	14.704	-0.173		3314	15918	20.819	0.229		0.028
Cefazolin sodium	104170051	3147	17389	18.098	-0.038		4073	15037	27.087	-0.071		-0.054
Cefdinir	46386833	3194	17261	18.504	-0.137		4158	16112	25.807	-0.434		-0.286
Cefixime trihydrate	46386832	1350	14079	9.589	-0.105		3085	16988	18.160	-0.814		-0.459
Cefotaxime sodium	104170202	1872	15999	11.701	0.826		3701	16953	21.831	0.477		0.651
Cefoxitin sodium	104170054	3043	17342	17.547	-0.215		3736	14122	26.455	-0.222		-0.218
Cefpodoxime proxetil	46386731	2403	13373	17.969	-0.310		3332	11873	28.064	0.243		-0.033
Cefuroxime	104170159	1604	16606	9.659	-0.260		3554	17862	19.897	-0.247		-0.253
Celecoxib	104170206	1297	12844	10.098	-0.026		2932	14299	20.505	-0.020		-0.023
Cephalexin hydrate	46386774	2743	14890	18.422	1.030		2613	12636	20.679	0.181		0.605
Cerivastatin sodium	46386572	2730	14795	18.452	1.040		3607	14140	25.509	1.828		1.434
Cetirizine	104170194	1550	14739	10.516	0.268		3597	16533	21.756	-0.073		0.097
Cetraxate hydrochloride	46386678	3337	17467	19.105	-0.110		4528	17700	25.582	-0.191		-0.150
CGS 12066B dimaleate	46386975	951	11692	8.134	-0.776		2858	14617	19.553	-0.449		-0.613
CGS 15943	46386800	2738	15750	17.384	0.549		4190	16031	26.137	1.085		0.817
Chlorambucil	104170053	1093	10543	10.367	-0.004		2915	13474	21.634	0.004		0.000
Chloramphenicol	104170151	1375	14287	9.624	-0.469		3640	16341	22.275	0.230		-0.120
Chlordiazepoxide	46386831	1464	14960	9.786	-0.014		3443	17023	20.226	-0.273		-0.143
Chlorothiazide	104169998	3207	16805	19.084	0.280		4410	15973	27.609	0.055		0.167
Chloroxine	104170003	3065	17408	17.607	-0.196		4374	15169	28.835	0.348		0.076
Chlorpheniramine maleate	46386872	2507	13409	18.696	-0.291		3321	12824	25.897	-0.083		-0.187
Chlorpromazine hydrochloride	104170050	2884	17420	16.556	-0.534		4155	15372	27.030	-0.084		-0.309
Chlorpropamide	104170001	3149	17627	17.865	-0.113		3913	14732	26.561	-0.196		-0.154
Chlorthalidone	104170188	1536	14969	10.261	0.061		3657	17498	20.900	0.128		0.094
Chlorzoxazone	104169997	1684	16393	10.273	0.067		3452	17737	19.462	-0.410		-0.172
Cilastatin sodium	46386570	2313	12905	17.923	-0.633		3365	12637	26.628	0.167		-0.233
Cimetidine	104169999	2897	16824	17.219	-0.320		4107	15440	26.600	-0.187		-0.254
Cinanserin	46386801	2134	16797	12.705	-0.279		3593	17211	20.876	-0.086		-0.183
Cisapride hydrate	46386802	3272	16478	19.857	0.986		4886	16227	30.110	1.970		1.478
Citalopram hydrobromide	46386617	2676	17052	15.693	0.147		3156	15317	20.605	0.156		0.151
Cladribine	46386544	1238	11082	11.171	0.625		3151	12712	24.788	0.922		0.774
Clarithromycin	46386761	3430	17486	19.616	1.416		2951	15049	19.609	-0.184		0.616
Clobenpropit	46387016	1784	15566	11.461	0.681		4020	17074	23.545	0.678		0.679
Clobetasol propionate	104170049	2938	12290	23.906	1.832		4085	11736	34.807	1.777		1.805
Clofazimine	46386952	1374	17415	7.890	-2.378		2633	15552	16.930	-1.097		-1.737
Clomifene citrate	104170129	1460	14973	9.751	-0.030		3482	16993	20.491	-0.204		-0.117
Clomipramine hydrochloride	104170176	1366	16638	8.210	-1.355		3257	17114	19.031	-0.914		-1.135
Clonidine hydrochloride	46386982	2458	17215	14.278	-0.311		3211	15335	20.939	0.270		-0.021
Clopidogrel	104170201	1572	14846	10.589	0.307		4158	17457	23.819	0.521		0.414
Clotrimazole	46386926	2589	15415	16.795	0.445		3692	15751	23.440	0.485		0.465
Clozapine	104170165	1340	16070	8.339	-0.962		3089	17233	17.925	-0.986		-0.974
Corticosterone	46386953	1503	14044	10.702	0.409		3879	16504	23.503	0.585		0.497
Cortisol 21-acetate	104169955	1630	13483	12.089	1.130		4333	16111	26.895	1.407		1.268
Cortisone	46386956	1629	14796	11.010	0.398		3550	16827	21.097	-0.186		0.106
Cortisone acetate	104170175	3352	17454	19.205	0.319		4230	15541	27.218	-0.039		0.140
Cromolyn sodium	104170109	1448	15286	9.473	-0.359		3533	17333	20.383	-0.065		-0.212
Crotamiton	46386684	1410	14323	9.844	0.013		3557	17398	20.445	-0.216		-0.101
Cyclophosphamide hydrate	104170160	1140	11239	10.143	-0.144		3017	14614	20.645	-0.345		-0.245
Cyproheptadine hydrochloride	46386957	1300	14714	8.835	-0.453		3125	16790	18.612	-0.696		-0.574
Cytarabine	46386862	2937	12310	23.859	1.996		3890	11800	32.966	2.338		2.167
D-Cycloserine	46386864	2524	17723	14.241	-0.323		3326	16769	19.834	-0.107		-0.215
Dactinomycin	46386883	2733	10907	25.057	3.177		3325	10282	32.338	4.156		3.666
Danazol	104170055	3254	17310	18.798	0.188		4162	15212	27.360	-0.005		0.091
Dantrolene sodium	104170142	1448	14619	9.905	-0.294		3526	16859	20.915	-0.250		-0.272
Dapsone	104169986	1193	11146	10.703	0.206		3352	14554	23.031	0.497		0.352
Daunorubicin hydrochloride	104170197	295	3477	8.484	-0.846		1709	8981	19.029	-0.858		-0.852
Deferiprone	46386865	1347	14070	9.574	-0.112		3717	17468	21.279	0.003		-0.055
Dehydrocholic acid	46386890	1035	11407	9.073	-0.814		2962	14676	20.183	-0.508		-0.661
Dehydroepiandrosterone	46387028	1510	15183	9.945	-0.268		3858	17234	22.386	0.269		0.000
Demeclocycline	104170101	1464	15273	9.586	-0.106		3596	16933	21.237	-0.008		-0.057
Desipramine hydrochloride	104170179	1614	16281	9.913	-0.124		3421	17928	19.082	-0.552		-0.338
Desloratadine	46386563	1572	16636	9.449	-1.873		1978	15801	12.518	-2.601		-2.237
Desoximetasone	46386959	1489	11217	13.274	1.596		3483	13457	25.882	1.208		1.402
Dexamethasone	104170143	1242	10381	11.964	1.061		3382	13511	25.031	0.870		0.966
Dexbrompheniramine maleate	46386574	2673	13675	19.547	0.086		3386	12781	26.492	0.121		0.103

Dexchlorpheniramine maleate	46386575	2309	17006	13.578	-0.125		3806	17303	21.996	0.163		0.019
Dextromethorphan hydrobromide, monohydrate	46386932	2575	16933	15.207	0.164		3849	17054	22.569	0.291		0.227
Dextrorphan D-tartrate	46386873	3461	17451	19.833	0.213		4283	16430	26.068	-0.025		0.094
Diazepam	46386554	2984	15856	18.819	-0.036		3956	14390	27.491	0.071		0.018
Diazoxide	46386946	1462	14515	10.072	0.118		3515	16613	21.158	-0.029		0.045
Dichloroacetic acid	46386944	2875	16028	17.937	-0.320		4056	15333	26.453	-0.240		-0.280
Diclofenac sodium	46386927	2173	13442	16.166	-0.890		3133	11768	26.623	-0.189		-0.540
Dicloxacillin sodium	104170195	1696	15265	11.110	0.512		3672	17054	21.532	0.364		0.438
Dicyclomine hydrochloride	104170002	3830	16902	22.660	1.431		4946	15477	31.957	1.095		1.263
Didanosine	46386730	2428	17477	13.893	-0.435		3005	15755	19.073	-0.366		-0.401
Diflunisal	104170004	887	10836	8.186	-1.010		2974	14925	19.926	-0.600		-0.805
Digoxin	104170057	8	9479	0.084	-4.491		91	11121	0.818	-5.355		-4.923
Dihydrexidine hydrochloride	46386992	1835	15030	12.209	-0.980		2264	12980	17.442	-0.922		-0.951
Dilantin	104170140	1673	16048	10.425	0.032		3742	17333	21.589	-0.012		0.010
Diphenhydramine hydrochloride	46386874	1146	11920	9.614	-0.284		3108	14750	21.071	0.192		-0.046
Diphenoxylate hydrochloride	46386550	3354	17418	19.256	-0.043		4320	16527	26.139	0.000		-0.022
Diphenylcyclopropenone	46386897	897	12100	7.413	-1.109		2547	14627	17.413	-1.010		-1.059
Dipyridamole	104169946	1080	11181	9.659	-0.447		3118	13799	22.596	0.343		-0.052
Disopyramide phosphate	104170181	2940	17322	16.973	-0.400		4028	14899	27.035	-0.083		-0.241
Disulfiram	46386898	3726	17283	21.559	0.977		4364	16666	26.185	0.015		0.496
DL-Penicillamine	104169974	1634	15850	10.309	0.154		3854	17415	22.130	0.035		0.094
DMSO-Mock		2	14457	0.014	-8.566		1	14359	0.007	-8.952		-8.759
DMSO-Mock		3	13247	0.023	-8.562		1	12778	0.008	-8.952		-8.757
DMSO-Mock		5	14722	0.034	-8.557		1	14374	0.007	-8.952		-8.754
DMSO-Mock		5	14419	0.035	-8.557		36	14237	0.253	-8.868		-8.712
DMSO-Mock		1	12425	0.008	-6.490		1	15209	0.007	-7.625		-7.058
DMSO-Mock		1	12211	0.008	-6.490		0	15649	0.000	-7.627		-7.059
DMSO-Mock		2	11906	0.017	-6.485		5	15134	0.033	-7.615		-7.050
DMSO-Mock		2	10999	0.018	-6.484		12	14125	0.085	-7.597		-7.041
DMSO-Mock		0	14066	0.000	-6.093		1	14360	0.007	-8.180		-7.136
DMSO-Mock		1	14197	0.007	-6.091		2	14389	0.014	-8.178		-7.134
DMSO-Mock		1	12684	0.008	-6.090		2	11909	0.017	-8.177		-7.134
DMSO-Mock		5	14111	0.035	-6.081		16	13150	0.122	-8.145		-7.113
DMSO-Mock		0	14413	0.000	-5.864		0	13412	0.000	-6.553		-6.209
DMSO-Mock		1	14919	0.007	-5.862		2	14404	0.014	-6.550		-6.206
DMSO-Mock		1	13620	0.007	-5.862		2	13294	0.015	-6.550		-6.206
DMSO-Mock		2	14500	0.014	-5.860		2	13610	0.015	-6.550		-6.205
DMSO-Mock		0	10665	0.000	-5.495		0	15530	0.000	-6.338		-5.917
DMSO-Mock		1	8725	0.011	-5.489		3	15252	0.020	-6.332		-5.911
DMSO-Mock		2	8614	0.023	-5.482		1	15372	0.007	-6.336		-5.909
DMSO-Mock		4	1857	0.215	-5.377		0	13851	0.000	-6.338		-5.858
DMSO-Mock		0	14906	0.000	-4.930		4	13249	0.030	-6.859		-5.895
DMSO-Mock		0	15148	0.000	-4.930		1	14738	0.007	-6.867		-5.899
DMSO-Mock		0	14200	0.000	-4.930		0	12652	0.000	-6.869		-5.900
DMSO-Mock		1	15221	0.007	-4.928		11	13302	0.083	-6.841		-5.885
DMSO-Mock		0	12060	0.000	-4.530		17	15361	0.111	-5.541		-5.035
DMSO-Mock		2	11643	0.017	-4.522		12	15262	0.079	-5.549		-5.036
DMSO-Mock		5	13226	0.038	-4.512		0	14479	0.000	-5.570		-5.041
DMSO-Mock		9	12277	0.073	-4.496		20	15109	0.132	-5.535		-5.016
DMSO-Mock		0	15208	0.000	-2.527		39	16632	0.234	-4.684		-3.605
DMSO-Mock		6	17101	0.035	-2.521		22	16309	0.135	-4.706		-3.613
DMSO-Mock		6	15091	0.040	-2.520		1	15474	0.006	-4.734		-3.627
DMSO-Mock		7	14972	0.047	-2.519		2	16570	0.012	-4.733		-3.626
DMSO-Mock		1036	13721	7.550	-1.381		1	15076	0.007	-7.692		-4.537
DMSO-Mock		1121	13450	8.335	-0.964		1	15610	0.006	-7.693		-4.328
DMSO-Mock		1131	12664	8.931	-0.647		0	14503	0.000	-7.695		-4.171
DMSO-Mock		1274	13302	9.578	-0.303		6	15538	0.039	-7.680		-3.992
DMSO-Reo		2551	13648	18.691	-0.293		1528	5124	29.820	1.261		0.484
DMSO-Reo		1086	11366	9.555	-0.259		2891	14485	19.959	-0.591		-0.425
DMSO-Reo		1190	11782	10.100	-0.171		3214	14386	22.341	0.253		0.041
DMSO-Reo		1164	11845	9.827	-0.110		3093	14903	20.754	-0.362		-0.236
DMSO-Reo		1064	11042	9.636	-0.083		3319	15035	22.075	0.211		0.064
DMSO-Reo		2671	13829	19.314	-0.017		1347	4411	30.537	1.506		0.745
DMSO-Reo		2128	14603	14.572	0.051		3447	15907	21.670	0.090		0.071
DMSO-Reo		2679	13721	19.525	0.076		1549	4856	31.899	1.973		1.025
DMSO-Reo		2072	14047	14.750	0.083		3352	15730	21.310	0.010		0.047
DMSO-Reo		2560	13207	19.384	0.146		3440	12393	27.758	0.151		0.148
DMSO-Reo		2335	11861	19.686	0.148		1197	3513	34.073	2.718		1.433
DMSO-Reo		2255	14693	15.347	0.189		3267	15721	20.781	-0.108		0.041
DMSO-Reo		2626	13964	18.805	0.190		3160	11272	28.034	0.156		0.173
DMSO-Reo		1203	11446	10.510	0.264		3000	14496	20.695	-0.379		-0.057
DMSO-Reo		1410	13192	10.688	0.288		3241	14916	21.728	0.438		0.363
DMSO-Reo		2522	12692	19.871	0.302		3437	12429	27.653	0.120		0.211
DMSO-Reo		2717	14094	19.278	0.342		3149	11303	27.860	0.115		0.228
DMSO-Reo		2662	13294	20.024	0.352		3486	12844	27.141	-0.034		0.159
DMSO-Reo		1234	11634	10.607	0.365		3283	15204	21.593	0.085		0.225
DMSO-Reo		1450	13288	10.912	0.407		3134	15037	20.842	0.106		0.256
DMSO-Reo		2348	13800	17.014	0.484		3373	15521	21.732	0.104		0.294
DMSO-Reo		2752	13839	19.886	0.538		3472	12784	27.159	-0.053		0.242
DMSO-Reo		1286	11623	11.064	0.576		3370	15274	22.064	0.208		0.392
DMSO-Reo		1329	11760	11.301	0.581		3067	14438	21.243	-0.134		0.223
DMSO-Reo		2525	12041	20.970	0.656		3396	11444	29.675	0.727		0.692
DMSO-Reo		1347	11741	11.473	0.688		3210	14540	22.077	0.160		0.424
DMSO-Reo		1538	13144	11.701	0.826		3100	14507	21.369	0.304		0.565
DMSO-Reo		1297	10700	12.121	1.064		3266	14369	22.729	0.383		0.723
DMSO-Reo		970	7946	12.207	1.194		2771	13438	20.621	-0.400		0.397

DMSO-Reo		2769	14439	19.177	1.274		2408	12087	19.922	-0.077		0.599
DMSO-Reo		1300	10461	12.427	1.286		3058	13811	22.142	0.183		0.734
DMSO-Reo		2946	15289	19.269	1.304		2313	11475	20.157	0.003		0.653
DMSO-Reo		1552	12136	12.788	1.404		3075	14107	21.798	0.464		0.934
DMSO-Reo		2972	14981	19.838	1.488		1967	10260	19.172	-0.333		0.578
DMSO-Reo		2818	13985	20.150	1.589		2336	10694	21.844	0.578		1.084
DMSO-Reo		2971	12775	23.256	1.623		3171	11619	27.292	-0.021		0.801
Docetaxel	46386672	465	7167	6.488	-1.536		1410	8316	16.955	-1.129		-1.333
Dofetilide	46386638	3268	17241	18.955	0.008		4437	16465	26.948	-0.092		-0.042
Dolasetron mesylate	46386881	3156	14551	21.689	1.119		3836	12928	29.672	0.548		0.834
Donepezil hydrochloride	46386644	4129	17065	24.196	2.145		4841	15139	31.977	1.999		2.072
Dopamine hydrochloride	104170043	3037	16398	18.521	0.099		3950	14911	26.491	-0.213		-0.057
Doxapram hydrochloride	46386821	1047	11320	9.249	-0.262		3156	14297	22.075	0.211		-0.025
Doxazosin	104170183	2074	16775	12.364	1.280		4603	17542	26.240	1.218		1.249
Doxepin hydrochloride	104169945	1546	14684	10.528	0.097		3963	17255	22.967	0.474		0.285
Doxorubicin hydrochloride	46386781	3010	5071	59.357	7.976		3707	7131	51.984	6.842		7.409
Doxycycline	104170107	1062	11505	9.231	-0.437		3107	14709	21.123	-0.255		-0.346
Doxylamine succinate	46386900	1244	14065	8.845	-0.448		3602	16522	21.801	0.140		-0.154
Droperidol	46386863	4336	16945	25.589	2.762		5156	16909	30.493	1.491		2.127
Duloxetine hydrochloride	46386541	2284	14329	15.940	0.293		3588	15504	23.142	0.418		0.356
DuP 697	46387010	2447	16521	14.811	0.094		3563	16797	21.212	-0.012		0.041
Duvadilan	104170012	1550	14926	10.385	0.126		3651	16325	22.364	0.676		0.401
E-4031 dihydrochloride	46387000	3461	16889	20.493	0.505		4268	16364	26.082	-0.020		0.243
E64d-Mock		0	15020	0.000	-8.572		2	14130	0.014	-8.950		-8.761
E64d-Mock		0	13528	0.000	-8.572		1	13381	0.007	-8.952		-8.762
E64d-Mock		0	14666	0.000	-8.572		1	14037	0.007	-8.952		-8.762
E64d-Mock		3	14561	0.021	-8.563		1	13998	0.007	-8.952		-8.757
E64d-Mock		0	12895	0.000	-6.496		6	15722	0.038	-7.614		-7.055
E64d-Mock		0	12257	0.000	-6.496		1	15543	0.006	-7.625		-7.060
E64d-Mock		0	11144	0.000	-6.496		0	14656	0.000	-7.627		-7.061
E64d-Mock		2	12065	0.017	-6.485		8	15582	0.051	-7.609		-7.047
E64d-Mock		0	14540	0.000	-6.093		4	14122	0.028	-8.173		-7.133
E64d-Mock		1	14636	0.007	-6.091		1	14209	0.007	-8.180		-7.135
E64d-Mock		2	13244	0.015	-6.088		0	12847	0.000	-8.182		-7.135
E64d-Mock		8	14473	0.055	-6.075		1	13770	0.007	-8.180		-7.127
E64d-Mock		0	14313	0.000	-5.864		2	12547	0.016	-6.550		-6.207
E64d-Mock		0	15025	0.000	-5.864		1	14386	0.007	-6.552		-6.208
E64d-Mock		0	14877	0.000	-5.864		0	12886	0.000	-6.553		-6.209
E64d-Mock		5	14651	0.034	-5.853		2	14406	0.014	-6.550		-6.202
E64d-Mock		0	11069	0.000	-5.495		1	15430	0.006	-6.336		-5.916
E64d-Mock		1	3239	0.031	-5.478		4	15431	0.026	-6.331		-5.904
E64d-Mock		4	9894	0.040	-5.473		0	15555	0.000	-6.338		-5.905
E64d-Mock		0	13251	0.000	-5.396		18	15849	0.114	-7.652		-6.524
E64d-Mock		0	13806	0.000	-5.396		9	16080	0.056	-7.674		-6.535
E64d-Mock		2	13007	0.015	-5.388		21	15574	0.135	-7.644		-6.516
E64d-Mock		10	12278	0.081	-5.353		3	14986	0.020	-7.687		-6.520
E64d-Mock		7	2484	0.282	-5.341		13	14292	0.091	-6.312		-5.826
E64d-Mock		0	15531	0.000	-4.930		14	14181	0.099	-6.835		-5.883
E64d-Mock		0	15245	0.000	-4.930		3	14869	0.020	-6.862		-5.896
E64d-Mock		0	14240	0.000	-4.930		0	13036	0.000	-6.869		-5.900
E64d-Mock		0	15319	0.000	-4.930		0	13576	0.000	-6.869		-5.900
E64d-Mock		0	11436	0.000	-4.530		4	15630	0.026	-5.563		-5.046
E64d-Mock		0	11613	0.000	-4.530		1	14839	0.007	-5.568		-5.049
E64d-Mock		1	12031	0.008	-4.526		2	15530	0.013	-5.566		-5.046
E64d-Mock		3	12040	0.025	-4.518		5	15360	0.033	-5.561		-5.040
E64d-Mock		2	14244	0.014	-2.525		15	16449	0.091	-4.716		-3.620
E64d-Mock		16	15244	0.105	-2.509		4	16899	0.024	-4.731		-3.620
E64d-Mock		24	14668	0.164	-2.498		26	16605	0.157	-4.701		-3.600
E64d-Mock		43	14588	0.295	-2.475		17	16933	0.100	-4.713		-3.594
E64d-Reo		19	13616	0.140	-8.510		41	5058	0.811	-8.677		-8.593
E64d-Reo		19	12552	0.151	-8.505		57	11638	0.490	-8.787		-8.646
E64d-Reo		37	12824	0.289	-8.444		29	4037	0.718	-8.708		-8.576
E64d-Reo		40	13350	0.300	-8.439		27	4413	0.612	-8.745		-8.592
E64d-Reo		0	11704	0.000	-6.496		27	14853	0.182	-7.563		-7.029
E64d-Reo		1	12067	0.008	-6.490		13	14459	0.090	-7.595		-7.043
E64d-Reo		5	12085	0.041	-6.470		20	14634	0.137	-7.579		-7.024
E64d-Reo		7	10207	0.069	-6.453		12	13824	0.087	-7.596		-7.025
E64d-Reo		14	13193	0.106	-6.059		59	13027	0.453	-8.046		-7.052
E64d-Reo		16	12506	0.128	-6.052		44	11593	0.380	-8.068		-7.060
E64d-Reo		20	12613	0.159	-6.042		31	12637	0.245	-8.108		-7.075
E64d-Reo		39	13159	0.296	-5.998		26	12956	0.201	-8.122		-7.060
E64d-Reo		10	13968	0.072	-5.841		23	12055	0.191	-6.508		-6.174
E64d-Reo		13	13819	0.094	-5.834		35	11627	0.301	-6.481		-6.158
E64d-Reo		15	13976	0.107	-5.830		23	11353	0.203	-6.505		-6.167
E64d-Reo		16	13404	0.119	-5.826		23	10884	0.211	-6.503		-6.164
E64d-Reo		0	10146	0.000	-5.495		23	14739	0.156	-6.293		-5.894
E64d-Reo		1	10139	0.010	-5.490		50	15005	0.333	-6.242		-5.866
E64d-Reo		2	9602	0.021	-5.484		16	15010	0.107	-6.307		-5.895
E64d-Reo		4	3424	0.117	-5.431		17	13892	0.122	-6.303		-5.867
E64d-Reo		0	13058	0.000	-5.396		23	15637	0.147	-7.640		-6.518
E64d-Reo		1	13256	0.008	-5.392		40	15159	0.264	-7.596		-6.494
E64d-Reo		1	12725	0.008	-5.392		9	15414	0.058	-7.673		-6.532
E64d-Reo		3	11514	0.026	-5.382		10	14164	0.071	-7.669		-6.525
E64d-Reo		11	14213	0.077	-4.905		19	10055	0.189	-6.805		-5.855
E64d-Reo		16	14977	0.107	-4.896		30	10870	0.276	-6.775		-5.835
E64d-Reo		17	14771	0.115	-4.893		20	9896	0.202	-6.800		-5.847

E64d-Reo		19	14741	0.129	-4.889		7	10461	0.067	-6.846		-5.867
E64d-Reo		1	11072	0.009	-4.526		27	15862	0.170	-5.525		-5.025
E64d-Reo		3	10351	0.029	-4.516		20	15151	0.132	-5.535		-5.026
E64d-Reo		10	11305	0.088	-4.489		39	16008	0.244	-5.506		-4.997
E64d-Reo		11	10907	0.101	-4.483		29	15819	0.183	-5.522		-5.002
E64d-Reo		7	14046	0.050	-2.519		24	16201	0.148	-4.703		-3.611
E64d-Reo		11	14437	0.076	-2.514		25	16099	0.155	-4.701		-3.608
E64d-Reo		14	14045	0.100	-2.510		21	16649	0.126	-4.708		-3.609
E64d-Reo		19	13687	0.139	-2.503		62	15391	0.403	-4.646		-3.574
Ebselen	46386980	810	11024	7.348	-1.139		3171	14917	21.258	-0.003		-0.571
Econazole nitrate	104170005	1778	16427	10.824	0.360		3805	17202	22.120	0.585		0.472
Edrophonium chloride	104170059	1409	14948	9.426	-0.180		3543	17431	20.326	-0.247		-0.213
Efavirenz	46386724	2482	16656	14.902	0.110		4212	16279	25.874	1.027		0.568
Enalapril maleate	104170123	1707	15881	10.749	0.235		3811	17452	21.837	0.075		0.155
Enalaprilat	46386741	2668	14384	18.548	0.108		3260	12213	26.693	-0.165		-0.029
Enrofloxacin	46386889	1266	11271	11.232	0.538		3104	13783	22.520	0.316		0.427
Epigallocatechin gallate	46386901	2362	13233	17.849	-0.666		3334	13124	25.404	-0.252		-0.459
Epirubicin hydrochloride	46386577	1455	4466	32.579	3.238		1978	6524	30.319	2.017		2.627
Eryped	104170095	1417	15546	9.115	-0.500		3753	17997	20.853	-0.333		-0.417
Escitalopram oxalate	46386725	2310	16807	13.744	-0.095		3766	17605	21.392	0.028		-0.033
Esmolol hydrochloride	46386551	2214	16325	13.562	-0.127		3468	16791	20.654	-0.136		-0.132
Esomeprazole magnesium	46386556	3664	17230	21.265	0.847		4711	17136	27.492	0.463		0.655
Estradiol valerate	104170058	3384	17807	19.004	0.254		4108	16173	25.400	-0.474		-0.110
Estrone 3-sulfate sodium salt	46386974	982	11179	8.784	-0.476		3070	15209	20.185	-0.284		-0.380
Eszopiclone	104170161	1230	11891	10.344	-0.019		3045	14489	21.016	-0.214		-0.116
Ethacrynic acid	104169948	1499	14710	10.190	0.173		3444	17222	19.998	-0.333		-0.080
Ethambutol	104170193	1677	16446	10.197	0.026		3566	17437	20.451	-0.040		-0.007
Ethionamide	104170006	1485	14825	10.017	-0.006		3826	16627	23.011	0.288		0.141
Ethylestrenol	46386573	1986	14191	13.995	-0.402		2309	12208	18.914	-0.421		-0.412
Ethynylestradiol	46386858	1171	14199	8.247	-0.724		3459	17165	20.151	-0.292		-0.508
Etodolac	104170216	1563	16286	9.597	-0.293		3439	17880	19.234	-0.496		-0.394
Etomidate	46386983	3082	15750	19.568	0.205		4229	15619	27.076	-0.053		0.076
Etomoxir	46386895	2941	15326	19.190	0.083		4161	14857	28.007	0.226		0.155
Etoposide	46386954	1703	9973	17.076	3.350		3478	11627	29.913	2.264		2.807
Exemestane	46386592	2393	16788	14.254	-0.318		3092	15021	20.585	0.149		-0.085
Ezetimibe	46386640	3137	16938	18.520	1.062		3069	14304	21.456	0.446		0.754
Famciclovir	46386745	2733	14827	18.433	-0.160		4242	15917	26.651	-0.181		-0.171
Famotidine	46386903	2802	14034	19.966	0.272		3316	13098	25.317	-0.282		-0.005
Felbamate	46386855	1428	14328	9.966	0.070		3544	16263	21.792	0.137		0.103
Felodipine	104170219	1343	12962	10.361	0.183		3708	17397	21.314	-0.200		-0.009
Fenofibrate	104169950	2158	15796	13.662	1.869		4542	16825	26.996	2.410		2.139
Fenoldopam mesylate	46386722	2283	16237	14.060	-0.039		3845	17450	22.034	0.172		0.066
Fenpiverinium bromide	46386658	2361	16907	13.965	-0.412		3142	15674	20.046	-0.035		-0.223
Fexofenadine hydrochloride	104170222	1463	13377	10.937	0.498		3809	15818	24.080	0.596		0.547
Finasteride	46386559	2914	16543	17.615	0.769		2869	14408	19.913	-0.080		0.344
Flecainide hydrochloride		3968	16962	23.393	1.790		4902	17170	28.550	0.825		1.308
Floxuridine	104170121	845	10139	8.334	-0.964		2319	11744	19.746	-0.304		-0.634
Flubendazole	46386742	492	6799	7.236	-3.534		1079	5714	18.883	-2.034		-2.784
Fluconazole	104170148	3150	17352	18.154	-0.020		4205	15356	27.383	0.001		-0.010
Flucytosine	46386766	1675	16534	10.131	-0.009		3390	16457	20.599	0.015		0.003
Fludarabine	104170131	1382	12438	11.111	0.594		3314	14001	23.670	0.478		0.536
Flumadine hydrochloride	104170172	2015	16454	12.246	1.116		4141	17269	23.979	1.281		1.198
Flumazenil	46386776	1304	13579	9.603	-0.098		3610	17269	20.905	-0.095		-0.097
Flunisolide	104170214	1386	15621	8.873	-0.633		3619	17420	20.775	-0.356		-0.494
Fluocinolone acetonide	104170060	2784	12011	23.179	1.598		4028	11561	34.841	1.786		1.692
Fluocinolone acetonide 21-acetate	104170119	1955	14055	13.910	2.001		3802	15636	24.316	1.407		1.704
Fluorometholone	104170223	1376	11690	11.771	0.955		3713	14544	25.529	1.013		0.984
Fluoxetine hydrochloride	104170213	1593	13765	11.573	0.847		4366	16390	26.638	1.333		1.090
Fluperlapine	46386904	2315	17112	13.529	-0.133		3680	17669	20.827	-0.097		-0.115
Fluphenazine dihydrochloride	46386937	1094	14435	7.579	-1.032		2960	17184	17.225	-1.059		-1.046
Flurbiprofen	46386788	2543	17308	14.693	-0.177		3101	15382	20.160	0.004		-0.086
Flutamide	104169949	3197	17958	17.803	-0.133		3812	14003	27.223	-0.038		-0.085
Fluticasone propionate	46386601	2273	12537	18.130	0.681		3563	14569	24.456	0.711		0.696
Fluvastatin	104170157	1507	9966	15.121	2.448		3829	12054	31.765	2.749		2.599
Fluvoxamine maleate	46386804	2405	16566	14.518	0.042		3839	16831	22.809	0.344		0.193
Folic acid	104169953	1503	12411	12.110	1.141		3962	17719	22.360	0.101		0.621
Formoterol fumarate dihydrate	46386732	2300	16625	13.835	-0.079		3431	17180	19.971	-0.288		-0.184
Furosemide	104169951	1515	14592	10.382	0.194		4020	17837	22.537	0.152		0.173
Gabexate mesilate	46386710	1302	14447	9.012	-0.371		3679	16708	22.019	0.197		-0.087
Galanthamine hydrobromide	46386805	3318	17455	19.009	-0.152		4322	16979	25.455	-0.235		-0.193
Ganciclovir	104170145	2976	16482	18.056	-0.051		3716	13930	26.676	-0.169		-0.110
Gatifloxacin	104170200	1402	14916	9.399	-0.344		3584	16724	21.430	-0.167		-0.256
Gemfibrozil	104170063	2952	17274	17.089	-0.362		3951	14987	26.363	-0.244		-0.303
Glimepiride	46386690	3503	17841	19.635	0.125		4556	17784	25.619	-0.179		-0.027
Glipizide	104170062	1569	14993	10.465	0.169		3298	17005	19.394	-0.436		-0.133
Glyburide	104170064	3199	16756	19.092	0.282		3881	14235	27.264	-0.028		0.127
Glycopyrronium bromide	46386646	3024	16125	18.753	-0.057		4127	14872	27.750	0.149		0.046
Goserelin acetate		2381	13503	17.633	-0.761		3623	13699	26.447	0.105		-0.328
GR 79236	46387015	1418	14439	9.821	-0.346		3540	16883	20.968	-0.231		-0.289
GR 89696 fumarate	46386996	3147	16489	19.085	0.050		4416	15588	28.329	0.323		0.186
Granisetron hydrochloride	46386545	2521	16332	15.436	0.204		3864	16647	23.211	0.434		0.319
Griseofulvin	104170114	1557	15416	10.100	-0.025		3432	17196	19.958	-0.224		-0.125
Halometasone monohydrate	46386633	1210	9648	12.541	1.258		3721	14437	25.774	1.180		1.219
Haloperidol hydrochloride	46386806	3242	17055	19.009	0.836		4869	16880	28.845	1.688		1.262
Hexachlorophene	104170010	668	11131	6.001	-2.207		2303	14676	15.692	-1.819		-2.013
Hexamethylenebisacetamide	46386869	2131	15158	14.059	-0.040		3439	15721	21.875	0.136		0.048

Homoharringtonine	46386877	4	5267	0.076	-5.840		13	6000	0.217	-6.502		-6.171
Homoveratrylamine	46386943	3201	16609	19.273	0.110		4452	16124	27.611	0.107		0.109
Honokiol	46386673	3240	17356	18.668	-0.085		4443	16666	26.659	-0.179		-0.132
HTMT dimaleate	46386998	2404	15066	15.956	0.232		2954	12892	22.913	0.943		0.588
Huperzine A	46386885	3457	18159	19.037	-0.139		4394	17531	25.064	-0.369		-0.254
Hydrochlorothiazide	104170008	1664	15816	10.521	0.270		3950	17170	23.005	0.287		0.278
Hydrocortisone	104169954	1339	10992	12.182	1.180		3490	14090	24.769	0.795		0.987
Hydrocortisone 17-valerate	104170102	3105	14507	21.403	1.027		4462	13993	31.887	1.079		1.053
Hydrocortisone hemisuccinate	104170065	2546	13105	19.428	0.391		3749	11789	31.801	1.058		0.724
Hydroflumethiazide	104169994	1838	15674	11.726	0.840		3573	15553	22.973	0.904		0.872
Hydroxyzine pamoate	104170009	1458	15656	9.313	-0.392		3730	17262	21.608	-0.116		-0.254
Hyperoside	46386811	2219	16143	13.746	-0.095		3619	17417	20.779	-0.108		-0.101
Ibuprofen	104169956	1211	12140	9.975	0.074		3315	14863	22.304	0.271		0.172
Icariin	46386578	3021	16847	17.932	0.871		3188	15364	20.750	0.205		0.538
Idarubicin hydrochloride	46386733	1299	7517	17.281	-0.531		2016	6905	29.196	0.583		0.026
Idebenone	46386682	1089	11578	9.406	-0.606		3069	14031	21.873	0.088		-0.259
Ifenprodil hemitartrate	46386807	3527	17496	20.159	1.592		3985	15278	26.083	2.023		1.808
Imatinib mesylate	46386639	1367	16866	8.105	-1.093		1943	16939	11.471	-2.181		-1.637
Imipramine hydrochloride	104170068	1318	13157	10.017	-0.069		3159	15273	20.684	0.047		-0.011
Indapamide	104170066	1266	12595	10.052	-0.051		3207	15264	21.010	0.169		0.059
Indatraline hydrochloride	46386808	2606	14520	17.948	0.649		4100	15160	27.045	1.288		0.968
Indinavir sulfate	46386606	1991	15283	13.028	-0.222		3285	15502	21.191	-0.016		-0.119
Indirubin	46386581	4016	17120	23.458	1.819		4837	16452	29.401	1.117		1.468
Indomethacin hydrate	46386809	1190	11144	10.678	0.191		3126	14965	20.889	-0.259		-0.034
Ipidacrine	46386925	3067	17058	17.980	-0.306		4206	15986	26.311	-0.283		-0.295
Ipratropium bromide	104170067	1427	14791	9.648	-0.208		3695	17250	21.420	-0.170		-0.189
Ipriflavone	46386694	1729	16681	10.365	0.116		3512	17331	20.264	-0.110		0.003
Irbesartan	46386566	2971	15576	19.074	0.046		4090	14987	27.290	0.011		0.029
Irinotecan hydrochloride	46386616	2455	12612	19.466	0.917		3802	13669	27.815	1.459		1.188
Irsogladine maleate	46386698	2734	16128	16.952	-0.637		4139	15342	26.978	-0.083		-0.360
Isoniazid	104170011	1401	15084	9.288	-0.457		3400	16541	20.555	-0.001		-0.229
Isoproterenol hydrochloride	104170013	1458	15345	9.501	-0.546		3665	16779	21.843	0.077		-0.234
Isoquercitrin	46386780	2462	17543	14.034	-0.390		3195	15681	20.375	0.077		-0.156
Isotretinoin	104170133	3003	16374	18.340	0.040		4090	14612	27.991	0.146		0.093
Isradipine	46386602	2810	16563	16.966	-0.633		4187	16092	26.019	-0.371		-0.502
Itavastatin calcium	46386827	3368	14431	23.339	1.766		4277	13469	31.754	1.923		1.844
Itopride hydrochloride	46386560	1919	14417	13.311	-0.172		3654	14620	24.993	0.831		0.329
Itraconazole	46386736	1620	16098	10.063	-2.854		3138	14302	21.941	-1.595		-2.224
Ketoconazole	46386810	3113	17103	18.201	-0.235		4578	16045	28.532	0.384		0.074
Ketoprofen	104169957	1620	15763	10.277	-0.060		3798	17480	21.728	0.037		-0.012
Ketorolac tromethamine	46386614	3361	17163	19.583	1.406		2943	15545	18.932	-0.415		0.496
Ketotifen fumarate	46386834	2491	13461	18.505	-0.375		3478	13145	26.459	0.109		-0.133
Kitasamycin	46386711	964	12174	7.919	-1.185		3038	14682	20.692	0.050		-0.568
L-694,247	46386999	3187	16932	18.822	-0.035		4699	16121	29.148	0.569		0.267
L-NMMA acetate	46386919	2105	14288	14.733	0.080		3395	16221	20.930	-0.074		0.003
L-Thyroxine	104169983	1335	14340	9.310	-0.666		3871	16941	22.850	0.433		-0.117
Labetalol hydrochloride	104170069	1732	16631	10.414	0.212		4254	18003	23.629	0.466		0.339
Lacidipine	46386664	2424	16867	14.371	-1.468		3620	15853	22.835	-1.327		-1.397
Lamivudine	46386600	2283	16380	13.938	-0.061		3448	17043	20.231	-0.230		-0.145
Lamotrigine	46386680	2936	16510	17.783	-0.369		3966	15381	25.785	-0.441		-0.405
Lansoprazole	46386562	2341	16049	14.587	0.054		3913	16039	24.397	0.698		0.376
Latanoprost	46386728	2911	17585	16.554	0.426		3097	15675	19.758	-0.133		0.146
Letrozole	46386665	1358	14055	9.662	-0.071		3647	17537	20.796	-0.124		-0.097
Levetiracetam	46386557	2587	17536	14.753	-0.157		3087	15809	19.527	-0.212		-0.185
Levocetirizine	46386593	3310	16928	19.553	0.200		4382	16426	26.677	-0.173		0.014
Levofloxacin	46386771	1318	13809	9.544	-0.125		3684	17428	21.138	-0.034		-0.080
Levonorgestrel	46386677	1580	15844	9.972	-0.251		3432	16645	20.619	-0.354		-0.303
Levosulpiride	46386685	1758	16346	10.755	0.239		3463	15864	21.829	0.073		0.156
Lidocaine	46386868	3657	17618	20.757	0.622		4461	17571	25.388	-0.257		0.182
Lincomycin hydrochloride	104170115	1624	16229	10.007	-0.075		3508	17724	19.792	-0.287		-0.181
Linezolid	46386641	3303	14991	22.033	2.198		2957	12619	23.433	1.120		1.659
Linopirdine dihydrochloride	46386985	2069	16675	12.408	-0.916		2956	15692	18.838	-0.447		-0.681
Lobeline hydrochloride	46386920	1807	14748	12.253	1.124		4381	17043	25.706	1.162		1.143
Lofepramine	46386649	3187	17699	18.007	0.896		2705	15013	18.018	-0.726		0.085
Lofexidine hydrochloride	46386875	3059	16085	19.018	0.028		4271	15272	27.966	0.214		0.121
Lomerizine dihydrochloride	46386707	1015	14579	6.962	-1.317		3289	17537	18.755	-0.658		-0.988
Lomifylline	46386754	1827	15950	11.455	0.677		3563	17066	20.878	-0.263		0.207
Loperamide hydrochloride	104170070	2	14905	0.013	-5.488		26	18123	0.143	-6.297		-5.892
Loratadine	46386837	2030	16719	12.142	-0.379		3573	17392	20.544	-0.160		-0.270
Lorazepam	46386878	2252	13012	17.307	-0.906		3480	12937	26.900	0.260		-0.323
Losartan potassium	46386652	2108	14843	14.202	-0.014		3156	15622	20.202	-0.236		-0.125
Loteprednol etabonate	46386647	1328	11144	11.917	0.970		3518	13599	25.870	1.205		1.087
Lovastatin	104170211	1645	12430	13.234	1.757		4152	13597	30.536	2.455		2.106
Loxapine succinate	46386931	1555	14211	10.942	0.356		3677	16336	22.509	0.312		0.334
Loxoprofen sodium	46386612	2312	16496	14.016	-0.047		3643	17449	20.878	-0.086		-0.067
LY 171883	46386838	2692	14115	19.072	0.276		3472	12359	28.093	0.170		0.223
Mafenide acetate	104170207	1738	15802	10.999	0.532		4153	18276	22.724	0.206		0.369
Maltol	46386945	3214	17058	18.842	-0.029		4408	16529	26.668	-0.176		-0.102
Maprotiline hydrochloride	46386839	2745	16836	16.304	0.358		4048	17362	23.315	0.457		0.407
MDL 73005EF hydrochloride	46387017	1865	15845	11.770	0.874		3990	16748	23.824	0.776		0.825
Mebendazole	104170137	547	5683	9.625	-2.765		988	4952	19.952	-1.778		-2.272
Mecillinam	46386744	1250	14049	8.897	-0.424		3844	17431	22.053	0.205		-0.109
Meclizine hydrochloride	104170138	3109	17619	17.646	-0.183		3906	15762	24.781	-0.622		-0.403
Meclofenamic acid sodium salt	104170147	3175	17752	17.885	-0.106		4181	15751	26.544	-0.200		-0.153
Medroxyprogesterone	46387018	2611	15918	16.403	0.377		3418	14982	22.814	0.909		0.643
Medroxyprogesterone 17-acetate	104170072	1753	14937	11.736	0.936		4507	17456	25.819	1.097		1.016

Medrysone	104170097	1651	13688	12.062	1.114		4070	16558	24.580	0.740		0.927
Mefenamic acid	104170015	3235	17715	18.261	0.015		3981	13921	28.597	0.291		0.153
Mefloquine hydrochloride	104170120	3535	16701	21.166	0.950		5403	14731	36.678	2.225		1.588
Megestrol acetate	46386702	2901	15277	18.989	0.019		4088	15020	27.217	-0.011		0.004
Meloxicam	104170196	800	9147	8.746	-0.702		3156	14630	21.572	-0.126		-0.414
Memantine hydrochloride	104170178	3512	17820	19.708	0.481		4374	14943	29.271	0.452		0.467
Mepenzolate bromide	104170016	2801	16437	17.041	-0.378		4068	15145	26.860	-0.125		-0.251
Mepirizole	46386965	2558	12914	19.808	0.282		3465	12506	27.707	0.136		0.209
Mepivacaine hydrochloride	46386949	1650	16543	9.974	-0.092		3608	17548	20.561	0.001		-0.046
Mercaptopurine	104170111	362	13660	2.650	-3.987		1619	15940	10.157	-3.893		-3.940
Meropenem	46386666	2387	13278	17.977	-0.307		3333	12198	27.324	0.021		-0.143
Mesalamine	46386870	1314	12644	10.392	0.130		3233	15678	20.621	0.024		0.077
Mesna	104170146	1632	15438	10.571	0.124		3769	17093	22.050	0.151		0.137
Mesoridazine besylate	46386921	1046	12788	8.180	-1.046		3178	15379	20.665	0.040		-0.503
Mestanolone	46386759	2276	14641	15.545	0.099		2810	13458	20.880	0.249		0.174
Mestranol	46386940	678	13750	4.931	-2.254		2697	17223	15.659	-1.469		-1.862
Metaproterenol	104170149	3031	16220	18.687	0.152		3788	13501	28.057	0.162		0.157
Methazolamide	104170116	1007	10841	9.289	-0.405		3205	14456	22.171	0.046		-0.179
Methimazole	104170134	3276	18019	18.181	-0.011		4141	15570	26.596	-0.188		-0.099
Methocarbamol	104170007	1488	15297	9.727	-0.165		3898	17295	22.538	0.152		-0.006
Methotrexate trihydrate	46386835	1717	15835	10.843	0.294		3546	16870	21.020	-0.213		0.040
Methoxsalen	104170150	2978	16876	17.646	-0.183		3827	14673	26.082	-0.311		-0.247
Methylandrostenediol	46386580	2850	12857	22.167	1.041		3678	12005	30.637	1.016		1.029
Methyldopa	104170018	2444	14023	17.429	-0.253		3633	13050	27.839	0.110		-0.072
Methylperone hydrochloride	46387011	1506	13979	10.773	0.442		3941	16251	24.251	0.781		0.611
Methylprednisolone	104170189	1682	13252	12.692	1.460		3898	14438	26.998	1.436		1.448
Methylprednisolone acetate	104170126	1811	13815	13.109	1.713		3907	15185	25.729	1.448		1.580
Methyltestosterone	46386739	3031	13313	22.767	1.235		4375	15898	27.519	0.080		0.657
Metoclopramide hydrochloride	104170017	3179	17557	18.107	-0.035		4622	16202	28.527	0.274		0.120
Metronidazole	46386860	3376	17546	19.241	-0.049		4364	16694	26.141	0.000		-0.025
Metyrapone	104169960	1537	15152	10.144	0.064		3747	16949	22.107	0.028		0.046
Mevastatin	46386660	1474	10176	14.485	2.155		3831	12663	30.253	2.353		2.254
Mexiletine hydrochloride	104170180	1788	15440	11.580	0.762		3967	17583	22.562	0.750		0.756
Miconazole nitrate	104169959	1329	12525	10.611	0.246		3228	14514	22.241	0.630		0.438
Midazolam hydrochloride	46386603	1166	11293	10.325	0.235		3331	14944	22.290	0.268		0.251
Midodrine hydrochloride	104170071	1654	15407	10.735	0.388		3881	17777	21.832	-0.051		0.168
Miglitol	46386758	1683	16187	10.397	0.015		3936	17524	22.461	0.295		0.155
Milnacipran hydrochloride	46386905	2373	16331	14.531	0.044		3652	17181	21.256	-0.002		0.021
Milrinone	46386629	2558	17465	14.646	-0.192		2913	14905	19.544	-0.206		-0.199
Minocycline hydrochloride	104169958	1316	13110	10.038	0.006		3721	17005	21.882	-0.037		-0.016
Minoxidil	104170184	1498	14862	10.079	0.028		3932	17294	22.736	0.209		0.119
Mirtazapine	46386716	2168	14351	15.107	-0.043		2499	13117	19.052	-0.374		-0.208
Mitoxantrone hydrochloride	104170122	1519	7801	19.472	0.405		1473	7316	20.134	-1.735		-0.665
MK 886	46386984	2225	16686	13.335	-0.168		3545	17518	20.236	-0.229		-0.198
Moclobemide	46386631	1451	14112	10.282	0.215		3449	16498	20.906	-0.095		0.060
Modafinil	46386605	2922	13583	21.512	0.831		3457	12518	27.616	0.109		0.470
Molindone hydrochloride	104170156	2485	13657	18.196	-0.006		3705	12713	29.143	0.422		0.208
Montelukast sodium	46386714	3278	16347	20.053	0.361		4451	15627	28.483	0.369		0.365
Mosapride citrate	46386693	2441	16681	14.633	0.062		3659	16851	21.714	0.100		0.081
Moxifloxacin hydrochloride	46386670	2387	15091	15.817	0.272		3463	16103	21.505	0.054		0.163
Moxonidine hydrochloride	46386777	2092	15165	13.795	-0.086		3549	14895	23.827	0.571		0.242
Mupirocin	104170118	1230	12303	9.998	-0.080		3098	14713	21.056	0.187		0.053
Nabumetone	104170077	1711	15624	10.951	0.506		3813	17857	21.353	-0.189		0.158
Nadolol	104169962	1093	12526	8.726	-0.714		3539	17585	20.125	-0.543		-0.628
Nafadotride	46387001	2950	16965	17.389	0.550		4479	17769	25.207	0.878		0.714
Nafcillin sodium	104170104	1637	15770	10.380	0.004		3884	17309	22.439	0.288		0.146
Naftopidil	46386715	996	10819	9.206	-0.281		3309	15065	21.965	0.182		-0.050
Nalbuphine hydrochloride	46386933	3352	16951	19.775	0.187		4136	16276	25.412	-0.250		-0.031
Nalidixic acid	104169992	3257	17801	18.297	0.027		4096	15730	26.039	-0.321		-0.147
Naloxone hydrochloride	104170085	1379	14336	9.619	-0.473		3329	16673	19.966	-0.584		-0.528
Naltrexone hydrochloride	104170191	1573	16392	9.596	-0.293		3591	18256	19.670	-0.332		-0.313
Naltrindole hydrochloride hydrate	46386854	1887	13284	14.205	-2.280		3098	13194	23.480	-0.911		-1.596
Naphazoline hydrochloride	104170021	1552	14086	11.018	0.555		3902	16854	23.152	0.493		0.524
Naproxen sodium	46386948	2504	13207	18.960	0.009		3287	12189	26.967	-0.086		-0.038
Nateglinide	46386701	1765	16319	10.816	0.355		3462	16807	20.599	0.015		0.185
Nefazodone hydrochloride	46386669	2322	15117	15.360	0.191		3663	15362	23.845	0.575		0.383
Nelfinavir mesylate	46386712	2036	16117	12.633	-0.292		3297	17605	18.728	-0.565		-0.428
Nevirapine	46386569	2403	17356	13.845	-0.451		2678	12409	21.581	0.489		0.019
Nialamide	46386894	3320	17024	19.502	0.184		4245	16216	26.178	-0.323		-0.070
Nicardipine hydrochloride	104170076	949	10972	8.649	-0.755		3040	14564	20.873	-0.327		-0.541
Nicorandil	46386683	2717	15586	17.432	-0.482		4311	16079	26.811	-0.133		-0.308
Nicotinamide	46386893	1704	16231	10.498	0.078		3655	17408	20.996	-0.221		-0.072
Nicotine	104170075	895	10335	8.660	-0.750		2901	14876	19.501	-0.722		-0.736
Nicotinic acid	104170022	3113	17453	17.836	-0.122		4345	15782	27.531	0.036		-0.043
Nifedipine	46386790	3507	17467	20.078	0.321		4537	17746	25.566	-0.197		0.062
Nifekalant hydrochloride	46386697	1956	14403	13.581	-0.124		3278	15699	20.880	-0.085		-0.105
Nimetazepam	46386768	1400	14294	9.794	-0.010		3564	16891	21.100	-0.044		-0.027
Nimodipine	46386964	2398	14611	16.412	0.380		3062	12963	23.621	1.184		0.782
Nisoldipine	46386699	1099	10292	10.678	0.191		3201	13652	23.447	0.643		0.417
Nitazoxanide	46386689	1162	16086	7.224	-1.972		2814	16695	16.855	-1.682		-1.827
Nitrazepam	46386691	2520	13585	18.550	0.108		3560	12928	27.537	0.037		0.073
Nitrendipine	46386549	1097	13063	8.398	-0.654		3421	16311	20.974	-0.077		-0.366
Nitrofurantoin	104170019	3189	18074	17.644	-0.184		3982	15196	26.204	-0.282		-0.233
Nizatidine	46386765	3087	15604	19.783	0.274		4068	16131	25.219	-0.611		-0.168
Nobiletin	46386719	3907	15309	25.521	2.121		5503	14526	37.884	3.191		2.656
Norfloxacin	104169961	1591	15487	10.273	0.067		3431	16647	20.610	0.020		0.043

Nornicotine	46386896	2192	16608	13.198	-0.192		3567	17093	20.868	-0.088		-0.140
Nortriptyline hydrochloride	104170020	1231	14551	8.460	-0.626		3002	17635	17.023	-1.112		-0.869
Ofloxacin	104169964	1633	15865	10.293	0.145		3741	17590	21.268	-0.214		-0.034
Olanzapine	46386668	3271	16989	19.254	1.299		2913	14465	20.138	-0.003		0.648
Oligomycin A		3757	15432	24.346	2.212		6101	14923	40.883	5.050		3.631
Olmesartan medoxomil	46386651	3174	17601	18.033	0.904		3379	16568	20.395	0.084		0.494
Olopatadine hydrochloride	46386826	2175	14717	14.779	-0.149		2887	12864	22.442	0.782		0.317
Omeprazole	46386973	1295	13231	9.788	-0.013		3563	16519	21.569	0.079		0.033
Ondansetron	104170204	1905	12399	15.364	2.774		3981	14475	27.503	2.599		2.687
Orlistat	46386654	2079	17662	11.771	-1.122		2629	15259	17.229	-0.995		-1.059
Ormetoprim	46386708	1491	14448	10.320	-0.034		3849	16375	23.505	0.664		0.315
Ornidazole	46386947	3046	16179	18.827	-0.034		3983	14968	26.610	-0.193		-0.113
Orphenadrine hydrochloride	104169963	1558	15614	9.978	-0.027		4009	17421	23.012	0.289		0.131
Otenzepad	46386986	2222	17083	13.007	-0.722		2887	15329	18.834	-0.448		-0.585
Oxacillin sodium	104170106	1079	11166	9.663	-0.200		3015	14690	20.524	-0.428		-0.314
Oxaprozin	46386783	1453	14267	10.184	0.170		3710	16752	22.147	0.230		0.200
Oxcarbazepine	46386767	2604	16942	15.370	0.043		3366	16383	20.546	0.136		0.089
Oxiconazole nitrate	46386704	2120	16329	12.983	1.634		4114	17076	24.092	0.871		1.252
Oxybutynin hydrochloride	104170078	950	10749	8.838	-0.652		3296	14965	22.025	0.004		-0.324
Oxymetholone	46386778	2604	14169	18.378	0.053		3143	11712	26.836	-0.131		-0.039
Oxyphenonium bromide	46386961	2325	16919	13.742	-0.096		3394	17348	19.564	-0.379		-0.237
Oxytetracycline hydrochloride	104170024	1497	15288	9.792	-0.189		3528	17357	20.326	-0.087		-0.138
Ozagrel hydrochloride	46386611	2084	14966	13.925	-0.063		3442	16273	21.152	-0.025		-0.044
P1075	46386997	2710	17582	15.413	0.057		3597	13836	25.997	1.994		1.025
Palonosetron hydrochloride	46386820	3454	13106	26.354	2.389		4329	11915	36.332	2.726		2.557
Pancuronium dibromide	46386853	2145	15812	13.566	-0.127		3535	17381	20.338	-0.206		-0.166
Pantoprazole sodium	46386609	2629	17593	14.943	-0.095		3220	15939	20.202	0.018		-0.039
Parecoxib sodium	46386785	2528	13729	18.414	-0.167		3220	11854	27.164	-0.027		-0.097
Paroxetine maleate	46386841	3473	14164	24.520	2.289		4472	13503	33.119	2.391		2.340
Pazufloxacin	46386755	3116	17247	18.067	-0.278		4340	16413	26.442	-0.244		-0.261
PD 81723	46386976	2989	15383	19.431	0.161		3931	14548	27.021	-0.070		0.045
Pefloxacin mesylate	46386589	2281	16844	13.542	-0.131		3642	17396	20.936	-0.073		-0.102
Pemolide	46386687	3384	17585	19.244	-0.048		4288	17515	24.482	-0.568		-0.308
Penciclovir	46386598	2215	16122	13.739	-0.096		3430	17252	19.882	-0.308		-0.202
Penicillin G potassium	104170081	1504	15172	9.913	-0.063		3932	17908	21.957	-0.015		-0.039
Penicillin V	104170199	1552	15104	10.275	0.136		3702	16969	21.816	-0.056		0.040
Pentoxifylline	46386861	2208	16236	13.599	-0.121		3602	17495	20.589	-0.150		-0.136
Pergolide mesylate	46386979	3319	17667	18.786	-0.047		4655	16289	28.578	0.397		0.175
Perospirone hydrochloride	46386671	2604	16405	15.873	0.282		4834	17151	28.185	1.541		0.912
Perphenazine	104169970	1055	15197	6.942	-1.704		2645	16662	15.874	-1.753		-1.729
Phenelzine sulfate	46386907	3451	15941	21.649	1.017		4143	15468	26.784	0.221		0.619
Phenothiazine	46386888	1134	10975	10.333	-0.026		3034	14137	21.461	-0.057		-0.041
Phenoxybenzamine hydrochloride	104170096	1596	15233	10.477	0.246		3768	17131	21.995	-0.004		0.121
Phenprobamate	46386753	1547	14819	10.439	0.041		3616	16843	21.469	-0.054		-0.007
Phentolamine mono-hydrochloride	104170130	1865	16458	11.332	0.630		3682	17287	21.299	0.278		0.454
Phylloquinone	104170094	1429	13002	10.991	0.448		3191	14727	21.668	0.415		0.432
Physostigmine hemisulfate	46386842	2271	16531	13.738	-0.096		3688	17537	21.030	-0.052		-0.074
Piceid	46386700	1090	11519	9.463	-0.571		3212	14860	21.615	-0.003		-0.287
Picrotin - Picrotoxinin	46386843	2324	17242	13.479	-0.569		3144	16076	19.557	-0.201		-0.385
Pidotimod	46386775	2951	16971	17.388	0.696		3041	15615	19.475	-0.229		0.233
Pilocarpine hydrochloride	46386789	3026	16634	18.192	-0.238		4383	16737	26.187	-0.320		-0.279
Pinacidil monohydrate	46387019	1383	14649	9.441	-0.173		3727	16977	21.953	0.179		0.003
Pindolol	104169965	1476	16390	9.005	-0.560		3651	17465	20.905	-0.318		-0.439
Pioglitazone hydrochloride	46386618	2438	15675	15.553	0.225		3424	15468	22.136	0.194		0.210
Piperacillin sodium	104169975	1693	16334	10.365	-0.006		3702	17114	21.631	0.003		-0.001
Pirenperone	46386967	1645	14160	11.617	0.831		4142	16094	25.736	1.170		1.001
Piribedil hydrochloride	46386844	2441	16388	14.895	0.108		3423	16891	20.265	-0.222		-0.057
Piroxicam	46386918	1475	14744	10.004	0.087		3713	16839	22.050	0.205		0.146
Pizotyline maleate	46386908	1999	16024	12.475	-0.320		3105	16837	18.442	-0.629		-0.474
Podofilox	104170173	320	8761	3.653	-3.454		804	7388	10.883	-3.622		-3.538
Pralidoxime chloride	104170029	1621	15961	10.156	0.005		3546	17686	20.050	-0.190		-0.093
Pramipexole	46386856	2401	13318	18.028	-0.586		3433	12527	27.405	0.433		-0.077
Pravastatin sodium	46386713	3044	15724	19.359	0.138		4143	14664	28.253	0.300		0.219
Praziquantel	104169966	3130	17786	17.598	-0.198		4048	15347	26.376	-0.240		-0.219
Prazosin hydrochloride hydrate	46386845	3629	16094	22.549	1.416		4540	15725	28.871	0.936		1.176
Prednisolone	104169971	1662	13821	12.025	1.094		3835	14856	25.814	1.096		1.095
Prednisolone acetate	104169968	3297	15429	21.369	1.016		4083	13372	30.534	0.755		0.885
Prednisolone sodium succinate	46386971	2927	13113	22.321	1.322		3615	11535	31.339	0.947		1.135
Prednisone	104169973	1758	16554	10.620	0.324		4033	17689	22.799	0.227		0.276
Prilocaine hydrochloride	104169972	1673	15884	10.533	0.277		3951	17328	22.801	0.228		0.252
Primaquine diphosphate	104170105	2640	16035	16.464	-0.564		3702	15673	23.620	-0.900		-0.732
Primidone	104170030	1703	16729	10.180	0.017		3647	17734	20.565	0.003		0.010
Priscoline hydrochloride	104170110	1021	10455	9.766	-0.144		3263	14392	22.672	0.191		0.023
Probenecid	104170028	1796	16240	11.059	0.565		3519	16280	21.615	-0.114		0.226
Procainamide hydrochloride	104170033	2885	13376	21.568	1.080		3456	12776	27.051	-0.079		0.500
Procaine hydrochloride	104170025	1712	15274	11.209	0.564		3722	16703	22.283	0.646		0.605
Procarbazine hydrochloride	46386582	3363	16957	19.833	0.213		4485	17121	26.196	0.019		0.116
Prochlorperazine maleate	46386924	1940	16467	11.781	-0.443		3026	17183	17.610	-0.814		-0.628
Procyclidine hydrochloride	104170083	1732	16626	10.417	0.213		4199	17681	23.749	0.501		0.357
Procysteine	46386866	1520	14734	10.316	0.231		3593	16817	21.365	0.025		0.128
Progesterone	46386909	2417	16312	14.817	0.095		3619	16449	22.001	0.164		0.129
Promethazine hydrochloride	104169969	1178	14176	8.310	-0.942		3344	16771	19.939	-0.596		-0.769
Propafenone	104170080	1517	15143	10.018	-0.006		4012	17509	22.914	0.260		0.127
Propantheline bromide	104170027	1582	15486	10.216	0.036		3682	17648	20.864	0.114		0.075
Propofol	104169947	1830	15100	12.119	1.093		3959	16763	23.617	0.703		0.898
Propranolol hydrochloride	104170185	1855	14514	12.781	1.507		4212	16599	25.375	1.323		1.415

Propylthiouracil	104170031	1692	16488	10.262	0.061		3634	18081	20.098	-0.172		-0.056
Prostaglandin E1	46386879	1063	11375	9.345	-0.644		2974	14510	20.496	-0.398		-0.521
Proxymetacaine	104170084	1106	10372	10.663	0.348		3328	14522	22.917	0.261		0.305
Pterostilbene	46386623	2289	15874	14.420	-0.265		2693	14379	18.729	-0.484		-0.374
Pyrazinamide	104170032	1369	14359	9.534	-0.271		3800	17040	22.300	0.084		-0.093
Pyridostigmine bromide	104170079	1599	15678	10.199	0.094		4027	17874	22.530	0.150		0.122
Pyrimethamine	104170026	922	14910	6.184	-2.108		2532	16506	15.340	-1.953		-2.030
Quetiapine fumarate	46386812	3284	17269	19.017	-0.149		4498	17158	26.215	0.026		-0.061
Quinapril hydrochloride	104170220	1558	14674	10.617	0.250		3412	16349	20.870	0.117		0.183
Quinidine	104169976	1382	14939	9.251	-0.703		3793	17266	21.968	0.122		-0.291
R(+)-SCH-23390 hydrochloride	46387007	3418	16212	21.083	0.767		4412	15795	27.933	0.614		0.690
Rabeprazole	46386636	1537	14361	10.703	0.409		3644	17186	21.203	-0.017		0.196
Racecadotril	46386930	1380	14510	9.511	-0.141		3292	16946	19.426	-0.482		-0.312
Racepinephrine	104170169	2693	16170	16.654	-0.502		3921	14187	27.638	0.061		-0.220
Raclopride	46386981	2553	13726	18.600	-0.333		3711	13507	27.475	0.457		0.062
Raloxifene hydrochloride	104170163	1046	15617	6.698	-2.302		1913	17668	10.827	-3.808		-3.055
Raltitrexed	46386823	2859	15993	17.877	-0.339		4071	14890	27.340	0.026		-0.157
Ramipril	46386770	2560	17448	14.672	-0.183		3105	15843	19.599	-0.187		-0.185
Ranitidine hydrochloride	104169977	2407	14211	16.938	-0.411		3450	12601	27.379	-0.001		-0.206
Ranolazine dihydrochloride	46386552	3242	16939	19.139	-0.094		4279	16614	25.755	-0.132		-0.113
Remacemide hydrochloride	46386987	3053	15769	19.361	0.004		4167	15840	26.307	0.057		0.030
Repaglinide	46386564	1142	13794	8.279	-0.709		2659	16437	16.177	-1.333		-1.021
Resveratrol	46386962	1290	13845	9.317	-0.661		3226	16752	19.257	-0.834		-0.748
Ribavirin	104170186	1278	14872	8.593	-0.826		3259	17194	18.954	-0.600		-0.713
Rifabutin	104170218	1300	14619	8.893	-0.927		3630	16928	21.444	-0.063		-0.495
Rifampicin	104169978	2989	17337	17.241	-0.313		3718	14201	26.181	-0.287		-0.300
Rifapentine	104170198	1007	10807	9.318	-0.389		2901	14319	20.260	-0.504		-0.447
Rifaximin	46386615	3054	16569	18.432	-0.161		4036	14831	27.213	-0.012		-0.086
Riluzole hydrochloride	46386847	2538	16881	15.035	0.133		3737	17568	21.272	0.002		0.067
Rimcazole dihydrochloride	46387003	2230	13542	16.467	-1.278		3292	12812	25.695	-0.153		-0.715
Risperidone	46386613	3150	14530	21.679	2.084		2838	11664	24.331	1.426		1.755
Ritonavir	46386817	2855	17818	16.023	-1.475		3533	17545	20.137	-2.056		-1.766
Rizatriptan benzoate	46386632	2562	17169	14.922	-0.102		3116	15757	19.775	-0.127		-0.115
Rofecoxib	46386634	2871	17828	16.104	0.280		3170	16115	19.671	-0.163		0.059
Rolipram	46386779	1524	14765	10.322	0.233		3619	16418	22.043	0.203		0.218
Rolitetracycline	46386966	1496	15066	9.930	0.053		3476	16277	21.355	0.023		0.038
Ropivacaine hydrochloride	46386542	2208	16518	13.367	-0.162		3732	17237	21.651	0.086		-0.038
Rosiglitazone maleate	46386628	2398	16297	14.714	0.076		3493	16880	20.693	-0.127		-0.025
Roxatidine acetate hydrochloride	46386565	3278	16946	19.344	-0.004		4162	16350	25.456	-0.234		-0.119
Ru 24969 hemisuccinate	46387004	1340	15946	8.403	-0.927		3019	16410	18.397	-0.809		-0.868
RU-486	46386955	1977	14380	13.748	1.815		4386	16709	26.249	1.304		1.560
Rufloxacin hydrochloride	46386706	1713	16054	10.670	0.186		3576	16834	21.243	-0.134		0.026
Rutin	46386546	1570	14312	10.970	0.533		3663	17247	21.238	-0.008		0.262
S(-)-Timolol maleate	104170090	1186	15171	7.818	-1.211		3368	17273	19.499	-0.723		-0.967
Salbutamol sulfate	46386798	3081	16958	18.168	-0.524		4078	16022	25.453	-0.236		-0.380
Salmeterol	46387005	3932	16830	23.363	1.426		5369	15969	33.621	1.912		1.669
Saquinavir mesylate	46386596	1028	11797	8.714	-0.508		2761	14800	18.655	-0.684		-0.596
SB 205607 dihydrobromide	46387006	1569	15977	9.820	-0.347		3654	16891	21.633	0.003		-0.172
Scopolamine hydrobromide	46386794	3427	17359	19.742	0.173		4359	17373	25.091	-0.359		-0.093
SDM25N hydrochloride	46387008	2979	17100	17.421	-0.486		4339	16406	26.448	-0.242		-0.364
Secnidazole	46386696	1746	15844	11.020	0.405		3733	17322	21.551	-0.026		0.189
Secoisolariciresinol	46386735	1458	13974	10.434	0.038		3347	16604	20.158	-0.517		-0.240
Selegiline hydrochloride	46386796	2350	13036	18.027	-0.587		3497	13079	26.738	0.205		-0.191
Sertraline hydrochloride	46386723	2237	16368	13.667	-0.109		2913	15567	18.713	-0.568		-0.339
Sibutramine	46387014	2466	12702	19.414	0.155		3423	11946	28.654	0.420		0.288
Simvastatin	104170217	1690	11344	14.898	2.526		3864	13138	29.411	3.314		2.920
SKF 83566 hydrobromide	46386977	2623	13698	19.149	0.070		3247	12551	25.870	-0.415		-0.173
Sotalol hydrochloride	46386705	994	12766	7.786	-1.256		2828	14875	19.012	-0.579		-0.917
Spectinomycin	104170086	1558	15275	10.200	0.028		3419	16948	20.173	-0.144		-0.058
Spironolactone	104169980	3559	17775	20.023	0.582		4313	15310	28.171	0.189		0.386
SR 57227A	46386849	3122	14100	22.142	1.265		3841	11538	33.290	1.414		1.339
Stanozolol	46386608	1420	14654	9.690	-0.058		3527	16573	21.282	0.003		-0.027
Stavudine	104170182	1666	16195	10.287	0.074		3627	17492	20.735	0.066		0.070
Stiripentol	46386912	2535	13383	18.942	0.003		3212	11469	28.006	0.226		0.115
Sulfacetamide	104170036	1330	14263	9.325	-0.657		3553	16505	21.527	-0.034		-0.345
Sulfamethoxazole	104170035	1202	12196	9.856	-0.155		3118	14844	21.005	0.167		0.006
Sulfasalazine	46386548	1169	12177	9.600	-0.291		3075	15203	20.226	-0.124		-0.208
Sulfinpyrazone	104170037	3187	17668	18.038	-0.057		4024	15001	26.825	-0.133		-0.095
Sulfisoxazole	104170034	1664	15482	10.748	0.430		3567	17416	20.481	-0.206		0.112
Sulindac	104170038	2907	16240	17.900	-0.101		4473	15659	28.565	0.283		0.091
Sumatriptan succinate	46386597	3085	16273	18.958	-0.175		4414	15767	27.995	0.635		0.230
Symmetrel	104169987	1681	15161	11.088	0.500		3475	16645	20.877	0.120		0.310
Synephrine	46386970	2437	13784	17.680	-0.403		3363	12710	26.459	-0.238		-0.321
Tacrine hydrochloride	46386852	3732	17594	21.212	0.824		4940	17100	28.889	0.942		0.883
Tacrolimus	46386734	3146	16500	19.067	0.044		4496	15822	28.416	0.349		0.196
Tadalafil	46386604	3112	16717	18.616	1.093		2909	14696	19.795	-0.121		0.486
Tamoxifen	104170047	1006	11985	8.394	-1.240		3307	14354	23.039	0.499		-0.370
Taxifolin-(+)	46386813	1326	13687	9.688	-0.429		3453	16257	21.240	-0.135		-0.282
Taxifolin-(+/-)	46386773	1464	14165	10.335	0.240		3446	16667	20.676	-0.155		0.042
Tegafur	46386579	3440	17979	19.133	0.065		4433	16312	27.176	-0.023		0.021
Tegaserod maleate	46386624	2884	15161	19.022	0.839		4774	16273	29.337	1.798		1.318
Telithromycin	46386829	2638	14462	18.241	0.009		3334	11657	28.601	0.292		0.150
Telmisartan	46386620	2559	17608	14.533	-0.228		3193	16050	19.894	-0.087		-0.157
Temozolomide	46386653	2601	14488	17.953	0.878		2338	11119	21.027	0.300		0.589
Terazosin	104170187	1590	15194	10.465	0.169		3708	16889	21.955	0.523		0.346
Terbinafine hydrochloride	46386583	2625	16774	15.649	0.242		3876	17220	22.509	0.277		0.260

Terbutaline sulfate	104170117	1185	13845	8.559	-0.805		3520	16515	21.314	-0.200		-0.503
Testosterone	46501387	3083	15942	19.339	0.362		4621	15913	29.039	0.397		0.379
Tetracycline	104170039	1317	13660	9.641	-0.081		3326	17446	19.065	-0.577		-0.329
Tetrahydrozoline hydrochloride	104169982	1569	15620	10.045	-0.055		3589	17082	21.010	0.169		0.057
TFMPP hydrochloride	46386913	2776	15193	18.272	0.706		4452	16623	26.782	1.229		0.968
Thalidomide	104170098	3056	17304	17.661	-0.178		4260	15542	27.410	0.007		-0.086
Theophylline	104170040	2340	13772	16.991	-0.394		3640	12757	28.533	0.276		-0.059
Thiabendazole	104170091	1454	15011	9.686	-0.187		3524	16796	20.981	-0.296		-0.242
Thioridazine hydrochloride	104170092	980	12250	8.000	-1.142		2805	14515	19.325	-0.462		-0.802
Thiothixene	104170208	854	14015	6.093	-2.156		2142	17102	12.525	-2.731		-2.444
Tiagabine hydrochloride	46386642	2472	17164	14.402	-0.271		3047	15644	19.477	-0.229		-0.250
Tibolone	46386825	2910	15856	18.353	-0.186		4019	14643	27.447	0.058		-0.064
Ticlopidine hydrochloride	46386576	2350	16262	14.451	0.030		3542	17227	20.561	-0.157		-0.063
Tinidazole	46387025	2500	17349	14.410	-0.268		2935	14989	19.581	-0.193		-0.231
Tizanidine hydrochloride	104170152	1058	11709	9.036	-0.360		3210	14360	22.354	0.284		-0.038
Tocainide	46386772	3464	17222	20.114	0.381		4181	16494	25.349	-0.572		-0.096
Tolazamide	104170088	1463	15447	9.471	-0.305		3806	17247	22.068	0.017		-0.144
Tolbutamide	104170041	3133	17717	17.684	-0.171		3926	13413	29.270	0.452		0.141
Tolterodine tartrate	46386674	2902	17078	16.993	-1.045		4081	16476	24.769	-0.470		-0.757
Topiramate	46386619	2274	15093	15.067	-0.056		2649	11856	22.343	0.748		0.346
Topotecan hydrochloride	46386667	4461	12513	35.651	5.381		5830	12398	47.024	5.935		5.658
Torasemide	46386585	936	10973	8.530	-1.154		3039	14409	21.091	-0.188		-0.671
Toremifene citrate	46386786	1405	16753	8.387	-0.936		3390	18027	18.805	-0.656		-0.796
Tosufloxacin tosilate	46386743	2376	16863	14.090	-0.034		3564	17194	20.728	-0.119		-0.077
Tramadol hydrochloride	46386884	2592	13311	19.473	0.174		3529	12499	28.234	0.294		0.234
Tranilast	46386750	1721	15708	10.956	0.365		3745	16764	22.340	0.253		0.309
trans-Retinoic acid	104169979	3058	16772	18.233	0.006		4027	14713	27.370	-0.003		0.002
Trazodone hydrochloride	46386915	3217	16195	19.864	0.227		4338	16068	26.998	0.294		0.260
Tremulacin	46386886	2448	16520	14.818	-0.136		3115	15056	20.689	0.185		0.024
Triamcinolone acetonide	104170089	1962	13954	14.060	2.210		4054	15871	25.543	1.018		1.614
Triamterene	104170042	1865	13202	14.127	-1.316		2871	12551	22.875	-1.079		-1.197
Triclabendazole	46386738	2940	17290	17.004	0.571		3692	15958	23.136	1.019		0.795
Triclosan	104170014	3053	16187	18.861	0.208		4372	15365	28.454	0.257		0.233
Trifluoperazine hydrochloride	46386916	3016	17709	17.031	-1.028		4129	17714	23.309	-0.970		-0.999
Trihexyphenidyl hydrochloride	104169984	1711	16545	10.341	0.103		3794	17277	21.960	0.525		0.314
Trimebutine maleate	46386760	2430	16650	14.595	0.055		4057	17332	23.408	0.477		0.266
Trimethoprim	104169981	1356	12749	10.636	0.260		3305	15101	21.886	0.497		0.379
Tripelennamine hydrochloride	46386917	2664	13799	19.306	0.121		3651	13094	27.883	0.189		0.155
Triptolide	46386571	1437	10256	14.011	-0.397		1783	8725	20.436	0.098		-0.150
Tropicamide	104170087	1678	15492	10.831	0.440		3887	17744	21.906	-0.030		0.205
Tropisetron hydrochloride	46386594	3124	16580	18.842	0.807		4988	16565	30.112	1.971		1.389
Troxipide	46386769	1665	14985	11.111	0.462		3683	17262	21.336	-0.101		0.180
Tryptoline	46386936	3212	15933	20.159	0.395		4199	14602	28.756	0.451		0.423
Urapidil hydrochloride	46386851	2421	17429	13.891	-0.069		3411	17027	20.033	-0.274		-0.172
Ursodeoxycholic acid	104169985	1083	11009	9.837	0.010		3161	14847	21.290	0.006		0.008
Valaciclovir hydrochloride	46386762	3128	16498	18.960	-0.174		4126	15790	26.130	-0.003		-0.089
Valdecoxib	46386621	3437	17135	20.058	0.363		4567	16618	27.482	0.069		0.216
Valproic acid	104170082	1077	12163	8.855	-0.643		2982	14542	20.506	-0.433		-0.538
Valsartan	46386599	2288	16956	13.494	-0.565		2901	14719	19.709	-0.150		-0.357
Vardenafil citrate	46386591	2547	16503	15.434	0.204		3889	17197	22.614	0.301		0.252
Vecuronium bromide	46386876	2419	13500	17.919	-0.326		3544	12745	27.807	0.166		-0.080
Venlafaxine hydrochloride	46386590	2391	17054	14.020	-0.046		3572	17125	20.858	-0.090		-0.068
Verapamil hydrochloride	46386795	1570	14104	11.132	0.607		4102	16332	25.116	1.008		0.807
Vidarabine	104170045	2987	15282	19.546	0.429		3879	13458	28.823	0.345		0.387
Vincristine sulfate	46386588	334	7110	4.698	-2.362		905	7266	12.455	-2.308		-2.335
Vindesine sulfate	46386586	425	4236	10.033	-2.864		969	3806	25.460	-0.539		-1.701
Vinorelbine tartrate	46386815	178	5376	3.311	-3.859		392	6039	6.491	-4.656		-4.258
Voriconazole	46386721	3172	16602	19.106	0.056		4086	14879	27.462	0.062		0.059
Warfarin sodium	104169988	3081	16818	18.320	0.034		3781	14810	25.530	-0.443		-0.205
Xanthinol nicotinate	46387024	2565	17528	14.634	-0.196		3221	16020	20.106	-0.014		-0.105
Zacopride hydrochloride hydrate	46386978	1677	12745	13.158	1.542		4020	14439	27.841	1.721		1.632
Zafirlukast	46386595	2985	17268	17.286	0.663		3311	16305	20.307	0.054		0.358
Zalcitabine	46386814	3027	15660	19.330	0.128		4043	15062	26.842	-0.123		0.002
Zaleplon	46386657	2696	14629	18.429	1.032		2428	12098	20.069	-0.027		0.503
Zardaverine	46386923	1270	13809	9.197	-0.737		3336	15681	21.274	-0.123		-0.430
Zeranol	46386627	2485	16889	14.714	-0.170		3083	15778	19.540	-0.207		-0.189
Zidovudine	104170164	1734	16193	10.708	0.298		3433	17224	19.931	-0.234		0.032
Zileuton	46386751	1178	12435	9.473	-0.358		3004	14713	20.417	-0.053		-0.206
Zolmitriptan	46386880	2532	14212	17.816	-0.128		3443	12175	28.279	0.215		0.043
Zolpidem tartrate	46386567	3170	17097	18.541	0.105		3853	14399	26.759	-0.149		-0.022
Zonisamide	104170135	1429	13998	10.209	0.181		3540	16338	21.667	0.104		0.143
Zucapsaicin	46386797	1442	14586	9.886	0.032		3401	17101	19.888	-0.362		-0.165
		Std Dev	2452.65				**Std Dev**	2269				
		Average	14826.66				**Average**	15225				
		Median	15279.50				**Median**	15903				

Chapter 3: Doxorubicin Conjugation to Reovirus Improves Oncolytic Efficacy in Triple-Negative Breast Cancer

This research is being submitted to *Molecular Therapeutics, Oncolytics*

Authors: Jameson T.L. Berry, Luis E. Muñoz, Roxana M. Rodríguez Stewart, Periasamy Selvaraj, and Bernardo A. Mainou

Doxorubicin conjugation to reovirus improves oncolytic efficacy in triple-negative breast cancer

Jameson T.L. Berry[1,2], Luis E. Muñoz[1,3], Roxana M. Rodríguez Stewart[1,2], Periasamy Selvaraj[1,3], and Bernardo A. Mainou[1,2,4*]

Emory University,[1] Department of Pediatrics,[2] Department of Pathology and Laboratory Medicine,[3] Emory University School of Medicine, Atlanta, GA 30032, Children's Healthcare of Atlanta,[4] Atlanta, GA, 30322

*To whom correspondence should be addressed: Emory University School of Medicine, Department of Pediatrics, ECC 564, 2015 Uppergate Drive, Atlanta, GA 30322. Tel.: (404) 727-1605. Fax: (404) 727-9223. E-mail: bernardo.mainou@emory.edu

Running Title: Conjugated Doxorubicin Augments Reovirus Oncolysis

GRAPHICAL ABSTRACT

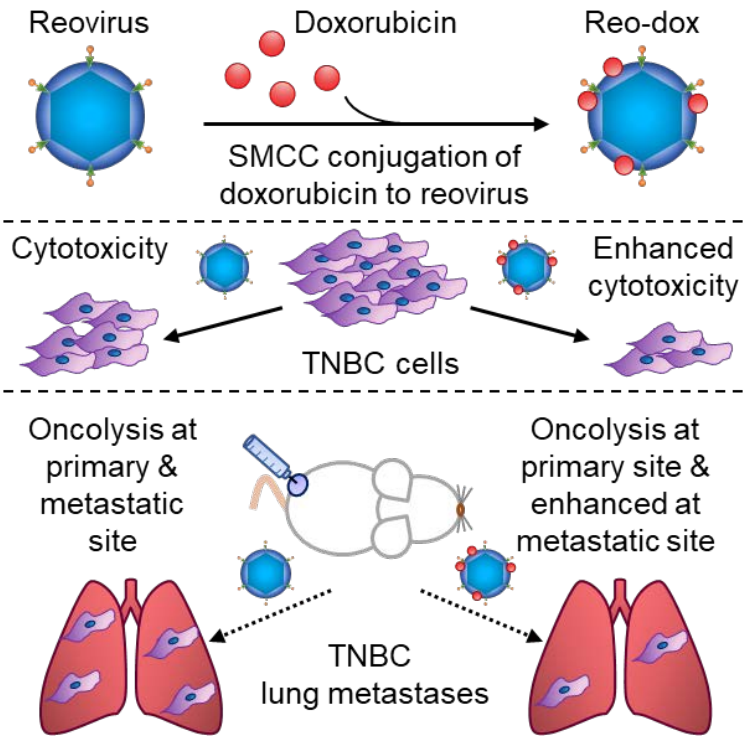

ABSTRACT

Breast cancer is the second leading cause of cancer-related deaths in women in the United States. The triple-negative subtype (TNBC) associates with higher rates of relapse, shorter overall survival, and aggressive metastatic disease. Hormone therapy is ineffective against TNBC, leaving patients with limited therapeutic options. Mammalian orthoreovirus (reovirus) preferentially infects and kills transformed cells, and a genetically engineered reassortant reovirus infects and kills TNBC cells more efficiently than prototypical strains. Reovirus oncolytic efficacy is further augmented by combination with topoisomerase inhibitors, including the frontline chemotherapeutic doxorubicin. However, long-term doxorubicin use correlates with toxicity to healthy tissues. Here, we conjugated doxorubicin to reovirus (reo-dox) to control drug delivery and enhance reovirus-mediated oncolysis. Our data indicate that conjugation does not impair viral biology and enhances reovirus oncolytic capacity in TNBC cells. Reo-dox infection promotes innate immune activation, and crosslinked doxorubicin retains DNA damaging properties within infected cells. Importantly, reovirus and reo-dox significantly reduce primary TNBC tumor burden *in vivo*, with greater reduction in metastatic burden after reo-dox inoculation. Together, these data demonstrate that crosslinking chemotherapeutic agents to oncolytic viruses facilitates functional drug delivery to cells targeted by the virus, making it a viable approach for combination therapy against TNBC.

INTRODUCTION

Breast cancer is most prevalent among new cancer diagnoses and the second leading cause of cancer-related deaths in women in the United States (11). Breast cancer subtypes are categorized according to the surface expression of three receptor proteins: estrogen receptor (ER), progesterone receptor (PR), and human epidermal growth factor receptor 2 (HER2). The triple-negative subtype (TNBC) characteristically lacks expression of ER, PR, and HER2. TNBC accounts for approximately 12% of breast tumors (254, 255), and among metastatic breast cancers, TNBC exhibits higher rates of relapse and shorter overall survival compared to other subtypes of breast cancer(256, 257).

Treatment of TNBCs is largely limited to chemotherapy, radiation therapy, and surgery. Hormone therapies, which have been efficacious in the treatment of other types of breast cancer, are inadequate in TNBC due to the lack of the hormone therapy targets, ER, PR, and HER2 (21, 183). TNBCs are initially more sensitive to chemotherapy compared to other breast cancer subtypes, but patients with residual disease after neoadjuvant chemotherapy and surgery suffer higher rates of mortality (256, 257). Thus, there is great need for efficacious, targeted therapies to improve therapeutic outcomes in TNBC.

The concept that viral infection can correlate with decreased tumor burden has existed nearly as long as knowledge about viruses (73). Recent developments in genetic engineering of viruses has allowed the development of oncolytic viruses with increased recognition of receptors overexpressed in tumor tissue (258, 259) and viruses that encode or package suicide or pro-apoptotic genes or agents for delivery to cancer cells (260, 261). Viruses can also be manipulated to upregulate antigen presentation and T cell antitumor response (262, 263). Despite ongoing efforts, talimogene laherparepvec (T-Vec, OncoVEX$^{GM\text{-}CSF}$, Imlygic®), an attenuated and genetically engineered herpes simplex virus (HSV) that overexpresses granulocyte-macrophage

colony-stimulating factor (GM-CSF), is the only oncolytic virus that has been approved for clinical use in the United States and Europe (ClinicalTrials.gov identifier NCT00769704) (77-80).

Mammalian orthoreovirus (reovirus) is a nonenveloped, segmented dsRNA virus (93). Most humans are infected with reovirus during childhood, but infection rarely causes disease (264). Reovirus preferentially replicates in transformed cells, making it an attractive oncolytic agent (189). Tropism to cancer cells is linked to many factors, including overexpression of the proteinaceous virus receptor junctional adhesion molecule A (JAM-A) (108, 150), dysregulated Ras signaling (265), downregulated dsRNA-dependent protein kinase R (PKR) (266), and increased expression of cathepsins (151-153). A laboratory-adapted reovirus is in clinical trials to test its efficacy against several cancers (159, 177, 188, 267), but its efficacy against TNBC has not been extensively investigated.

We previously generated a reassortant reovirus (henceforward referred to as reovirus) with enhanced infectivity and cytotoxic properties in TNBC cells (268). The oncolytic properties of reovirus in TNBC are enhanced when combined with topoisomerase inhibitors topotecan, etoposide, and doxorubicin (dox) (268). Dox is a topoisomerase II inhibitor that is a frontline chemotherapeutic for many cancers. Dox intercalates with DNA, inhibiting topoisomerase II binding with DNA and strand relegation (24). Dox is a potent anticancer agent, but its clinical use is limited by severe systemic toxicity and association with cardiomyopathy, especially during long-term treatment (21-23). Improving the specificity of cytotoxic agents to cancer cells can increase their efficacy and improve quality of care for patients (269).

In this study, we show that dox conjugation to reovirus (reo-dox) enhances cytotoxicity to TNBC cells without impairing reovirus biology. We demonstrate that infection with reo-dox elicits an innate immune response to the virus and promotes DNA damage resulting in activation of the

double strand break response pathway, indicative of dox bioactivity. Additionally, in a murine TNBC model, reo-dox dramatically reduced primary tumor and metastatic burden compared to dox-treated animals. Together, our data indicate that crosslinking small molecules to oncolytic reovirus can serve as a platform for efficacious, targeted delivery of drugs and oncolytic virus to infected cells, limiting the progression of aggressive metastatic breast cancer.

RESULTS

Doxorubicin conjugation to reovirus enhances cytotoxicity in TNBC cells.

We previously identified that infecting TNBC cells with a genetically engineered reovirus in the presence of doxorubicin (dox) yields additive cytotoxicity (268). Dox is an effective chemotherapy for the treatment of TNBC (21), but toxicity to healthy cells and tissues limits its clinical utility (22, 23). Conjugation of small molecule fluorescent dyes to reovirus to generate fluorescently-labeled viral particles has little impact on virus biology or cargo function (210, 270, 271). To minimize off-tumor effects of dox and selectively deliver the drug to virus-infected cells, dox was conjugated to reovirus (reo-dox) using the heterobifunctional covalent crosslinker succinimidyl 4-(n-maleimidomethyl)cyclohexane-1-carboxylate (SMCC) (Figure 3.1A). To determine the concentration of dox crosslinked to reovirus, dox absorbance at 480 nm was measured by ultraviolet-visible spectroscopy (Figure 3.1B, Table 3.S1). On average, 5.01×10^{-15} μmol of dox are present on one reovirus particle. Dox concentration positively correlates with μmol of dox per reovirus particle with an r^2 value of 0.9917 (Figure 3.1B) and negatively correlates with viral titer with an r^2 value of 0.6589 (Figure 3.1C), indicating that higher concentrations of crosslinked dox dampen reovirus infectivity. These data indicate that dox can be successfully conjugated to reovirus using SMCC with minimal impact on the infective properties of the virus.

To determine the cytotoxic properties of reo-dox in TNBC cells, MDA-MB-231 and MDA-MB-436 cells (both of the mesenchymal stem-like (MSL) cellular subtype (182)) were pretreated with vehicle (DMSO) or increasing concentrations of dox and infected with mock, reovirus, or reo-dox at an MOI of 100 PFU/cell (Figure 3.1D). In MDA-MB-231 cells, reo-dox (red) significantly reduced viability by day 3 post infection compared to reovirus alone (orange) and reovirus infection after 0.1 μM dox pretreatment (violet) (Figure 3.1E). Reo-dox also impaired cell

viability with faster kinetics than virus alone or virus infection after 0.1 μM dox. In MDA-MB-436 cells, reovirus infection alone induced mild cytotoxicity, and pretreatment with 0.1 or 1.0 μM dox followed by reovirus infection enhanced viral cytotoxicity. Infection with reo-dox reduced MDA-MB-436 cell viability to similar levels as reovirus infection of dox-pretreated cells and significantly reduced viability compared to cells treated with dox alone or reovirus infection alone (Figure 3.1D-E). These data indicate that infection of TNBC cells with reo-dox yields greater cytotoxicity than virus alone.

Dox conjugation does not affect reovirus replication kinetics.

To evaluate the effect of dox conjugation on reovirus biology, reo-dox attachment, infectivity, and replication were evaluated in TNBC cells. Reovirus cell attachment is mediated by a strength-adhesion mechanism in which the viral attachment fiber σ1 binds cell-surface carbohydrate and proteinaceous receptor junctional adhesion molecule-A (JAM-A) (108, 206). To investigate whether dox conjugation altered the ability of reovirus to attach to TNBC cells, MDA-MB-231 and MDA-MB-436 cells were pretreated with vehicle (DMSO) or dox, adsorbed with mock, reovirus, or reo-dox at an MOI of 1×10^5 particles/cell at 4°C, and assessed for cell surface reovirus by flow cytometry using indirect immunofluorescence with reovirus-specific antiserum (Figures 3.2A, 3.S1A). In both cell lines, cell-surface reovirus and the percent of cells with virus were similar in cells adsorbed with reovirus alone, reovirus pretreated with dox, or reo-dox. Interestingly, 3-4 times more reovirus bound to MDA-MB-436 cells than MDA-MB-231 cells. This is likely due to different levels of cell-surface JAM-A. These data indicate that dox conjugation to reovirus does not affect the ability of reovirus to attach to TNBC cells.

To test if dox conjugation to reovirus impacted reovirus infectivity, MDA-MB-231 cells and MDA-MB-436 cells were pretreated with vehicle (DMSO), dox, or the cysteine protease inhibitor E64-d, which blocks reovirus cell entry by preventing proteolytic processing of virions during endocytosis (207). Cells were infected with mock, reovirus, or reo-dox at an MOI of 100 PFU/cell, and assessed for infectivity after 18 h by indirect immunofluorescence using reovirus-specific antiserum (Figure 3.2B). Similar to previous observations (268), 1.0 μM dox pretreatment of MDA-MB-231 cells slightly enhanced reovirus infectivity, whereas 1.0 μM dox pretreatment of MDA-MB-436 cells slightly decreased reovirus infectivity. Reo-dox infectivity was slightly higher or similar to virus alone or virus following dox pretreatment in both MDA-MB-231 and MDA-MB-436 cells (Figure 3.2B). These data indicate that reo-dox can efficiently infect TNBC cells and that crosslinking dox to virus has negligible effects on infectivity.

To determine if crosslinking dox to reovirus alters viral replication in TNBC cells, MDA-MB-231 and MDA-MB-436 cells were pretreated with vehicle (DMSO) or 1.0 μM dox, infected with mock, reovirus, or reo-dox at an MOI of 100 PFU/cell, and assessed for viral replication by qPCR over a 2 day time course of infection (Figure 3.2C). In parallel, cells were adsorbed with mock, reovirus, or reo-dox at an MOI of 10 PFU/cell and assessed for replication by plaque assay on L929 mouse fibroblasts over a 3 day time course of infection (Figures 3.2D, 3.S1B). Reo-dox replicated to similar levels with similar kinetics as reovirus alone or in in the context of dox-pretreated cells. Viral RNA levels in MDA-MB-436 cells were 10-fold higher over the first day of infection than in MDA-MB-231 cells (Figure 3.2C). Viral yield was similar in cells infected with reo-dox compared to cells infected with reovirus alone (Figure 3.2D). Peak titers reached 10^8 PFU/mL by 2 days post infection (dpi) in MDA-MB-436 cells and 3 dpi in MDA-MB-231 cells (Figure 3.S1B), corroborating the finding that MDA-MB-436 cells support faster replication

kinetics. These data indicate that infection of MDA-MB-436 cells is more efficient than MDA-MB-231 cells correlating with differences in attachment. Further, dox conjugation to reovirus does not alter virus attachment and infection kinetics compared to reovirus alone.

Dox conjugation to reovirus does not alter innate immune response to virus infection.

Reovirus infection of MDA-MB-231 cells induces *IFNL1* transcription and cytokine production with no transcription of *IFNB1* (268). To investigate the IFN response to reo-dox infection in TNBC cells, MDA-MB-231 (Figure 3.3A) and MDA-MB-436 (Figure 3.3B) cells were treated with vehicle (DMSO) or 1.0 μM dox and infected with mock, reovirus, or reo-dox at an MOI of 100 PFU/cell for 0-48 h, and *IFNL1, IFNB1,* and *IFNG* mRNA levels were assessed by qPCR. In MDA-MB-231 cells, there was no detectable *IFNB1*, but *IFNL1* RNA levels were 100-fold higher by 8 hours post infection (hpi) under all conditions with reovirus, peaking at 24 hpi, compared to uninfected cells. Reovirus infection following dox pretreatment (teal) resulted in slightly greater *IFNL1* RNA levels. Dox treatment alone induced *IFNL1* transcription by 48 hpi, consistent with previous findings (268). Dox treatment alone or followed by reovirus induced elevated *IFNG* RNA levels by 12 hpi, peaking by 48 hpi. Reovirus infection following dox pretreatment yielded 10-fold greater *IFNG* RNA levels than dox treatment alone by 48 hpi. Reo-dox infection yielded increased *IFNG* RNA levels by 24 hpi, peaking at 48 hpi, though to a lesser extent than free dox alone or with reovirus infection. In MDA-MB-436 cells, *IFNL1* and *IFNB1* RNA were detected under all conditions with reovirus as early as 8 hpi. Whereas *IFNB1* RNA remained at similar levels throughout the times tested, *IFNL1* RNA levels increased and peaked at 24 hpi. Dox treatment alone induced transcription of *IFNL1* and *IFNB1* RNA by 24 h post treatment, peaking by 48 hpi. Interestingly, *IFNL1,* but not *IFNB1*, RNA levels increased over

time with vehicle treatment. *IFNG* RNA was detected following dox treatment in the presence or absence of reovirus and in reo-dox infected cells. *IFNG* RNA was 10-fold higher in cells infected with reovirus after dox treatment compared to vehicle-treated cells at 0 hpi, with levels increasing over the course of the infection. In MDA-MB-436 cells infected in the absence of dox, little *IFNG* RNA was detected. The lower levels of *IFNG* after reo-dox infection in both cell lines likely reflects a delay in dox delivery to infected cells compared to the addition of dox directly to cells and suggest that a lower concentration of dox is delivered on a per-cell basis (Table 3.S1).

To determine if transcriptional upregulation of *IFNL1*, *IFNB1*, and *IFNG* results in increased secreted IFN proteins, supernatants from MDA-MB-231 and MDA-MB-436 cells pretreated with vehicle (DMSO) or dox and infected with mock, reovirus, or reo-dox were assessed for IFNλ, IFNβ, and IFNγ by ELISA (Figure 3.3C-D). In MDA-MB-231 cells, IFNλ was only detected after infection with reovirus, reovirus following dox pretreatment, or reo-dox (Figure 3.3C). Following reo-dox infection, IFNλ was detected by12 hpi, peaking at 24 hpi, In cells infected with reovirus after dox pretreatment, IFNλ was not detected until 24 hpi with levels increasing at 48 hpi. IFNλ levels were greater in cells infected in the presence of dox (following pretreatment or conjugated to reovirus) than reovirus alone. *IFNB1* RNA was not detected, so we did not test for secreted IFNβ levels in these cells. In MDA-MB-436 cells, reovirus infection induced robust IFNλ and IFNβ secretion, with detectable levels at 12 hpi and increasing through the course of infection (Figure 3.3D). Levels of detected IFNλ were 5-10x those of IFNβ. IFNλ and IFNβ levels were greater in infected cells in the presence of dox than virus alone. Although *IFNL1* RNA was detected by 24 and 48 h after treatment with vehicle and dox in the absence of virus, secreted cytokine was not detected in DMSO-treated cells, and low levels of IFNλ were detected in dox-treated cells.

In both MDA-MB-231 and MDA-MB-436 cells, all conditions promoted low levels of IFNγ throughout the experiment despite changes in RNA levels. IFNγ levels in MDA-MB-436 cells were about 10x those observed in MDA-MB-231 cells (Figure 3.3C-D). Together, these data suggest a context-dependent innate immune response to reovirus infection. In both MDA-MB-231 and MDA-MB-436 cells, infection resulted in robust Type III IFN production with some additive enhancement conferred by the presence of dox, whether in soluble or crosslinked form. Interestingly, IFNλ and β have minimal to no direct effect on TNBC cell viability, despite substantial activation of signaling pathways responsive to the cytokines (Figure 3.S2) (268).

To determine if MDA-MB-231 and MDA-MB-436 cells respond to IFN in the context of dox treatment and reovirus infection, cells were pretreated with vehicle (DMSO) or dox, infected with mock, reovirus, or reo-dox at an MOI of 100 PFU/cell, and assessed the activation status of STAT1 and STAT2 by immunoblot over a two day time course of infection (Figures 3.4, 3.S3). In MDA-MB-231, phospho-STAT1 (p-STAT1) levels were slightly elevated in cells treated with dox in the absence of reovirus, and reovirus infection in the presence or absence of dox decreased p-STAT1 levels. Infection of MDA-MB-231 cells with reo-dox induced robust levels of p-STAT1 and p-STAT2 at 1 dpi. In MDA-MB-436 cells, p-STAT1 levels were consistently high with the exception of a small increase in p-STAT1 levels 1 day following dox treatment in the absence of reovirus and reovirus infection leading to decreased p-STAT1 levels at 2 dpi. Infection in the presence or absence of dox had little effect on p-STAT2 levels, with no p-STAT2 detected at 2 dpi. Infection of MDA-MB-436 cells with reo-dox did not significantly increase p-STAT1 or p-STAT2 levels as observed in MDA-MB-231 cells.

Activated STAT3 is associated with epithelial-to-mesenchymal transition, survival, and proliferation, and is constitutively activated in 40% of breast cancers (217). While IL-6 is the

primary agonist for STAT3 activation, Type I and Type III IFN can activate STAT3. In MDA-MB-231 and MDA-MB-436 cells, p-STAT3 levels decreased in the presence of dox alone, and reovirus alone or combined with soluble or conjugated dox decreased p-STAT3 to a greater degree than drug alone. These data indicate that while dox dampens the activation of STAT3, reovirus infection potently inhibits the activation of this protein.

Crosslinking dox to reovirus does not affect the DNA damaging properties of dox.

To determine if the DNA damaging properties of dox remain intact when conjugated to reovirus, MDA-MB-231 and MDA-MB-436 cells were treated with vehicle (DMSO) or dox, infected with mock, reovirus, or reo-dox at an MOI of 100 PFU/cell, and analyzed for DNA damage by single-cell electrophoresis comet assay (Figure 3.5). In both cells, dox treatment, reovirus infection after dox pretreatment, and reo-dox infection resulted in greater DNA fragmentation than mock or reovirus infection alone by 2 dpi. Unconjugated dox-induced DNA damage was greater in MDA-MB-231 cells (Figure 3.5A) than in MDA-MB-436 cells (Figure 3.5C), corroborating cell viability data (Figure 3.1D).

H2A histone family member X (H2AX) is phosphorylated (γH2AX) by ataxia telangiectasia mutated (ATM) in response to DNA double strand breaks (56, 57). ATM and p53 are phosphorylated as part of the response to double strand breaks (58, 63). To assess if dox-induced DNA damage promotes activation of the double strand break response, the activation levels of ATM, p53, and H2AX were assessed in MDA-MB-231 and MDA-MB-436 cells in the presence or absence of dox and reovirus or reo-dox infection (Figure 3.4). MDA-MB-436 cells do not express full-length p53 due to a nonsense frameshift mutation at position E204 in p53 (272). Reovirus infection alone did not induce activation of ATM, but γH2AX levels in MDA-MB-436

cells were elevated by 1 and 2 dpi. Treatment with dox alone, infection of dox-treated cells, and reo-dox infection led to robust increase of levels of p-ATM, p-p53, and γH2AX in MDA-MB-231 cells and p-ATM and γH2AX in MDA-MB-436 cells. Reovirus infection dampened dox-induced H2AX phosphorylation in MDA-MB-231 cells, but dox-induced γH2AX levels increased after reovirus infection of MDA-MB-436 cells, suggesting some cell-specific effects by reovirus on H2AX phosphorylation. DNA damage response was enhanced by reo-dox infection, though to a lesser extent as exogenous dox treatment, correlating with less DNA fragmentation observed by comet assay. The lower levels of DNA damage response activity detected biochemically in MDA-MB-436 cells correlate with higher basal ATM phosphorylation (Figure 3.4), lower levels of measured DNA fragmentation (Figure 3.5), and less cytotoxic effects of dox in these cells (Figures 3.1C-D). Together, these data indicate that reovirus does not interfere with dox-induced DNA damage response, and crosslinking dox to reovirus does not impair the pharmacological properties of dox.

Reovirus and reo-dox reduce 4T1 murine tumors and metastases *in vivo*

The 4T1 murine mammary carcinoma cell line is widely used TNBC model (273-276). To determine if the 4T1 cell line is a viable model for reovirus and reo-dox oncolysis, cells pretreated in the absence or presence of dox were infected with mock, reovirus, or reo-dox at increasing MOIs, and infectivity was assessed (Figure 3.6A). At all MOIs tested, reo-dox and reovirus infectivity were similar and infection after dox pretreatment enhanced reovirus infectivity to varying degrees depending on the MOI, mimicking the effect observed in MDA-MB-231 cells (Figure 3.2B) (268). To assess the impact of reovirus infection on cell viability, 4T1 cells were treated with DMSO or dox, or infected with mock or increasing MOIs of reovirus or reo-dox, and cell viability was

measured over a 6 day time course of infection (Figure 3.6B). At all MOIs tested, reovirus and reo-dox infection negatively affected cell viability in a dose-dependent manner, with reo-dox impairing cell viability with faster kinetics than reovirus alone. Infection with reo-dox at MOIs of 50 and 100 PFU/cell resulted in similar cell viability levels as 10 μM dox treatment alone at day 6. Together, these data indicate that reovirus and reo-dox can efficiently infect and impair cell viability of 4T1 cells *in vitro* and that 4T1 cells are sensitive to dox.

To assess the ability of reovirus and reo-dox to impair TNBC tumor growth and metastasis *in vivo*, female Balb/c mice were challenged with 5×10^4 4T1 cells subcutaneously in the hind flank, and PBS, 54.4 μg/mL dox, or 5×10^8 PFU reovirus or reo-dox were administered intratumorally on days 10 and 14 post tumor challenge (Figure 3.6C). Mouse weight (Figure 3.6D) and primary tumor area (Figure 3.6E) were assessed through 21 days post tumor challenge. Treatments had minimal effect on mouse weight. Animals treated with dox (pink) or inoculated with reovirus (teal) had a greater reduction in weight from day 10 to 14 compared to PBS (black) or reo-dox (violet), possibly indicating lower toxicity of the initial dose (Figure 3.6D). Intratumoral delivery of reovirus and reo-dox significantly impaired tumor growth, with tumors being ~60% smaller compared to PBS treatment and ~50% smaller than dox treatment by endpoint (Figure 3.6E). These data indicate that intratumoral reovirus and reo-dox can limit tumor growth at the primary site.

To determine the extent of viral antigen and DNA damage in the primary tumors, reovirus antigen and γH2AX levels were assessed by immunohistochemistry (IHC) (Figures 3.7, 3.S4). Reovirus antigen staining was detected only in tumors infected with reovirus or reo-dox, with viral antigen detected in 7.5% (reovirus) and 5.6% (reo-dox) of cells in the tumor (Figure 3.7A). γH2AX staining was only slightly elevated in reo-dox-infected tumors, with 1.5-2 times more γH2AX-positive cells than any other condition (Figure 3.7B). To determine the levels of viral replication

at primary and metastatic (lung) tumor sites, viral titers were assessed by plaque assay (Figure 3.7C-D). Viral titers were similar at the primary tumor site for animals inoculated with reovirus or reo-dox (Figure 3.7C), reflecting that observed by IHC staining (Figure 3.7A). To determine if virus and 4T1 cells were present in the lungs, a site of TNBC metastasis, viral titers (Figure 3.7D) and 4T1 cell numbers (Figure 3.7E) were assessed at this site. The number of 4T1 cells in the lungs was determined by clonogenic assay using 6-thioguanine selection (Figure 3.7E) (275, 277). In the lungs, reovirus levels were approximately 3 times greater in mice that received reo-dox than those inoculated with reovirus. In PBS-treated mice, a median of 1.85×10^5 4T1 cells was present in the lungs, and dox treatment did not significantly impact the number of 4T1 cells. Infection with reovirus reduced the median number of 4T1 cells per lung by ~80-85%, and infection with reo-dox reduced the median number of 4T1 cells per lung by ~95%. Together, these data indicate that reovirus and reo-dox replicate to a similar extent within the primary tumor and that reo-dox can promote DNA damage in the primary tumor site. Further, reovirus and reo-dox replicate at the metastatic site. These data also suggest that reovirus and reo-dox limit the metastatic potential of TNBC cells *in vivo*. The results of work presented here show that crosslinking dox to reovirus is a viable alternative for the codelivery of oncolytic virus and anti-neoplastic drugs to tumor sites, with potential benefits at primary and metastatic tumor sites.

DISCUSSION

Reovirus is a prime platform for the development of enhanced oncolytic virotherapies. Reovirus preferentially infects and replicates in tumor cells (189), can be delivered via intratumoral and intravenous administration (93), and can be combined with genotoxic and immunogenic agents that enhance oncolysis (187, 188, 268, 278-282). A lab-adapted serotype 3 reovirus is in phase I-III clinical trials (ClinicalTrials.gov identifier NCT01656538) (80), though success has been limited and evaluation of reovirus as an oncolytic in breast cancers is minimal (159, 177, 188, 267). For this study, we used a genetically engineered reassortant reovirus (r2Reovirus), which more efficiently infects and promotes greater cytotoxic effects in triple-negative breast cancer (TNBC) cells compared to prototypical strains, including the reovirus that is currently in clinical trials (268). In TNBC cells, topoisomerase inhibitors augment reovirus infectivity, cytotoxicity, and innate immune activation (268). In this study, we show that conjugation of doxorubicin (dox) to oncolytic reovirus (reo-dox) using a heterobifunctional covalent crosslinker allows delivery of bioactive dox to cells, promoting enhanced cytotoxicity through the effects of the drug and the virus.

We estimate that reo-dox carries an average of 3000 molecules of dox per viral particle (Table 3.S1). Crosslinking fluorescent molecules to reovirus using succinimidyl esters preferentially labels reovirus outer capsid structural proteins λ2, μ1, σ1, and σ3 (270). Crystal structures of reovirus structural proteins μ1 and σ3 and reovirus virions suggest the presence of multiple solvent-exposed cysteine residues (283), indicating that the estimation of dox molecules per virion is biologically feasible. Here we show that dox conjugation on reovirus has minimal effects on virus biology.

Reo-dox attaches to cells to similar levels compared to unlabeled reovirus, suggesting that dox conjugation does not hinder reovirus attachment fiber σ1 binding to cell surface carbohydrate or proteinaceous receptor junctional adhesion molecule A (JAM-A) (106-108, 150). Based on the σ1 crystal structure, a single cysteine residue is hidden within the monomeric tertiary structure (284), suggesting that dox is unlikely to be crosslinked to σ1. Although we did not observe a difference in overall levels of reo-dox attached to cells compared to unlabeled reovirus, we observed a small reduction in the percentage of cells with attached reo-dox compared to unlabeled virus (Figure 3.S1). It is possible that this is the result of SMCC-dox causing some aggregation of viral particles, thus resulting in no change in the number of viral particles attached to cells, but fewer cells with virus. Reovirus attachment to MDA-MB-436 cells was 3-5x that observed in MDA-MB-231 cells, likely due to higher cell surface levels of JAM-A.

Reo-dox efficiently infects and replicates in TNBC cells. Paralleling that observed by attachment, reovirus infects MDA-MB-436 cells more efficiently than MDA-MB-231 cells. Pretreatment of MDA-MB-231 cells with 1 μM dox slightly increases infectivity, similar to previous observations (268). Intriguingly, pretreatment of MDA-MB-436 cells with 1 μM dox slightly reduced infectivity despite MDA-MB-436 cells being less sensitive to the cytotoxic effects of dox. It is not known how exogenous dox effects these alterations to reovirus infectivity. In contrast to pretreatment of cells with dox, reovirus infectivity after dox crosslinking is largely unaffected. Reo-dox likely delivers dox to cells after attachment and endocytic uptake, whereas exogenous dox can affect cells before virus attachment, endocytic uptake, and transport of the virus. Thus, the effects of dox on reovirus infectivity likely impact a post-attachment step in the virus replication cycle. Reo-dox also exhibits similar replication kinetics as unlabeled virus in MDA-MB-231 cells and MDA-MB-436 cells. Viral RNA levels and viral yield of unlabeled

reovirus and reo-dox are greater in MDA-MB-436 cells than MDA-MB-231 cells at 1 dpi, indicating that MDA-MB-436 cells are more permissive to reovirus infection than MDA-MB-231 cells.

Conjugation of dox to reovirus does not significantly impact virus biology, but reo-dox elicits more robust cytotoxicity with faster kinetics than unlabeled reovirus in MDA-MB-231 and MDA-MB-436 cells. While exogenous 1 μM dox with and without reovirus impairs cell viability to slightly greater levels than reo-dox in MDA-MB-231 cells, reo-dox performs as well as exogenous dox with and without virus in MDA-MB-436 cells (Figure 3.1D). The differences observed between combination and conjugation treatment in MDA-MB-231 cells are likely due to the lower effective dose of dox delivered via conjugation and that only cells initially infected with reo-dox receive the drug, with progeny unlabeled virus being responsible for subsequent cytotoxicity. While reo-dox likely delivers a lower effective dose of the drug per cell, the delivery is also controlled and contained to only those cells taking up virus. Moreover, there is likely a proportion of cells that take up virions that do not result in productive infection but still receive the drug.

Virus infection can induce potent innate immune responses, and dox conjugation to reovirus does not hinder the TNBC response to virus infection. Reovirus and reo-dox infection of MDA-MB-231 cells upregulate transcription of *IFNL1* but not *IFNB1* (Figure 3.3A) (268). In MDA-MB-436 cells, reovirus and reo-dox infection induce transcription of both *IFNL1* and *IFNB1* (Figure 3.3B), but only IFNλ is secreted at high levels by both TNBC cell lines (Figure 3.3C-D). Little is known about the role of Type III IFN on TNBC cell biology. Treatment of MDA-MB-231 and MDA-MB-436 cells with recombinant IFNβ or IFNλ results in robust STAT1 and STAT2 activation with little effect on cellular proliferation (Figure 3.S2) (268), suggesting that both cell

lines express the cognate receptors for Type-I and –III IFNs. Gut mucosal epithelial cells depend on Type-III IFN to protect against viral pathogens (285, 286). An antiviral role for IFNλ has been described in other tissues and cell lineages including human placental trophoblast protection against Zika virus (287) and in *in vitro* human cervical epithelial cell resistance to dengue virus (288). Mucosal epithelia with high concentrations of peroxisomes in relation to mitochondria favor transcription of Type III IFN over Type I (289). It is possible that the skewed Type III IFN response observed in TNBC cells is due to increased peroxisome abundance in these cells. Epithelial cells in brain and kidney tissues also respond to IFNλ (290), and IFNλ in murine mammary epithelial cells recruits $CD4^+$ T cells to the tumor microenvironment (291). TNBC cells secrete high levels of IFNλ in response to reovirus alone and when combined with topoisomerase inhibitors (268). As such, it is possible that IFNλ secretion by TNBC cells promotes a favorable environment for the recruitment of immune modulatory cells to the site of infection.

Despite the upregulated levels of *IFNL1* and secreted IFNλ, only reo-dox infection of MDA-MB-231 cells robustly activated STAT1 and STAT2 (Figure 3.4). It is possible that reovirus infection of MDA-MB-231 cells in the presence of topoisomerase inhibitors can favor STAT1 and STAT2 activation. We previously observed that pretreatment of MDA-MB-231 cell with the topoisomerase I inhibitor topotecan followed by reovirus infection induces a similar STAT1 and STAT2 activation phenotype (268). MDA-MB-436 cells exhibit basal activation of STAT 1, STAT2, and STAT3. This activity may be related to MDA-MB-436 cells having higher basal levels of secreted IFNγ than MDA-MB-231 cells (Figure 3.3). IFNγ primarily signals through STAT1 but can also activate other STAT proteins (292). Despite robust secretion of IFNλ after reovirus infection, STAT activity decreases by 2 dpi.

DNA damaging agents including topoisomerase inhibitors can induce elevated secretion of Type I IFN in a STING-dependent, cGAS-independent pathway (216). It is possible that dox-induced DNA damage activates STING by this mechanism to promote Type III IFN and autocrine or paracrine activation of STAT1 and STAT2. Additionally, treatment with doxorubicin correlates with increased activation of STAT1 and STAT2 in some epithelial cell lines, though in an IFNγ-dependent manner (293, 294). In both TNBC cell lines, dox treatment, and not reovirus infection, results in robust amplification of *IFNG* (Figure 3.3A-B) but only low levels of secreted IFNγ. Because the concentration of exogenous dox followed by reovirus infection is greater than the concentration of drug delivered by reo-dox, it is possible that cells treated with exogenous dox are killed too rapidly for robust innate immune responses to be detected. Delivery of dox after reo-dox attachment may also afford an optimal timing for cells to mount robust innate immune and DNA damage responses.

One critical question was whether crosslinking dox to reovirus affects the pharmacological properties of the drug. We show that cells infected with reo-dox exhibit clear evidence of DNA damage and response, with the number of cells harboring DNA double strand breaks increasing by 2 dpi to comparable levels as dox treatment (Figure 3.5). Reo-dox also induces robust levels of γH2AX and activated ATM in both cell lines, as well as phosphorylated p53 in MDA-MB-231 cells (Figure 3.4). While the mechanism by which dox is released from the viral particle remains unclear, we hypothesize that proteolytic processing during endocytosis of the virus results in dox being released from the viral particle. It is possible that extracellular proteases secreted by some TNBC that can interact with the virus (295) may facilitate removal of SMCC-dox from viral particles before endocytic uptake. While SMCC forms an uncleavable thioether bond (296), SMCC and dox bind through succinimidyl ester chemistry yielding an amide bond. As such, dox

may undergo cleavage by amidases or other amide-targeting enzymes delivered to late endosomes, restoring the primary amine of dox and releasing it from viral protein or peptides to interact with nuclear DNA (297-299).

This study is the first to evaluate the effects of this particular reassortant reovirus and reo-dox in an *in vivo* model of TNBC. Reovirus and reo-dox significantly reduce tumor area compared to PBS control and greatly enhances tumor reduction compared to dox treatment (Figure 3.6). Viral antigen staining and assessment of viral titers of tumors indicate that viable virus is present in primary tumors over a week after inoculation (Figure 3.7). Replicating virus at the tumor site likely contributes to virus-mediated tumor regression. Shrinking primary tumors are accompanied by diminished levels of metastasized 4T1 cells in the lungs with both reovirus alone and reo-dox. Reo-dox inoculation results in greater reduction in metastatic 4T1 cells and up to 3x more actively replicating virus in lung tissue than reovirus alone (Figure 3.7D). Metastatic TNBC PDX models can exhibit elevated transcription of oxidative phosphorylation metabolism (OXPHOS) genes compared to primary tumors (300). Inhibition of OXPHOS significantly reduces micrometastatic seeding of lungs in MDA-MB-231 and 4T1 *in vivo* models, indicating a dependence on the shift from glycolytic to OXPHOS metabolism for TNBC cell metastasis (300). It is possible that reovirus infection disrupts mitochondrial membrane potential, interfering with mitochondrial enzymes involved in electron transport chain and limiting metastatic potential. Interestingly, cancer cells shifted toward OXPHOS metabolism exhibit increased sensitivity to antineoplastic agents like dox (301, 302). As such, cells with greater metastatic potential due to a metabolic shift to OXPHOS may be more susceptible to cytotoxic effects of reo-dox. It remains to be seen if the reduced metastatic burden in the lungs is primarily due to enhanced 4T1 cell death in primary tumors or oncolytic activity in the metastatic site. Alternatively, an antiviral immune response like

that elicited *in vitro* in human cell lines may potentiate anti-tumor responses in the tumor microenvironment in mice inoculated with reo-dox.

In this study, we have shown that crosslinking dox to reovirus is a viable alternative to deliver chemotherapeutic agents in combination with oncolytic viruses. This approach mitigates off-target effects of small molecule therapeutics by selectively delivering the drug to cells and tissues targeted by the oncolytic virus. Drug-virus conjugation also enhances the anti-neoplastic effects of chemotherapeutic agents and oncolytic viruses by simultaneously delivering both agents to the same cell. This study presents evidence that reovirus conjugated with a genotoxic drug is a promising advancement in metastatic TNBC therapy.

MATERIALS AND METHODS

Cells, virus, and antibodies

MDA-MB-231 cells (gift from Jennifer Pietenpol, Vanderbilt University) and MDA-MB-436 cells (ATCC HTB-130) were grown in Dulbecco's modified Eagle's medium (DMEM) supplemented with 10% fetal bovine serum (FBS) (Life Technologies) and 100 U per mL penicillin and streptomycin (Life Technologies). Spinner-adapted L929 cells (Terry Dermody, University of Pittsburgh) were grown in Joklik's modified minimal essential medium (MEM) with 5% FBS, 2 mM L-glutamine (Life Technologies), penicillin and streptomycin, and 0.25 mg per mL amphotericin B (Life Technologies). 4T1 cells (gift from Periasamy Selvaraj, Emory University) were grown in DMEM supplemented with 10% FBS, 100 U per mL penicillin and streptomycin, 5 mM L-glutamine, and 5 mM HEPES buffer (Life Technologies).

Working stocks of reassortant reovirus were prepared by plaque purification and passage in L929 cells (247). Purified virions were prepared using second-passage L929 cell lysate stocks. Virus was purified from infected cell lysates by Vertrel XF (TMC Industries Inc.) extraction and CsCl gradient centrifugation (249). The band corresponding to the density of reovirus particles (1.36 g/cm^3) was collected and dialyzed exhaustively against virion storage buffer (150 mM NaCl, 15 mM MgCl 2, 10 mM Tris-HCl [pH 7.4]). The reovirus particle concentration was determined from the equivalence of 1 unit of optical density at 260 nm to 2.1×10^{12} particles (250). Viral titers were determined by plaque assay using L929 cells (251).

Reovirus polyclonal rabbit antiserum raised against reovirus strains T1L and T3D was purified (252) and cross-adsorbed for MDA-MB-231 or 4T1 cells. Secondary IRDye 680 and 800 antibodies (Li-Cor Biosciences) and goat anti-rabbit A488 (Life Technologies) were used.

Doxorubicin conjugation to reovirus

10 mM doxorubicin was diluted to 7.5 mM in PBS. Doxorubicin was mixed with 3.7 mg/mL succinimidyl 4-(N-maleimidomethyl)cyclohexane-1-carboxylate (SMCC) in a 10:1 ratio and incubated at room temperature for 30 min. Doxorubicin and SMCC solution was dialyzed against cold PBS for 1 h at 4°C. Desalted SMCC-doxorubicin solution was measured for doxorubicin concentration by UV-vis spectroscopy on a Nanodrop Nd-8000 (Thermo Scientific). Absorbance at 480 nm (A480) was assessed and compared to a doxorubicin gradient standard curve. 3×10^{12} particles of reovirus were diluted in PBS up to 100 µL and combined with 400 µL of 500 µM SMCC-dox. Reovirus plus SMCC-dox solution was incubated for 30 min at room temperature with agitation on a tube revolver (Thermo Scientific) on reciprocating setting. The solution was dialyzed exhaustively against cold PBS overnight at 4°C.

Cell viability assay

To determine the effect of reo-dox on cell viability, MDA-MB-231 and MDA-MB-436 cells were pretreated with increasing concentrations of doxorubicin for 1 h at 37°C. Reovirus or reo-dox was added to cells at an MOI of 100 PFU/cell, and incubated in the presence of doxorubicin for 0-3 days. 4T1 cells were treated with vehicle (DMSO) or 10 µM doxorubicin, or infected with reovirus or reo-dox at MOIs of 10, 50, and 100 PFU/cell for 0-3 days. Presto Blue (Invitrogen) was added at each time point for 30 min at 37°C and fluorescence (540 nm excitation/590 nm emission) was measured with a Synergy HT or Synergy H1 plate reader (Biotek).

Flow cytometric analysis of cell-surface reovirus

MDA-MB-231 and MDA-MB-436 cells were treated with vehicle or 1 μM doxorubicin for 30 min at 37°C and then 4°C for 30 min. Media was removed and cells were adsorbed with reovirus or reo-dox at an MOI of 1×10^5 particles/cell in OMEM (Gibco) for 1 h at 4°C. Cells were washed with PBS, detached with Cellstripper (Cellgro) for 10 min at 37°C, quenched and washed with PBS containing 2% FBS. Surface reovirus antigen was stained using reovirus-specific antiserum and Alexa Fluor 488 secondary antibody (A488, Thermo Scientific). Cells were fixed in 1% EM-grade paraformaldehyde (Electron Microscopy Sciences). Mean fluorescence intensity (MFI) and percent reovirus-positive cells were assessed using a CytoFLEX flow cytometer (Beckman Coulter) and quantified using FlowJo software.

Reovirus infectivity assay

Reo-dox infectivity was assessed by indirect immunofluorescence assay. MDA-MB-231, MDA-MB-436, and 4T1 cells were pretreated with vehicle (DMSO), 2.0 μM or 0.2 μM doxorubicin, or 8 μM E64-d for 1 h at 37°C. Reovirus or reo-dox was added to cells and incubated for 18 h at 37°C. Cells were fixed with ice-cold methanol for at least 30 min. Methanol was removed, cells were washed twice with PBS, and blocked with PBS containing 1% BSA for 15 min at room temperature. Cells were stained with reovirus-specific polyclonal antiserum (1:2000) for 1 h at room temperature, washed twice with PBS, stained with A488 (1:1000) for 1 h at room temperature, stained with 0.5 ng/ml DAPI for 5 min at room temperature, and washed twice with PBS. Immunofluorescence was detected using a Lionheart FX Automated Microscope (Biotek) with a 4x-PLFL phase objective (NA 0.13), and percent infectivity was determined (reovirus positive cells/DAPI positive cells) using Gen5 software (Biotek).

Reovirus replication assay

MDA-MB-231 and MDA-MB-436 cells were adsorbed with reovirus or reo-dox at an MOI of 10 PFU/cell in OMEM (Gibco) for 1 h at room temperature, washed with PBS, and incubated for 0-3 days with complete media at 37°C. Cells were freeze-thawed three times and viral titers were determined by plaque assay using L929 cells. Viral yields were calculated by dividing viral titers by the viral titer from day 0.

qPCR assessment of Type-I and -III interferon transcript levels

MDA-MB-231 and MDA-MB-436 cells were treated with DMSO or 2 μM doxorubicin for 1 h at 37°C, infected with mock, reovirus, or reo-dox at an MOI of 100 PFU/cell, and incubated for 0, 8, 12, 24, and 48 h. RNA was isolated using a QIAGEN RNeasy kit with on-column DNase digestion. cDNAs were generated using 500 ng of RNA and random primers with the High-Capacity cDNA Reverse Transcription Kit (ThermoFisher) in a SimpliAmp Thermal Cycler (ThermoFisher). cDNA was diluted 1:5 in nuclease-free water and qPCR reactions were performed in MicroAmp Fast Optical 96-Well Reaction Plates (Applied Biosystems) using Primetime qPCR assays (IDT) for *IFNB1*, *IFNL1*, *HPRT1*, and a custom assay for the reovirus *S1* gene segment (Probe: 5'-/56-FAM/TCAATGCTG/ZEN/TCGAACCACGAGTTGA/3IABkFQ/-3'; Primer 1: 5'-CGAGTCAGGTCACGCAATTA-3'; Primer 2: 5'-GGATGTTCGTCCAGTGAGATTAG-3') using a 7500 Fast Real-Time PCR System (Applied Biosystems) and accompanying software to analyze qPCR data.

IFN ELISA

MDA-MB-231and MDA-MB-436 cells were treated with DMSO or 2 μM doxorubicin for 1 h at 37°C, infected with mock, reovirus, or reo-dox at an MOI of 100 PFU/cell, and incubated for 0, 8, 12, 24, and 48 h. Cell supernatants were collected and levels of IFNl or IFNβ were determined with the Human IFN-λ 1/3 and Human IFN-β DuoSet ELISA kits (R&D Systems). Plates were read on a Synergy HT or Synergy H1 plate reader (Biotek) using 450 nm for sample detection and 540 nm for wavelength correction.

Immunoblotting for DNA damage response and innate immune molecules

MDA-MB-231 or MDA-MB-436 cells were treated with DMSO or 2 μM doxorubicin for 1 h at 37°C, infected with mock, reovirus, or reo-dox at an MOI of 100 PFU/cell, and incubated for 0-2 days at 37°C. To assess the ability of IFNs to stimulate immune signaling, MDA-MB-436 cells were treated with 10 and 100 ng/ml of IFNl or 100 and 1000 IU/ml IFNb for 1 h at 37°C. Whole cell lysates were prepared using RIPA buffer (20 mM Tris-HCl [pH 7.5], 150 mM NaCl, 1 mM EDTA, 1% NP-40, 0.1% sodium dodecyl sulfate, 0.1% sodium deoxycholate) and fresh Protease Inhibitor Cocktail (P8340, Sigma-Aldrich), Phosphatase Inhibitor Cocktail 2 (P5726, Sigma-Aldrich), 1 mM sodium vanadate, and 1 mM phenylmethylsulfonyl fluoride (PMSF) and protein concentration was determined using the DC protein assay (Bio-Rad). Whole cell lysates were resolved by SDS-PAGE in 4-20% gradient Mini-PROTEAN TGX gels (Bio-Rad) and transferred to 0.2 mm pore size nitrocellulose membranes (Bio-Rad). Membranes were incubated for 1 h in blocking buffer (Tris-buffered saline [TBS] with 5% powdered milk), incubated with primary antibodies specific for phospho-ATM(S1981, clone 10H11.E12, #4526), -p53(S15, #9284), -H2AX (S139, #2577), -STAT1 (Y701, clone D4A7 #7649), -STAT2 (Y690,

clone D3P2P, #88410), -STAT3 (Y705, clone D3A7, #9145), total ATM (clone D2E2, #2873), p53 (clone 1C12, #2524), STAT1 (clone D3A7, #9145), STAT2 (clone D9J7L, #72604), STAT3 (clone 124H6, #9139), and GAPDH (clone GA1R, MA5-15738), and reovirus polyclonal antiserum overnight at 4°C. Antibodies are from Cell Signaling Technology except for GAPDH (ThermoFisher). Membranes were washed with TBS-T (TBS with 0.1% Tween 20), incubated with secondary antibodies conjugated to IRDye 680 or IRDye 800, and imaged using a LiCor Odyssey CLx and processed in ImageStudio (LI-COR Biosciences).

Comet Assay

Protocol adapted from Olive and Banáth, 2006 (303). MDA-MB-231 and MDA-MB-436 cells were pretreated with vehicle (DMSO) or 2 μM doxorubicin for 1 h at 37°C. Without changing media, cells were infected with mock, reovirus, or reo-dox at an MOI of 100 PFU/cell in an equal volume of media for 1 h at 37°C. At 0 and 2 days post infection, trypsin was added and cells were diluted to 2×10^4 cells/mL in cold PBS. 1% low melting point agarose (Lonza) in pure water was added to each cell solution in a 3:1 ratio. Agarose-cell solution was dispensed on a glass microscope slide, and a glass coverslip was placed on top of the agarose solution. Slides were allowed to gel at 4°C for 10 min, coverslips were removed, and slides were incubated for 10 min at 4°C. Slides were arranged in single layers in 150 mm culture dishes, lysis buffer (2% sarkosyl, 0.5M Na2EDTA, 0.5 mg/ml proteinase K) were added to each slide, and slides were incubated for 18 h at 37°C. Gels were washed three times for 20 min with 1x TBE (tris-HCl, borate, EDTA) at room temperature. Slides were electrophoresed in TBE for 25 min at 0.6 V/cm (12 V on a Bio-Rad Wide Mini-Sub Cell GT gel rig), then washed with water before submerging in 1:10,000

DAPI in water for 20 min with occasional rocking. Slides were washed with water and imaged on an epifluorescent microscope. Cells were scored with the Comet Score software.

In vivo 4T1 model

Female BALB/c mice, 6-8 weeks of age, were purchased from Jackson Laboratories and were maintained in accordance with IACUC approved institutional guidelines and protocols. Mice were housed in static racks with Micro-Isolator housing with individual water and food supplies. 4T1 breast cancer cells were inoculated subcutaneously on the hind flank with $5x10^4$ cells in 100 μL of PBS. Mice were monitored for tumor growth and weight loss and were euthanized if tumors became ulcerated or reached $>2cm^2$ or lost 25% of their initial weight following IACUC protocols. Doxorubicin was delivered intratumorally at a concentration of 0.14 mg/kg in 50 μL of PBS, and reovirus or reo-dox was delivered intratumorally at a concentration of 5×10^8 PFU in 50 μL of PBS once tumors reached 7mm in diameter. After inoculation, mice were housed in Animal Biocontainment Level 2 (ABSL2) rooms and handled following the Division of Animal Resources (DAR) guidelines based on the Biosafety in Microbiological and Biomedical Laboratories (BMBL) 5th edition guidelines.

Immunohistochemistry on 4T1 tissue samples

Tissue samples were fixed in 10% formalin for 24 h. Formalin was aspirated from samples and tissues were stored in 70% ethanol until processed for paraffin embedding and slide mounting (Emory Cancer Tissue and Pathology Shared Resource Core). Mounted tumor tissues were stained for γH2AX (Cell Signaling, S139, clone 20E3 #9781) at 1:480 and reovirus using polyclonal antibody crossadsorbed in L929 mouse fibroblasts and 4T1 murine mammary adenocarcinoma

cells. Reovirus antibody was used at 1:8000. Stained tissues were scanned using an Olympus Nanozoomer whole-slide scanner (Emory Cancer Tissue and Pathology Shared Resource Core). Images were analyzed using QuPath software (304) with the following scripts:

Reovirus polyclonal antibody detection was run on manually selected whole tissues:

```
setImageType('BRIGHTFIELD_H_DAB');
setColorDeconvolutionStains('{"Name" : "H-DAB default", "Stain 1" :
"Hematoxylin", "Values 1" : "0.65111 0.70119 0.29049 ", "Stain 2" : "DAB",
"Values 2" : "0.26917 0.56824 0.77759 ", "Background" : " 255 255 255 "}');
runPlugin('qupath.imagej.detect.nuclei.PositiveCellDetection',
'{"detectionImageBrightfield": "Hematoxylin OD",
"requestedPixelSizeMicrons": 0.5,  "backgroundRadiusMicrons": 8.0,
"medianRadiusMicrons": 0.0,  "sigmaMicrons": 1.5,  "minAreaMicrons": 2.0,
"maxAreaMicrons": 400.0,  "threshold": 0.1,  "maxBackground": 2.0,
"watershedPostProcess": true,  "excludeDAB": false,  "cellExpansionMicrons":
5.0,  "includeNuclei": true,  "smoothBoundaries": true,  "makeMeasurements":
true,  "thresholdCompartment": "Cell: DAB OD mean",  "thresholdPositive1":
0.2,  "thresholdPositive2": 0.4,  "thresholdPositive3": 0.6,
"singleThreshold": false}');
```

γH2AX:

```
setImageType('BRIGHTFIELD_H_DAB');
setColorDeconvolutionStains('{"Name" : "H-DAB default", "Stain 1" :
"Hematoxylin", "Values 1" : "0.65111 0.70119 0.29049 ", "Stain 2" : "DAB",
"Values 2" : "0.26917 0.56824 0.77759 ", "Background" : " 255 255 255 "}');
runPlugin('qupath.imagej.detect.tissue.SimpleTissueDetection2',
'{"threshold": 212,  "requestedPixelSizeMicrons": 5.0,  "minAreaMicrons":
10000.0,  "maxHoleAreaMicrons": 1000000.0,  "darkBackground":
false,  "smoothImage": true,  "medianCleanup": true,  "dilateBoundaries":
false,  "smoothCoordinates": true,  "excludeOnBoundary":
false,  "singleAnnotation": true}');
selectAnnotations();
runPlugin('qupath.imagej.detect.nuclei.PositiveCellDetection',
'{"detectionImageBrightfield": "Hematoxylin
OD",  "requestedPixelSizeMicrons": 0.5,  "backgroundRadiusMicrons":
8.0,  "medianRadiusMicrons": 0.0,  "sigmaMicrons": 2.0,  "minAreaMicrons":
2.0,  "maxAreaMicrons": 400.0,  "threshold": 0.1,  "maxBackground":
2.0,  "watershedPostProcess": true,  "excludeDAB":
false,  "cellExpansionMicrons": 5.0,  "includeNuclei":
true,  "smoothBoundaries": true,  "makeMeasurements":
true,  "thresholdCompartment": "Nucleus: DAB OD
mean",  "thresholdPositive1": 0.3,  "thresholdPositive2":
0.4,  "thresholdPositive3": 0.5,  "singleThreshold": false}');
```

Clonogenic assay for metastatic 4T1 cells in lungs

Mice were euthanized on day 21 post tumor challenge. Lungs were digested and processed to a single cell suspension using collagenase type IV (Sigma-Aldrich) for 3 h at 37°C with constant motion. Homogenates were strained using a 70 μm cell strainer. Cells were washed and suspended in DMEM with 10%FBS (Hyclone) containing 6-thioguanine (Sigma-Aldrich). Serial dilutions were made and cultures were grown in a 6-well plate at 37°C with 5% CO_2 until the first well reached confluence. Cell counts were obtained using a hemocytometer.

Statistical analysis

Mean values for triplicate and quadruplicate experiments were compared using one or two-way analysis of variance (ANOVA) with Dunnett's or Tukey's multiple-comparisons test (Graph Pad Prism). *P* values of < 0.05 were considered statistically significant.

ACKNOWLEDGEMENTS

We thank Dr. Curtis Henry, Emily Greene, and Allison Wolf for critical revision and feedback during manuscript preparation. This work was supported by funding from the Children's Healthcare of Atlanta and the Pediatric Research Institute, Winship Comprehensive Cancer Institute #IRG-14-188-01 from the American Cancer Society, and the National Institutes of Health (R01 AI146260) (B.A.M.)., NCI/NIH R01 grant (R01 CA202763 to P.S.), and Diversity Supplement grant (R01 CA202763-S to L.E.M.). Flow cytometry experiments were performed in the Emory Pediatrics Flow Cytometry Core (UL1TR002378). Imaging was performed at the Emory Integrated Cellular Imaging Core (2P30CA138292-04 and the Emory Pediatrics Institute). Mouse tissue histology and imaging was performed by the Cancer Tissue and Pathology shared resource of Winship Cancer Institute of Emory University and NIH/NCI (P30CA138292). The funders had no role in the study design, data collection and analysis, decision to publish, or preparation of manuscript.

AUTHOR CONTRIBUTIONS

J.T.L.B., L.E.M., R.M.R.S., and B.A.M. designed *in vitro* and *in vivo* experiments. J.T.L.B., L.E.M., and R.M.R.S. contributed to carrying out experiments and data analysis. J.T.L.B. and B.A.M. wrote the manuscript and prepared figures. P.S. provided *in vivo* study support.

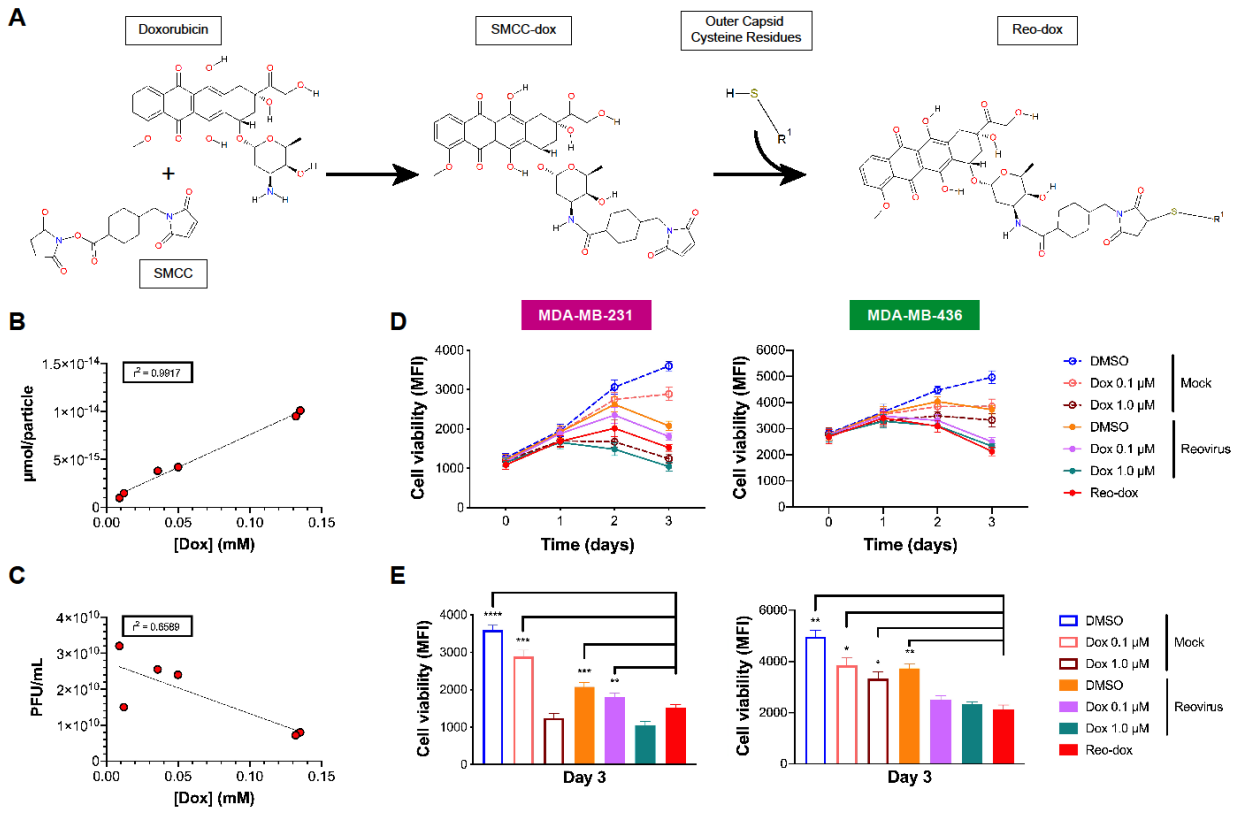

Figure 3.1. Doxorubicin conjugation to reovirus enhances viral cytotoxicity in TNBC cells.

(A) Chemistry of doxorubicin conjugation to reovirus. The lone primary amine of doxorubicin reacts with the succinimide functional group of succinimidyl 4-(n-maleimidomethyl) cyclohexane-1-carboxylate (SMCC) to form SMCC-dox. Cysteine residues on viral capsid proteins (R^1) react with the maleimide functional group of SMCC-dox, yielding a final crosslinked product or doxorubicin bound to reovirus (reo-dox). (B-C) UV-vis spectroscopy was performed on reo-dox preparations (Table 3.S1). (B) Doxorubicin concentration was correlated with the amount of drug per reovirus particle and (C) viral titer. r^2 values are presented for six independently labeled reo-dox preparations. (D-E) TNBC cells were pretreated with vehicle (DMSO) or doxorubicin. Cells were infected with mock, reovirus, or reo-dox at an MOI of 100 PFU/cell. (D) Cell viability was measured over three days post infection. (E) Cell viability at 3 dpi. From (D). Data represent the

mean of four independent experiments. Error bars = SEM. *, $P \leq 0.05$; **, $P \leq 0.01$; ***, $P \leq 0.001$; ****, $P \leq 0.0001$ by one-way ANOVA for reo-dox compared to all conditions.

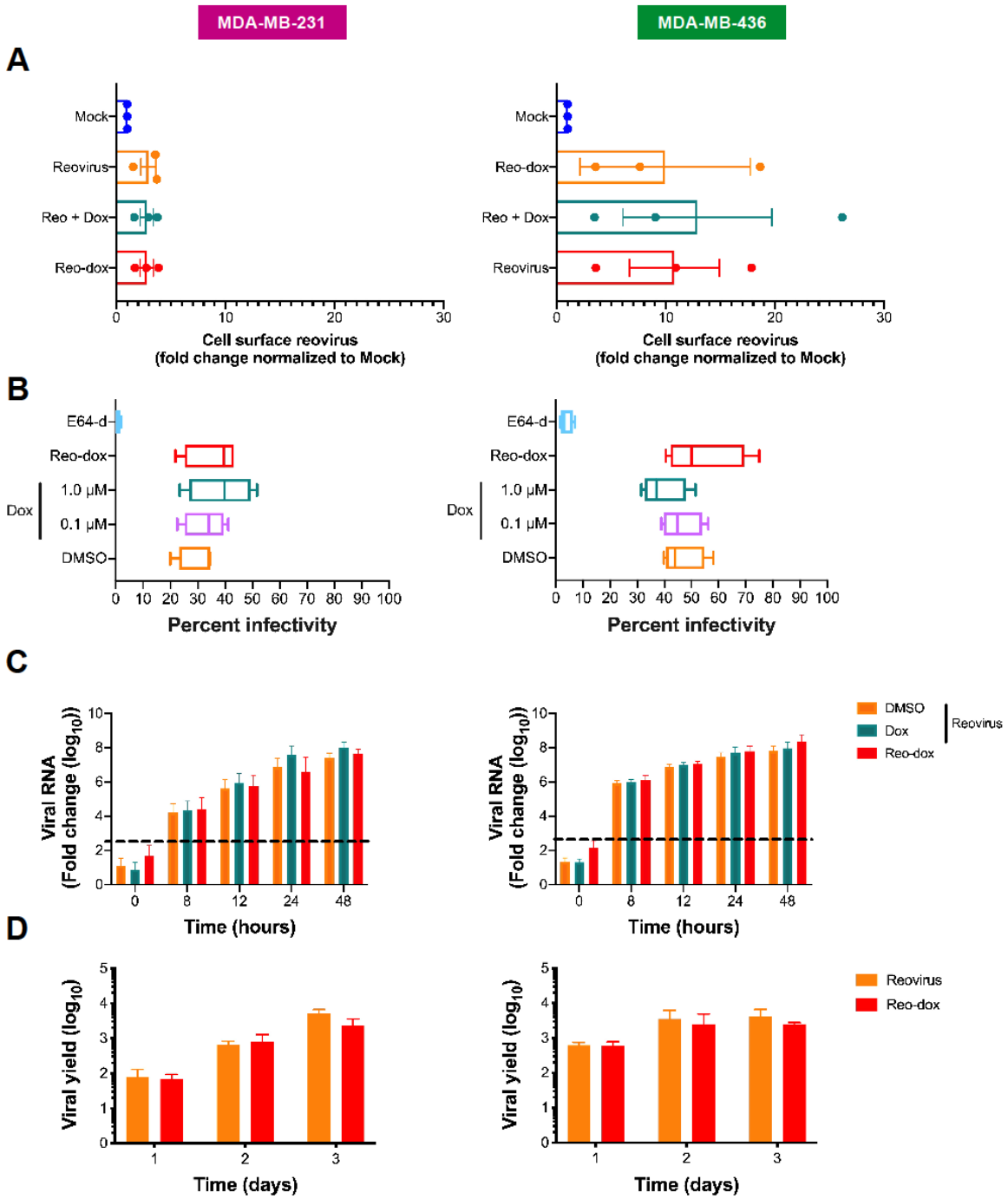

Figure 3.2. Reo-dox has similar attachment, infectivity, and replication kinetics as reovirus, but enhanced cytotoxicity in TNBC cells.

Results for MDA-MB-231 cells are displayed on left and MDA-MB-436 cells are displayed on right for all panels. (A) TNBC cells were pretreated with vehicle (DMSO) or doxorubicin and

adsorbed with mock, reovirus, or reo-dox at an MOI of 1×10^5 particles/cell for 1 h at 4°C. Cells were assessed for cell surface reovirus by flow cytometry using indirect immunofluorescence. (B) TNBC cells were pretreated with vehicle (DMSO), E64-d, or doxorubicin and infected with mock, reovirus, or reo-dox at an MOI of 100 PFU/cell for 18 h. Infectivity was assessed by indirect immunofluorescence. (C) TNBC cells were pretreated with vehicle (DMSO) or doxorubicin and infected with mock, reovirus, or reo-dox, and qPCR was performed to assess RNA levels of reovirus *S1* gene. Dashed line represents background baseline levels observed in mock. Data are shown as fold change normalized to a housekeeping gene. (D) TNBC cells were adsorbed with reovirus or reo-dox at an MOI of 10 PFU/cell over a three day time course. Viral titers were assessed by plaque assay on L929 mouse fibroblasts and viral yield was calculated as fold increase in titer compared to day 0. Error bars = SEM. Data represent the means of three (A) or four (B-D) independent experiments. Error bars = SEM.

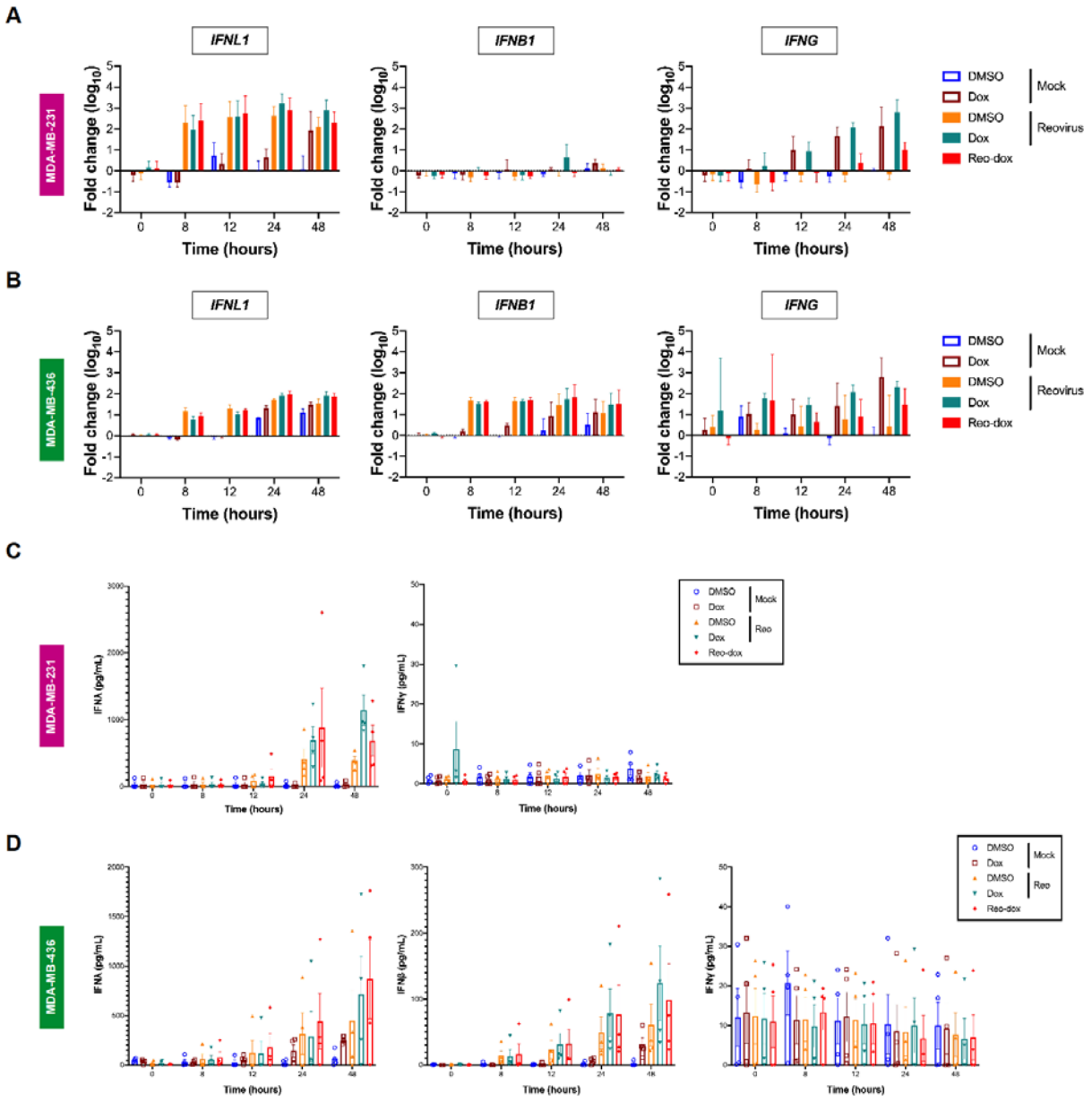

Figure 3.3. Reo-dox induces Type-III IFN in TNBC cells.

(A) MDA-MB-231 and (B) MDA-MB-436 cells were pretreated with vehicle (DMSO) or doxorubicin and infected with mock, reovirus, or reo-dox. RNA was isolated from cells at times shown and qPCR was performed to assess mRNA levels of *IFNL1*, *IFNB1*, and *IFNG*. Data are shown as fold change to DMSO Mock at 0 h for four independent experiments. Error bars = SEM.

(C-D) Levels of IFNλ, IFNβ (MDA-MB-436 only), and IFNγ in cell supernatants were detected by ELISA. Data are shown as pg/mL of IFN for four independent experiments. Error bars = SEM.

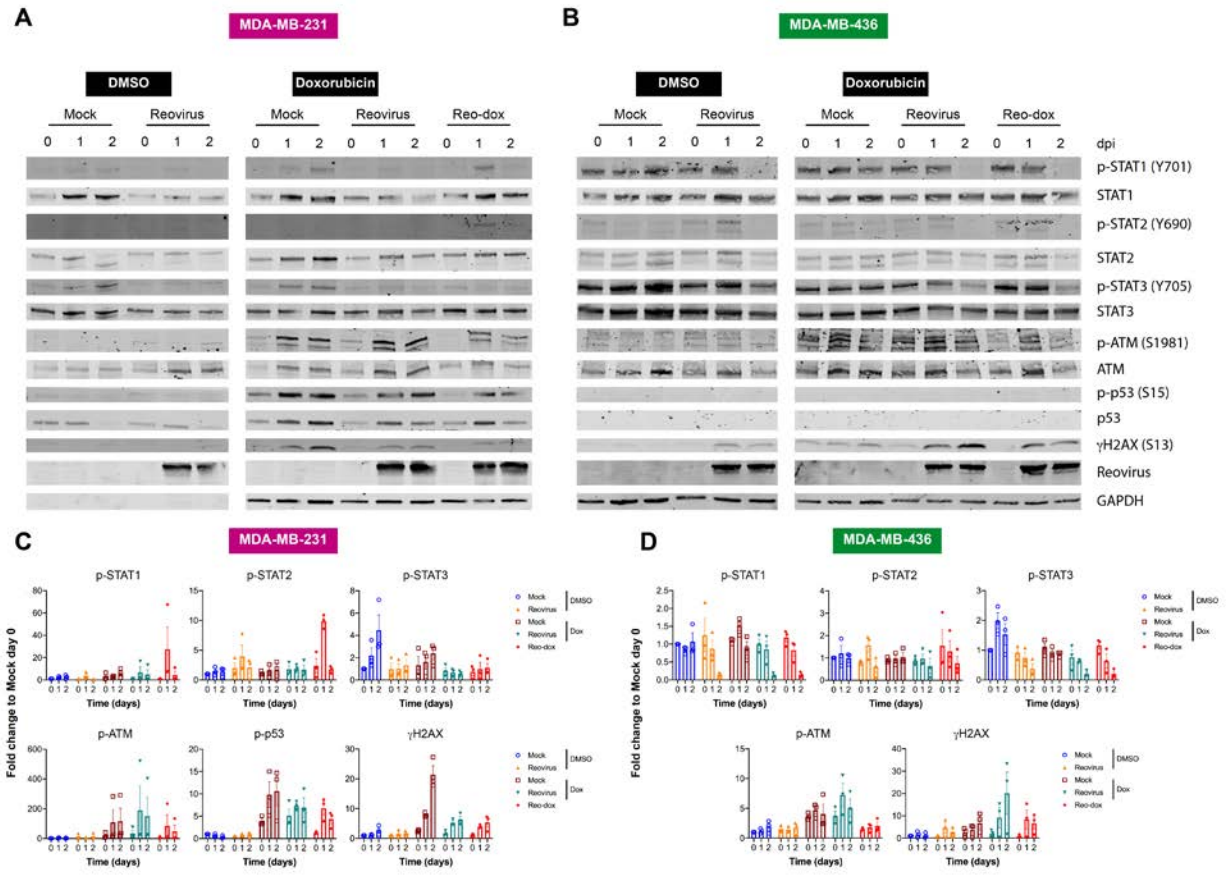

Figure 3.4. Reo-dox activates DNA damage response pathways and modulates innate immune activity in TNBC cells.

(A, C) MDA-MB-231 and (B, D) MDA-MB-436 cells were treated with vehicle (DMSO) or doxorubicin and infected with reovirus or reo-dox at an MOI of 100 PFU/cell. (A-B) Whole cell lysates for 0, 1, and 2 dpi were resolved by SDS-PAGE and immunoblotted with antibodies specific for phosphorylated and total STAT1, STAT2, STAT3, ATM, p53, H2AX, reovirus, and GAPDH. Residues recognized by phosphorylation-specific antibodies are shown in parentheses. Blots are representative of three independent experiments. (C-D) Quantitative densitometry was performed on all phosphorylated and total proteins. Data represent means of three independent experiments normalized to respective mock day 0 values. Error bars = SEM.

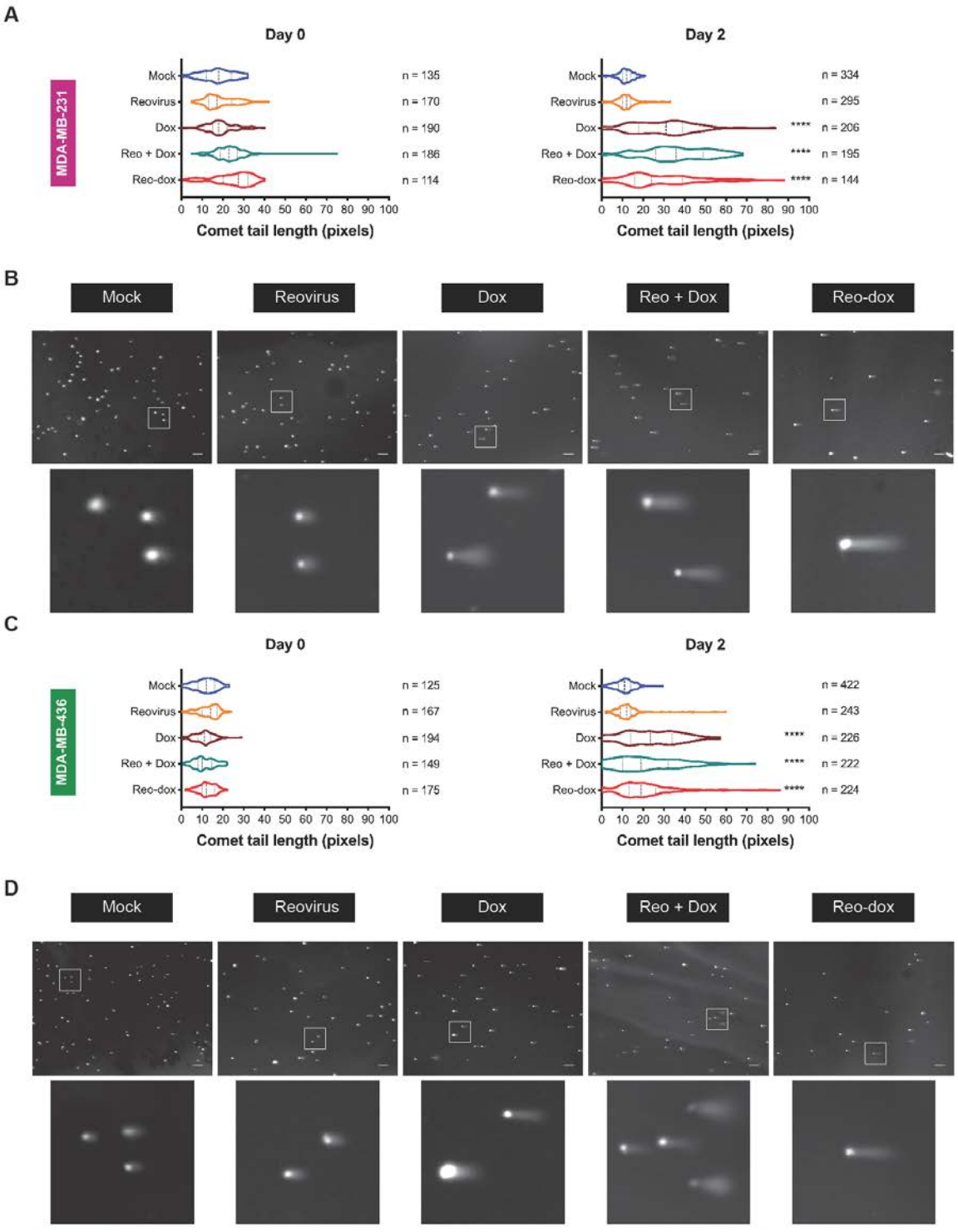

Figure 3.5. Reo-dox infection of TNBC cells induces DNA double strand breaks.

(A-B) MDA-MB-231 and (C-D) MDA-MB-436 cells were pretreated with vehicle (DMSO) or doxorubicin and infected with mock, reovirus, or reo-dox at an MOI of 100 PFU/cell. DNA double

strand break damage was assessed by single cell electrophoresis (comet assay) on 0 and 2 dpi. Chromatin was visualized by epifluorescence using DAPI staining. (A, C) Comet tail length was measured for imaged cells. Data represented as violin plots. Median and upper and lower quartiles are presented as dotted lines within violins. ****, $P \leq 0.0001$ compared to mock and reovirus by one-way ANOVA for reo-dox compared to all conditions. (B, D) Representative images of comets on 2 dpi. Scale bar = 200 μm. Inset highlights boxed cells. Data are representative of two independent experiments.

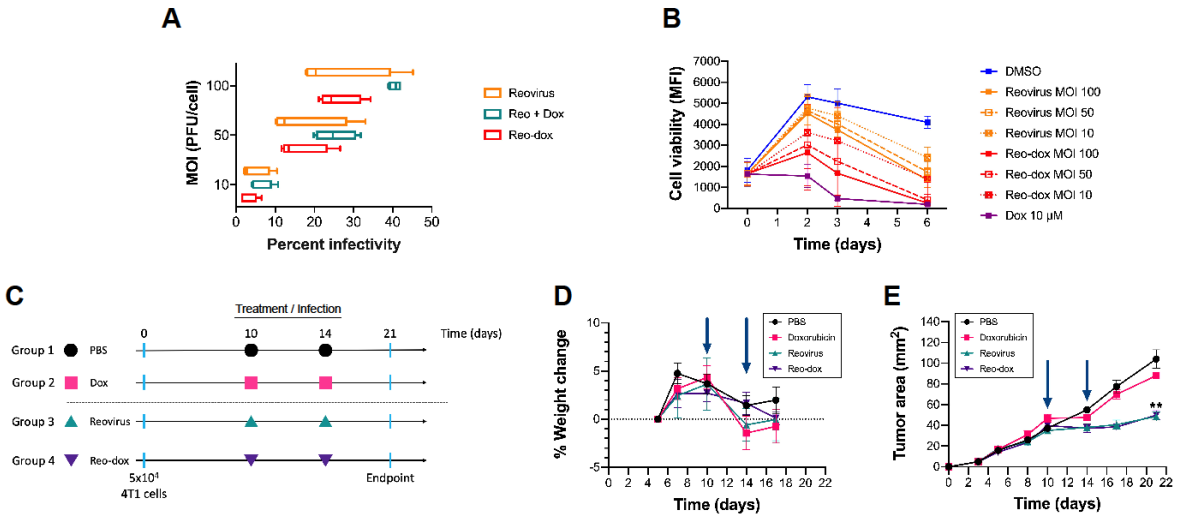

Figure 3.6. Reo-dox and reovirus infect and kill 4T1 cells *in vitro* and *in vivo*, and reduce 4T1 cell metastatic potential to the lungs.

(A) 4T1 cells were pretreated with vehicle (DMSO) or doxorubicin and infected with mock, reovirus, or reo-dox. Infectivity was assessed after 20 h by indirect immunofluorescence using reovirus-specific antiserum. (B) 4T1 cells were treated with vehicle (DMSO) or doxorubicin, or infected with reovirus or reo-dox at increasing MOIs. Cell viability was assessed at times shown. (A-B) Data represent mean of four independent experiments. Error bars = SEM. (C) Female, 8-week-old Balb/c mice were challenged with 5×10^4 4T1 cells via subcutaneous injection in the hind flank. At day 10 and 14 post challenge (arrows in D and E), mice were treated with PBS, 54.4 µg/mL doxorubicin, or 5×10^8 PFU of reovirus or reo-dox. The experimental endpoint was 21 days post tumor challenge. (D) Percent change in weight of mice was calculated as the weight on day of measurement normalized to weight at day 5. (E) Tumor area was measured at days indicated by data points. **, $P < 0.01$, Reovirus and Reo-dox compared to PBS by two-way ANOVA. (C-E) n = 5 mice per treatment group. Error bars = SEM.

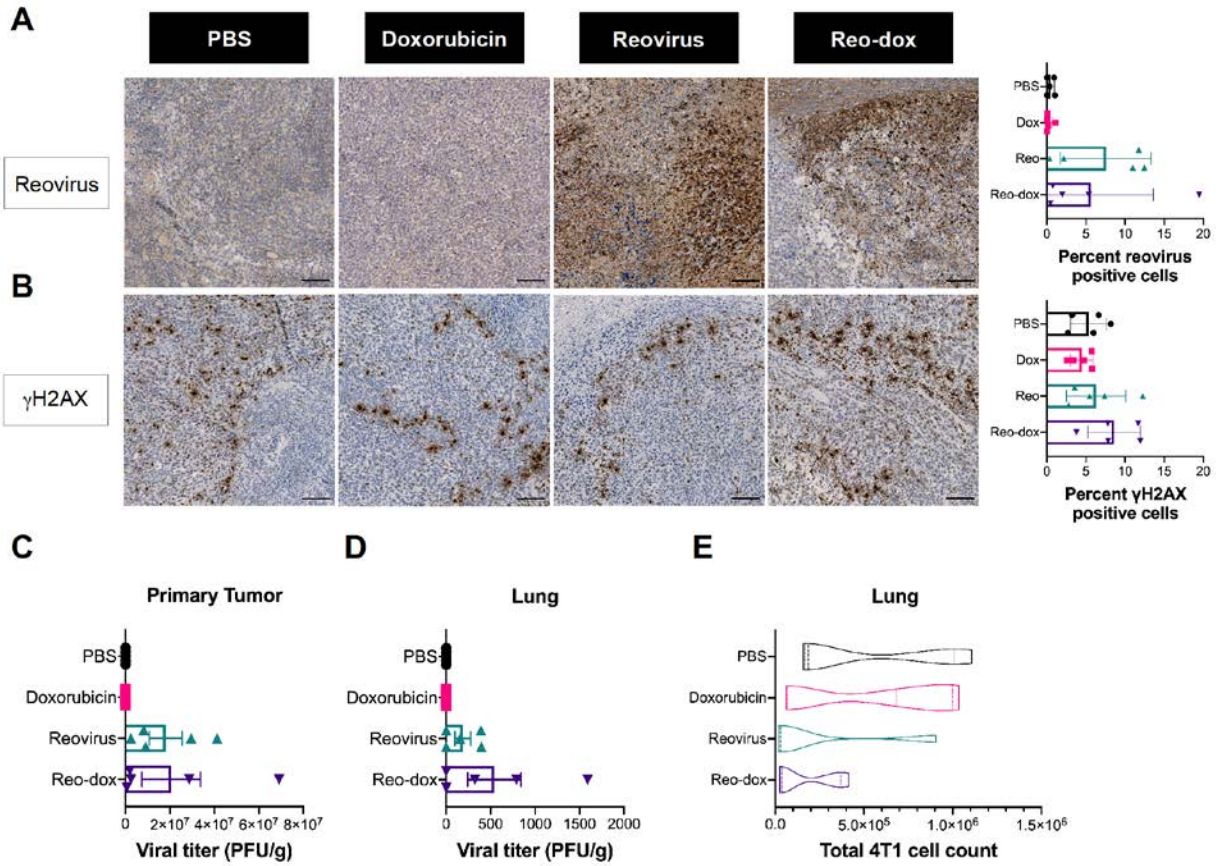

Figure 3.7. Reovirus antigen γH2AX are detected in 4T1 tumors infected with reo-dox.

Primary tumor tissues were assessed for (A) reovirus antigen and (B) γH2AX levels by indirect immunohistochemistry. (A-B) Inset images enlarged from representative whole tissue scans in Figure 3.S4. Scale bars = 100 μm. Percent of cells in whole tissue scans positive for reovirus antigen and γH2AX presented on right. Bar graphs represent mean of representative tissue from each mouse. n = 5. Error bars = SD. (C) Titers for reovirus or reo-dox present in primary tumor tissue and (D) lungs were assessed by plaque assay on L929 mouse fibroblasts. (E) Total number of metastatic 4T1 cells in lungs were counted. Data are represented as violin plots with median and upper and lower quartiles indicated by vertical dotted lines within violins. (C-E) n = 5 mice. Error bars = SEM.

Table 3.S1. UV-vis Spectroscopy to Determine the Amount of Doxorubicin in Reo-dox Preparations.

	Reo-dox Sample						
	1	2	3	4	5	6	AVG
A480	0.15	0.12	0.12	0.16	0.24	0.24	0.17
[Dox] (mM)	3.57×10^{-2}	9.08×10^{-3}	1.21×10^{-2}	4.99×10^{-2}	1.35×10^{-1}	1.32×10^{-1}	6.30×10^{-2}
PFU/mL	2.55×10^{10}	3.20×10^{10}	1.50×10^{10}	2.40×10^{10}	8.00×10^{9}	7.20×10^{9}	1.86×10^{10}
Particles/mL	9.36×10^{12}	9.26×10^{12}	8.15×10^{12}	1.19×10^{13}	1.34×10^{13}	1.39×10^{13}	1.10×10^{13}
μmol/PFU	1.40×10^{-12}	2.84×10^{-13}	8.05×10^{-13}	2.08×10^{-12}	1.69×10^{-11}	1.83×10^{-11}	6.63×10^{-12}
μmol/particle	3.81×10^{-15}	9.81×10^{-16}	1.48×10^{-15}	4.20×10^{-15}	1.01×10^{-14}	9.50×10^{-15}	5.01×10^{-15}
	SMCC-dox pre-dialysis		Mock SMCC-dox dialysate		Parental Reovirus		
A480	1.34		3.33×10^{-4}		0		
[Dox] (mM)	1.23		0		0		
	Doxorubicin Standard						
A480	0.17	0.46	1.39	2.96	4.79	7.05	10.65
[Dox] (mM)	0.1	0.5	1.0	2.5	5.0	7.5	10.0

A480 values represent the absorbance measured for each sample at 480 nm. Each value presented is the average of three readings for the sample.

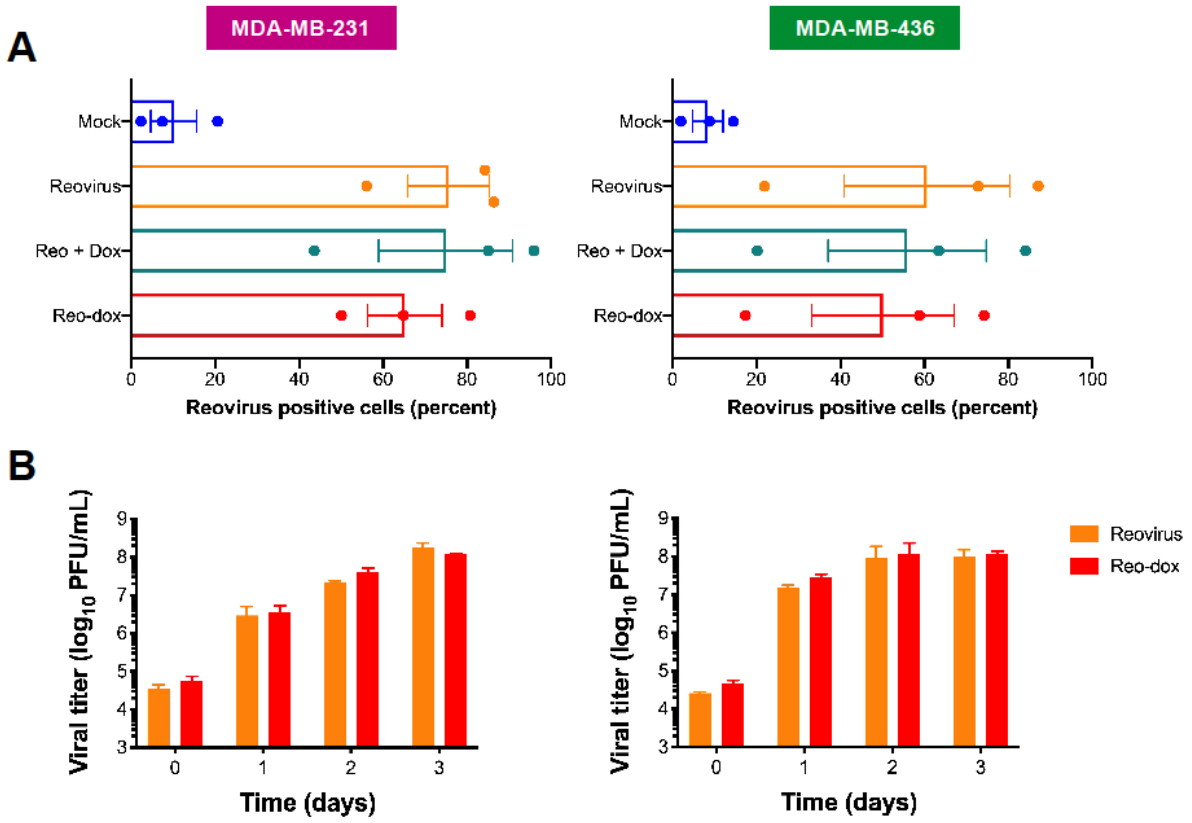

Figure 3.S1. Reo-dox exhibits similar attachment and replication kinetics as reovirus in TNBC cells.

(A) TNBC cells were pretreated with vehicle (DMSO) or doxorubicin and adsorbed with mock, reovirus, or reo-dox at an MOI of 1×10^5 particles/cell for 1 h at 4°C. Cells were assessed for surface-attached reovirus by flow cytometry using indirect immunofluorescence. Data are presented as mean of percent of cells with attached reovirus for three independent experiments. Error bars = SEM. (B) TNBC cells were adsorbed with reovirus or reo-dox at an MOI of 10 PFU/cell over a three day time course. Viral titers were assessed by plaque assay on L929 mouse fibroblasts. n = 4. Error bars = SEM.

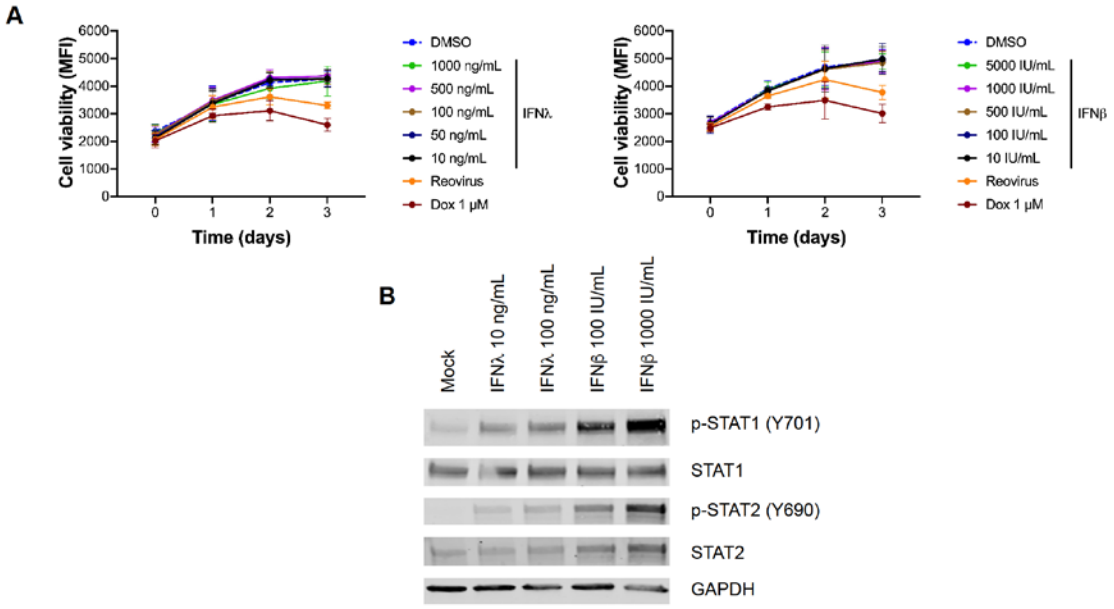

Figure 3.S2. IFNλ does have cytotoxic effects on MDA-MB-436 cells but induces activation of STAT1 and STAT2.

(A) MDA-MB-436 cells were treated with vehicle (DMSO), 1 µM doxorubicin, recombinant human IFNλ or IFNβ, or infected with reovirus at an MOI of 100 PFU/cell for 1 h and assessed for cell viability at 0-3 days post treatment or infection. Data are shown as mean fluorescence intensity (MFI) for the average of four independent experiments. Error bars = SEM. (B) MDA-MB-436 cells were treated with recombinant IFNλ or IFNβ for 1 h. Whole cell lysates were resolved by SDS-PAGE and immunoblotted with antibodies specific for phosphorylated and total STAT1, STAT2, and GAPDH. Residues recognized by phosphorylation-specific antibodies are shown in parentheses.

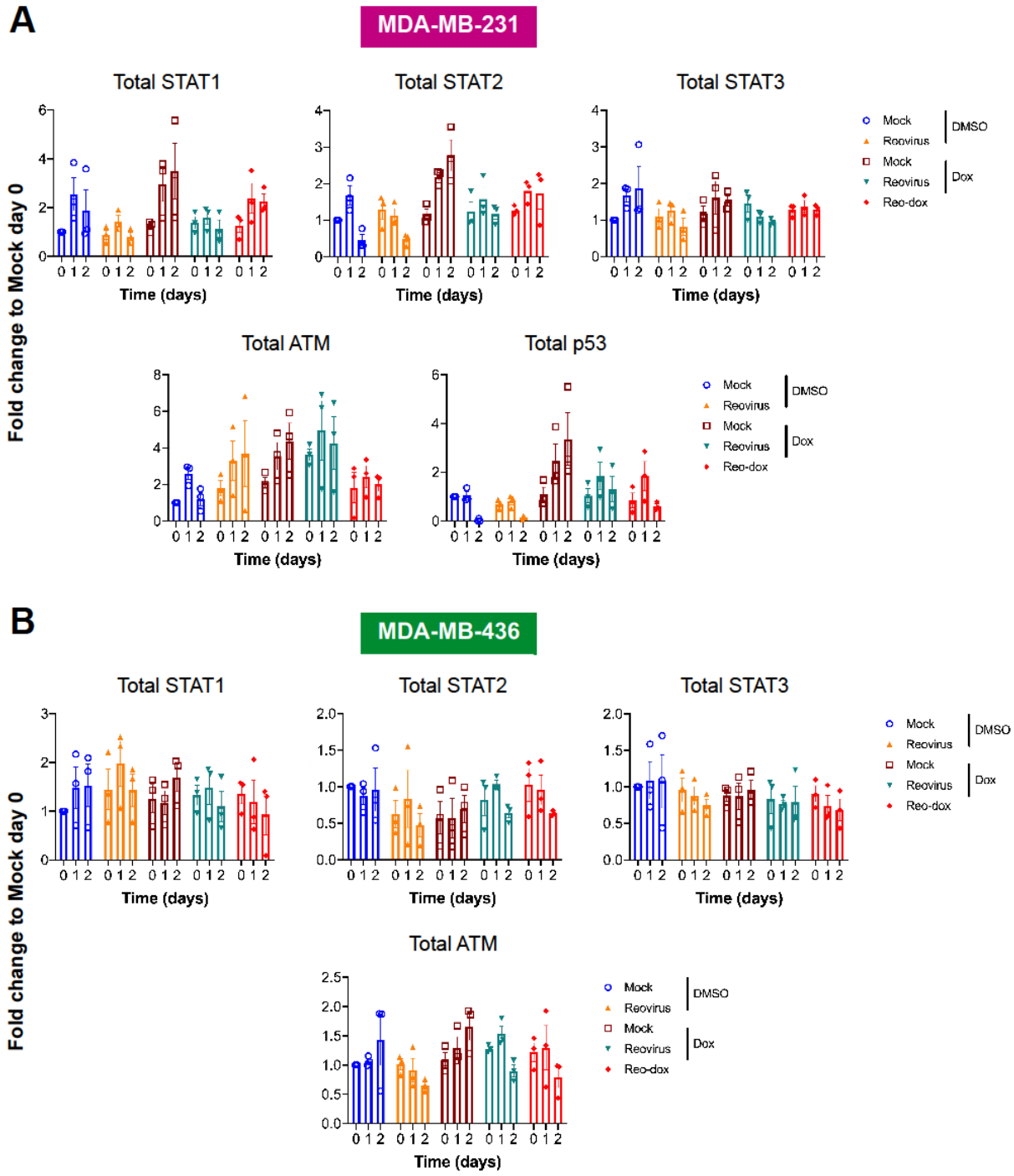

Figure 3.S3. Total protein densitometry.

Quantitative densitometry was performed on total protein levels from immunoblots of MDA-MB-231 (A) and MDA-MB-436 (B) whole cell lysates (Figure 3.4). Data represent mean of three independent experiments normalized to respective Mock day 0 values. Error bars = SEM.

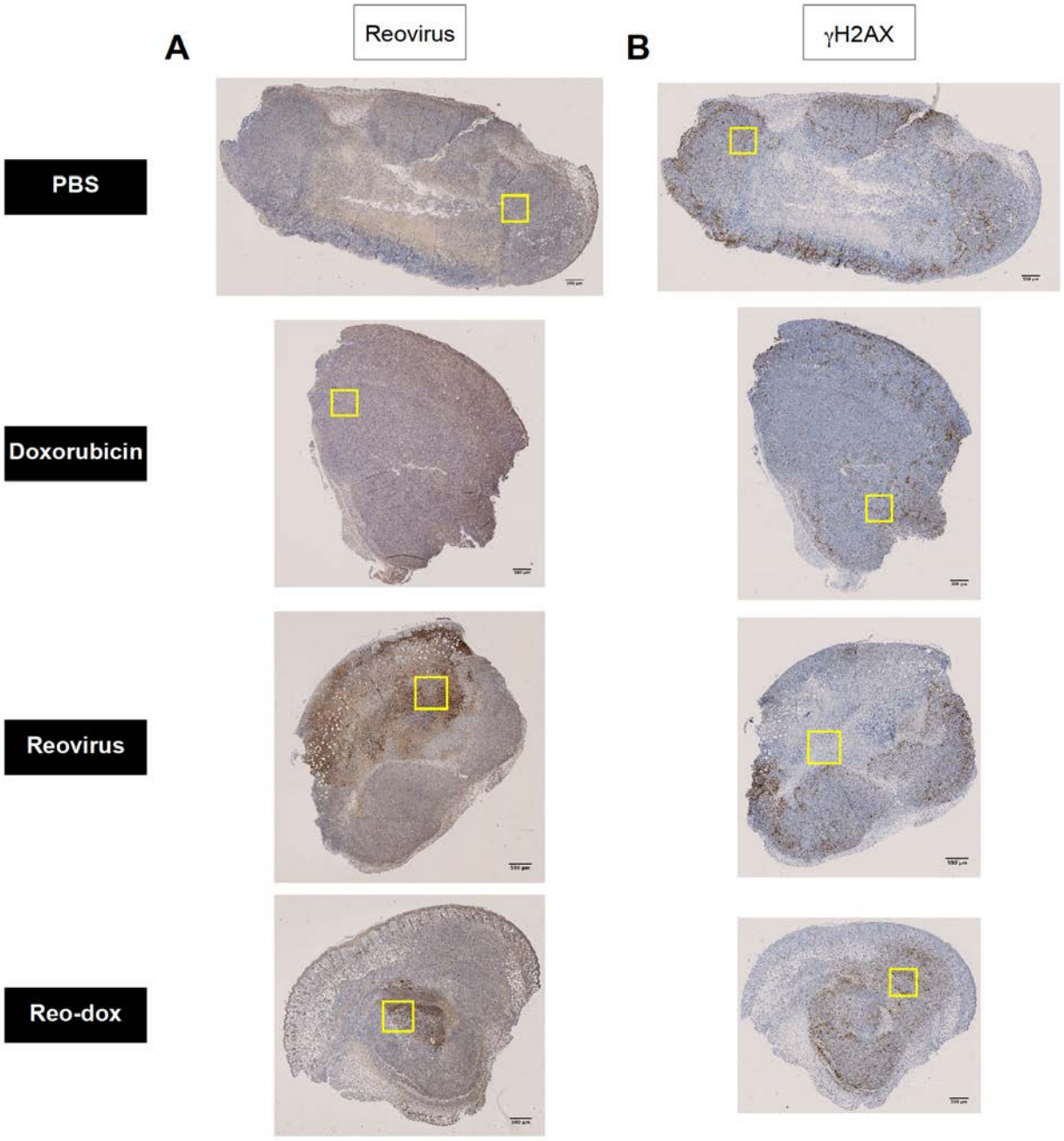

Figure 3.S4. Whole tissue scans of 4T1 *in vivo* primary tumors.

Primary tumor tissues were assessed for (A) reovirus antigen and (B) γH2AX levels by indirect immunohistochemistry. Yellow boxes indicate inset regions presented in Figure 7. Tissues are representative of five mice in a single experiment. Scale bars = 500 μm.

Chapter 4: Discussion and Conclusions

Triple-negative breast cancer (TNBC) continues to be a difficult disease to effectively target and treat. Despite the development of effective targeted therapies against other types of breast cancer, the characteristic lack of cell-surface hormone receptors and HER2 in TNBC restricts treatment options to surgery, radiation therapy, and systemic chemotherapy. Treating TNBC is further complicated by the aggressive nature of TNBC which often gives rise to metastatic tumors.

The oncolytic potential of reovirus has been investigated for over forty years in a variety of cancers. Though reovirus exhibits a preference to infect and replicate within cancer cells, clinical success is limited. Some attributes that make reovirus a prospective oncolytic virus are a double-edged sword. Serological studies reveal that the majority of humans are exposed to reovirus during childhood. Around 35% of infants younger than 1 year and 60% of children age 11-19 are reovirus positive (90, 91), and 70%-100% are seropositive by adulthood (91). High rate of exposure in childhood, subclinical disease, and rapid clearance of infection indicate a high level of safety when considering reovirus as an oncolytic (90, 93). However, preexposure correlates with more rapid viral clearance when reovirus is administered as an oncolytic. Neutralizing antibody levels are robustly elevated in clinical trial patients treated with reovirus (158, 305-307). Such studies have indicated that repeated administration of reovirus can be used and relatively high viral titers are safe for patients, but long-term efficacy of reovirus remains limited and requires combination with other therapeutics or modifications to the virus to enhance tumor-directed toxicity. A laboratory-isolated serotype 3 (T3C$) reovirus (Reolysin®, pelareorep) has been assessed in phase I-III clinical trials, including in breast cancer in combination with paclitaxel (170). Multiple studies have evaluated mutant reoviruses for increased specificity to cancer cells and limited toxicity to non-tumor sites (i.e. altering JAM-A binding by mutating σ1, altering virus

sensitivity to IFN-stimulated antiviral responses which tend to be more active in non-tumor cells, increasing efficiency of viral uncoating) (308). Little work has been conducted to genetically engineer reovirus to be more specific for aggressive breast cancer (268).

In Chapter II, a reassortant reovirus was engineered to infect and kill TNBC cell lines more effectively than prototypical strains and assessed for oncolytic efficacy alone and combined with topoisomerase inhibitors. Through serial passage of TNBC cells with T1L, T2J, and T3D reoviruses, a predominant reassortant variant, r2Reovirus, was isolated. r2Reovirus has a T3D M2 gene segment in an otherwise T1L genetic background with several nonsynonymous and synonymous point mutations. Even though r2Reovirus attaches to MDA-MB-231 cells to similar levels as T1L, but at lower levels than T3D and T3C$, r2Reovirus is significantly more efficient at infecting MDA-MB-231 cells than T1L, T3D, or T3C$. Greater levels of infection by r2Reovirus do not correlate to faster replication kinetics except compared to T3D. In MDA-MB-231 and MDA-MB-436 cells, r2Reovirus exhibits greater cytotoxicity than parental strains or T3C$, suggesting that the T3D M2 gene alone or combined with the point mutations confer an oncolytic advantage to reovirus in TNBC cells.

Infectivity and cytotoxicity are further augmented by combination of r2Reovirus when cells are pretreated with topoisomerase inhibitors topotecan, epirubicin, and doxorubicin. Characteristic DNA double strand break response pathway activation is maintained in the presence of r2Reovirus for all three inhibitors. Further, each agent combined with r2Reovirus induces secretion of IFNλ. Combining topotecan with r2Reovirus induces the most robust secretory response and may potentiate the phosphorylation of signal transducer and activator of transcription 1 (STAT1) and STAT2 in MDA-MB-231 TNBC cells, but interferon treatment of TNBC cells does not directly impact cell viability (Figures 2.12, 3.S2).

In Chapter III, doxorubicin was conjugated to r2Reovirus. The impact of drug crosslinking on virus biology, TNBC biology, drug delivery, and tumor progression were assessed. In the chemical screen to identify small molecule inhibitors, doxorubicin conferred the most robust enhancement of infectivity. Given the observed benefits to r2Reovirus infection and toxicity in TNBC cells after combination, an approach to enhance delivery of genotoxic agents to TNBC cells was evaluated and characterized. Many genotoxic inhibitors are not specifically targeted to cancer cells. As such, systemic administration leads to toxicity in various non-tumor tissues, causing damage to healthy organs over extended periods of drug use (dox refs from paper). Given the tropism of reovirus for cancer cells, the ability of r2Reovirus to more efficiently infect and kill TNBC cells, and the enhancement to cytotoxic and immunostimulatory responses conferred by doxorubicin, doxorubicin was chemically conjugated to reovirus (reo-dox). Conjugation augments r2Reovirus cytotoxicity in MDA-MB-231 and MDA-MB-436 TNBC cell lines without diminishing viral attachment, establishment of infection, or replication kinetics. Reo-dox infection yields similar *IFNB1* and *IFNL1* transcriptional regulation and secretion as r2Reovirus or virus combined with doxorubicin, and *IFNG* levels increase only in the context of exogenous or crosslinked dox. Infection of both MDA-MB-231 and MDA-MB-436 cells leads to elevated IFNλ secretion, indicating that reo-dox infection and r2Reovirus infection preferentially promote Type-III IFN secretion over Type-I, and dox combination and crosslinking enhances the levels of secreted IFNλ. In MDA-MB-231 cells, reo-dox infection induces robust activation of STAT1 and STAT2, whereas phosphorylated STATs 1, 2, and 3 are diminished after 2 days in MDA-MB-436 cells.

For reo-dox to be an effective combination therapy and drug delivery method, it was important to verify the pharmacological activity of dox after infection. Cells infected with reo-dox

exhibit similar levels of fragmented DNA by 2 dpi as cells treated with dox alone or in combination with r2Reovirus. Reo-dox infection also promotes phosphorylation of H2AX and ATM in TNBC cells, which indicates that the DNA double strand break response pathway is activated and corroborates the observed physical damage. In a 4T1 *in vivo* model, r2Reovirus and reo-dox significantly reduce primary tumor burden. Further, inoculation with reovirus or reo-dox reduce metastatic burden in lungs. Reo-dox inoculation results in slightly better elimination of metastatic cells than r2Reovirus, and reo-dox viral titers were slightly higher in lungs compared to r2Reovirus.

MODEL OF FINDINGS

Reassortant r2Reovirus infectivity in the MDA-MB-231 cell line is enhanced when cells are pretreated with topoisomerase inhibitors. Topoisomerase inhibitors do not alter r2Reovirus attachment to cells, nor affect the expression levels of JAM-A in TNBC cells (Figures 3.2, 3.S1, Appendix 1), so topoisomerase inhibitors affects a step after attachment in the virus replication cycle to enhance infectivity. Topotecan, epirubicin, and doxorubicin induce DNA damage which activates ATM (58, 59). ATM activates tumor suppressor p53 directly or through phosphorylating Chk2 (61, 63). The DNA damage response pathway arrests cell cycle progression, at which point the cell is fated for cell death or DNA repair, contingent upon the level of damage and response signaling within the cell. ATM and Chk2 activate BRCA1 (breast cancer type 1 susceptibility protein), which promotes DNA repair (309-311). Both p53 and BRCA1 promote the activity of PTEN (phosphatase and tensin homolog deleted on chromosome 10), which directly antagonizes the PI3K/AKT (phosphoinositide 3-kinase/protein kinase B) cell proliferation pathway and survival. PI3K phosphorylates PIP2 (phosphatidylinositol (4,5)-bisphosphate), forming PIP3

(phosphatidylinositol (3,4,5)-triphosphate) which activates AKT. PTEN antagonizes this pathway by removing the phosphate group from PIP3, forming PIP2 (312, 313).

The proposed shift in membrane-bound PIP2 abundance may directly impact the events of reovirus cell entry at the cell surface. Reovirus enters cells through clathrin-mediated endocytosis after adhesion to cell surface receptors JAM-A and carbohydrates (111, 112). Adaptor proteins initiate the nucleation of clathrins, leading to the formation of clathrin-coated pits (314-316). As the clathrin-coated pits invaginates to endocytose the virus, the endocytic vesicle is released into the cytoplasm through dynamin-dependent and independent fission (111, 317-320). One of the major clathrin adaptor proteins is adaptor protein 2 (AP-2). AP-2 is a heterotetrameric protein with α, β2, μ2, and σ2 subunits (321-323). PIP2 binding domains are present on the α, β2, and μ2 subunits (321, 324, 325) and are required for AP-2 to transition from “closed” to “open” conformation (322, 325, 326). Only when AP-2 is in the “open” state is the clathrin binding site accessible, therefore indicating a reliance on PIP2 interaction for effective endocytosis. Given that topoisomerase inhibitors may promote PTEN activities in treated cells, the levels of PIP2 likely increase relative to untreated cells. Higher PIP2 levels may promote greater levels of “open” AP-2, mediating an increased rate of clathrin assembly and subsequent endocytosis. This process could mediate topoisomerase inhibitor pretreatment-dependent enhancement in reovirus infectivity observed in Chapter II in MDA-MB-231 cells. However, other mechanisms must be explored to understand the interaction of doxorubicin and r2Reovirus when delivered as a drug-virus-conjugate.

Doxorubicin can be crosslinked to r2Reovirus (reo-dox) using heterobifunctional covalent chemistry of succinimidyl 4-(N-maleimidomethyl)cyclohexane-1-carboxylate (SMCC). Fluorescent labeling of reovirus using succinimidyl esters preferentially conjugates the outer

capsid structural proteins (270). Crystal structures indicate that μ2 and σ3 likely have solvent exposed cysteine residues to which dox is likely crosslinked (283). Attachment fiber protein σ1 is likely not targeted because cysteine residues are not apparently solvent exposed in the tertiary structure of the homotrimeric protein (284). Reo-dox is thus fully capable to attach and infect TNBC cells with similar efficiency as r2Reovirus (Figure 3.2A-B).

Once within the cell, reo-dox must leave the endosome to continue the virus replication cycle and for drug to translocate to the nucleus and damage DNA. We know that reo-dox replicates with similar efficiency and kinetics as r2Reovirus alone or with exogenous topoisomerase inhibitor pretreatment (Figures 2.8, 3.2C-D), indicating that in reo-dox-infected cells, reovirus likely still undergoes transition to ISVP, translocation across endosomal membrane to the cytoplasm, formation of viral factories, and conversion to transcriptionally active viral cores. Additionally, cells infected with reo-dox have significant levels of DNA fragmentation and robustly elevated levels of activated DNA damage response proteins (Figures 3.4, 3.5). Preliminary observations indicate that chemical inhibition of cathepsin proteases (required for reovirus to leave endosomes and enter the cytoplasm) by E64-d (a cysteine protease inhibitor) (207, 327) and ammonium chloride (an inhibitor of endosome acidification) (328) fail to abrogate activation of ATM or p53 in reo-dox infected cells (Appendix 2). This indicates that dox is removed from r2Reovirus particles at a step before or independent of endocytic processing of the virus to an infections subvirion particle (ISVP). As suggested in the discussion section of Chapter III, extracellular proteases are capable of interacting with oncolytic reovirus and affecting the ability of reovirus to infect TNBC cells (295). Such proteases may cleave short peptide-bound SMCC-dox from the outer capsid proteins, or remove dox itself from viral particles, before reo-dox is internalized in the cell. The thioether bond formed from SMCC is highly stable (296). SMCC and dox are bound

through the formation of a succinimidyl ester, which includes the formation of an amide bond. Amide bonds are cleavable by endogenous proteases and other cellular enzymes (297-299). It is possible that such intracellular catabolic enzyme may cleave the succinimidyl ester, restoring the primary amine of dox and releasing it from viral protein or peptides to interact with nuclear DNA.

Reo-dox and r2Reovirus infection alone and after topoisomerase inhibitor treatment result in elevated levels of Type III IFN RNA and secreted IFNλ. Reovirus typically induces a Type I IFN antiviral response in epithelial cells and a Type III IFN response in mucosal epithelial cells (135, 136, 285, 286), though other non-mucosal epithelia are capable of mounting Type III IFN antiviral responses (268, 287, 288). Viral dsRNA is detected in the cytoplasm by PRR proteins RIG-I and MDA5, which signal through mitochondria-associated protein MAVS to activate IRF3 and NF-κB. MAVS can associate with peroxisomes as well as the mitochondria. In cells with MAVS preferentially associated with peroxisomes, IFN responses are shifted toward Type III over Type I (289).

Etoposide-induced DNA fragmentation can lead to activation of STING, a protein typically responsive to cGAS/cGAMP recognition of foreign DNA in cytosol. ATM-activated p53 associates with IFI16, and together with TRAF6 form a complex with STING which induces production of Type I IFN in an NF-κB-dependent fashion (216). Topoisomerase inhibitors may promote a similar signaling cascade in TNBC cells that induces low levels of *IFNL* transcription and IFNλ secretion. In the context of r2Reovirus infection, topoisomerase inhibitors augment the virus-induced Type III IFN response. The additive effect observed in combination treatment and reo-dox infection may be brought about by concomitant induction of rig-like receptor (RLR)-dependent antiviral response and DNA damage-induced noncanonical STING activity. TNBC cells express modest levels of total STING (data not shown), and others have observed STING-

dependent antitumor stimulation in TNBC cells. Inhibition of PARP (poly ADP-ribose polymerase) with olaparib in BRCA1-deficient TNBC cells leads to robust activation of cGAS/STING in tumor cells *in vivo* and promotes TBK1/IRF3 signaling in dendritic cells (DC)s. This signaling associated with DC maturation, antigen presentation, and subsequent $CD8^+$ T cell infiltration and activation against the tumor cells (329). If r2Reovirus with topoisomerase inhibitors is stimulating STING, combination and conjugation approaches may lead to STING-dependent tumor associated antigen (TAA) presentation by DCs to the adaptive immune system, generating a systemic immune response to TNBC cells.

Type I and type III IFN are regulated by a shared set of proteins but with different dependencies. AP-1 (activator protein 1), IRF3, IRF7, and NF-κB localize to DNA binding sites in close proximity to each other. The cooperative binding of all four transcription factors (enhanceasome complex) is required for IFNβ transcription (330). The promoter for IFNλ1 contains binding sites for the same transcription factors, but AP-1, nor activation by upstream MAP kinases, are not required for Type III IFN transcription (289). Further, IRF1 specifically induces Type III IFN and not Type I IFN (289, 331, 332), and IRFs or NF-κB can independently induce Type III IFN transcription (333). The multifactorial regulation of IFNλ may allow this antiviral, innate immune response to be less susceptible to shutdown when cancerous cells transform and evolve immune evasion mechanisms. Additionally, any cancer cells, including MDA-MB-231 cells harbor a constitutively activated Ras pathway, which signals through MAPK, activating AP-1 (334-339). r2Reovirus infection of TNBC cells may suppress oncogenic survival and proliferation pathways, like MAPK signaling, as part of virus-induced cell death, shifting the immune response toward Type III IFN.

Although MDA-MB-231 and MDA-MB-436 cells are responsive to Type III IFN, direct treatment of cells with recombinant human IFNλ has no detectable impact on cell viability (Figures 2.12, 3.S2). Further, IFNλ secreted from cells infected with r2Reovirus in the presence or absence of topoisomerase inhibitors has little direct impact on cell viability. When IFNλ is rendered inactive by neutralizing antibody in cell supernatant, cell viability remains similar to that of cells treated with isotype control antibody (Appendix 3). IFNλ likely promotes the transcription of interferon-stimulated genes (ISGs) that activate neighboring cells in culture, but without dramatic impact on viability due to the lack of immune cell types. In the context of an immunocompetent animal model, the virus and drug-stimulated immune secretory responses likely recruit TILs (tumor infiltrating lymphocytes) that may assist in greater levels of tumor cell clearance. In a 2013 study using a spontaneous metastatic mammary adenocarcinoma mouse model, knockout of Usp18 led to a Th1 $CD4^+$ T cell tumor suppressive microenvironment with elevated IFNλ-mediated Cxcl10 and Cxcl11 secretion (291). Cxcl10 and Cxcl11 are two of the three chemokine ligands for Cxcr3, a receptor that is highly expressed on Th1 $CD4^+$ T cells, cytotoxic $CD8^+$ T cells, and NK cells, among other immune cell types (340-342). Both chemokines serve to attract lymphocytes; further, MDA-MB-231 TNBC cells infected with r2Reovirus display a 4-fold and 10-fold increase in RNA levels for Cxcl10 and Cxcl11, respectively (Mainou lab Nanostring data, not shown). It is possible that when administered *in vivo*, r2Reovirus infection of TNBC cells induces IFNλ production which in turn promotes increased secretion of Cxcl10 and Cxcl11. These chemokines may then serve to attract NK cells and $CD8^+$ T cells to a tumor suppressive microenvironment. Although IFNλ has been shown to indirectly influence NK cell antitumor activity (343), NK cells experience significant reduction in their protective capacity against tumor metastases when IL-

28R is deleted (344), suggesting the cytokine remains important for stimulating this arm of the innate antitumor immune response.

In vivo, r2Reovirus and reo-dox significantly diminish subcutaneous hind flank 4T1 tumor burden in Balb/c mice when administered intratumorally. Both conditions dramatically reduce the median number of metastatic 4T1 cells in the lungs of inoculated animals. The slight increase in the percent of γH2AX positive cells in tumors of mice inoculated with reo-dox compared to r2Reovirus alone indicates DNA damage by dox. Although the effect of dox conjugation on primary tumor size is negligible compared to r2Reovirus alone, animals treated with reo-dox had fewer metastatic cells than animals treated with r2Reovirus. As posited in Chapter III, reo-dox may perform better than r2Reovirus or dox alone by virtue of altered metabolism of metastatic TNBC cells. In a study on genome-wide transcriptional differences among patient-derived xenograft (PDX) models of TNBC, genes related to oxidative phosphorylation (OXPHOS) were found to be more abundantly expressed in metastatic cells compared to primary tumor (300). Murine models of MDA-MB-231 and 4T1 cell lines were treated with oligomycin to inhibit OXPHOS; micrometastatic seeding of the lungs was significantly reduced, indicating that metastatic TNBC cells require a metabolic shift from glycolysis to OXPHOS in order to migrate to and populate a secondary tumor niche (300). It is possible that r2Reovirus infection disrupts mitochondrial membrane potential. This would inhibit the ability of Complex I-IV enzymes and ATP synthase in the inner mitochondrial membrane to transport electrons across the membrane and ablate the proton gradient required for electron transport chain. OXPHOS would be interrupted and 4T1 cells would lose their metastatic potential, leading to less 4T1 cells seeded in the lungs of infected animals. Interestingly, cancer cells shifted toward OXPHOS metabolism exhibit increased sensitivity to antineoplastic agents like dox (301, 302). As such, if TNBC cells rely on OXPHOS

for metastasis, these cells may be more susceptible to the lytic effects of reo-dox, leading to further ablation of metastatic seeding. By intratumoral injection, reo-dox-mediated reduction in metastatic burden likely results from oncolytic activity in the primary tumor. However, progeny virus may circulate to the lungs or be carried by infected metastatic cells and continue killing TNBC cells locally in the secondary site. Alternatively, infected cells may produce cytokines such as Type III IFN and TAAs, mounting a tumor-specific immune response in the tumor microenvironment.

FUTURE DIRECTIONS

One significant gap in knowledge that served as a foundation for the presented work is the lack of target therapies for TNBC. The generation of r2Reovirus indicates that oncolytic reovirus can be engineered to more preferentially infect and kill specific cell types, especially compared to the wild-type lab-isolated reovirus currently studied in clinical trials. Reo-dox serves as a platform to develop other virus-drug conjugates to simultaneously infect cells and deliver small molecule inhibitor payloads to cells targeted by virus. It may be possible to arm reovirus with agents that specifically target key pathways that support cancer cell survival and proliferation, including microtubule inhibitors to disrupt unregulated growth, or Bcl2 inhibitors to abrogate apoptosis dysregulation. While crosslinking chemotherapeutic agents to reovirus can specifically kill infected cells, limiting off-tumor infection and toxicity remains an area for future work.

Reo-dox or other drug-conjugated reoviruses may be of benefit for treating tumors that are not directly accessible to chemotherapeutics. Doxorubicin is incapable of crossing the blood brain barrier when administered as a free systemic agent (28). Encapsulation methods have altered the bioavailability of the drug and allow it to pass into neural tissues to kill cancer cells (25). If enhancements in cytotoxicity observed by combination and conjugation of topoisomerase

inhibitors with reovirus in triple-negative breast cancer (TNBC) apply within the context of neurological malignancies, drug conjugation to reovirus may be a viable therapeutic option. Oncolytic reovirus is able to cross the blood brain barrier and has been assessed in brain tumors in several clinical trials, though long-term efficacy needs to be improved (Table 1.1).

Cancer therapy will continue to evolve with new combination approaches. As a complex set of diseases with extreme cell type, phenotype, and genotype heterogeneity within and among tumors, no single therapeutic agent is likely to completely cure every cancer in every patient. While advances in chemical and immunological therapeutics continue to broaden treatment options, mounting safe, long-lasting, autonomous detection and destruction of cancer cells will be of massive benefit. Oncolytic viruses (OVs) are one such method that can help improve the long-term antineoplastic effect. Until neutralized by immune recognition, replication competent OVs can continue to infect and kill cancer cells, increasing in concentration over time rather than becoming more dilute as in the case of chemical agents. OVs have the potential to directly kill cancer cells and stimulate adaptive immune responses specific to the cancer, with theoretical systemic impact, aiding in reducing metastatic burden. The combination of chemical and immunological agents with OVs potentially augments the potency of either method. As more OVs succeed in clinical trials and gain FDA approval, the largest advances will likely be seen in viruses that are adapted in patient-specific manners. Individualized therapy has the potential to dramatically enhance how well a patient tolerates and responds to treatment. OVs such as r2Reovirus, which was developed by allowing the virus to adapt to its cancer cell environment, may prove to be invaluable tools for cancer therapy in the future. In an evolutionary tug-of-war, a biological agent like a virus can adapt to more efficiently infect, replicate, and kill its host, (e.g. heterogeneous tumor tissue). OVs could be developed for individual patients *ex vivo* using tissue

samples, then administered to the patient. Engineering OVs using heterogeneous cells with representative phenotypes matching common genetic profiles of similar tumors may even provide a broader and more feasibly approvable method to enhancing OV-mediated cancer therapy. Regardless of the approach, improving cancer therapy will require multidisciplinary insight and methods, branching not only fields in biology (i.e. immunology, microbiology, genetics), but also across natural science fields (i.e. chemistry, physics, engineering). As complex and heterogenous a disease as cancer is, treating it will require equally clever, multifaceted, cooperative evolution of scientific thought and therapeutic development.

Appendix: Unpublished Data

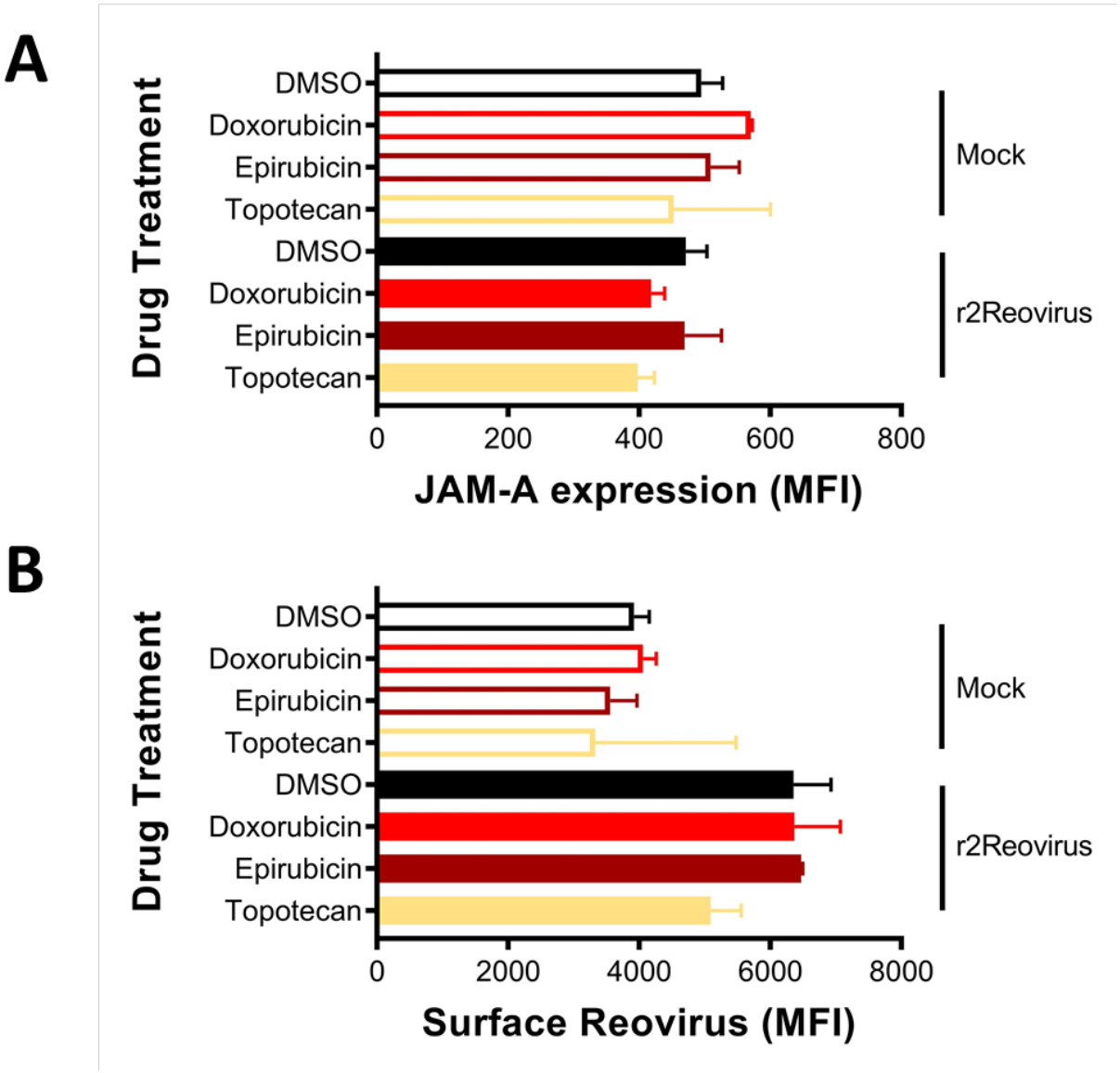

Appendix 0.1. JAM-A and r2Reovirus attachment in topoisomerase inhibitor-treated TNBC cells.

MDA-MB-231 cells were treated with vehicle (DMSO) or topoisomerase inhibitors and infected with mock or r2Reovirus. Surface-expressed JAM-A and attached reovirus were measured by flow cytometry and expressed as mean fluorescence intensity (MFI).

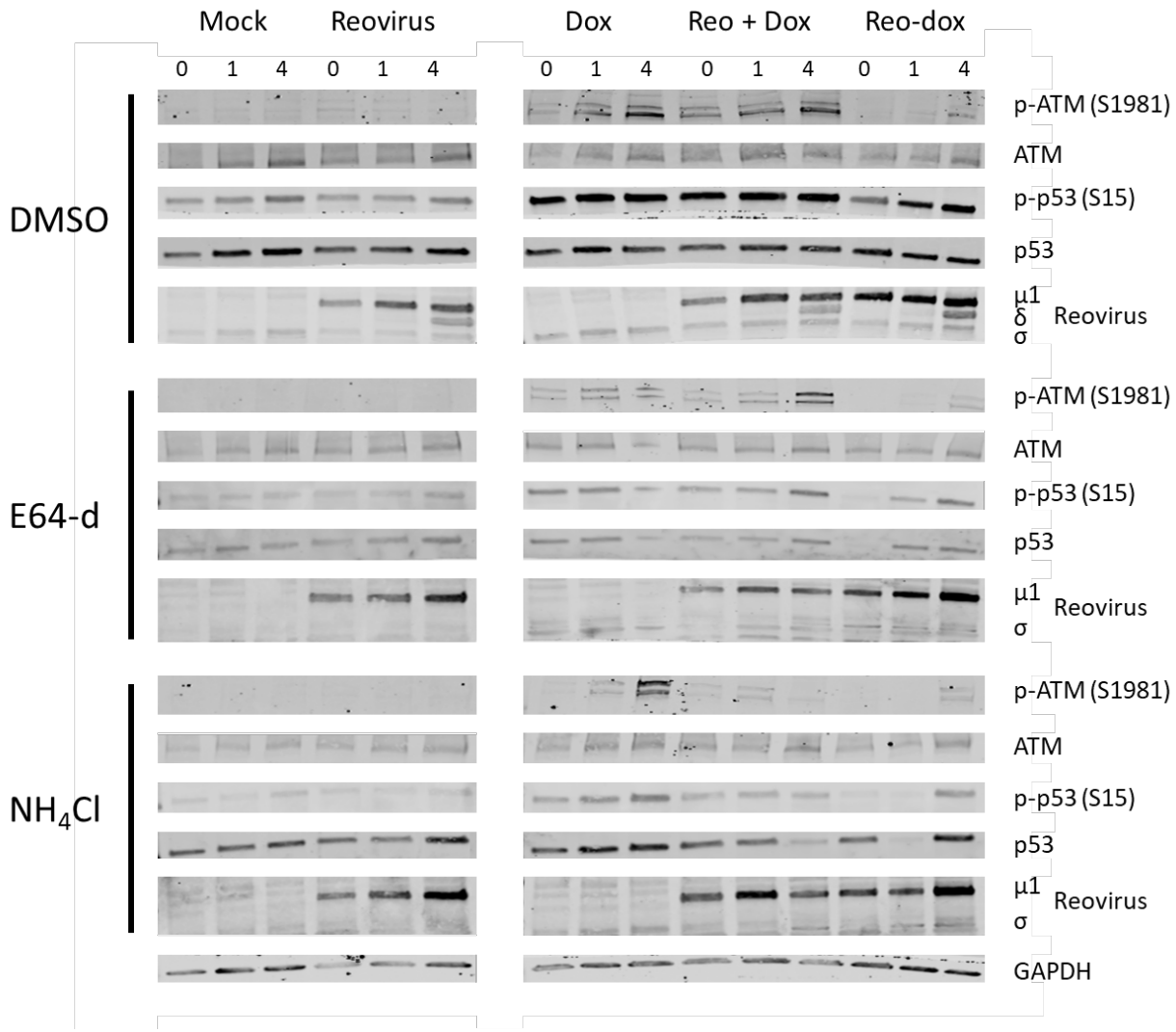

Appendix 0.2. Doxorubicin crosslinked to reovirus retains pharmacological activity despite inhibition of endocytic processing of virus.

MDA-MB-231 cells were treated with vehicle (DMSO) or doxorubicin alone or combined with E64-d, or NH_4Cl. Cell were infected with mock, r2Reovirus, or reo-dox. Levels of total and activated DNA damage response proteins and reovirus structural proteins were measured over the first four hours of infection.

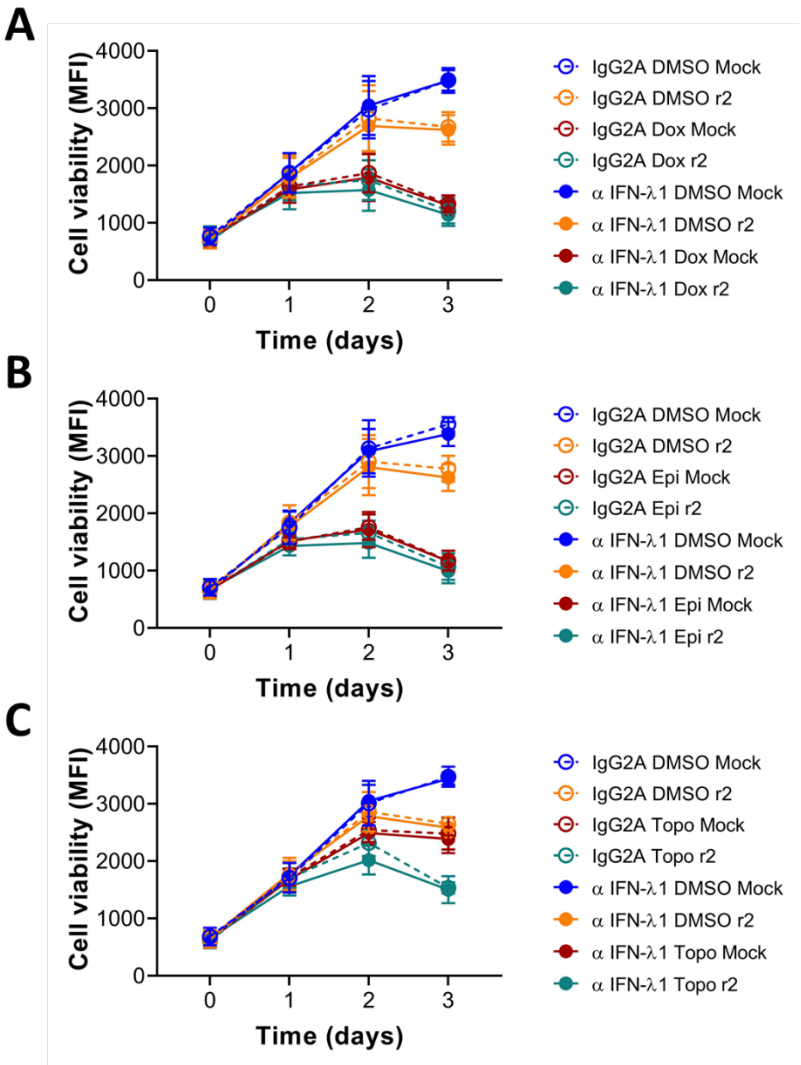

Appendix 3. Neutralizing IFNλ does not impact cytotoxicity by r2Reovirus or topoisomerase inhibitors.

MDA-MB-231 cells were treated with vehicle (DMSO) or 1 μM topoisomerase inhibitors and infected with mock or r2Reovirus at an MOI of 100 PFU/cell. Isotype control or anti-IFNλ neutralizing antibody was added, and cell viability was assessed over a 3 day time course of infection.

References

1. Heron M. Deaths: Leading Causes for 2017. Natl Vital Stat Rep. 2019;68(6):1-77. Epub 2020/06/06. PubMed PMID: 32501203.
2. Fisher R, Pusztai L, Swanton C. Cancer heterogeneity: implications for targeted therapeutics. Br J Cancer. 2013;108(3):479-85. Epub 2013/01/10. doi: 10.1038/bjc.2012.581. PubMed PMID: 23299535; PMCID: PMC3593543.
3. Marusyk A, Polyak K. Tumor heterogeneity: causes and consequences. Biochim Biophys Acta. 2010;1805(1):105-17. Epub 2009/11/26. doi: 10.1016/j.bbcan.2009.11.002. PubMed PMID: 19931353; PMCID: PMC2814927.
4. Dagogo-Jack I, Shaw AT. Tumour heterogeneity and resistance to cancer therapies. Nat Rev Clin Oncol. 2018;15(2):81-94. Epub 2017/11/09. doi: 10.1038/nrclinonc.2017.166. PubMed PMID: 29115304.
5. Prasetyanti PR, Medema JP. Intra-tumor heterogeneity from a cancer stem cell perspective. Mol Cancer. 2017;16(1):41. Epub 2017/02/18. doi: 10.1186/s12943-017-0600-4. PubMed PMID: 28209166; PMCID: PMC5314464.
6. Hanahan D, Weinberg RA. The hallmarks of cancer. Cell. 2000;100(1):57-70. Epub 2000/01/27. doi: 10.1016/s0092-8674(00)81683-9. PubMed PMID: 10647931.
7. Hanahan D, Weinberg RA. Hallmarks of cancer: the next generation. Cell. 2011;144(5):646-74. Epub 2011/03/08. doi: 10.1016/j.cell.2011.02.013. PubMed PMID: 21376230.
8. Nishida N, Yano H, Nishida T, Kamura T, Kojiro M. Angiogenesis in cancer. Vasc Health Risk Manag. 2006;2(3):213-9. Epub 2007/03/01. doi: 10.2147/vhrm.2006.2.3.213. PubMed PMID: 17326328; PMCID: PMC1993983.
9. Liu T, Han C, Wang S, Fang P, Ma Z, Xu L, Yin R. Cancer-associated fibroblasts: an emerging target of anti-cancer immunotherapy. J Hematol Oncol. 2019;12(1):86. Epub 2019/08/30. doi: 10.1186/s13045-019-0770-1. PubMed PMID: 31462327; PMCID: PMC6714445.
10. Coussens LM, Raymond WW, Bergers G, Laig-Webster M, Behrendtsen O, Werb Z, Caughey GH, Hanahan D. Inflammatory mast cells up-regulate angiogenesis during squamous epithelial carcinogenesis. Genes Dev. 1999;13(11):1382-97. Epub 1999/06/11. doi: 10.1101/gad.13.11.1382. PubMed PMID: 10364156; PMCID: PMC316772.
11. American Cancer Society. Cancer Facts & Figures 2020. 2020.
12. SEER Cancer Statistics Review (CSR) 1975-2016 5-year Survival Rates: National Cancer Institute; 2020 [cited 2020]. Available from: https://seer.cancer.gov/archive/csr/1975_2016/results_merged/topic_survival.pdf.
13. American Cancer Society. Global Cancer Facts & Figures 4th Edition. 2018.
14. Organization WH. Global Cancer Profile. 2020.
15. Weigelt B, Peterse JL, van 't Veer LJ. Breast cancer metastasis: markers and models. Nature reviews Cancer. 2005;5(8):591-602. Epub 2005/08/02. doi: 10.1038/nrc1670. PubMed PMID: 16056258.
16. Howlader N, Cronin KA, Kurian AW, Andridge R. Differences in Breast Cancer Survival by Molecular Subtypes in the United States. Cancer Epidemiol Biomarkers Prev. 2018;27(6):619-26. Epub 2018/03/30. doi: 10.1158/1055-9965.EPI-17-0627. PubMed PMID: 29593010.

17. Parise CA, Caggiano V. Risk of mortality of node-negative, ER/PR/HER2 breast cancer subtypes in T1, T2, and T3 tumors. Breast Cancer Res Treat. 2017;165(3):743-50. Epub 2017/07/10. doi: 10.1007/s10549-017-4383-5. PubMed PMID: 28689363.
18. Plevritis SK, Munoz D, Kurian AW, Stout NK, Alagoz O, Near AM, Lee SJ, van den Broek JJ, Huang X, Schechter CB, Sprague BL, Song J, de Koning HJ, Trentham-Dietz A, van Ravesteyn NT, Gangnon R, Chandler Y, Li Y, Xu C, Ergun MA, Huang H, Berry DA, Mandelblatt JS. Association of Screening and Treatment With Breast Cancer Mortality by Molecular Subtype in US Women, 2000-2012. JAMA. 2018;319(2):154-64. Epub 2018/01/11. doi: 10.1001/jama.2017.19130. PubMed PMID: 29318276; PMCID: PMC5833658.
19. Wolff AC, Tung NM, Carey LA. Implications of Neoadjuvant Therapy in Human Epidermal Growth Factor Receptor 2-Positive Breast Cancer. J Clin Oncol. 2019;37(25):2189-92. Epub 2019/06/04. doi: 10.1200/JCO.19.01159. PubMed PMID: 31157582.
20. Sharma P. Biology and Management of Patients With Triple-Negative Breast Cancer. Oncologist. 2016;21(9):1050-62. Epub 2016/07/13. doi: 10.1634/theoncologist.2016-0067. PubMed PMID: 27401886; PMCID: PMC5016071.
21. Wahba HA, El-Hadaad HA. Current approaches in treatment of triple-negative breast cancer. Cancer Biol Med. 2015;12(2):106-16. Epub 2015/07/16. doi: 10.7497/j.issn.2095-3941.2015.0030. PubMed PMID: 26175926; PMCID: PMC4493381.
22. Buzdar AU, Marcus C, Smith TL, Blumenschein GR. Early and delayed clinical cardiotoxicity of doxorubicin. Cancer. 1985;55(12):2761-5. Epub 1985/06/15. doi: 10.1002/1097-0142(19850615)55:12<2761::aid-cncr2820551206>3.0.co;2-p. PubMed PMID: 3922612.
23. Johnson-Arbor K, Dubey R. Doxorubicin. StatPearls. Treasure Island (FL)2020.
24. Tewey KM, Rowe TC, Yang L, Halligan BD, Liu LF. Adriamycin-induced DNA damage mediated by mammalian DNA topoisomerase II. Science. 1984;226(4673):466-8. Epub 1984/10/26. doi: 10.1126/science.6093249. PubMed PMID: 6093249.
25. Tacar O, Sriamornsak P, Dass CR. Doxorubicin: an update on anticancer molecular action, toxicity and novel drug delivery systems. J Pharm Pharmacol. 2013;65(2):157-70. Epub 2013/01/03. doi: 10.1111/j.2042-7158.2012.01567.x. PubMed PMID: 23278683.
26. Mizutani H, Tada-Oikawa S, Hiraku Y, Kojima M, Kawanishi S. Mechanism of apoptosis induced by doxorubicin through the generation of hydrogen peroxide. Life Sci. 2005;76(13):1439-53. Epub 2005/02/01. doi: 10.1016/j.lfs.2004.05.040. PubMed PMID: 15680309.
27. Carvalho C, Santos RX, Cardoso S, Correia S, Oliveira PJ, Santos MS, Moreira PI. Doxorubicin: the good, the bad and the ugly effect. Curr Med Chem. 2009;16(25):3267-85. Epub 2009/06/25. doi: 10.2174/092986709788803312. PubMed PMID: 19548866.
28. Bigotte L, Arvidson B, Olsson Y. Cytofluorescence localization of adriamycin in the nervous system. I. Distribution of the drug in the central nervous system of normal adult mice after intravenous injection. Acta Neuropathol. 1982;57(2-3):121-9. Epub 1982/01/01. doi: 10.1007/BF00685379. PubMed PMID: 7124341.
29. Tangpong J, Cole MP, Sultana R, Joshi G, Estus S, Vore M, St Clair W, Ratanachaiyavong S, St Clair DK, Butterfield DA. Adriamycin-induced, TNF-alpha-mediated central nervous system toxicity. Neurobiol Dis. 2006;23(1):127-39. Epub 2006/05/16. doi: 10.1016/j.nbd.2006.02.013. PubMed PMID: 16697651.

30. Zhao N, Woodle MC, Mixson AJ. Advances in delivery systems for doxorubicin. J Nanomed Nanotechnol. 2018;9(5). Epub 2019/01/08. doi: 10.4172/2157-7439.1000519. PubMed PMID: 30613436; PMCID: PMC6319900.
31. Goldstein LJ, Galski H, Fojo A, Willingham M, Lai SL, Gazdar A, Pirker R, Green A, Crist W, Brodeur GM, et al. Expression of a multidrug resistance gene in human cancers. Journal of the National Cancer Institute. 1989;81(2):116-24. Epub 1989/01/18. doi: 10.1093/jnci/81.2.116. PubMed PMID: 2562856.
32. Ramachandra M, Ambudkar SV, Chen D, Hrycyna CA, Dey S, Gottesman MM, Pastan I. Human P-glycoprotein exhibits reduced affinity for substrates during a catalytic transition state. Biochemistry. 1998;37(14):5010-9. Epub 1998/05/16. doi: 10.1021/bi973045u. PubMed PMID: 9538020.
33. Abolhoda A, Wilson AE, Ross H, Danenberg PV, Burt M, Scotto KW. Rapid activation of MDR1 gene expression in human metastatic sarcoma after in vivo exposure to doxorubicin. Clin Cancer Res. 1999;5(11):3352-6. Epub 1999/12/10. PubMed PMID: 10589744.
34. Genovese I, Fiorillo A, Ilari A, Masciarelli S, Fazi F, Colotti G. Binding of doxorubicin to Sorcin impairs cell death and increases drug resistance in cancer cells. Cell Death Dis. 2017;8(7):e2950. Epub 2017/07/21. doi: 10.1038/cddis.2017.342. PubMed PMID: 28726784; PMCID: PMC5550883.
35. Rafiyath SM, Rasul M, Lee B, Wei G, Lamba G, Liu D. Comparison of safety and toxicity of liposomal doxorubicin vs. conventional anthracyclines: a meta-analysis. Exp Hematol Oncol. 2012;1(1):10. Epub 2012/12/06. doi: 10.1186/2162-3619-1-10. PubMed PMID: 23210520; PMCID: PMC3514106.
36. Chatterjee K, Zhang J, Honbo N, Karliner JS. Doxorubicin cardiomyopathy. Cardiology. 2010;115(2):155-62. Epub 2009/12/18. doi: 10.1159/000265166. PubMed PMID: 20016174; PMCID: PMC2848530.
37. Zhang Y, Yang C, Wang W, Liu J, Liu Q, Huang F, Chu L, Gao H, Li C, Kong D, Liu Q, Liu J. Co-delivery of doxorubicin and curcumin by pH-sensitive prodrug nanoparticle for combination therapy of cancer. Sci Rep. 2016;6:21225. Epub 2016/02/16. doi: 10.1038/srep21225. PubMed PMID: 26876480; PMCID: PMC4753416.
38. Hadla M, Palazzolo S, Corona G, Caligiuri I, Canzonieri V, Toffoli G, Rizzolio F. Exosomes increase the therapeutic index of doxorubicin in breast and ovarian cancer mouse models. Nanomedicine (Lond). 2016;11(18):2431-41. Epub 2016/08/26. doi: 10.2217/nnm-2016-0154. PubMed PMID: 27558906.
39. Dan N, Setua S, Kashyap VK, Khan S, Jaggi M, Yallapu MM, Chauhan SC. Antibody-Drug Conjugates for Cancer Therapy: Chemistry to Clinical Implications. Pharmaceuticals (Basel). 2018;11(2). Epub 2018/04/13. doi: 10.3390/ph11020032. PubMed PMID: 29642542; PMCID: PMC6027311.
40. Kratz F, Muller IA, Ryppa C, Warnecke A. Prodrug strategies in anticancer chemotherapy. ChemMedChem. 2008;3(1):20-53. Epub 2007/10/30. doi: 10.1002/cmdc.200700159. PubMed PMID: 17963208.
41. Trail PA, Willner D, Lasch SJ, Henderson AJ, Hofstead S, Casazza AM, Firestone RA, Hellstrom I, Hellstrom KE. Cure of xenografted human carcinomas by BR96-doxorubicin immunoconjugates. Science. 1993;261(5118):212-5. Epub 1993/07/09. doi: 10.1126/science.8327892. PubMed PMID: 8327892.
42. Yin BW, Finstad CL, Kitamura K, Federici MG, Welshinger M, Kudryashov V, Hoskins WJ, Welt S, Lloyd KO. Serological and immunochemical analysis of Lewis y (Ley) blood group

antigen expression in epithelial ovarian cancer. International journal of cancer Journal international du cancer. 1996;65(4):406-12. Epub 1996/02/08. doi: 10.1002/(SICI)1097-0215(19960208)65:4<406::AID-IJC2>3.0.CO;2-0. PubMed PMID: 8621218.
43. Miyake M, Taki T, Hitomi S, Hakomori S. Correlation of expression of H/Le(y)/Le(b) antigens with survival in patients with carcinoma of the lung. N Engl J Med. 1992;327(1):14-8. Epub 1992/07/02. doi: 10.1056/NEJM199207023270103. PubMed PMID: 1317941.
44. Sakamoto J, Furukawa K, Cordon-Cardo C, Yin BW, Rettig WJ, Oettgen HF, Old LJ, Lloyd KO. Expression of Lewisa, Lewisb, X, and Y blood group antigens in human colonic tumors and normal tissue and in human tumor-derived cell lines. Cancer research. 1986;46(3):1553-61. Epub 1986/03/01. PubMed PMID: 3510728.
45. Asakura T, Yokoyama M, Shiraishi K, Aoki K, Ohkawa K. Chemotherapeutic Effect of CD147 Antibody-labeled Micelles Encapsulating Doxorubicin Conjugate Targeting CD147-Expressing Carcinoma Cells. Anticancer Res. 2018;38(3):1311-6. Epub 2018/03/02. doi: 10.21873/anticanres.12353. PubMed PMID: 29491054.
46. Marcinkowska M, Sobierajska E, Stanczyk M, Janaszewska A, Chworos A, Klajnert-Maculewicz B. Conjugate of PAMAM Dendrimer, Doxorubicin and Monoclonal Antibody-Trastuzumab: The New Approach of a Well-Known Strategy. Polymers (Basel). 2018;10(2). Epub 2018/02/14. doi: 10.3390/polym10020187. PubMed PMID: 30966223; PMCID: PMC6414888.
47. Munster P, Krop IE, LoRusso P, Ma C, Siegel BA, Shields AF, Molnar I, Wickham TJ, Reynolds J, Campbell K, Hendriks BS, Adiwijaya BS, Geretti E, Moyo V, Miller KD. Safety and pharmacokinetics of MM-302, a HER2-targeted antibody-liposomal doxorubicin conjugate, in patients with advanced HER2-positive breast cancer: a phase 1 dose-escalation study. Br J Cancer. 2018;119(9):1086-93. Epub 2018/10/27. doi: 10.1038/s41416-018-0235-2. PubMed PMID: 30361524; PMCID: PMC6219487.
48. Wang JC. Interaction between DNA and an Escherichia coli protein omega. J Mol Biol. 1971;55(3):523-33. Epub 1971/02/14. doi: 10.1016/0022-2836(71)90334-2. PubMed PMID: 4927945.
49. Champoux JJ, Dulbecco R. An activity from mammalian cells that untwists superhelical DNA--a possible swivel for DNA replication (polyoma-ethidium bromide-mouse-embryo cells-dye binding assay). Proc Natl Acad Sci U S A. 1972;69(1):143-6. Epub 1972/01/01. doi: 10.1073/pnas.69.1.143. PubMed PMID: 4333036; PMCID: PMC427563.
50. Hanai R, Caron PR, Wang JC. Human TOP3: a single-copy gene encoding DNA topoisomerase III. Proc Natl Acad Sci U S A. 1996;93(8):3653-7. Epub 1996/04/16. doi: 10.1073/pnas.93.8.3653. PubMed PMID: 8622991; PMCID: PMC39666.
51. Zhang H, Barcelo JM, Lee B, Kohlhagen G, Zimonjic DB, Popescu NC, Pommier Y. Human mitochondrial topoisomerase I. Proc Natl Acad Sci U S A. 2001;98(19):10608-13. Epub 2001/08/30. doi: 10.1073/pnas.191321998. PubMed PMID: 11526219; PMCID: PMC58513.
52. Gellert M, Mizuuchi K, O'Dea MH, Nash HA. DNA gyrase: an enzyme that introduces superhelical turns into DNA. Proc Natl Acad Sci U S A. 1976;73(11):3872-6. Epub 1976/11/01. doi: 10.1073/pnas.73.11.3872. PubMed PMID: 186775; PMCID: PMC431247.
53. Rybenkov VV, Ullsperger C, Vologodskii AV, Cozzarelli NR. Simplification of DNA topology below equilibrium values by type II topoisomerases. Science. 1997;277(5326):690-3. Epub 1997/08/01. doi: 10.1126/science.277.5326.690. PubMed PMID: 9235892.

54. Negri C, Bernardi R, Donzelli M, Scovassi AI. Induction of apoptotic cell death by DNA topoisomerase II inhibitors. Biochimie. 1995;77(11):893-9. Epub 1995/01/01. doi: 10.1016/0300-9084(95)90009-8. PubMed PMID: 8824770.
55. Kizaki H, Onishi Y. Topoisomerase II inhibitor-induced apoptosis in thymocytes and lymphoma cells. Adv Enzyme Regul. 1997;37:403-23. Epub 1997/01/01. doi: 10.1016/s0065-2571(96)00014-3. PubMed PMID: 9381984.
56. Rogakou EP, Pilch DR, Orr AH, Ivanova VS, Bonner WM. DNA double-stranded breaks induce histone H2AX phosphorylation on serine 139. J Biol Chem. 1998;273(10):5858-68. Epub 1998/04/16. doi: 10.1074/jbc.273.10.5858. PubMed PMID: 9488723.
57. Burma S, Chen BP, Murphy M, Kurimasa A, Chen DJ. ATM phosphorylates histone H2AX in response to DNA double-strand breaks. J Biol Chem. 2001;276(45):42462-7. Epub 2001/09/26. doi: 10.1074/jbc.C100466200. PubMed PMID: 11571274.
58. Bakkenist CJ, Kastan MB. DNA damage activates ATM through intermolecular autophosphorylation and dimer dissociation. Nature. 2003;421(6922):499-506. Epub 2003/01/31. doi: 10.1038/nature01368. PubMed PMID: 12556884.
59. Dupre A, Boyer-Chatenet L, Gautier J. Two-step activation of ATM by DNA and the Mre11-Rad50-Nbs1 complex. Nat Struct Mol Biol. 2006;13(5):451-7. Epub 2006/04/20. doi: 10.1038/nsmb1090. PubMed PMID: 16622404.
60. Zhao H, Piwnica-Worms H. ATR-mediated checkpoint pathways regulate phosphorylation and activation of human Chk1. Mol Cell Biol. 2001;21(13):4129-39. Epub 2001/06/08. doi: 10.1128/MCB.21.13.4129-4139.2001. PubMed PMID: 11390642; PMCID: PMC87074.
61. Matsuoka S, Rotman G, Ogawa A, Shiloh Y, Tamai K, Elledge SJ. Ataxia telangiectasia-mutated phosphorylates Chk2 in vivo and in vitro. Proc Natl Acad Sci U S A. 2000;97(19):10389-94. Epub 2000/09/06. doi: 10.1073/pnas.190030497. PubMed PMID: 10973490; PMCID: PMC27034.
62. Peng CY, Graves PR, Thoma RS, Wu Z, Shaw AS, Piwnica-Worms H. Mitotic and G2 checkpoint control: regulation of 14-3-3 protein binding by phosphorylation of Cdc25C on serine-216. Science. 1997;277(5331):1501-5. Epub 1997/09/05. doi: 10.1126/science.277.5331.1501. PubMed PMID: 9278512.
63. Canman CE, Lim DS, Cimprich KA, Taya Y, Tamai K, Sakaguchi K, Appella E, Kastan MB, Siliciano JD. Activation of the ATM kinase by ionizing radiation and phosphorylation of p53. Science. 1998;281(5383):1677-9. Epub 1998/09/11. doi: 10.1126/science.281.5383.1677. PubMed PMID: 9733515.
64. Harper JW, Adami GR, Wei N, Keyomarsi K, Elledge SJ. The p21 Cdk-interacting protein Cip1 is a potent inhibitor of G1 cyclin-dependent kinases. Cell. 1993;75(4):805-16. Epub 1993/11/19. doi: 10.1016/0092-8674(93)90499-g. PubMed PMID: 8242751.
65. Innocente SA, Abrahamson JL, Cogswell JP, Lee JM. p53 regulates a G2 checkpoint through cyclin B1. Proc Natl Acad Sci U S A. 1999;96(5):2147-52. Epub 1999/03/03. doi: 10.1073/pnas.96.5.2147. PubMed PMID: 10051609; PMCID: PMC26751.
66. Hermeking H, Lengauer C, Polyak K, He TC, Zhang L, Thiagalingam S, Kinzler KW, Vogelstein B. 14-3-3sigma is a p53-regulated inhibitor of G2/M progression. Mol Cell. 1997;1(1):3-11. Epub 1998/07/11. doi: 10.1016/s1097-2765(00)80002-7. PubMed PMID: 9659898.

67. Pucci B, Kasten M, Giordano A. Cell cycle and apoptosis. Neoplasia. 2000;2(4):291-9. Epub 2000/09/27. doi: 10.1038/sj.neo.7900101. PubMed PMID: 11005563; PMCID: PMC1550296.
68. DiPaola RS. To arrest or not to G(2)-M Cell-cycle arrest : commentary re: A. K. Tyagi et al., Silibinin strongly synergizes human prostate carcinoma DU145 cells to doxorubicin-induced growth inhibition, G(2)-M arrest, and apoptosis. Clin. cancer res., 8: 3512-3519, 2002. Clin Cancer Res. 2002;8(11):3311-4. Epub 2002/11/14. PubMed PMID: 12429616.
69. Miyashita T, Krajewski S, Krajewska M, Wang HG, Lin HK, Liebermann DA, Hoffman B, Reed JC. Tumor suppressor p53 is a regulator of bcl-2 and bax gene expression in vitro and in vivo. Oncogene. 1994;9(6):1799-805. Epub 1994/06/01. PubMed PMID: 8183579.
70. Nakano K, Vousden KH. PUMA, a novel proapoptotic gene, is induced by p53. Mol Cell. 2001;7(3):683-94. Epub 2001/07/21. doi: 10.1016/s1097-2765(01)00214-3. PubMed PMID: 11463392.
71. Oda E, Ohki R, Murasawa H, Nemoto J, Shibue T, Yamashita T, Tokino T, Taniguchi T, Tanaka N. Noxa, a BH3-only member of the Bcl-2 family and candidate mediator of p53-induced apoptosis. Science. 2000;288(5468):1053-8. Epub 2000/05/12. doi: 10.1126/science.288.5468.1053. PubMed PMID: 10807576.
72. Sax JK, Fei P, Murphy ME, Bernhard E, Korsmeyer SJ, El-Deiry WS. BID regulation by p53 contributes to chemosensitivity. Nat Cell Biol. 2002;4(11):842-9. Epub 2002/10/29. doi: 10.1038/ncb866. PubMed PMID: 12402042.
73. Dock G. The Influence of Complicating Diseases Upon Leukemia. Am J Med Sci. 1904;127(4):563-92.
74. Kelly E, Russell SJ. History of oncolytic viruses: genesis to genetic engineering. Mol Ther. 2007;15(4):651-9. Epub 2007/02/15. doi: 10.1038/sj.mt.6300108. PubMed PMID: 17299401.
75. Bell J, McFadden G. Viruses for tumor therapy. Cell host & microbe. 2014;15(3):260-5. Epub 2014/03/19. doi: 10.1016/j.chom.2014.01.002. PubMed PMID: 24629333; PMCID: PMC3963258.
76. Toda M, Rabkin SD, Kojima H, Martuza RL. Herpes simplex virus as an in situ cancer vaccine for the induction of specific anti-tumor immunity. Hum Gene Ther. 1999;10(3):385-93. Epub 1999/02/27. doi: 10.1089/10430349950018832. PubMed PMID: 10048391.
77. FDA Approves First Oncolytic Virus Therapy Imlygic for Melanom. Oncolygy Times. 2015;37(23). doi: 10.1097/01.COT.0000475724.97729.9e.
78. Franke V, Berger DMS, Klop WMC, van der Hiel B, van de Wiel BA, Ter Meulen S, Wouters M, van Houdt WJ, van Akkooi ACJ. High response rates for T-VEC in early metastatic melanoma (stage IIIB/C-IVM1a). International journal of cancer Journal international du cancer. 2019;145(4):974-8. Epub 2019/01/30. doi: 10.1002/ijc.32172. PubMed PMID: 30694555.
79. Andtbacka RHI, Collichio F, Harrington KJ, Middleton MR, Downey G, hrling K, Kaufman HL. Final analyses of OPTiM: a randomized phase III trial of talimogene laherparepvec versus granulocyte-macrophage colony-stimulating factor in unresectable stage III-IV melanoma. J Immunother Cancer. 2019;7(1):145. Epub 2019/06/07. doi: 10.1186/s40425-019-0623-z. PubMed PMID: 31171039; PMCID: PMC6554874.
80. ClinicalTrials.gov [cited 2018]. Available from: https://clinicaltrials.gov.
81. Liu BL, Robinson M, Han ZQ, Branston RH, English C, Reay P, McGrath Y, Thomas SK, Thornton M, Bullock P, Love CA, Coffin RS. ICP34.5 deleted herpes simplex virus with

enhanced oncolytic, immune stimulating, and anti-tumour properties. Gene Ther. 2003;10(4):292-303. Epub 2003/02/22. doi: 10.1038/sj.gt.3301885. PubMed PMID: 12595888.
82. He B, Gross M, Roizman B. The gamma(1)34.5 protein of herpes simplex virus 1 complexes with protein phosphatase 1alpha to dephosphorylate the alpha subunit of the eukaryotic translation initiation factor 2 and preclude the shutoff of protein synthesis by double-stranded RNA-activated protein kinase. Proc Natl Acad Sci U S A. 1997;94(3):843-8. Epub 1997/02/04. doi: 10.1073/pnas.94.3.843. PubMed PMID: 9023344; PMCID: PMC19601.
83. MacLean AR, ul-Fareed M, Robertson L, Harland J, Brown SM. Herpes simplex virus type 1 deletion variants 1714 and 1716 pinpoint neurovirulence-related sequences in Glasgow strain 17+ between immediate early gene 1 and the 'a' sequence. J Gen Virol. 1991;72 (Pt 3):631-9. Epub 1991/03/01. doi: 10.1099/0022-1317-72-3-631. PubMed PMID: 1848598.
84. Mineta T, Rabkin SD, Yazaki T, Hunter WD, Martuza RL. Attenuated multi-mutated herpes simplex virus-1 for the treatment of malignant gliomas. Nat Med. 1995;1(9):938-43. Epub 1995/09/01. doi: 10.1038/nm0995-938. PubMed PMID: 7585221.
85. Todo T, Martuza RL, Rabkin SD, Johnson PA. Oncolytic herpes simplex virus vector with enhanced MHC class I presentation and tumor cell killing. Proc Natl Acad Sci U S A. 2001;98(11):6396-401. Epub 2001/05/17. doi: 10.1073/pnas.101136398. PubMed PMID: 11353831; PMCID: PMC33479.
86. Taneja S, MacGregor J, Markus S, Ha S, Mohr I. Enhanced antitumor efficacy of a herpes simplex virus mutant isolated by genetic selection in cancer cells. Proc Natl Acad Sci U S A. 2001;98(15):8804-8. Epub 2001/07/05. doi: 10.1073/pnas.161011798. PubMed PMID: 11438715; PMCID: PMC37516.
87. Mohr I, Sternberg D, Ward S, Leib D, Mulvey M, Gluzman Y. A herpes simplex virus type 1 gamma34.5 second-site suppressor mutant that exhibits enhanced growth in cultured glioblastoma cells is severely attenuated in animals. J Virol. 2001;75(11):5189-96. Epub 2001/05/03. doi: 10.1128/JVI.75.11.5189-5196.2001. PubMed PMID: 11333900; PMCID: PMC114924.
88. Goldsmith K, Chen W, Johnson DC, Hendricks RL. Infected cell protein (ICP)47 enhances herpes simplex virus neurovirulence by blocking the CD8+ T cell response. J Exp Med. 1998;187(3):341-8. Epub 1998/03/21. doi: 10.1084/jem.187.3.341. PubMed PMID: 9449714; PMCID: PMC2212130.
89. Hill A, Jugovic P, York I, Russ G, Bennink J, Yewdell J, Ploegh H, Johnson D. Herpes simplex virus turns off the TAP to evade host immunity. Nature. 1995;375(6530):411-5. Epub 1995/06/01. doi: 10.1038/375411a0. PubMed PMID: 7760935.
90. Tai JH, Williams JV, Edwards KM, Wright PF, Crowe JE, Jr., Dermody TS. Prevalence of reovirus-specific antibodies in young children in Nashville, Tennessee. The Journal of infectious diseases. 2005;191(8):1221-4. Epub 2005/03/19. doi: 10.1086/428911. PubMed PMID: 15776366.
91. Minuk GY, Paul RW, Lee PW. The prevalence of antibodies to reovirus type 3 in adults with idiopathic cholestatic liver disease. Journal of medical virology. 1985;16(1):55-60. Epub 1985/05/01. doi: 10.1002/jmv.1890160108. PubMed PMID: 2995568.
92. Bouziat R, Hinterleitner R, Brown JJ, Stencel-Baerenwald JE, Ikizler M, Mayassi T, Meisel M, Kim SM, Discepolo V, Pruijssers AJ, Ernest JD, Iskarpatyoti JA, Costes LM, Lawrence I, Palanski BA, Varma M, Zurenski MA, Khomandiak S, McAllister N, Aravamudhan P, Boehme KW, Hu F, Samsom JN, Reinecker HC, Kupfer SS, Guandalini S, Semrad CE, Abadie V, Khosla C, Barreiro LB, Xavier RJ, Ng A, Dermody TS, Jabri B. Reovirus infection

triggers inflammatory responses to dietary antigens and development of celiac disease. Science. 2017;356(6333):44-50. doi: 10.1126/science.aah5298. PubMed PMID: 28386004.
93. Dermody TS, Parker J, Sherry B. Orthoreoviruses. In: Knipe DM, Howley PM, editors. Fields Virology. Sixth ed. Philadelphia: Lippincott Williams & Wilkins; 2013. p. 1304-46.
94. Dryden KA, Wang G, Yeager M, Nibert ML, Coombs KM, Furlong DB, Fields BN, Baker TS. Early steps in reovirus infection are associated with dramatic changes in supramolecular structure and protein conformation: analysis of virions and subviral particles by cryoelectron microscopy and image reconstruction. J Cell Biol. 1993;122(5):1023-41. Epub 1993/09/01. PubMed PMID: 8394844; PMCID: PMC2119633.
95. Nibert ML, Dermody TS, Fields BN. Structure of the reovirus cell-attachment protein: a model for the domain organization of sigma 1. J Virol. 1990;64(6):2976-89. PubMed PMID: 2335823; PMCID: PMC249482.
96. Dietrich MH, Ogden KM, Long JM, Ebenhoch R, Thor A, Dermody TS, Stehle T. Structural and Functional Features of the Reovirus sigma1 Tail. J Virol. 2018;92(14). Epub 2018/04/27. doi: 10.1128/JVI.00336-18. PubMed PMID: 29695426; PMCID: PMC6026731.
97. Chappell JD, Prota AE, Dermody TS, Stehle T. Crystal structure of reovirus attachment protein sigma1 reveals evolutionary relationship to adenovirus fiber. EMBO J. 2002;21(1-2):1-11. doi: 10.1093/emboj/21.1.1. PubMed PMID: 11782420; PMCID: PMC125343.
98. Ramos-Alvarez M, Sabin AB. Characteristics of poliomyelitis and other enteric viruses recovered in tissue culture from healthy American children. Proc Soc Exp Biol Med. 1954;87(3):655-61. PubMed PMID: 13237336.
99. Ramos-Alvarez M, Sabin AB. Intestinal viral flora of healthy children demonstrable by monkey kidney tissue culture. Am J Public Health Nations Health. 1956;46(3):295-9. PubMed PMID: 13292578; PMCID: PMC1623578.
100. ENTERIC cytopathogenic human orphan (ECHO) viruses. Science. 1955;122(3181):1187-8. Epub 1955/12/16. PubMed PMID: 13274079.
101. Ramos-Alvarez M, Sabin AB. Enteropathogenic viruses and bacteria; role in summer diarrheal diseases of infancy and early childhood. J Am Med Assoc. 1958;167(2):147-56. PubMed PMID: 13538681.
102. Sabin AB. Reoviruses. A new group of respiratory and enteric viruses formerly classified as ECHO type 10 is described. Science. 1959;130(3386):1387-9. PubMed PMID: 14440555.
103. Rosen L. Serologic grouping of reoviruses by hemagglutination-inhibition. Am J Hyg. 1960;71:242-9. PubMed PMID: 14438891.
104. Barton ES, Connolly JL, Forrest JC, Chappell JD, Dermody TS. Utilization of sialic acid as a coreceptor enhances reovirus attachment by multistep adhesion strengthening. J Biol Chem. 2001;276(3):2200-11. Epub 2000/10/31. doi: 10.1074/jbc.M004680200. PubMed PMID: 11054410.
105. Gentsch JR, Pacitti AF. Differential interaction of reovirus type 3 with sialylated receptor components on animal cells. Virology. 1987;161(1):245-8. PubMed PMID: 3672931.
106. Reiss K, Stencel JE, Liu Y, Blaum BS, Reiter DM, Feizi T, Dermody TS, Stehle T. The GM2 glycan serves as a functional coreceptor for serotype 1 reovirus. PLoS pathogens. 2012;8(12):e1003078. Epub 2012/12/14. doi: 10.1371/journal.ppat.1003078. PubMed PMID: 23236285; PMCID: PMC3516570.
107. Reiter DM, Frierson JM, Halvorson EE, Kobayashi T, Dermody TS, Stehle T. Crystal structure of reovirus attachment protein sigma1 in complex with sialylated oligosaccharides.

PLoS pathogens. 2011;7(8):e1002166. doi: 10.1371/journal.ppat.1002166. PubMed PMID: 21829363; PMCID: PMC3150272.
108. Barton ES, Forrest JC, Connolly JL, Chappell JD, Liu Y, Schnell FJ, Nusrat A, Parkos CA, Dermody TS. Junction adhesion molecule is a receptor for reovirus. Cell. 2001;104(3):441-51. Epub 2001/03/10. doi: S0092-8674(01)00231-8 [pii]. PubMed PMID: 11239401.
109. Martin-Padura I, Lostaglio S, Schneemann M, Williams L, Romano M, Fruscella P, Panzeri C, Stoppacciaro A, Ruco L, Villa A, Simmons D, Dejana E. Junctional adhesion molecule, a novel member of the immunoglobulin superfamily that distributes at intercellular junctions and modulates monocyte transmigration. J Cell Biol. 1998;142(1):117-27. PubMed PMID: 9660867; PMCID: PMC2133024.
110. Maginnis MS, Forrest JC, Kopecky-Bromberg SA, Dickeson SK, Santoro SA, Zutter MM, Nemerow GR, Bergelson JM, Dermody TS. Beta1 integrin mediates internalization of mammalian reovirus. J Virol. 2006;80(6):2760-70. doi: 10.1128/JVI.80.6.2760-2770.2006. PubMed PMID: 16501085; PMCID: PMC1395463.
111. Maginnis MS, Mainou BA, Derdowski A, Johnson EM, Zent R, Dermody TS. NPXY motifs in the beta1 integrin cytoplasmic tail are required for functional reovirus entry. J Virol. 2008;82(7):3181-91. doi: 10.1128/JVI.01612-07. PubMed PMID: 18216114; PMCID: PMC2268482.
112. Ehrlich M, Boll W, Van Oijen A, Hariharan R, Chandran K, Nibert ML, Kirchhausen T. Endocytosis by random initiation and stabilization of clathrin-coated pits. Cell. 2004;118(5):591-605. doi: 10.1016/j.cell.2004.08.017. PubMed PMID: 15339664.
113. Doyle JD, Danthi P, Kendall EA, Ooms LS, Wetzel JD, Dermody TS. Molecular determinants of proteolytic disassembly of the reovirus outer capsid. J Biol Chem. 2012;287(11):8029-38. Epub 2012/01/19. doi: 10.1074/jbc.M111.334854. PubMed PMID: 22253447; PMCID: PMC3318753.
114. Ebert DH, Deussing J, Peters C, Dermody TS. Cathepsin L and cathepsin B mediate reovirus disassembly in murine fibroblast cells. J Biol Chem. 2002;277(27):24609-17. doi: 10.1074/jbc.M201107200. PubMed PMID: 11986312.
115. Johnson EM, Doyle JD, Wetzel JD, McClung RP, Katunuma N, Chappell JD, Washington MK, Dermody TS. Genetic and pharmacologic alteration of cathepsin expression influences reovirus pathogenesis. J Virol. 2009;83(19):9630-40. Epub 2009/07/31. doi: 10.1128/JVI.01095-09. PubMed PMID: 19640986; PMCID: PMC2748054.
116. Boulant S, Stanifer M, Kural C, Cureton DK, Massol R, Nibert ML, Kirchhausen T. Similar uptake but different trafficking and escape routes of reovirus virions and infectious subvirion particles imaged in polarized Madin-Darby canine kidney cells. Mol Biol Cell. 2013;24(8):1196-207. Epub 2013/02/22. doi: 10.1091/mbc.E12-12-0852. PubMed PMID: 23427267; PMCID: PMC3623640.
117. Mainou BA, Dermody TS. Transport to late endosomes is required for efficient reovirus infection. J Virol. 2012;86(16):8346-58. Epub 2012/06/08. doi: 10.1128/JVI.00100-12. PubMed PMID: 22674975; PMCID: PMC3421701.
118. Golden JW, Bahe JA, Lucas WT, Nibert ML, Schiff LA. Cathepsin S supports acid-independent infection by some reoviruses. J Biol Chem. 2004;279(10):8547-57. doi: 10.1074/jbc.M309758200. PubMed PMID: 14670972.
119. Ebert DH, Wetzel JD, Brumbaugh DE, Chance SR, Stobie LE, Baer GS, Dermody TS. Adaptation of reovirus to growth in the presence of protease inhibitor E64 segregates with a mutation in the carboxy terminus of viral outer-capsid protein sigma3. J Virol. 2001;75(7):3197-

206. Epub 2001/03/10. doi: 10.1128/JVI.75.7.3197-3206.2001. PubMed PMID: 11238846; PMCID: PMC114113.
120. Danthi P, Holm GH, Stehle T, Dermody TS. Reovirus receptors, cell entry, and proapoptotic signaling. Advances in experimental medicine and biology. 2013;790:42-71. doi: 10.1007/978-1-4614-7651-1_3. PubMed PMID: 23884585; PMCID: PMC4724410.
121. Snyder AJ, Danthi P. Cleavage of the C-Terminal Fragment of Reovirus mu1 Is Required for Optimal Infectivity. J Virol. 2018;92(6). Epub 2018/01/05. doi: 10.1128/JVI.01848-17. PubMed PMID: 29298891; PMCID: PMC5827373.
122. Drayna D, Fields BN. Activation and characterization of the reovirus transcriptase: genetic analysis. J Virol. 1982;41(1):110-8. PubMed PMID: 7086953; PMCID: PMC256731.
123. Lemay G. Synthesis and Translation of Viral mRNA in Reovirus-Infected Cells: Progress and Remaining Questions. Viruses. 2018;10(12). Epub 2018/11/30. doi: 10.3390/v10120671. PubMed PMID: 30486370; PMCID: PMC6315682.
124. Fernandez de Castro I, Zamora PF, Ooms L, Fernandez JJ, Lai CM, Mainou BA, Dermody TS, Risco C. Reovirus forms neo-organelles for progeny particle assembly within reorganized cell membranes. mBio. 2014;5(1). doi: 10.1128/mBio.00931-13. PubMed PMID: 24549844; PMCID: PMC3944815.
125. Tenorio R, Fernandez de Castro I, Knowlton JJ, Zamora PF, Lee CH, Mainou BA, Dermody TS, Risco C. Reovirus sigmaNS and muNS Proteins Remodel the Endoplasmic Reticulum to Build Replication Neo-Organelles. mBio. 2018;9(4). Epub 2018/08/09. doi: 10.1128/mBio.01253-18. PubMed PMID: 30087167; PMCID: PMC6083906.
126. Broering TJ, Kim J, Miller CL, Piggott CD, Dinoso JB, Nibert ML, Parker JS. Reovirus nonstructural protein mu NS recruits viral core surface proteins and entering core particles to factory-like inclusions. J Virol. 2004;78(4):1882-92. Epub 2004/01/30. PubMed PMID: 14747553; PMCID: PMC369481.
127. Miller CL, Broering TJ, Parker JS, Arnold MM, Nibert ML. Reovirus sigma NS protein localizes to inclusions through an association requiring the mu NS amino terminus. J Virol. 2003;77(8):4566-76. Epub 2003/03/29. doi: 10.1128/jvi.77.8.4566-4576.2003. PubMed PMID: 12663763; PMCID: PMC152138.
128. Farsetta DL, Chandran K, Nibert ML. Transcriptional activities of reovirus RNA polymerase in recoated cores. Initiation and elongation are regulated by separate mechanisms. J Biol Chem. 2000;275(50):39693-701. Epub 2000/09/29. doi: 10.1074/jbc.M004562200. PubMed PMID: 11007773.
129. Yoneyama M, Kikuchi M, Natsukawa T, Shinobu N, Imaizumi T, Miyagishi M, Taira K, Akira S, Fujita T. The RNA helicase RIG-I has an essential function in double-stranded RNA-induced innate antiviral responses. Nat Immunol. 2004;5(7):730-7. Epub 2004/06/23. doi: 10.1038/ni1087. PubMed PMID: 15208624.
130. Kawai T, Takahashi K, Sato S, Coban C, Kumar H, Kato H, Ishii KJ, Takeuchi O, Akira S. IPS-1, an adaptor triggering RIG-I- and Mda5-mediated type I interferon induction. Nat Immunol. 2005;6(10):981-8. Epub 2005/08/30. doi: 10.1038/ni1243. PubMed PMID: 16127453.
131. Seth RB, Sun L, Ea CK, Chen ZJ. Identification and characterization of MAVS, a mitochondrial antiviral signaling protein that activates NF-kappaB and IRF 3. Cell. 2005;122(5):669-82. Epub 2005/08/30. doi: 10.1016/j.cell.2005.08.012. PubMed PMID: 16125763.
132. Meylan E, Curran J, Hofmann K, Moradpour D, Binder M, Bartenschlager R, Tschopp J. Cardif is an adaptor protein in the RIG-I antiviral pathway and is targeted by hepatitis C virus.

Nature. 2005;437(7062):1167-72. Epub 2005/09/24. doi: 10.1038/nature04193. PubMed PMID: 16177806.
133. Sadler AJ, Williams BR. Structure and function of the protein kinase R. Curr Top Microbiol Immunol. 2007;316:253-92. Epub 2007/11/01. doi: 10.1007/978-3-540-71329-6_13. PubMed PMID: 17969452.
134. Phillips MB, Stuart JD, Rodriguez Stewart RM, Berry JT, Mainou BA, Boehme KW. Current understanding of reovirus oncolysis mechanisms. Oncolytic Virother. 2018;7:53-63. Epub 2018/06/27. doi: 10.2147/OV.S143808. PubMed PMID: 29942799; PMCID: PMC6005300.
135. Imani F, Jacobs BL. Inhibitory activity for the interferon-induced protein kinase is associated with the reovirus serotype 1 sigma 3 protein. Proc Natl Acad Sci U S A. 1988;85(21):7887-91. Epub 1988/11/01. doi: 10.1073/pnas.85.21.7887. PubMed PMID: 2460857; PMCID: PMC282302.
136. Yue Z, Shatkin AJ. Double-stranded RNA-dependent protein kinase (PKR) is regulated by reovirus structural proteins. Virology. 1997;234(2):364-71. Epub 1997/08/04. doi: 10.1006/viro.1997.8664. PubMed PMID: 9268168.
137. Boriack-Sjodin PA, Margarit SM, Bar-Sagi D, Kuriyan J. The structural basis of the activation of Ras by Sos. Nature. 1998;394(6691):337-43. Epub 1998/08/05. doi: 10.1038/28548. PubMed PMID: 9690470.
138. Nandan MO, Yang VW. An Update on the Biology of RAS/RAF Mutations in Colorectal Cancer. Curr Colorectal Cancer Rep. 2011;7(2):113-20. Epub 2011/06/01. doi: 10.1007/s11888-011-0086-1. PubMed PMID: 21625338; PMCID: PMC3103074.
139. Avruch J, Khokhlatchev A, Kyriakis JM, Luo Z, Tzivion G, Vavvas D, Zhang XF. Ras activation of the Raf kinase: tyrosine kinase recruitment of the MAP kinase cascade. Recent Prog Horm Res. 2001;56:127-55. Epub 2001/03/10. doi: 10.1210/rp.56.1.127. PubMed PMID: 11237210.
140. Giltnane JM, Balko JM. Rationale for targeting the Ras/MAPK pathway in triple-negative breast cancer. Discov Med. 2014;17(95):275-83. Epub 2014/06/03. PubMed PMID: 24882719.
141. Cerami E, Gao J, Dogrusoz U, Gross BE, Sumer SO, Aksoy BA, Jacobsen A, Byrne CJ, Heuer ML, Larsson E, Antipin Y, Reva B, Goldberg AP, Sander C, Schultz N. The cBio cancer genomics portal: an open platform for exploring multidimensional cancer genomics data. Cancer Discov. 2012;2(5):401-4. doi: 10.1158/2159-8290.CD-12-0095. PubMed PMID: 22588877; PMCID: PMC3956037.
142. Cancer Genome Atlas N. Comprehensive molecular portraits of human breast tumours. Nature. 2012;490(7418):61-70. Epub 2012/09/25. doi: 10.1038/nature11412. PubMed PMID: 23000897; PMCID: PMC3465532.
143. Adeyinka A, Nui Y, Cherlet T, Snell L, Watson PH, Murphy LC. Activated mitogen-activated protein kinase expression during human breast tumorigenesis and breast cancer progression. Clin Cancer Res. 2002;8(6):1747-53. Epub 2002/06/13. PubMed PMID: 12060612.
144. Sivaraman VS, Wang H, Nuovo GJ, Malbon CC. Hyperexpression of mitogen-activated protein kinase in human breast cancer. J Clin Invest. 1997;99(7):1478-83. Epub 1997/04/01. doi: 10.1172/JCI119309. PubMed PMID: 9119990; PMCID: PMC507966.
145. Craig DW, O'Shaughnessy JA, Kiefer JA, Aldrich J, Sinari S, Moses TM, Wong S, Dinh J, Christoforides A, Blum JL, Aitelli CL, Osborne CR, Izatt T, Kurdoglu A, Baker A, Koeman J, Barbacioru C, Sakarya O, De La Vega FM, Siddiqui A, Hoang L, Billings PR, Salhia B, Tolcher

AW, Trent JM, Mousses S, Von Hoff D, Carpten JD. Genome and transcriptome sequencing in prospective metastatic triple-negative breast cancer uncovers therapeutic vulnerabilities. Mol Cancer Ther. 2013;12(1):104-16. Epub 2012/11/23. doi: 10.1158/1535-7163.MCT-12-0781. PubMed PMID: 23171949.
146. Wallace MD, Pfefferle AD, Shen L, McNairn AJ, Cerami EG, Fallon BL, Rinaldi VD, Southard TL, Perou CM, Schimenti JC. Comparative oncogenomics implicates the neurofibromin 1 gene (NF1) as a breast cancer driver. Genetics. 2012;192(2):385-96. Epub 2012/08/02. doi: 10.1534/genetics.112.142802. PubMed PMID: 22851646; PMCID: PMC3454871.
147. Fernandes J. Oncogenes: The Passport for Viral Oncolysis Through PKR Inhibition. Biomark Cancer. 2016;8:101-10. Epub 2016/08/04. doi: 10.4137/BIC.S33378. PubMed PMID: 27486347; PMCID: PMC4966488.
148. Shmulevitz M, Pan LZ, Garant K, Pan D, Lee PW. Oncogenic Ras promotes reovirus spread by suppressing IFN-beta production through negative regulation of RIG-I signaling. Cancer research. 2010;70(12):4912-21. Epub 2010/05/27. doi: 10.1158/0008-5472.CAN-09-4676. PubMed PMID: 20501842.
149. Zhang P, Samuel CE. Protein kinase PKR plays a stimulus- and virus-dependent role in apoptotic death and virus multiplication in human cells. J Virol. 2007;81(15):8192-200. Epub 2007/05/25. doi: 10.1128/JVI.00426-07. PubMed PMID: 17522227; PMCID: PMC1951329.
150. Kirchner E, Guglielmi KM, Strauss HM, Dermody TS, Stehle T. Structure of reovirus sigma1 in complex with its receptor junctional adhesion molecule-A. PLoS pathogens. 2008;4(12):e1000235. doi: 10.1371/journal.ppat.1000235. PubMed PMID: 19079583; PMCID: PMC2588538.
151. Marcato P, Shmulevitz M, Pan D, Stoltz D, Lee PW. Ras transformation mediates reovirus oncolysis by enhancing virus uncoating, particle infectivity, and apoptosis-dependent release. Mol Ther. 2007;15(8):1522-30. Epub 2007/04/26. doi: 10.1038/sj.mt.6300179. PubMed PMID: 17457318.
152. Nouh MA, Mohamed MM, El-Shinawi M, Shaalan MA, Cavallo-Medved D, Khaled HM, Sloane BF. Cathepsin B: a potential prognostic marker for inflammatory breast cancer. J Transl Med. 2011;9:1. Epub 2011/01/05. doi: 10.1186/1479-5876-9-1. PubMed PMID: 21199580; PMCID: PMC3022726.
153. Vasiljeva O, Korovin M, Gajda M, Brodoefel H, Bojic L, Kruger A, Schurigt U, Sevenich L, Turk B, Peters C, Reinheckel T. Reduced tumour cell proliferation and delayed development of high-grade mammary carcinomas in cathepsin B-deficient mice. Oncogene. 2008;27(30):4191-9. Epub 2008/03/18. doi: 10.1038/onc.2008.59. PubMed PMID: 18345026.
154. Withana NP, Blum G, Sameni M, Slaney C, Anbalagan A, Olive MB, Bidwell BN, Edgington L, Wang L, Moin K, Sloane BF, Anderson RL, Bogyo MS, Parker BS. Cathepsin B inhibition limits bone metastasis in breast cancer. Cancer research. 2012;72(5):1199-209. Epub 2012/01/24. doi: 10.1158/0008-5472.CAN-11-2759. PubMed PMID: 22266111; PMCID: PMC3538126.
155. Jedeszko C, Sloane BF. Cysteine cathepsins in human cancer. Biol Chem. 2004;385(11):1017-27. Epub 2004/12/04. doi: 10.1515/BC.2004.132. PubMed PMID: 15576321.
156. Alain T, Kim TS, Lun X, Liacini A, Schiff LA, Senger DL, Forsyth PA. Proteolytic disassembly is a critical determinant for reovirus oncolysis. Mol Ther. 2007;15(8):1512-21. Epub 2007/05/24. doi: 10.1038/sj.mt.6300207. PubMed PMID: 17519890; PMCID: PMC7185731.

157. Rosen L, Evans HE, Spickard A. Reovirus infections in human volunteers. Am J Hyg. 1963;77:29-37. Epub 1963/01/01. doi: 10.1093/oxfordjournals.aje.a120293. PubMed PMID: 13974840.
158. Vidal L, Pandha HS, Yap TA, White CL, Twigger K, Vile RG, Melcher A, Coffey M, Harrington KJ, DeBono JS. A phase I study of intravenous oncolytic reovirus type 3 Dearing in patients with advanced cancer. Clin Cancer Res. 2008;14(21):7127-37. Epub 2008/11/05. doi: 10.1158/1078-0432.CCR-08-0524. PubMed PMID: 18981012.
159. Lolkema MP, Arkenau HT, Harrington K, Roxburgh P, Morrison R, Roulstone V, Twigger K, Coffey M, Mettinger K, Gill G, Evans TR, de Bono JS. A phase I study of the combination of intravenous reovirus type 3 Dearing and gemcitabine in patients with advanced cancer. Clin Cancer Res. 2011;17(3):581-8. Epub 2010/11/26. doi: 10.1158/1078-0432.CCR-10-2159. PubMed PMID: 21106728.
160. Coffey MC, Strong JE, Forsyth PA, Lee PW. Reovirus therapy of tumors with activated Ras pathway. Science. 1998;282(5392):1332-4. Epub 1998/11/13. PubMed PMID: 9812900.
161. Ilett EJ, Prestwich RJ, Kottke T, Errington F, Thompson JM, Harrington KJ, Pandha HS, Coffey M, Selby PJ, Vile RG, Melcher AA. Dendritic cells and T cells deliver oncolytic reovirus for tumour killing despite pre-existing anti-viral immunity. Gene Ther. 2009;16(5):689-99. doi: 10.1038/gt.2009.29. PubMed PMID: 19282847; PMCID: PMC4562026.
162. Berkeley RA, Steele LP, Mulder AA, van den Wollenberg DJM, Kottke TJ, Thompson J, Coffey M, Hoeben RC, Vile RG, Melcher A, Ilett EJ. Antibody-Neutralized Reovirus Is Effective in Oncolytic Virotherapy. Cancer Immunol Res. 2018;6(10):1161-73. Epub 2018/09/14. doi: 10.1158/2326-6066.CIR-18-0309. PubMed PMID: 30209061.
163. Qiao J, Kottke T, Willmon C, Galivo F, Wongthida P, Diaz RM, Thompson J, Ryno P, Barber GN, Chester J, Selby P, Harrington K, Melcher A, Vile RG. Purging metastases in lymphoid organs using a combination of antigen-nonspecific adoptive T cell therapy, oncolytic virotherapy and immunotherapy. Nat Med. 2008;14(1):37-44. Epub 2007/12/11. doi: 10.1038/nm1681. PubMed PMID: 18066076.
164. Gromeier M, Alexander L, Wimmer E. Internal ribosomal entry site substitution eliminates neurovirulence in intergeneric poliovirus recombinants. Proc Natl Acad Sci U S A. 1996;93(6):2370-5. Epub 1996/03/19. doi: 10.1073/pnas.93.6.2370. PubMed PMID: 8637880; PMCID: PMC39803.
165. Mosaheb MM, Dobrikova EY, Brown MC, Yang Y, Cable J, Okada H, Nair SK, Bigner DD, Ashley DM, Gromeier M. Genetically stable poliovirus vectors activate dendritic cells and prime antitumor CD8 T cell immunity. Nat Commun. 2020;11(1):524. Epub 2020/01/29. doi: 10.1038/s41467-019-13939-z. PubMed PMID: 31988324; PMCID: PMC6985231.
166. Kicielinski KP, Chiocca EA, Yu JS, Gill GM, Coffey M, Markert JM. Phase 1 clinical trial of intratumoral reovirus infusion for the treatment of recurrent malignant gliomas in adults. Mol Ther. 2014;22(5):1056-62. Epub 2014/02/21. doi: 10.1038/mt.2014.21. PubMed PMID: 24553100; PMCID: PMC4015229.
167. Forsyth P, Roldan G, George D, Wallace C, Palmer CA, Morris D, Cairncross G, Matthews MV, Markert J, Gillespie Y, Coffey M, Thompson B, Hamilton M. A phase I trial of intratumoral administration of reovirus in patients with histologically confirmed recurrent malignant gliomas. Mol Ther. 2008;16(3):627-32. Epub 2008/02/07. doi: 10.1038/sj.mt.6300403. PubMed PMID: 18253152.
168. Cohn DE, Sill MW, Walker JL, O'Malley D, Nagel CI, Rutledge TL, Bradley W, Richardson DL, Moxley KM, Aghajanian C. Randomized phase IIB evaluation of weekly

paclitaxel versus weekly paclitaxel with oncolytic reovirus (Reolysin(R)) in recurrent ovarian, tubal, or peritoneal cancer: An NRG Oncology/Gynecologic Oncology Group study. Gynecol Oncol. 2017;146(3):477-83. Epub 2017/08/02. doi: 10.1016/j.ygyno.2017.07.135. PubMed PMID: 28756871; PMCID: PMC5570536.
169. Jonker DJ, Tang PA, Kennecke H, Welch SA, Cripps MC, Asmis T, Chalchal H, Tomiak A, Lim H, Ko YJ, Chen EX, Alcindor T, Goffin JR, Korpanty GJ, Feilotter H, Tsao MS, Theis A, Tu D, Seymour L. A Randomized Phase II Study of FOLFOX6/Bevacizumab With or Without Pelareorep in Patients With Metastatic Colorectal Cancer: IND.210, a Canadian Cancer Trials Group Trial. Clin Colorectal Cancer. 2018;17(3):231-9 e7. Epub 2018/04/15. doi: 10.1016/j.clcc.2018.03.001. PubMed PMID: 29653857.
170. Bernstein V, Ellard SL, Dent SF, Tu D, Mates M, Dhesy-Thind SK, Panasci L, Gelmon KA, Salim M, Song X, Clemons M, Ksienski D, Verma S, Simmons C, Lui H, Chi K, Feilotter H, Hagerman LJ, Seymour L. A randomized phase II study of weekly paclitaxel with or without pelareorep in patients with metastatic breast cancer: final analysis of Canadian Cancer Trials Group IND.213. Breast Cancer Res Treat. 2018;167(2):485-93. Epub 2017/10/14. doi: 10.1007/s10549-017-4538-4. PubMed PMID: 29027598.
171. Eigl BJ, Chi K, Tu D, Hotte SJ, Winquist E, Booth CM, Canil C, Potvin K, Gregg R, North S, Zulfiqar M, Ellard S, Ruether JD, Le L, Kakumanu AS, Salim M, Allan AL, Feilotter H, Theis A, Seymour L. A randomized phase II study of pelareorep and docetaxel or docetaxel alone in men with metastatic castration resistant prostate cancer: CCTG study IND 209. Oncotarget. 2018;9(8):8155-64. Epub 2018/03/01. doi: 10.18632/oncotarget.24263. PubMed PMID: 29487723; PMCID: PMC5814290.
172. Noonan AM, Farren MR, Geyer SM, Huang Y, Tahiri S, Ahn D, Mikhail S, Ciombor KK, Pant S, Aparo S, Sexton J, Marshall JL, Mace TA, Wu CS, El-Rayes B, Timmers CD, Zwiebel J, Lesinski GB, Villalona-Calero MA, Bekaii-Saab TS. Randomized Phase 2 Trial of the Oncolytic Virus Pelareorep (Reolysin) in Upfront Treatment of Metastatic Pancreatic Adenocarcinoma. Mol Ther. 2016;24(6):1150-8. Epub 2016/04/05. doi: 10.1038/mt.2016.66. PubMed PMID: 27039845; PMCID: PMC4923331.
173. Bradbury PA, Morris DG, Nicholas G, Tu D, Tehfe M, Goffin JR, Shepherd FA, Gregg RW, Rothenstein J, Lee C, Kuruvilla S, Keith BD, Torri V, Blais N, Hao D, Korpanty GJ, Goss G, Melosky BL, Mates M, Leighl N, Ayoub JP, Sederias J, Feilotter H, Seymour L, Laurie SA. Canadian Cancer Trials Group (CCTG) IND211: A randomized trial of pelareorep (Reolysin) in patients with previously treated advanced or metastatic non-small cell lung cancer receiving standard salvage therapy. Lung Cancer. 2018;120:142-8. Epub 2018/05/12. doi: 10.1016/j.lungcan.2018.03.005. PubMed PMID: 29748010.
174. Karapanagiotou EM, Roulstone V, Twigger K, Ball M, Tanay M, Nutting C, Newbold K, Gore ME, Larkin J, Syrigos KN, Coffey M, Thompson B, Mettinger K, Vile RG, Pandha HS, Hall GD, Melcher AA, Chester J, Harrington KJ. Phase I/II trial of carboplatin and paclitaxel chemotherapy in combination with intravenous oncolytic reovirus in patients with advanced malignancies. Clin Cancer Res. 2012;18(7):2080-9. Epub 2012/02/10. doi: 10.1158/1078-0432.CCR-11-2181. PubMed PMID: 22316603; PMCID: PMC5553618.
175. Galanis E, Markovic SN, Suman VJ, Nuovo GJ, Vile RG, Kottke TJ, Nevala WK, Thompson MA, Lewis JE, Rumilla KM, Roulstone V, Harrington K, Linette GP, Maples WJ, Coffey M, Zwiebel J, Kendra K. Phase II trial of intravenous administration of Reolysin((R)) (Reovirus Serotype-3-dearing Strain) in patients with metastatic melanoma. Mol Ther.

2012;20(10):1998-2003. Epub 2012/08/09. doi: 10.1038/mt.2012.146. PubMed PMID: 22871663; PMCID: PMC3464629.
176. Comins C, Spicer J, Protheroe A, Roulstone V, Twigger K, White CM, Vile R, Melcher A, Coffey MC, Mettinger KL, Nuovo G, Cohn DE, Phelps M, Harrington KJ, Pandha HS. REO-10: a phase I study of intravenous reovirus and docetaxel in patients with advanced cancer. Clin Cancer Res. 2010;16(22):5564-72. Epub 2010/10/12. doi: 10.1158/1078-0432.CCR-10-1233. PubMed PMID: 20926400; PMCID: PMC3934355.
177. Harrington KJ, Karapanagiotou EM, Roulstone V, Twigger KR, White CL, Vidal L, Beirne D, Prestwich R, Newbold K, Ahmed M, Thway K, Nutting CM, Coffey M, Harris D, Vile RG, Pandha HS, Debono JS, Melcher AA. Two-stage phase I dose-escalation study of intratumoral reovirus type 3 dearing and palliative radiotherapy in patients with advanced cancers. Clin Cancer Res. 2010;16(11):3067-77. Epub 2010/05/21. doi: 10.1158/1078-0432.CCR-10-0054. PubMed PMID: 20484020; PMCID: PMC3907942.
178. Morris DG, Feng X, DiFrancesco LM, Fonseca K, Forsyth PA, Paterson AH, Coffey MC, Thompson B. REO-001: A phase I trial of percutaneous intralesional administration of reovirus type 3 dearing (Reolysin(R)) in patients with advanced solid tumors. Investigational new drugs. 2013;31(3):696-706. Epub 2012/08/14. doi: 10.1007/s10637-012-9865-z. PubMed PMID: 22886613.
179. Kim M. Naturally occurring reoviruses for human cancer therapy. BMB Rep. 2015;48(8):454-60. Epub 2015/06/11. doi: 10.5483/bmbrep.2015.48.8.076. PubMed PMID: 26058397; PMCID: PMC4576953.
180. Surveilance, Epidemiology, and End Results Program 2018 [cited 2018]. Available from: https://seer.cancer.gov/.
181. Abramson VG, Lehmann BD, Ballinger TJ, Pietenpol JA. Subtyping of triple-negative breast cancer: implications for therapy. Cancer. 2015;121(1):8-16. doi: 10.1002/cncr.28914. PubMed PMID: 25043972; PMCID: PMC4270831.
182. Lehmann BD, Bauer JA, Chen X, Sanders ME, Chakravarthy AB, Shyr Y, Pietenpol JA. Identification of human triple-negative breast cancer subtypes and preclinical models for selection of targeted therapies. J Clin Invest. 2011;121(7):2750-67. doi: 10.1172/JCI45014. PubMed PMID: 21633166; PMCID: PMC3127435.
183. Zeichner SB, Terawaki H, Gogineni K. A Review of Systemic Treatment in Metastatic Triple-Negative Breast Cancer. Breast Cancer (Auckl). 2016;10:25-36. Epub 2016/04/05. doi: 10.4137/BCBCR.S32783. PubMed PMID: 27042088; PMCID: PMC4807882.
184. Cattaneo R, Miest T, Shashkova EV, Barry MA. Reprogrammed viruses as cancer therapeutics: targeted, armed and shielded. Nat Rev Microbiol. 2008;6(7):529-40. doi: 10.1038/nrmicro1927. PubMed PMID: 18552863; PMCID: PMC3947522.
185. Brown MC, Holl EK, Boczkowski D, Dobrikova E, Mosaheb M, Chandramohan V, Bigner DD, Gromeier M, Nair SK. Cancer immunotherapy with recombinant poliovirus induces IFN-dominant activation of dendritic cells and tumor antigen-specific CTLs. Sci Transl Med. 2017;9(408). Epub 2017/09/22. doi: 10.1126/scitranslmed.aan4220. PubMed PMID: 28931654; PMCID: PMC6034685.
186. El-Sherbiny YM, Holmes TD, Wetherill LF, Black EV, Wilson EB, Phillips SL, Scott GB, Adair RA, Dave R, Scott KJ, Morgan RS, Coffey M, Toogood GJ, Melcher AA, Cook GP. Controlled infection with a therapeutic virus defines the activation kinetics of human natural killer cells in vivo. Clin Exp Immunol. 2015;180(1):98-107. Epub 2014/12/04. doi: 10.1111/cei.12562. PubMed PMID: 25469725; PMCID: PMC4367098.

187. Kelly KR, Espitia CM, Zhao W, Wu K, Visconte V, Anwer F, Calton CM, Carew JS, Nawrocki ST. Oncolytic reovirus sensitizes multiple myeloma cells to anti-PD-L1 therapy. Leukemia. 2018;32(1):230-3. Epub 2017/08/24. doi: 10.1038/leu.2017.272. PubMed PMID: 28832023; PMCID: PMC5844271.
188. Rajani K, Parrish C, Kottke T, Thompson J, Zaidi S, Ilett L, Shim KG, Diaz RM, Pandha H, Harrington K, Coffey M, Melcher A, Vile R. Combination Therapy With Reovirus and Anti-PD-1 Blockade Controls Tumor Growth Through Innate and Adaptive Immune Responses. Mol Ther. 2016;24(1):166-74. doi: 10.1038/mt.2015.156. PubMed PMID: 26310630; PMCID: PMC4754544.
189. Duncan MR, Stanish SM, Cox DC. Differential sensitivity of normal and transformed human cells to reovirus infection. J Virol. 1978;28(2):444-9. Epub 1978/11/01. PubMed PMID: 214572; PMCID: PMC354293.
190. Kemp V, Hoeben RC, van den Wollenberg DJ. Exploring Reovirus Plasticity for Improving Its Use as Oncolytic Virus. Viruses. 2015;8(1). Epub 2015/12/30. doi: 10.3390/v8010004. PubMed PMID: 26712782; PMCID: PMC4728564.
191. Shatkin AJ, Sipe JD, Loh P. Separation of ten reovirus genome segments by polyacrylamide gel electrophoresis. J Virol. 1968;2(10):986-91. PubMed PMID: 5723704; PMCID: PMC375428.
192. Ouattara LA, Barin F, Barthez MA, Bonnaud B, Roingeard P, Goudeau A, Castelnau P, Vernet G, Paranhos-Baccala G, Komurian-Pradel F. Novel human reovirus isolated from children with acute necrotizing encephalopathy. Emerging infectious diseases. 2011;17(8):1436-44. Epub 2011/08/02. doi: 10.3201/eid1708.101528. PubMed PMID: 21801621; PMCID: PMC3381585.
193. Berger AK, Danthi P. Reovirus activates a caspase-independent cell death pathway. mBio. 2013;4(3):e00178-13. doi: 10.1128/mBio.00178-13. PubMed PMID: 23674612; PMCID: PMC3656442.
194. Berger AK, Hiller BE, Thete D, Snyder AJ, Perez E, Jr., Upton JW, Danthi P. Viral RNA at Two Stages of Reovirus Infection Is Required for the Induction of Necroptosis. J Virol. 2017;91(6). Epub 2017/01/13. doi: 10.1128/JVI.02404-16. PubMed PMID: 28077640; PMCID: PMC5331789.
195. Brown JJ, Short SP, Stencel-Baerenwald J, Urbanek K, Pruijssers AJ, McAllister N, Ikizler M, Taylor G, Aravamudhan P, Khomandiak S, Jabri B, Williams CS, Dermody TS. Reovirus-Induced Apoptosis in the Intestine Limits Establishment of Enteric Infection. J Virol. 2018;92(10). Epub 2018/03/09. doi: 10.1128/JVI.02062-17. PubMed PMID: 29514905; PMCID: PMC5923068.
196. Clarke P, Beckham JD, Leser JS, Hoyt CC, Tyler KL. Fas-mediated apoptotic signaling in the mouse brain following reovirus infection. J Virol. 2009;83(12):6161-70. Epub 2009/03/27. doi: 10.1128/JVI.02488-08. PubMed PMID: 19321603; PMCID: PMC2687381.
197. Clarke P, Meintzer SM, Spalding AC, Johnson GL, Tyler KL. Caspase 8-dependent sensitization of cancer cells to TRAIL-induced apoptosis following reovirus-infection. Oncogene. 2001;20(47):6910-9. doi: 10.1038/sj.onc.1204842. PubMed PMID: 11687970.
198. Danthi P, Coffey CM, Parker JS, Abel TW, Dermody TS. Independent regulation of reovirus membrane penetration and apoptosis by the mu1 phi domain. PLoS pathogens. 2008;4(12):e1000248. doi: 10.1371/journal.ppat.1000248. PubMed PMID: 19112493; PMCID: PMC2600812.

199. Pruijssers AJ, Hengel H, Abel TW, Dermody TS. Apoptosis induction influences reovirus replication and virulence in newborn mice. J Virol. 2013;87(23):12980-9. Epub 2013/09/27. doi: 10.1128/JVI.01931-13. PubMed PMID: 24067960; PMCID: PMC3838116.
200. Simon EJ, Howells MA, Stuart JD, Boehme KW. Serotype-Specific Killing of Large Cell Carcinoma Cells by Reovirus. Viruses. 2017;9(6). Epub 2017/06/08. doi: 10.3390/v9060140. PubMed PMID: 28587298; PMCID: PMC5490817.
201. Connolly JL, Barton ES, Dermody TS. Reovirus binding to cell surface sialic acid potentiates virus-induced apoptosis. J Virol. 2001;75(9):4029-39. Epub 2001/04/05. doi: 10.1128/JVI.75.9.4029-4039.2001. PubMed PMID: 11287552; PMCID: PMC114148.
202. Danthi P, Hansberger MW, Campbell JA, Forrest JC, Dermody TS. JAM-A-independent, antibody-mediated uptake of reovirus into cells leads to apoptosis. J Virol. 2006;80(3):1261-70. Epub 2006/01/18. doi: 10.1128/JVI.80.3.1261-1270.2006. PubMed PMID: 16415003; PMCID: PMC1346953.
203. Tyler KL, Squier MK, Rodgers SE, Schneider BE, Oberhaus SM, Grdina TA, Cohen JJ, Dermody TS. Differences in the capacity of reovirus strains to induce apoptosis are determined by the viral attachment protein sigma 1. J Virol. 1995;69(11):6972-9. PubMed PMID: 7474116; PMCID: PMC189616.
204. Nibert ML, Margraf RL, Coombs KM. Nonrandom segregation of parental alleles in reovirus reassortants. J Virol. 1996;70(10):7295-300. Epub 1996/10/01. PubMed PMID: 8794386; PMCID: PMC190792.
205. Wenske EA, Chanock SJ, Krata L, Fields BN. Genetic reassortment of mammalian reoviruses in mice. J Virol. 1985;56(2):613-6. Epub 1985/11/01. PubMed PMID: 4057359; PMCID: PMC252619.
206. Konopka-Anstadt JL, Mainou BA, Sutherland DM, Sekine Y, Strittmatter SM, Dermody TS. The Nogo receptor NgR1 mediates infection by mammalian reovirus. Cell host & microbe. 2014;15(6):681-91. doi: 10.1016/j.chom.2014.05.010. PubMed PMID: 24922571; PMCID: PMC4100558.
207. Baer GS, Dermody TS. Mutations in reovirus outer-capsid protein sigma3 selected during persistent infections of L cells confer resistance to protease inhibitor E64. J Virol. 1997;71(7):4921-8. Epub 1997/07/01. PubMed PMID: 9188554; PMCID: PMC191722.
208. Oberhaus SM, Smith RL, Clayton GH, Dermody TS, Tyler KL. Reovirus infection and tissue injury in the mouse central nervous system are associated with apoptosis. J Virol. 1997;71(3):2100-6. Epub 1997/03/01. PubMed PMID: 9032342; PMCID: PMC191302.
209. Lee MJ, Ye AS, Gardino AK, Heijink AM, Sorger PK, MacBeath G, Yaffe MB. Sequential application of anticancer drugs enhances cell death by rewiring apoptotic signaling networks. Cell. 2012;149(4):780-94. doi: 10.1016/j.cell.2012.03.031. PubMed PMID: 22579283; PMCID: PMC3501264.
210. Mainou BA, Zamora PF, Ashbrook AW, Dorset DC, Kim KS, Dermody TS. Reovirus cell entry requires functional microtubules. mBio. 2013;4(4). Epub 2013/07/04. doi: 10.1128/mBio.00405-13. PubMed PMID: 23820395; PMCID: PMC3705452.
211. Ashbrook AW, Lentscher AJ, Zamora PF, Silva LA, May NA, Bauer JA, Morrison TE, Dermody TS. Antagonism of the Sodium-Potassium ATPase Impairs Chikungunya Virus Infection. mBio. 2016;7(3). Epub 2016/05/26. doi: 10.1128/mBio.00693-16. PubMed PMID: 27222471; PMCID: PMC4895112.
212. Mainou BA, Ashbrook AW, Smith EC, Dorset DC, Denison MR, Dermody TS. Serotonin Receptor Agonist 5-Nonyloxytryptamine Alters the Kinetics of Reovirus Cell Entry. J

Virol. 2015;89(17):8701-12. doi: 10.1128/JVI.00739-15. PubMed PMID: 26109733; PMCID: PMC4524060.
213. Das S, Tripathi N, Siddharth S, Nayak A, Nayak D, Sethy C, Bharatam PV, Kundu CN. Etoposide and doxorubicin enhance the sensitivity of triple negative breast cancers through modulation of TRAIL-DR5 axis. Apoptosis. 2017;22(10):1205-24. Epub 2017/07/14. doi: 10.1007/s10495-017-1400-4. PubMed PMID: 28702823.
214. Sherry B, Torres J, Blum MA. Reovirus induction of and sensitivity to beta interferon in cardiac myocyte cultures correlate with induction of myocarditis and are determined by viral core proteins. J Virol. 1998;72(2):1314-23. Epub 1998/01/28. PubMed PMID: 9445032; PMCID: PMC124610.
215. Stuart JD, Holm GH, Boehme KW. Differential Delivery of Genomic Double-Stranded RNA Causes Reovirus Strain-Specific Differences in Interferon Regulatory Factor 3 Activation. J Virol. 2018;92(9). Epub 2018/02/14. doi: 10.1128/JVI.01947-17. PubMed PMID: 29437975; PMCID: PMC5899194.
216. Dunphy G, Flannery SM, Almine JF, Connolly DJ, Paulus C, Jonsson KL, Jakobsen MR, Nevels MM, Bowie AG, Unterholzner L. Non-canonical Activation of the DNA Sensing Adaptor STING by ATM and IFI16 Mediates NF-kappaB Signaling after Nuclear DNA Damage. Mol Cell. 2018;71(5):745-60 e5. Epub 2018/09/08. doi: 10.1016/j.molcel.2018.07.034. PubMed PMID: 30193098; PMCID: PMC6127031.
217. Alvarez JV, Febbo PG, Ramaswamy S, Loda M, Richardson A, Frank DA. Identification of a genetic signature of activated signal transducer and activator of transcription 3 in human tumors. Cancer research. 2005;65(12):5054-62. Epub 2005/06/17. doi: 10.1158/0008-5472.CAN-04-4281. PubMed PMID: 15958548.
218. Banerjee K, Resat H. Constitutive activation of STAT3 in breast cancer cells: A review. International journal of cancer Journal international du cancer. 2016;138(11):2570-8. Epub 2015/11/13. doi: 10.1002/ijc.29923. PubMed PMID: 26559373; PMCID: PMC4801660.
219. Cui H, Lin Y, Yue L, Zhao X, Liu J. Differential expression of the alpha2,3-sialic acid residues in breast cancer is associated with metastatic potential. Oncol Rep. 2011;25(5):1365-71. Epub 2011/02/24. doi: 10.3892/or.2011.1192. PubMed PMID: 21344161.
220. McSherry EA, McGee SF, Jirstrom K, Doyle EM, Brennan DJ, Landberg G, Dervan PA, Hopkins AM, Gallagher WM. JAM-A expression positively correlates with poor prognosis in breast cancer patients. International journal of cancer Journal international du cancer. 2009;125(6):1343-51. Epub 2009/06/18. doi: 10.1002/ijc.24498. PubMed PMID: 19533747.
221. Naik MU, Naik TU, Suckow AT, Duncan MK, Naik UP. Attenuation of junctional adhesion molecule-A is a contributing factor for breast cancer cell invasion. Cancer research. 2008;68(7):2194-203. Epub 2008/04/03. doi: 10.1158/0008-5472.CAN-07-3057. PubMed PMID: 18381425.
222. Noble S, Nibert ML. Characterization of an ATPase activity in reovirus cores and its genetic association with core-shell protein lambda1. J Virol. 1997;71(3):2182-91. Epub 1997/03/01. PubMed PMID: 9032352; PMCID: PMC191325.
223. Coombs KM, Mak SC, Petrycky-Cox LD. Studies of the major reovirus core protein sigma 2: reversion of the assembly-defective mutant tsC447 is an intragenic process and involves back mutation of Asp-383 to Asn. J Virol. 1994;68(1):177-86. Epub 1994/01/01. PubMed PMID: 8254727; PMCID: PMC236276.
224. Becker MM, Goral MI, Hazelton PR, Baer GS, Rodgers SE, Brown EG, Coombs KM, Dermody TS. Reovirus sigmaNS protein is required for nucleation of viral assembly complexes

and formation of viral inclusions. J Virol. 2001;75(3):1459-75. Epub 2001/01/11. doi: 10.1128/JVI.75.3.1459-1475.2001. PubMed PMID: 11152519; PMCID: PMC114052.
225. Tyler KL, Squier MK, Brown AL, Pike B, Willis D, Oberhaus SM, Dermody TS, Cohen JJ. Linkage between reovirus-induced apoptosis and inhibition of cellular DNA synthesis: role of the S1 and M2 genes. J Virol. 1996;70(11):7984-91. Epub 1996/11/01. PubMed PMID: 8892922; PMCID: PMC190871.
226. Rodgers SE, Barton ES, Oberhaus SM, Pike B, Gibson CA, Tyler KL, Dermody TS. Reovirus-induced apoptosis of MDCK cells is not linked to viral yield and is blocked by Bcl-2. J Virol. 1997;71(3):2540-6. Epub 1997/03/01. PubMed PMID: 9032397; PMCID: PMC191370.
227. Thete D, Snyder AJ, Mainou BA, Danthi P. Reovirus mu1 Protein Affects Infectivity by Altering Virus-Receptor Interactions. J Virol. 2016;90(23):10951-62. doi: 10.1128/JVI.01843-16. PubMed PMID: 27681135; PMCID: PMC5110151.
228. Boehme KW, Hammer K, Tollefson WC, Konopka-Anstadt JL, Kobayashi T, Dermody TS. Nonstructural protein sigma1s mediates reovirus-induced cell cycle arrest and apoptosis. J Virol. 2013;87(23):12967-79. doi: 10.1128/JVI.02080-13. PubMed PMID: 24067959; PMCID: PMC3838159.
229. Phillips MB, Stuart JD, Simon EJ, Boehme KW. Nonstructural Protein sigma1s Is Required for Optimal Reovirus Protein Expression. J Virol. 2018;92(7). Epub 2018/01/13. doi: 10.1128/JVI.02259-17. PubMed PMID: 29321319; PMCID: PMC5972882.
230. Arcamone F, Penco S, Vigevani A, Redaelli S, Franchi G, DiMarco A, Casazza AM, Dasdia T, Formelli F, Necco A, Soranzo C. Synthesis and antitumor properties of new glycosides of daunomycinone and adriamycinone. Journal of medicinal chemistry. 1975;18(7):703-7. Epub 1975/07/01. PubMed PMID: 168385.
231. Burris HA, 3rd, Hanauske AR, Johnson RK, Marshall MH, Kuhn JG, Hilsenbeck SG, Von Hoff DD. Activity of topotecan, a new topoisomerase I inhibitor, against human tumor colony-forming units in vitro. Journal of the National Cancer Institute. 1992;84(23):1816-20. Epub 1992/12/02. PubMed PMID: 1331485.
232. Hsiang YH, Hertzberg R, Hecht S, Liu LF. Camptothecin induces protein-linked DNA breaks via mammalian DNA topoisomerase I. J Biol Chem. 1985;260(27):14873-8. Epub 1985/11/25. PubMed PMID: 2997227.
233. Ross WE, Bradley MO. DNA double-stranded breaks in mammalian cells after exposure to intercalating agents. Biochim Biophys Acta. 1981;654(1):129-34. Epub 1981/06/26. PubMed PMID: 7272306.
234. Danthi P, Kobayashi T, Holm GH, Hansberger MW, Abel TW, Dermody TS. Reovirus apoptosis and virulence are regulated by host cell membrane penetration efficiency. J Virol. 2008;82(1):161-72. Epub 2007/10/26. doi: 10.1128/JVI.01739-07. PubMed PMID: 17959662; PMCID: PMC2224352.
235. Danthi P, Pruijssers AJ, Berger AK, Holm GH, Zinkel SS, Dermody TS. Bid regulates the pathogenesis of neurotropic reovirus. PLoS pathogens. 2010;6:e1000980. doi: 10.1371/journal.ppat.1000980. PubMed PMID: 20617182; PMCID: PMC2895667.
236. Zhang X, Wu H, Liu C, Tian J, Qu L. PI3K/Akt/p53 pathway inhibits reovirus infection. Infect Genet Evol. 2015;34:415-22. Epub 2015/06/13. doi: 10.1016/j.meegid.2015.06.008. PubMed PMID: 26066464.
237. Yang L, Wei J, He S. Integrative genomic analyses on interferon-lambdas and their roles in cancer prediction. Int J Mol Med. 2010;25(2):299-304. Epub 2010/01/01. PubMed PMID: 20043142.

238. Onoguchi K, Yoneyama M, Takemura A, Akira S, Taniguchi T, Namiki H, Fujita T. Viral infections activate types I and III interferon genes through a common mechanism. J Biol Chem. 2007;282(10):7576-81. Epub 2007/01/06. doi: 10.1074/jbc.M608618200. PubMed PMID: 17204473.
239. Schafer SL, Lin R, Moore PA, Hiscott J, Pitha PM. Regulation of type I interferon gene expression by interferon regulatory factor-3. J Biol Chem. 1998;273(5):2714-20. Epub 1998/02/28. PubMed PMID: 9446577.
240. Stanifer ML, Kischnick C, Rippert A, Albrecht D, Boulant S. Reovirus inhibits interferon production by sequestering IRF3 into viral factories. Sci Rep. 2017;7(1):10873. Epub 2017/09/09. doi: 10.1038/s41598-017-11469-6. PubMed PMID: 28883463; PMCID: PMC5589761.
241. Pervolaraki K, Rastgou Talemi S, Albrecht D, Bormann F, Bamford C, Mendoza JL, Garcia KC, McLauchlan J, Hofer T, Stanifer ML, Boulant S. Differential induction of interferon stimulated genes between type I and type III interferons is independent of interferon receptor abundance. PLoS pathogens. 2018;14(11):e1007420. Epub 2018/11/30. doi: 10.1371/journal.ppat.1007420. PubMed PMID: 30485383; PMCID: PMC6287881.
242. Baldridge MT, Lee S, Brown JJ, McAllister N, Urbanek K, Dermody TS, Nice TJ, Virgin HW. Expression of Ifnlr1 on Intestinal Epithelial Cells Is Critical to the Antiviral Effects of Interferon Lambda against Norovirus and Reovirus. J Virol. 2017;91(7). doi: 10.1128/JVI.02079-16. PubMed PMID: 28077655; PMCID: PMC5355594.
243. Bowen JR, Quicke KM, Maddur MS, O'Neal JT, McDonald CE, Fedorova NB, Puri V, Shabman RS, Pulendran B, Suthar MS. Zika Virus Antagonizes Type I Interferon Responses during Infection of Human Dendritic Cells. PLoS pathogens. 2017;13(2):e1006164. Epub 2017/02/06. doi: 10.1371/journal.ppat.1006164. PubMed PMID: 28152048; PMCID: PMC5289613.
244. Kang JX, Liu J, Wang J, He C, Li FP. The extract of huanglian, a medicinal herb, induces cell growth arrest and apoptosis by upregulation of interferon-beta and TNF-alpha in human breast cancer cells. Carcinogenesis. 2005;26(11):1934-9. Epub 2005/06/17. doi: 10.1093/carcin/bgi154. PubMed PMID: 15958519.
245. Lindner DJ, Kolla V, Kalvakolanu DV, Borden EC. Tamoxifen enhances interferon-regulated gene expression in breast cancer cells. Mol Cell Biochem. 1997;167(1-2):169-77. Epub 1997/02/01. PubMed PMID: 9059994.
246. Yoon N, Park MS, Shigemoto T, Peltier G, Lee RH. Activated human mesenchymal stem/stromal cells suppress metastatic features of MDA-MB-231 cells by secreting IFN-beta. Cell Death Dis. 2016;7:e2191. Epub 2016/04/15. doi: 10.1038/cddis.2016.90. PubMed PMID: 27077807; PMCID: PMC4855669.
247. Kobayashi T, Antar AA, Boehme KW, Danthi P, Eby EA, Guglielmi KM, Holm GH, Johnson EM, Maginnis MS, Naik S, Skelton WB, Wetzel JD, Wilson GJ, Chappell JD, Dermody TS. A plasmid-based reverse genetics system for animal double-stranded RNA viruses. Cell host & microbe. 2007;1(2):147-57. doi: 10.1016/j.chom.2007.03.003. PubMed PMID: 18005692; PMCID: PMC2034303.
248. Cashdollar LW, Chmelo R, Esparza J, Hudson GR, Joklik WK. Molecular cloning of the complete genome of reovirus serotype 3. Virology. 1984;133(1):191-6. Epub 1984/02/01. PubMed PMID: 6546631.

249. Furlong DB, Nibert ML, Fields BN. Sigma 1 protein of mammalian reoviruses extends from the surfaces of viral particles. J Virol. 1988;62(1):246-56. Epub 1988/01/01. PubMed PMID: 3275434; PMCID: PMC250525.
250. Smith RE, Zweerink HJ, Joklik WK. Polypeptide components of virions, top component and cores of reovirus type 3. Virology. 1969;39(4):791-810. Epub 1969/12/01. doi: 0042-6822(69)90017-8 [pii]. PubMed PMID: 4311639.
251. Virgin HW, Dermody TS, Tyler KL. Cellular and humoral immunity to reovirus infection. Curr Top Microbiol Immunol. 1998;233(Pt 2):147-61. Epub 1998/05/26. PubMed PMID: 9599936.
252. Virgin HWt, Bassel-Duby R, Fields BN, Tyler KL. Antibody protects against lethal infection with the neurally spreading reovirus type 3 (Dearing). J Virol. 1988;62(12):4594-604. Epub 1988/12/01. PubMed PMID: 2460637; PMCID: PMC253571.
253. Berger AK, Yi H, Kearns DB, Mainou BA. Bacteria and bacterial envelope components enhance mammalian reovirus thermostability. PLoS pathogens. 2017;13(12):e1006768. Epub 2017/12/07. doi: 10.1371/journal.ppat.1006768. PubMed PMID: 29211815.
254. American Cancer Society. Breast Cancer Facts & Figures 2019-2020. 2019.
255. NAACCR.org. Available from: https://naaccr.org.
256. Haffty BG, Yang Q, Reiss M, Kearney T, Higgins SA, Weidhaas J, Harris L, Hait W, Toppmeyer D. Locoregional relapse and distant metastasis in conservatively managed triple negative early-stage breast cancer. J Clin Oncol. 2006;24(36):5652-7. doi: 10.1200/JCO.2006.06.5664. PubMed PMID: 17116942.
257. Dent R, Trudeau M, Pritchard KI, Hanna WM, Kahn HK, Sawka CA, Lickley LA, Rawlinson E, Sun P, Narod SA. Triple-negative breast cancer: clinical features and patterns of recurrence. Clin Cancer Res. 2007;13(15 Pt 1):4429-34. doi: 10.1158/1078-0432.CCR-06-3045. PubMed PMID: 17671126.
258. Dmitriev I, Krasnykh V, Miller CR, Wang M, Kashentseva E, Mikheeva G, Belousova N, Curiel DT. An adenovirus vector with genetically modified fibers demonstrates expanded tropism via utilization of a coxsackievirus and adenovirus receptor-independent cell entry mechanism. J Virol. 1998;72(12):9706-13. Epub 1998/11/13. PubMed PMID: 9811704; PMCID: PMC110480.
259. Morizono K, Xie Y, Ringpis GE, Johnson M, Nassanian H, Lee B, Wu L, Chen IS. Lentiviral vector retargeting to P-glycoprotein on metastatic melanoma through intravenous injection. Nat Med. 2005;11(3):346-52. Epub 2005/02/16. doi: 10.1038/nm1192. PubMed PMID: 15711560.
260. Doronin K, Toth K, Kuppuswamy M, Ward P, Tollefson AE, Wold WS. Tumor-specific, replication-competent adenovirus vectors overexpressing the adenovirus death protein. J Virol. 2000;74(13):6147-55. Epub 2000/06/14. doi: 10.1128/jvi.74.13.6147-6155.2000. PubMed PMID: 10846098; PMCID: PMC112113.
261. Hirvinen M, Rajecki M, Kapanen M, Parviainen S, Rouvinen-Lagerstrom N, Diaconu I, Nokisalmi P, Tenhunen M, Hemminki A, Cerullo V. Immunological effects of a tumor necrosis factor alpha-armed oncolytic adenovirus. Hum Gene Ther. 2015;26(3):134-44. Epub 2015/01/06. doi: 10.1089/hum.2014.069. PubMed PMID: 25557131.
262. Li JL, Liu HL, Zhang XR, Xu JP, Hu WK, Liang M, Chen SY, Hu F, Chu DT. A phase I trial of intratumoral administration of recombinant oncolytic adenovirus overexpressing HSP70 in advanced solid tumor patients. Gene Ther. 2009;16(3):376-82. Epub 2008/12/19. doi: 10.1038/gt.2008.179. PubMed PMID: 19092859.

263. Burke JM, Lamm DL, Meng MV, Nemunaitis JJ, Stephenson JJ, Arseneau JC, Aimi J, Lerner S, Yeung AW, Kazarian T, Maslyar DJ, McKiernan JM. A first in human phase 1 study of CG0070, a GM-CSF expressing oncolytic adenovirus, for the treatment of nonmuscle invasive bladder cancer. J Urol. 2012;188(6):2391-7. Epub 2012/10/24. doi: 10.1016/j.juro.2012.07.097. PubMed PMID: 23088985.
264. Selb B, Weber B. A study of human reovirus IgG and IgA antibodies by ELISA and western blot. Journal of virological methods. 1994;47(1-2):15-25. PubMed PMID: 8051222.
265. Norman KL, Hirasawa K, Yang AD, Shields MA, Lee PW. Reovirus oncolysis: the Ras/RalGEF/p38 pathway dictates host cell permissiveness to reovirus infection. Proc Natl Acad Sci U S A. 2004;101(30):11099-104. Epub 2004/07/21. doi: 10.1073/pnas.0404310101. PubMed PMID: 15263068; PMCID: PMC503746.
266. Strong JE, Coffey MC, Tang D, Sabinin P, Lee PW. The molecular basis of viral oncolysis: usurpation of the Ras signaling pathway by reovirus. EMBO J. 1998;17(12):3351-62. doi: 10.1093/emboj/17.12.3351. PubMed PMID: 9628872; PMCID: PMC1170673.
267. Villalona-Calero MA, Lam E, Otterson GA, Zhao W, Timmons M, Subramaniam D, Hade EM, Gill GM, Coffey M, Selvaggi G, Bertino E, Chao B, Knopp MV. Oncolytic reovirus in combination with chemotherapy in metastatic or recurrent non-small cell lung cancer patients with KRAS-activated tumors. Cancer. 2016;122(6):875-83. Epub 2015/12/29. doi: 10.1002/cncr.29856. PubMed PMID: 26709987; PMCID: PMC5068485.
268. Rodriguez Stewart RM, Berry JTL, Berger AK, Yoon SB, Hirsch AL, Guberman JA, Patel NB, Tharp GK, Bosinger SE, Mainou BA. Enhanced Killing of Triple-Negative Breast Cancer Cells by Reassortant Reovirus and Topoisomerase Inhibitors. J Virol. 2019;93(23). Epub 2019/09/13. doi: 10.1128/JVI.01411-19. PubMed PMID: 31511390; PMCID: PMC6854488.
269. Birrer MJ, Moore KN, Betella I, Bates RC. Antibody-Drug Conjugate-Based Therapeutics: State of the Science. Journal of the National Cancer Institute. 2019;111(6):538-49. Epub 2019/03/13. doi: 10.1093/jnci/djz035. PubMed PMID: 30859213.
270. Fecek RJ, Busch R, Lin H, Pal K, Cunningham CA, Cuff CF. Production of Alexa Fluor 488-labeled reovirus and characterization of target cell binding, competence, and immunogenicity of labeled virions. Journal of immunological methods. 2006;314(1-2):30-7. Epub 2006/07/11. doi: 10.1016/j.jim.2006.05.008. PubMed PMID: 16822520.
271. Huang S, Wang H, Carroll CA, Hayes SJ, Weintraub ST, Serwer P. Analysis of proteins stained by Alexa dyes. Electrophoresis. 2004;25(6):779-84. Epub 2004/03/09. doi: 10.1002/elps.200305723. PubMed PMID: 15004835.
272. Cancer Cell Line Encyclopedia. Available from: https://portals.broadinstitute.org/ccle.
273. Pulaski BA, Ostrand-Rosenberg S. Reduction of established spontaneous mammary carcinoma metastases following immunotherapy with major histocompatibility complex class II and B7.1 cell-based tumor vaccines. Cancer research. 1998;58(7):1486-93. Epub 1998/04/16. PubMed PMID: 9537252.
274. Pulaski BA, Terman DS, Khan S, Muller E, Ostrand-Rosenberg S. Cooperativity of Staphylococcal aureus enterotoxin B superantigen, major histocompatibility complex class II, and CD80 for immunotherapy of advanced spontaneous metastases in a clinically relevant postoperative mouse breast cancer model. Cancer research. 2000;60(10):2710-5. Epub 2000/05/29. PubMed PMID: 10825145.
275. Pulaski BA, Ostrand-Rosenberg S. Mouse 4T1 breast tumor model. Curr Protoc Immunol. 2001;Chapter 20:Unit 20 2. Epub 2008/04/25. doi: 10.1002/0471142735.im2002s39. PubMed PMID: 18432775.

276. Kaur P, Nagaraja GM, Zheng H, Gizachew D, Galukande M, Krishnan S, Asea A. A mouse model for triple-negative breast cancer tumor-initiating cells (TNBC-TICs) exhibits similar aggressive phenotype to the human disease. BMC cancer. 2012;12:120. Epub 2012/03/29. doi: 10.1186/1471-2407-12-120. PubMed PMID: 22452810; PMCID: PMC3340297.
277. Franken NA, Rodermond HM, Stap J, Haveman J, van Bree C. Clonogenic assay of cells in vitro. Nat Protoc. 2006;1(5):2315-9. Epub 2007/04/05. doi: 10.1038/nprot.2006.339. PubMed PMID: 17406473.
278. Pan D, Marcato P, Ahn DG, Gujar S, Pan LZ, Shmulevitz M, Lee PW. Activation of p53 by chemotherapeutic agents enhances reovirus oncolysis. PloS one. 2013;8(1):e54006. Epub 2013/01/24. doi: 10.1371/journal.pone.0054006. PubMed PMID: 23342061; PMCID: PMC3546971.
279. Roulstone V, Twigger K, Zaidi S, Pencavel T, Kyula JN, White C, McLaughlin M, Seth R, Karapanagiotou EM, Mansfield D, Coffey M, Nuovo G, Vile RG, Pandha HS, Melcher AA, Harrington KJ. Synergistic cytotoxicity of oncolytic reovirus in combination with cisplatin-paclitaxel doublet chemotherapy. Gene Ther. 2013;20(5):521-8. Epub 2012/08/17. doi: 10.1038/gt.2012.68. PubMed PMID: 22895509; PMCID: PMC4821071.
280. Heinemann L, Simpson GR, Boxall A, Kottke T, Relph KL, Vile R, Melcher A, Prestwich R, Harrington KJ, Morgan R, Pandha HS. Synergistic effects of oncolytic reovirus and docetaxel chemotherapy in prostate cancer. BMC cancer. 2011;11:221. Epub 2011/06/08. doi: 10.1186/1471-2407-11-221. PubMed PMID: 21645351; PMCID: PMC3129324.
281. Sei S, Mussio JK, Yang QE, Nagashima K, Parchment RE, Coffey MC, Shoemaker RH, Tomaszewski JE. Synergistic antitumor activity of oncolytic reovirus and chemotherapeutic agents in non-small cell lung cancer cells. Mol Cancer. 2009;8:47. Epub 2009/07/15. doi: 10.1186/1476-4598-8-47. PubMed PMID: 19594950; PMCID: PMC2723073.
282. Samson A, Scott KJ, Taggart D, West EJ, Wilson E, Nuovo GJ, Thomson S, Corns R, Mathew RK, Fuller MJ, Kottke TJ, Thompson JM, Ilett EJ, Cockle JV, van Hille P, Sivakumar G, Polson ES, Turnbull SJ, Appleton ES, Migneco G, Rose AS, Coffey MC, Beirne DA, Collinson FJ, Ralph C, Alan Anthoney D, Twelves CJ, Furness AJ, Quezada SA, Wurdak H, Errington-Mais F, Pandha H, Harrington KJ, Selby PJ, Vile RG, Griffin SD, Stead LF, Short SC, Melcher AA. Intravenous delivery of oncolytic reovirus to brain tumor patients immunologically primes for subsequent checkpoint blockade. Sci Transl Med. 2018;10(422). Epub 2018/01/05. doi: 10.1126/scitranslmed.aam7577. PubMed PMID: 29298869; PMCID: PMC6276984.
283. Liemann S, Chandran K, Baker TS, Nibert ML, Harrison SC. Structure of the reovirus membrane-penetration protein, Mu1, in a complex with is protector protein, Sigma3. Cell. 2002;108(2):283-95. Epub 2002/02/08. doi: 10.1016/s0092-8674(02)00612-8. PubMed PMID: 11832217; PMCID: PMC4152834.
284. Dietrich MH, Ogden KM, Katen SP, Reiss K, Sutherland DM, Carnahan RH, Goff M, Cooper T, Dermody TS, Stehle T. Structural Insights into Reovirus sigma1 Interactions with Two Neutralizing Antibodies. J Virol. 2017;91(4). doi: 10.1128/JVI.01621-16. PubMed PMID: 27928010; PMCID: PMC5286903.
285. Peterson ST, Kennedy EA, Brigleb PH, Taylor GM, Urbanek K, Bricker TL, Lee S, Shin H, Dermody TS, Boon ACM, Baldridge MT. Disruption of type III interferon genes Ifnl2 and Ifnl3 recapitulates loss of the type III IFN receptor in the mucosal antiviral response. J Virol. 2019. Epub 2019/08/30. doi: 10.1128/JVI.01073-19. PubMed PMID: 31462571.

286. Mordstein M, Neugebauer E, Ditt V, Jessen B, Rieger T, Falcone V, Sorgeloos F, Ehl S, Mayer D, Kochs G, Schwemmle M, Gunther S, Drosten C, Michiels T, Staeheli P. Lambda interferon renders epithelial cells of the respiratory and gastrointestinal tracts resistant to viral infections. J Virol. 2010;84(11):5670-7. Epub 2010/03/26. doi: 10.1128/JVI.00272-10. PubMed PMID: 20335250; PMCID: PMC2876583.
287. Bayer A, Lennemann NJ, Ouyang Y, Bramley JC, Morosky S, Marques ET, Jr., Cherry S, Sadovsky Y, Coyne CB. Type III Interferons Produced by Human Placental Trophoblasts Confer Protection against Zika Virus Infection. Cell host & microbe. 2016;19(5):705-12. Epub 2016/04/14. doi: 10.1016/j.chom.2016.03.008. PubMed PMID: 27066743; PMCID: PMC4866896.
288. Palma-Ocampo HK, Flores-Alonso JC, Vallejo-Ruiz V, Reyes-Leyva J, Flores-Mendoza L, Herrera-Camacho I, Rosas-Murrieta NH, Santos-Lopez G. Interferon lambda inhibits dengue virus replication in epithelial cells. Virol J. 2015;12:150. Epub 2015/09/29. doi: 10.1186/s12985-015-0383-4. PubMed PMID: 26411318; PMCID: PMC4584467.
289. Odendall C, Dixit E, Stavru F, Bierne H, Franz KM, Durbin AF, Boulant S, Gehrke L, Cossart P, Kagan JC. Diverse intracellular pathogens activate type III interferon expression from peroxisomes. Nat Immunol. 2014;15(8):717-26. Epub 2014/06/24. doi: 10.1038/ni.2915. PubMed PMID: 24952503; PMCID: PMC4106986.
290. Sommereyns C, Paul S, Staeheli P, Michiels T. IFN-lambda (IFN-lambda) is expressed in a tissue-dependent fashion and primarily acts on epithelial cells in vivo. PLoS pathogens. 2008;4(3):e1000017. Epub 2008/03/29. doi: 10.1371/journal.ppat.1000017. PubMed PMID: 18369468; PMCID: PMC2265414.
291. Burkart C, Arimoto K, Tang T, Cong X, Xiao N, Liu YC, Kotenko SV, Ellies LG, Zhang DE. Usp18 deficient mammary epithelial cells create an antitumour environment driven by hypersensitivity to IFN-lambda and elevated secretion of Cxcl10. EMBO Mol Med. 2013;5(7):1035-50. Epub 2013/05/18. doi: 10.1002/emmm.201201864. PubMed PMID: 23681607; PMCID: PMC3721472.
292. Qing Y, Stark GR. Alternative activation of STAT1 and STAT3 in response to interferon-gamma. J Biol Chem. 2004;279(40):41679-85. Epub 2004/07/31. doi: 10.1074/jbc.M406413200. PubMed PMID: 15284232.
293. Hussner J, Ameling S, Hammer E, Herzog S, Steil L, Schwebe M, Niessen J, Schroeder HW, Kroemer HK, Ritter CA, Volker U, Bien S. Regulation of interferon-inducible proteins by doxorubicin via interferon gamma-Janus tyrosine kinase-signal transducer and activator of transcription signaling in tumor cells. Mol Pharmacol. 2012;81(5):679-88. Epub 2012/02/11. doi: 10.1124/mol.111.075994. PubMed PMID: 22323498.
294. Thomas M, Finnegan CE, Rogers KM, Purcell JW, Trimble A, Johnston PG, Boland MP. STAT1: a modulator of chemotherapy-induced apoptosis. Cancer research. 2004;64(22):8357-64. Epub 2004/11/19. doi: 10.1158/0008-5472.CAN-04-1864. PubMed PMID: 15548705.
295. Fernandes JP, Cristi F, Eaton HE, Chen P, Haeflinger S, Bernard I, Hitt MM, Shmulevitz M. Breast Tumor-Associated Metalloproteases Restrict Reovirus Oncolysis by Cleaving the sigma1 Cell Attachment Protein and Can Be Overcome by Mutation of sigma1. J Virol. 2019;93(22). Epub 2019/08/30. doi: 10.1128/JVI.01380-19. PubMed PMID: 31462562; PMCID: PMC6819916.
296. Liang Y, Li S, Wang X, He B, He B, Dai W, Zhang H, Wang X, Wang Y, Zhou D, Zhang Q. A Nanosystem of Amphiphilic Oligopeptide-Drug Conjugate Actualizing Both alphavbeta3 Targeting and Reduction-Triggered Release for Maytansinoid. Theranostics.

2017;7(13):3306-18. Epub 2017/09/14. doi: 10.7150/thno.20242. PubMed PMID: 28900511; PMCID: PMC5595133.
297. Hermanson GT. The Reactions of Bioconjugation. Bioconjugate Techniques. 3rd ed: Elsevier; 2013.
298. Pillay CS, Elliott E, Dennison C. Endolysosomal proteolysis and its regulation. Biochem J. 2002;363(Pt 3):417-29. Epub 2002/04/20. doi: 10.1042/0264-6021:3630417. PubMed PMID: 11964142; PMCID: PMC1222494.
299. Authier F, Posner BI, Bergeron JJ. Endosomal proteolysis of internalized proteins. FEBS letters. 1996;389(1):55-60. Epub 1996/06/24. doi: 10.1016/0014-5793(96)00368-7. PubMed PMID: 8682206.
300. Davis RT, Blake K, Ma D, Gabra MBI, Hernandez GA, Phung AT, Yang Y, Maurer D, Lefebvre A, Alshetaiwi H, Xiao Z, Liu J, Locasale JW, Digman MA, Mjolsness E, Kong M, Werb Z, Lawson DA. Transcriptional diversity and bioenergetic shift in human breast cancer metastasis revealed by single-cell RNA sequencing. Nat Cell Biol. 2020;22(3):310-20. Epub 2020/03/08. doi: 10.1038/s41556-020-0477-0. PubMed PMID: 32144411.
301. Yadav N, Kumar S, Marlowe T, Chaudhary AK, Kumar R, Wang J, O'Malley J, Boland PM, Jayanthi S, Kumar TK, Yadava N, Chandra D. Oxidative phosphorylation-dependent regulation of cancer cell apoptosis in response to anticancer agents. Cell Death Dis. 2015;6:e1969. Epub 2015/11/06. doi: 10.1038/cddis.2015.305. PubMed PMID: 26539916; PMCID: PMC4670921.
302. Alam SR, Wallrabe H, Svindrych Z, Chaudhary AK, Christopher KG, Chandra D, Periasamy A. Investigation of Mitochondrial Metabolic Response to Doxorubicin in Prostate Cancer Cells: An NADH, FAD and Tryptophan FLIM Assay. Sci Rep. 2017;7(1):10451. Epub 2017/09/07. doi: 10.1038/s41598-017-10856-3. PubMed PMID: 28874842; PMCID: PMC5585313.
303. Olive PL, Banath JP. The comet assay: a method to measure DNA damage in individual cells. Nat Protoc. 2006;1(1):23-9. Epub 2007/04/05. doi: 10.1038/nprot.2006.5. PubMed PMID: 17406208.
304. Bankhead P, Loughrey MB, Fernandez JA, Dombrowski Y, McArt DG, Dunne PD, McQuaid S, Gray RT, Murray LJ, Coleman HG, James JA, Salto-Tellez M, Hamilton PW. QuPath: Open source software for digital pathology image analysis. Sci Rep. 2017;7(1):16878. Epub 2017/12/06. doi: 10.1038/s41598-017-17204-5. PubMed PMID: 29203879; PMCID: PMC5715110.
305. Weiner HL, Fields BN. Neutralization of reovirus: the gene responsible for the neutralization antigen. J Exp Med. 1977;146(5):1305-10. PubMed PMID: 925604; PMCID: PMC2180977.
306. Thirukkumaran CM, Nodwell MJ, Hirasawa K, Shi ZQ, Diaz R, Luider J, Johnston RN, Forsyth PA, Magliocco AM, Lee P, Nishikawa S, Donnelly B, Coffey M, Trpkov K, Fonseca K, Spurrell J, Morris DG. Oncolytic viral therapy for prostate cancer: efficacy of reovirus as a biological therapeutic. Cancer research. 2010;70(6):2435-44. Epub 2010/03/11. doi: 10.1158/0008-5472.CAN-09-2408. PubMed PMID: 20215509.
307. White CL, Twigger KR, Vidal L, De Bono JS, Coffey M, Heinemann L, Morgan R, Merrick A, Errington F, Vile RG, Melcher AA, Pandha HS, Harrington KJ. Characterization of the adaptive and innate immune response to intravenous oncolytic reovirus (Dearing type 3) during a phase I clinical trial. Gene Ther. 2008;15(12):911-20. Epub 2008/03/08. doi: 10.1038/gt.2008.21. PubMed PMID: 18323793.

308. Mohamed A, Johnston RN, Shmulevitz M. Potential for Improving Potency and Specificity of Reovirus Oncolysis with Next-Generation Reovirus Variants. Viruses. 2015;7(12):6251-78. Epub 2015/12/04. doi: 10.3390/v7122936. PubMed PMID: 26633466; PMCID: PMC4690860.
309. Brew CT, Aronchik I, Hsu JC, Sheen JH, Dickson RB, Bjeldanes LF, Firestone GL. Indole-3-carbinol activates the ATM signaling pathway independent of DNA damage to stabilize p53 and induce G1 arrest of human mammary epithelial cells. International journal of cancer Journal international du cancer. 2006;118(4):857-68. Epub 2005/09/10. doi: 10.1002/ijc.21445. PubMed PMID: 16152627.
310. Li J, Stern DF. DNA damage regulates Chk2 association with chromatin. J Biol Chem. 2005;280(45):37948-56. Epub 2005/09/10. doi: 10.1074/jbc.M509299200. PubMed PMID: 16150728.
311. Yoshida K, Miki Y. Role of BRCA1 and BRCA2 as regulators of DNA repair, transcription, and cell cycle in response to DNA damage. Cancer Sci. 2004;95(11):866-71. Epub 2004/11/18. doi: 10.1111/j.1349-7006.2004.tb02195.x. PubMed PMID: 15546503.
312. Maehama T, Dixon JE. The tumor suppressor, PTEN/MMAC1, dephosphorylates the lipid second messenger, phosphatidylinositol 3,4,5-trisphosphate. J Biol Chem. 1998;273(22):13375-8. Epub 1998/06/05. doi: 10.1074/jbc.273.22.13375. PubMed PMID: 9593664.
313. Minami A, Murai, T., Nakanishi, A., Kitagishi, Y., Ichimura, M., Matsuda, S. Cell Cycle Regulation via the p53, PTEN, and BRCA1 Tumor Suppressors. In: Bulgin D, editor. New Aspects in Molecular and Cellular Mechanisms of Human Carcinogenesis2016.
314. Owen DJ, Collins BM, Evans PR. Adaptors for clathrin coats: structure and function. Annu Rev Cell Dev Biol. 2004;20:153-91. Epub 2004/10/12. doi: 10.1146/annurev.cellbio.20.010403.104543. PubMed PMID: 15473838.
315. Cocucci E, Aguet F, Boulant S, Kirchhausen T. The first five seconds in the life of a clathrin-coated pit. Cell. 2012;150(3):495-507. Epub 2012/08/07. doi: 10.1016/j.cell.2012.05.047. PubMed PMID: 22863004; PMCID: PMC3413093.
316. Traub LM, Bonifacino JS. Cargo recognition in clathrin-mediated endocytosis. Cold Spring Harb Perspect Biol. 2013;5(11):a016790. Epub 2013/11/05. doi: 10.1101/cshperspect.a016790. PubMed PMID: 24186068; PMCID: PMC3809577.
317. Schmid SL, Frolov VA. Dynamin: functional design of a membrane fission catalyst. Annu Rev Cell Dev Biol. 2011;27:79-105. Epub 2011/05/24. doi: 10.1146/annurev-cellbio-100109-104016. PubMed PMID: 21599493.
318. Ferguson SM, De Camilli P. Dynamin, a membrane-remodelling GTPase. Nature reviews Molecular cell biology. 2012;13(2):75-88. Epub 2012/01/12. doi: 10.1038/nrm3266. PubMed PMID: 22233676; PMCID: PMC3519936.
319. Morlot S, Roux A. Mechanics of dynamin-mediated membrane fission. Annu Rev Biophys. 2013;42:629-49. Epub 2013/04/02. doi: 10.1146/annurev-biophys-050511-102247. PubMed PMID: 23541160; PMCID: PMC4289195.
320. Schulz WL, Haj AK, Schiff LA. Reovirus uses multiple endocytic pathways for cell entry. J Virol. 2012;86(23):12665-75. Epub 2012/09/14. doi: 10.1128/JVI.01861-12. PubMed PMID: 22973022; PMCID: PMC3497677.
321. Collins BM, McCoy AJ, Kent HM, Evans PR, Owen DJ. Molecular architecture and functional model of the endocytic AP2 complex. Cell. 2002;109(4):523-35. Epub 2002/06/28. doi: 10.1016/s0092-8674(02)00735-3. PubMed PMID: 12086608.

322. Jackson LP, Kelly BT, McCoy AJ, Gaffry T, James LC, Collins BM, Honing S, Evans PR, Owen DJ. A large-scale conformational change couples membrane recruitment to cargo binding in the AP2 clathrin adaptor complex. Cell. 2010;141(7):1220-9. Epub 2010/07/07. doi: 10.1016/j.cell.2010.05.006. PubMed PMID: 20603002; PMCID: PMC3655264.
323. Kirchhausen T, Owen D, Harrison SC. Molecular structure, function, and dynamics of clathrin-mediated membrane traffic. Cold Spring Harb Perspect Biol. 2014;6(5):a016725. Epub 2014/05/03. doi: 10.1101/cshperspect.a016725. PubMed PMID: 24789820; PMCID: PMC3996469.
324. Gaidarov I, Keen JH. Phosphoinositide-AP-2 interactions required for targeting to plasma membrane clathrin-coated pits. J Cell Biol. 1999;146(4):755-64. Epub 1999/08/25. doi: 10.1083/jcb.146.4.755. PubMed PMID: 10459011; PMCID: PMC2156139.
325. Honing S, Ricotta D, Krauss M, Spate K, Spolaore B, Motley A, Robinson M, Robinson C, Haucke V, Owen DJ. Phosphatidylinositol-(4,5)-bisphosphate regulates sorting signal recognition by the clathrin-associated adaptor complex AP2. Mol Cell. 2005;18(5):519-31. Epub 2005/05/27. doi: 10.1016/j.molcel.2005.04.019. PubMed PMID: 15916959.
326. Kelly BT, Graham SC, Liska N, Dannhauser PN, Honing S, Ungewickell EJ, Owen DJ. Clathrin adaptors. AP2 controls clathrin polymerization with a membrane-activated switch. Science. 2014;345(6195):459-63. Epub 2014/07/26. doi: 10.1126/science.1254836. PubMed PMID: 25061211; PMCID: PMC4333214.
327. Barrett AJ, Kembhavi AA, Brown MA, Kirschke H, Knight CG, Tamai M, Hanada K. L-trans-Epoxysuccinyl-leucylamido(4-guanidino)butane (E-64) and its analogues as inhibitors of cysteine proteinases including cathepsins B, H and L. Biochem J. 1982;201(1):189-98. Epub 1982/01/01. doi: 10.1042/bj2010189. PubMed PMID: 7044372; PMCID: PMC1163625.
328. Sturzenbecker LJ, Nibert M, Furlong D, Fields BN. Intracellular digestion of reovirus particles requires a low pH and is an essential step in the viral infectious cycle. J Virol. 1987;61(8):2351-61. Epub 1987/08/01. PubMed PMID: 2885424; PMCID: PMC255643.
329. Pantelidou C, Sonzogni O, De Oliveria Taveira M, Mehta AK, Kothari A, Wang D, Visal T, Li MK, Pinto J, Castrillon JA, Cheney EM, Bouwman P, Jonkers J, Rottenberg S, Guerriero JL, Wulf GM, Shapiro GI. PARP Inhibitor Efficacy Depends on CD8(+) T-cell Recruitment via Intratumoral STING Pathway Activation in BRCA-Deficient Models of Triple-Negative Breast Cancer. Cancer Discov. 2019;9(6):722-37. Epub 2019/04/25. doi: 10.1158/2159-8290.CD-18-1218. PubMed PMID: 31015319; PMCID: PMC6548644.
330. Thanos D, Maniatis T. Virus induction of human IFN beta gene expression requires the assembly of an enhanceosome. Cell. 1995;83(7):1091-100. Epub 1995/12/29. doi: 10.1016/0092-8674(95)90136-1. PubMed PMID: 8548797.
331. Ueki IF, Min-Oo G, Kalinowski A, Ballon-Landa E, Lanier LL, Nadel JA, Koff JL. Respiratory virus-induced EGFR activation suppresses IRF1-dependent interferon lambda and antiviral defense in airway epithelium. J Exp Med. 2013;210(10):1929-36. Epub 2013/09/04. doi: 10.1084/jem.20121401. PubMed PMID: 23999497; PMCID: PMC3782052.
332. Siegel R, Eskdale J, Gallagher G. Regulation of IFN-lambda1 promoter activity (IFN-lambda1/IL-29) in human airway epithelial cells. J Immunol. 2011;187(11):5636-44. Epub 2011/11/08. doi: 10.4049/jimmunol.1003988. PubMed PMID: 22058416.
333. Thomson SJ, Goh FG, Banks H, Krausgruber T, Kotenko SV, Foxwell BM, Udalova IA. The role of transposable elements in the regulation of IFN-lambda1 gene expression. Proc Natl Acad Sci U S A. 2009;106(28):11564-9. Epub 2009/07/03. doi: 10.1073/pnas.0904477106. PubMed PMID: 19570999; PMCID: PMC2710658.

334. Hollestelle A, Elstrodt F, Nagel JH, Kallemeijn WW, Schutte M. Phosphatidylinositol-3-OH kinase or RAS pathway mutations in human breast cancer cell lines. Molecular cancer research : MCR. 2007;5(2):195-201. Epub 2007/02/23. doi: 10.1158/1541-7786.MCR-06-0263. PubMed PMID: 17314276.
335. Yao Z, Torres NM, Tao A, Gao Y, Luo L, Li Q, de Stanchina E, Abdel-Wahab O, Solit DB, Poulikakos PI, Rosen N. BRAF Mutants Evade ERK-Dependent Feedback by Different Mechanisms that Determine Their Sensitivity to Pharmacologic Inhibition. Cancer Cell. 2015;28(3):370-83. Epub 2015/09/08. doi: 10.1016/j.ccell.2015.08.001. PubMed PMID: 26343582; PMCID: PMC4894664.
336. Daud A, Bastian BC. Beyond BRAF in melanoma. Curr Top Microbiol Immunol. 2012;355:99-117. Epub 2011/08/10. doi: 10.1007/82_2011_163. PubMed PMID: 21826607.
337. Calvo F, Agudo-Ibanez L, Crespo P. The Ras-ERK pathway: understanding site-specific signaling provides hope of new anti-tumor therapies. Bioessays. 2010;32(5):412-21. Epub 2010/04/24. doi: 10.1002/bies.200900155. PubMed PMID: 20414899.
338. Malumbres M, Barbacid M. RAS oncogenes: the first 30 years. Nature reviews Cancer. 2003;3(6):459-65. Epub 2003/06/05. doi: 10.1038/nrc1097. PubMed PMID: 12778136.
339. Gou HF, Li X, Qiu M, Cheng K, Li LH, Dong H, Chen Y, Tang Y, Gao F, Zhao F, Men HT, Ge J, Su JM, Xu F, Bi F, Gao JJ, Liu JY. Epidermal growth factor receptor (EGFR)-RAS signaling pathway in penile squamous cell carcinoma. PloS one. 2013;8(4):e62175. Epub 2013/05/03. doi: 10.1371/journal.pone.0062175. PubMed PMID: 23637996; PMCID: PMC3634795.
340. Loetscher M, Gerber B, Loetscher P, Jones SA, Piali L, Clark-Lewis I, Baggiolini M, Moser B. Chemokine receptor specific for IP10 and mig: structure, function, and expression in activated T-lymphocytes. J Exp Med. 1996;184(3):963-9. Epub 1996/09/01. doi: 10.1084/jem.184.3.963. PubMed PMID: 9064356; PMCID: PMC2192763.
341. Loetscher M, Loetscher P, Brass N, Meese E, Moser B. Lymphocyte-specific chemokine receptor CXCR3: regulation, chemokine binding and gene localization. Eur J Immunol. 1998;28(11):3696-705. Epub 1998/12/08. doi: 10.1002/(SICI)1521-4141(199811)28:11<3696::AID-IMMU3696>3.0.CO;2-W. PubMed PMID: 9842912.
342. Groom JR, Luster AD. CXCR3 ligands: redundant, collaborative and antagonistic functions. Immunol Cell Biol. 2011;89(2):207-15. Epub 2011/01/12. doi: 10.1038/icb.2010.158. PubMed PMID: 21221121; PMCID: PMC3863330.
343. Lasfar A, de laTorre A, Abushahba W, Cohen-Solal KA, Castaneda I, Yuan Y, Reuhl K, Zloza A, Raveche E, Laskin DL, Kotenko SV. Concerted action of IFN-alpha and IFN-lambda induces local NK cell immunity and halts cancer growth. Oncotarget. 2016;7(31):49259-67. Epub 2016/07/01. doi: 10.18632/oncotarget.10272. PubMed PMID: 27363032; PMCID: PMC5226505.
344. Souza-Fonseca-Guimaraes F, Young A, Mittal D, Martinet L, Bruedigam C, Takeda K, Andoniou CE, Degli-Esposti MA, Hill GR, Smyth MJ. NK cells require IL-28R for optimal in vivo activity. Proc Natl Acad Sci U S A. 2015;112(18):E2376-84. Epub 2015/04/23. doi: 10.1073/pnas.1424241112. PubMed PMID: 25901316; PMCID: PMC4426428.